

**FLOOD PREDICTION LIMITATIONS IN SMALL  
WATERSHEDS WITH MOUNTAINOUS TERRAIN AND  
HIGH RAINFALL VARIABILITY**

by

Alejandra María Rojas González

A dissertation submitted in partial fulfillment of the requirements for the degree of

DOCTOR OF PHILOSOPHY

in

CIVIL ENGINEERING

UNIVERSITY OF PUERTO RICO

MAYAGÜEZ CAMPUS

2012

Approved by:

\_\_\_\_\_  
Raúl E. Zapata López, Ph.D.  
Member, Graduate Committee

\_\_\_\_\_  
Date

\_\_\_\_\_  
Jorge Rivera Santos, Ph.D.  
Member, Graduate Committee

\_\_\_\_\_  
Date

\_\_\_\_\_  
Rafael Segarra García, Ph.D.  
Member, Graduate Committee

\_\_\_\_\_  
Date

\_\_\_\_\_  
Eric W. Harmsen, Ph.D.  
President, Graduate Committee

\_\_\_\_\_  
Date

\_\_\_\_\_  
Aurelio Mercado Irizarry, M.S.  
Representative of Graduate Studies

\_\_\_\_\_  
Date

\_\_\_\_\_  
Ismael Pagán Trinidad, MSCE  
Chairperson of the Department

\_\_\_\_\_  
Date

## ABSTRACT

An evaluation of the interrelation between different up-scaling parameters and inputs were evaluated to quantify their influence on hydrologic predictability in complex terrain and small watersheds. An up-scaling experiment was performed, consisting of increasing the grid size to produce incrementally coarser resolution maps of each parameter, terrain and rainfall inputs. Each resolution was evaluated by an ensemble approach and generalized likelihood uncertainty estimation (GLUE) methodology using high resolution rain gauge network (rainfall resolution of 100 m) and fully distributed hydrologic model (10 meters). Each parameter perturbation, hydrologic model resolution, and rainfall resolution combination were modeled producing deterministic forecasts called “ensemble members”. Objective functions were used to evaluate the behavior of each ensemble with observed data using the variables time to peak, runoff depth and peak flow observations. Ensemble skill was evaluated using scalar measures of accuracy for continuous prediction as mean absolute errors (MAE), root mean square error (RMSE) and bias between the average ensembles to observation variable. Probabilistic distribution functions (PDF) were generated for each ensemble and prediction skill was measured by ranked probability score (RPS). Based on the analyses presented in this research, the recommended upscaled rainfall resolution, which will provide equivalent accuracy with the 100 m rainfall resolution, is 1000 m, and the recommended upscaled hydrologic

model grid resolution, which will provide equivalent accuracy with the 10 m resolution, is 100 m.

## RESUMEN

Una evaluación de la interrelación entre distintos tipos de escalamiento de parámetros e insumos fueron evaluados para cuantificar su influencia en la predictibilidad hidrológica en un terreno complejo y pequeñas cuencas hidrográficas. Un experimento de aumento de escala se llevó a cabo, el cual consistió en aumentar el tamaño de la cuadrícula para producir mapas de resolución más gruesa en forma incremental de cada parámetro, modelo hidrológico y entrada de precipitaciones. Cada resolución fue evaluada por un enfoque de ensamblaje y la metodología de incertidumbre generalizada de estimación de la probabilidad (GLUE), utilizando una red de pluviómetros de alta resolución (100 m) y el modelo hidrológico totalmente distribuido (10 metros). Cada perturbación de parámetros del modelo y la combinación de lluvias y modelos hidrológicos a distintas resoluciones fueron modelados para producir pronósticos determinísticos llamados "miembros del ensamblaje". Las funciones objetivo se utilizaron para evaluar el comportamiento de cada ensamblaje con los datos observados y con variables como el tiempo al pico, profundidad de la escorrentía y las observaciones de flujo máximo. La habilidad del ensamblaje se evaluó con el uso de medidas escalares de precisión para la predicción continua, como media de los errores absolutos (MAE), error cuadrático medio (RMSE) y el sesgo entre los conjuntos de medios a la variable de observación. Funciones de distribución probabilísticas (PDF) se generaron para cada ensamblado y la capacidad de predicción se midió por puntuación de probabilidad clasificado (RPS). En base a los

análisis presentados en esta investigación, la resolución de lluvia recomendada, que ofrecerá una precisión equivalente a la resolución de 100 metros, es de 1000 m, y la resolución recomendada para la rejilla del modelo hidrológico, que ofrecerá una precisión equivalente a la resolución de 10 m es 100m.

*To God and my family. Especially, my mother,  
Yadira González, my daughter, Mariajosé. Thanks  
for your majestic love, fidelity and spiritual support.*

## ACKNOWLEDGEMENTS

During the development of my graduate studies in the University of Puerto Rico several persons and institutions collaborated directly and indirectly with my research. Without their support it would be impossible for me to finish my work. That is why I wish to dedicate this section to recognize their support.

I want to start expressing a sincere acknowledgement to my advisor, Dr. Eric W. Harmsen because he gave me the opportunity to research under his guidance and supervision. I received motivation; encouragement and support from him during my studies. With him, I have learned how to write papers for conferences and sharing my ideas with the public. I also want to thank the example, motivation, inspiration and support. I also acknowledge Dr. Walter Silva for his financial support at the beginning of my doctoral studies and the committee members and Civil Engineering Department.

I would like to thank the CASA project supported by the Engineering Research Centers Program of the National Science Foundation under NSF award number 0313747, for their financial support during my graduate program, in the form of a graduate research assistantship, conferences, retreats and a summer internship to the National Weather Center at Oklahoma. I would like to thank Dra. Damaris Santana of the UPRM Mathematics Dept. for her help with the statistical analysis of the RPS data. Special thanks to CASA-Puerto Rico Test Bed students and professors for their friendship and

support during this project and for giving me the opportunity to work in a multidisciplinary team. Especially I am grateful to Dra. Sandra Cruz Pol and Dr. José Colom for the opportunity to participate and perform research on this project, under their supervision, support and guidance.

I also want to thank the UPRM NOAA-CREST project (grant NA06OAR4810162) for financial support and NOAA-CREST students for collecting and maintaining the rain gauge data, which was used in this project. Finally, but the most importantly, I would like to thank my family, for their unconditional support, inspiration and love.

Special thanks to the University of Costa Rica for its financial support in my last year of study and for giving me the opportunity to work in the institution.

# Table of Contents

ABSTRACT .....	II
RESUMEN .....	IV
ACKNOWLEDGEMENTS.....	VII
TABLE OF CONTENTS .....	IX
LIST OF TABLES.....	XI
LIST OF FIGURES .....	XIII
GLOSSARY OF TERMS .....	XVII
<b>1 INTRODUCTION .....</b>	<b>1</b>
1.1 JUSTIFICATION .....	6
1.2 RESEARCH QUESTIONS AND OBJECTIVES.....	7
<b>CHAPTER 2.....</b>	<b>12</b>
<b>2 THEORETICAL BACKGROUND.....</b>	<b>12</b>
2.1 QUANTITATIVE PRECIPITATION ESTIMATES.....	12
2.2 PHYSICALLY-BASED DISTRIBUTED HYDROLOGIC MODELS .....	17
2.3 CALIBRATION PROCESS .....	22
2.3.1 <i>Sensitivity Analysis</i> .....	22
2.3.2 <i>Calibration of distributed models</i> .....	23
2.4 FLOOD PREDICTION.....	27
<b>CHAPTER 3.....</b>	<b>32</b>
<b>3 STUDY AREA.....</b>	<b>32</b>
3.1 MAYAGÜEZ BAY DRAINAGE BASIN STUDY AREA.....	32
3.1.1 <i>General description and stations in the area</i> .....	32
3.1.2 <i>Soils Classification</i> .....	40
3.1.3 <i>Land Use Classification</i> .....	41
3.2 TEST BED SUB-WATERSHED.....	46
<b>CHAPTER 4.....</b>	<b>48</b>
<b>4 HYDROLOGIC MODEL CONFIGURATION AND SLOPE ANALYSIS .....</b>	<b>48</b>
4.1 FLOW DIRECTION AND STREAM DEFINITION .....	50
4.2 CHANNEL GEOMETRY .....	52
4.3 STAGE AND RATING CURVE FOR THE TBSW CREEK.....	54
4.4 SLOPE ANALYSIS .....	57
4.5 GREEN AMPT INFILTRATION PARAMETERS ASSIGNMENT .....	64

4.5.1	Assumptions for unclassified soil classes .....	66
4.6	SOIL DEPTH .....	69
4.7	OVERLAND ROUGHNESS, IMPERVIOUS AND CROP COEFFICIENT ASSIGNMENT .....	70
4.8	EVAPOTRANSPIRATION .....	75
<b>CHAPTER 5</b>	.....	<b>80</b>
<b>5</b>	<b>METHODOLOGY</b> .....	<b>80</b>
5.1	ADDITIONAL FIELD MEASUREMENTS .....	82
5.2	EVALUATION OF PARAMETER AGGREGATION TECHNIQUES WITHIN THE TBSW .....	84
5.3	DETERMINATION OF HYDROLOGIC MODEL SENSITIVITY DUE TO PARAMETERS AND RAINFALL PERTURBATIONS FOR THE MBDB MODEL .....	85
5.4	EVALUATION OF CURRENT QUANTITATIVE PRECIPITATION ESTIMATES .....	87
5.4.1	Evaluating rainfall detection accuracy and long term Bias quantification .....	89
5.4.2	Evaluation of flow response to Rainfall interpolation Methods .....	94
5.5	EVALUATION OF PREDICTABILITY DUE TO HYDROLOGIC MODEL PARAMETERS AND INPUTS RESOLUTIONS AT TBSW .....	95
5.5.1	Estimation of Uncertainty due to hydrologic model at TBSW .....	96
5.5.2	Estimation of Uncertainty due to Rainfall up-scaling and temporal variations .....	103
<b>CHAPTER 6</b>	.....	<b>106</b>
<b>6</b>	<b>SENSITIVITY ANALYSIS RESULTS</b> .....	<b>106</b>
6.1	PARAMETERS AND INPUT SENSITIVITY RESULTS .....	106
6.2	SENSITIVITY DUE TO QUANTITATIVE PRECIPITATION ESTIMATION WITHIN GAP AREAS .....	117
<b>CHAPTER 7</b>	.....	<b>121</b>
<b>7</b>	<b>BIAS ESTIMATION IN RADAR PRECIPITATION PRODUCT</b> .....	<b>121</b>
<b>CHAPTER 8</b>	.....	<b>136</b>
<b>8</b>	<b>PREDICTABILITY LIMITS DUE TO UP-SCALING</b> .....	<b>136</b>
8.1	PARAMETER UNCERTAINTY PROPAGATION DUE TO RAINFALL SPATIAL VARIABILITY AND HYDROLOGIC MODEL CONFIGURATIONS .....	136
8.1.1	Evaluating predictability limits .....	145
8.1.2	Evaluating hydrologic models resolutions and rainfall resolutions .....	158
8.2	SELECTION OF THE OPTIMAL RAINFALL AND GRID RESOLUTION FOR THE MBDB MODEL .....	171
<b>CHAPTER 9</b>	.....	<b>174</b>
<b>9</b>	<b>CALIBRATION/VALIDATION OF A DISTRIBUTED HYDROLOGIC MODEL AT MBDB</b> .....	<b>174</b>
<b>CHAPTER 10</b>	.....	<b>181</b>
<b>10</b>	<b>CONCLUSIONS AND FUTURE WORK</b> .....	<b>181</b>
<b>11</b>	<b>REFERENCES</b> .....	<b>187</b>

# List of Tables

Tables	Page
Table 3-1 Climatic and river flow stations located within the study area .....	38
Table 3-2 Temperature and Precipitation Normals for NOAA stations within the study area (NOAA, 2006).....	39
Table 4-1. Mean land surface slope and standard deviation for the sub-watersheds.....	59
Table 4-2 Summary of the infiltration values for the Green Ampt Model .....	65
Table 4-3. Soil classification (SSURGO), hydrologic group and infiltration parameters at TBSW .....	69
Table 4-4 Resized Grid Area for the land use map.....	71
Table 4-5 Land Use Classification with the Manning Roughness values and crop coefficient ( $K_c$ ) for MBDB .....	73
Table 4-6 Land use classification, Manning Roughness (n) values and $K_c$ for Evapotranspiration quantification in the TBSW.....	74
Table 5-1 Two-way contingency table .....	91
Table 6-1 Relative sensitivity analysis for peak flow evaluating 3 events and 3 USGS station outlet points for peak flow .....	115
Table 6-2 Relative sensitivity analysis for 3 events and 3 USGS station outlet points for runoff depth.....	115
Table 6-3 Comparison of hydrologic results and rainfall interpolation methods and radar .....	120
Table 7-1 Contingency tables for the MPE pixels.....	127
Table 7-2 Discrete validation scores for the MPE pixels and time scales.....	127
Table 7-3 Continuous validation scores for the MPE pixels and time scales.....	129
Table 7-4 Total rainfall in the MPE pixels and mean field daily bias calculation for year 2007.....	134
Table 8-1 Descriptive variables and statistical quantification for hydrologic model resolution TBSW configuration.....	138
Table 8-2 Inventory of observed events.....	140
Table 8-3 Total rainfall event measured in rain gauges network over 4 km x 4 km area	142
Table 8-4 Storm Total produced for different resolutions .....	144
Table 8-5 Ensemble statistics and skill of prediction according to rainfall resolution and hydrologic model resolution for October 22, 2007.....	164
Table 8-6 Ensemble statistics and skill of the prediction according to rainfall resolution and hydrologic model for May 2, 2008 .....	166
Table 8-7 Ensemble statistics and skill of the prediction according to rainfall resolution and hydrologic model for June 5, 2008 .....	167

Table 8-8 Ensemble statistics and skill of the prediction according to rainfall resolution and hydrologic model for August 28, 2008 .....	168
Table 8-9 Ensemble statistics and skill of the prediction according to rainfall resolution and hydrologic model for September 3, 2008.....	169
Table 8-10 Mean RPS values for Peak Flow, Volume and Time to Peak for 5 Storms, 5 Rainfall Resolutions and 5 Grid Resolutions.....	173
Table 9-1 Base flow separation at 3 USGS streamflow stations for 2003.....	175

# List of Figures

Figures	Page
Figure 3-1 Digital Elevation Model and Rio Guanajibo, Yaguez, and Grande de Añasco watersheds, rain gauges and flow gauging stations. ....	33
Figure 3-2 Soil Map distribution for the study area. Source: SSURGO data base, (USDA, 2006a, b, c, d).....	41
Figure 3-3 Soil Texture for the study area, SSURGO map (USDA, 2006a, b, c, d) .....	42
Figure 3-4 Map of Puerto Rico natural vegetation and land cover. Source: Helmer, E.H. et al., 2002.....	44
Figure 3-5 Land Use Classification at 30 m resolution from LandSat ETM, 2000. Source: Prieto (2006) and Helmer et al. (2002) .....	45
Figure 3-6 Land Use classification of the Mayagüez Bay Watershed.....	46
Figure 3-7 TBSW location within the 4 km by 4 km NEXRAD pixel and rain gauge network. ....	47
Figure 4-1 Fow accumulation and stream definition for Rio Grande de Añasco, Rio Guanajibo and Yaguez basin model. ....	52
Figure 4-2 Cross Sections Surveyed and interpolated for Mayagüez Bay Model.....	54
Figure 4-3 Cross section measured at the instrumentation place and rating curve to full bank condition.....	56
Figure 4-4 Photos of principal channel bed at TBSW (right) and location of the pressure transducer (left).....	56
Figure 4-5. TBSW hydrologic model configured in Vflo and identification of the river reaches.....	57
Figure 4-6. Sub Watersheds map belonging to MBDB .....	58
Figure 4-7 Land Surface slope map for the TBSW, slope values are given in percent ....	61
Figure 4-8 Slope calculated for TBSW using different resample techniques.....	61
Figure 4-9 Slope box plots (quartiles 25 and 75) for the MBDB study area calculated with Method 1 and nearest neighbor resample technique, mean slope (dashed lines), quartiles 5 and 95 (solid lines) and outliers (dots).....	62
Figure 4-10 Visual comparison between resample methods at 200 m resolution for the MBDB model by Method 1 .....	63
Figure 4-11 Visual comparison between resample methods at 200 m resolution for the MBDB model by Method 2 .....	63
Figure 4-12 Land Use general reclassification from Land Sat <sup>ET</sup> , 2004, PRWRERI (2004) .....	72
Figure 4-13 Land use classification for the TBSW extracted from Figure 4-13 .....	74
Figure 4-14 Photos describing the land use of the TBSW.....	75

Figure 4-15 Potential Evapotranspiration with Hargreaves-Samani relationship for observed $T_{max}$ , $T_{min}$ , $T_{ave}$ , solar radiation, extraterrestrial radiation; and temperatures predicted by Goyal relationships at TARS station.....	79
Figure 4-16 Potential Evapotranspiration with Hargreaves-Samani relationship for observed $T_{max}$ , $T_{min}$ , $T_{ave}$ , solar radiation, and extraterrestrial radiation; and temperatures predicted by Goyal relationships at Maricao Forest station.....	79
Figure 5-1 Rain gauge distribution and location within the HE pixel; TBSW location and Euclidean Distance between the stations .....	83
Figure 5-2 Coverage gap between terrain elevation and radar beam of 0.35 degrees with the detail of blockage at mountainous area.....	88
Figure 5-3 Flow chart of the ensemble for predictability limits .....	105
Figure 6-1 Total storm maps, (A) September, 1998; (B) November 2003; (C) September 2004.....	108
Figure 6-2 Spider plot for percentage change in peak flow due to rainfall multiplicative factors at 3 USGS station outputs .....	109
Figure 6-3 Spider plots for percentage change in runoff depth due to rainfall multiplicative factors at 3 USGS station outputs.....	110
Figure 6-4 Spider plots for changes in peak flow due to parameters multiplicative factors evaluated at USGS stations and 3 events. Parameters: A) Initial Saturation, B) Soil Depth, C) Channel Roughness, D) Overland Roughness, E) Channel hydraulic conductivity, F) Overland hydraulic conductivity. ....	111
Figure 6-5 Spider plots for changes in runoff depth due to parameter multiplicative factors evaluated at USGS stations and 3 events. Parameters: A) Initial Saturation, B) Soil Depth, C) Channel Roughness, D) Overland Roughness, E) Channel hydraulic conductivity, F) Overland hydraulic conductivity. ....	113
Figure 6-6 Mean relative sensitivity coefficients for peak flows at three USGS outlet points.....	116
Figure 6-7 Mean relative sensitivity coefficient for runoff depth at three USGS outlet points.....	116
Figure 6-8 Total Storm Rainfall Maps at Mayagüez Bay Drainage Basin for November 11-16, 2003 using Interpolation Methods: (A) Exponential Weighted; (B) Inverse Distance Weighted; and Radar data (C).....	118
Figure 6-9 Radar Bias correction for storm total, November 11-16, 2003.....	119
Figure 7-1 HE pixel (red box) and MPE pixels (black and colored boxes) (left) and Hourly Rainfall Product (N1P) from NEXRAD level 3 (right) orientated in shapefile and raster formats.....	122
Figure 7-2 Rainfall accumulation over the time for the MPE pixels.....	122
Figure 7-3 Monthly Total Rainfall calculation for the rain gauge stations belonging to MPE Pixel 1, for 2007. ....	123
Figure 7-4 Hourly average and standard deviation rainfall for the rain gauge network corresponding to MPE pixel 1 for 2007.....	124

Figure 7-5 Hourly average and standard deviation rainfall for rain gauge network for 2007.....	125
Figure 7-6 Average rain gauge rainfall vs. MPE radar rainfall within HE pixel at hourly time step.....	125
Figure 7-7 Hourly False Alarm Time Series for the MPE Pixel 1 for 2007.....	128
Figure 7-8 Hourly False Alarm Time Series for the MPE Pixels within a HE Pixel for June to December 2007.....	129
Figure 7-9 Hourly Mean Field Bias for the MPE Pixel 1 during 2007.....	130
Figure 7-10 Hourly Mean Field Bias for the four MPE Pixels during 2007 within a HE Pixel. ....	131
Figure 7-11. Hourly Mean Field Bias for the overall MPE Pixels within a HE Pixel for January to December, 2007.....	133
Figure 7-12 Probability plots for daily rainfall bias between rain gauges and MPE product .....	135
Figure 8-1 Observed flows for the events studied. ....	141
Figure 8-2 Hyetographs extracted from two cell (100 m resolution) for September 3, 2008 .....	145
Figure 8-3 Box plots of Peak flows for events on: (A) October 22, 2007; (B) May 2, 2008 .....	148
Figure 8-4 Box plots of Peak flows for events on: (A) June 5, 2008; (B) August 28, 2008 .....	150
Figure 8-5 Box plots of Peak flows for September 3, 2008 event.....	151
Figure 8-6 Box plots for runoff depth: (A) October 22, 2007; (B) May 2, 2008 .....	152
Figure 8-7 Box plots for runoff depth: (A) August 28, 2008; (B) September 3, 2008 ...	153
Figure 8-8 Box plots for runoff depth for September 3, 2008 .....	154
Figure 8-9 Box Plot of time to peak for (A) October 22, 2007; (B) May 2, 2008.....	155
Figure 8-10 Box Plot of time to peak for (A) June 5, 2008; (B) August 28, 2008 .....	156
Figure 8-11 Box Plot of time to peak for September 3, 2008.....	157
Figure 8-12 Probability plots for (A) Rain ensembles for peak flow, (B) Hydrologic model ensembles for peak flow, (C) Rain Ensembles for discharge depth volume, (D) Hydrologic Model ensembles for discharge depth volume. October 22, 2007 .....	159
Figure 8-13 Probability plots for (A) Rain ensembles for peak flow, (B) Hydrologic model ensembles for peak flow, (C) Rain Ensembles for discharge depth volume, (D) Hydrologic Model ensembles for discharge depth volume. May 2, 2008 .....	160
Figure 8-14 Box and probability plots for (A) Rain ensembles for peak flow, (B) Hydrologic model ensembles for peak flow, (C) Rain Ensembles for discharge depth volume, (D) Hydrologic Model ensembles for discharge depth volume. June 5, 2008 .....	161
Figure 8-15 Box and probability plots: (A) Rain ensembles for peak flow, (B) Hydrologic model ensembles for peak flow, (C) Rain Ensembles for discharge depth volume, (D) Hydrologic Model ensembles for discharge depth volume. August 28, 2008.....	162

Figure 8-16 Box and probability plots: (A) Rain ensembles for peak flow, (B) Hydrologic model ensembles for peak flow, (C) Rain Ensembles for discharge depth volume, (D) Hydrologic Model ensembles for discharge depth volume. September 3, 2008 ....	163
Figure 9-1 Daily stream flow and baseflow computation for 3 USGS stations, 2003....	176
Figure 9-2 Runoff depth accumulated for the USGS stations for 2003 year .....	177
Figure 9-3 Comparison between observed and simulated discharge for 2003 at hourly time step for: (A) Rio Grande de Añasco near San Sebastian and (B) Rio Rosario near Hormigueros stations. ....	178
Figure 9-4 Maximum, minimum and observed runoff for Añasco river (A) and Rosario river (B) outlet points for selected events .....	179

## GLOSSARY OF TERMS

A	flow area
a, b	coefficients in the radar rain rate equation
AMS	Annual Maximum Series
ArcGIS	Arc Geographical Information Systems
ASCII	data file in text format
Bias	bias
C	Celsius
CASA	Collaborative Adaptive Sensing of the Atmosphere
CASC2D	CASCade 2 Dimensional Sediment
CDA	Contributing drainage area
cdf	cumulative distribution function
cms	cubic meters per second
COEM	Centro Residencial de Oportunidades Educativas de Mayagüez
CREST	Cooperative Remote Sensing Science and Technology Center
CRIM	“Centro de Recaudación de Impuestos Municipales”, Center for Municipal Tax Revenues of Puerto Rico
CRR	Conceptual Rainfall-Runoff
DB	discrete bias
dBZ	decibels
DEM	digital elevation map
DHSVM	Distributed Hydrology Soils and Vegetation Model
$e_a$	actual vapor pressure
$e_s$	saturated vapor pressure
ET	evapotranspiration
ET <sub>o</sub>	reference evapotranspiration
EW	exponential weighted
FAR	false alarm rate
FAS	Flood Alarm System
FEM	finite element method
FEMA	Federal Emergency Management Agency
FIS	Flood Insurance Study
G	soil heat flux density
GIS	geographical information system
GLUE	generalized likelihood uncertainty estimation
GPD	generalized Pareto distribution
h	hour
$h$	flow depth
$H$	hit rate
HE	Hydro-Estimator

HEC	Hydrologic Engineering Center
HEC-RAS	Hydrologic Engineering Center-River Analysis System
HMS	Hydrologic Modeling System
HRAP	Hydrologic Rainfall Analysis Project
IDW	inverse distance weighting
$J$	number of categories and therefore also the number of probabilities included in each forecast
$K_c$	evapotranspiration crop coefficient
km	kilometer
kPa	kilopascal
$K_s$	saturated hydraulic conductivity
KWA	kinematic wave analogy
MAE	mean absolute error
MAR	mean annual rainfall
MBDB	Mayagüez Bay Drainage Basin
MPE	Multisensor Precipitation Estimation
$n$	Manning's roughness factor
NAD	North American Datum
NIP	precipitation radar product
NEXRAD	Next Generation Radar
$N_i$	adjustment factor
NOAA	National Oceanic and Atmospheric Administration
$O$	model output with input parameters set at base values
$O_{P+\Delta P}$ and $O_{P-\Delta P}$	are model outputs with the input parameter plus or minus a specified Percentage
$o_j$	cumulative probability of the observation in the $i^{\text{th}}$ category or vector component
OPPA	Ordered Physics-based Parameter Adjustment
P	value of input parameter
PBD	physically-based distributed
PDF	probability distribution function
PDS	partial duration series
PET	potential or reference evapotranspiration
POD	probability of detection
PR-1	CASA Student Testbed area 1
PRWRA	Puerto Rico Water Resources Authority
PRWRERI	Puerto Rico Water Resources and Environmental Research Insitute
$p_x(x)$	Gaussian or normal distribution function
Q	stream volumetric discharge
QPE	Quantitative Precipitation Estimation

QPe-SUMS	Quantitative Precipitation Estimation and Segregation Using Multiple Sensors
QPF	quantitative precipitation forecast
R	rain rate
$R^2$	Pearson correlation coefficient or coefficient of determination
$R_a$	extraterrestrial radiation
RMSE	root mean squared error
$R_n$	net radiation
RPS	ranked probability score
RQ	research question
S22, S23, S24	CASA projects
SCAN	Soil Climate Analysis Network
SHE	Systeme Hydrologique European
$S_o$	channel bed slope
$S_r$	relative sensitivity coefficient
SSURGO	refers to the Soil Survey Geographic Database
STD	standard deviation
$t$	time
TARS	Tropical Agriculture Research Station
$T_{ave}$	average air temperature
TBSW	Testbed Subwatershed
TM	Thermatic Mapper
$T_{max}$	maximum air temperature
$T_{min}$	minimum air temperature
TRMM	Tropical Rainfall Measuring Mission
$u$	channel velocity
$u_2$	wind velocity at 2 m height
USACE	U.S. Army Corps of Engineers
USDA	United States Department of Agriculture
USGS	U.S. Geological Survey
Vflo	physically-based hydrologic developed by Vieux and Associates, Inc.
X,Y	generic variables on a probability plot
$y$	prediction from the $k^{th}$ simulation for Time, Peak and volume
$y_j$	cumulative probability assigned o the category or vector component
$Y_m$ and $O_m$	cumulative forecast and observation
yr	year
Z	reflectivity
$\mu$	mean
$\Delta$	slope of the vapor pressure curve in Penman Monteith equation or change
$\sigma^2$	variance
$\gamma$	psychrometric constant in Penman Monteith equation

# CHAPTER 1

## 1 INTRODUCTION

Due to the complex terrain and the tropical climate influence, Puerto Rico is characterized by small watersheds, high rainfall intensity and spatial variability. The rainfall anomalies are produced by tropical waves, low pressure depressions, tropical storms, and hurricanes capable of producing flash flood in susceptible areas. As part of the model configuration, rainfall must be distributed over the model domain. Different theoretical methods are available to spatially distribute rainfall over a watershed, however, there is not typically enough rain gauge density to calculate the associated bias, and to obtain spatial variability of point rainfall at scales below the typical resolution of the radar-based products (2 x 2 kilometers), archived with the Next Generation Radar (NEXRAD) level 3.

New emerging radar technologies are being developed by the Student Test Bed of the Center for Collaborative Adaptive Sensing of the Atmosphere (CASA, 2006) in Puerto Rico and will be available for flash flood predictions. This new radar technology promises to revolutionize the way rainfall is detected, monitored and predicted, creating a dense sensor network of low-powered radars that overcome curvature blockage and significantly enhance resolution. This network will monitor the lower atmosphere where the principal atmospheric phenomena occur. The first step in the technology development has been the PR-1 radar located on the Stefani building at University of Puerto Rico,

Mayagüez Campus. The PR-1 radar is a marine radar adapted to sense reflectivity with an average pixel size of 150 m and the maximum coverage range of 25 km.

An important step for the hydrologic community and Puerto Rico in general will be the use of these advanced technologies as input to real-time flash flood prediction systems. Real-time flash flood estimates can allow decision makers to implement emergency plans only when it is necessary, since unnecessary preparations and evacuations are very costly. The technique also allows decision makers to better focus their emergency measures due to the variable rainfall patterns, since in the tropical region the locations where flood waters concentrate tend to vary in time and space. Rain gauge density is generally not sufficient to capture spatial variability at the NEXRAD radar sub-pixel scale and the new radar technology will help to fill gaps between rain gauges. Some methods for removing the systematic bias between radar and rain gauges are applied today. However, it is not known how much the intrinsic error due to spatial variability at the radar sub-pixel scale limit the reliability of the data for use in hydrologic models. Some scientific questions arise where complex terrain and climatological conditions increase the spatially dependent bias.

How does rainfall spatial distribution affect the hydrologic response in small subwatersheds? How can adjustments be made to radar rainfall estimates when there are not sufficient numbers of rain gauges within the network? Under these conditions, how can we produce reliable hydrologic estimates in small areas where high spatial variability exists? These questions are essential when using fully physics-based distributed

hydrologic models because the goal of their use is to produce accurate flood predictions at any location upstream of the watershed outlet.

Few studies have been conducted in Puerto Rico to forecast real-time rainfall runoff. In 1996 the US Geological Survey (USGS) developed a real time rainfall runoff simulation for Carraízo reservoir basin allowing the estimation of water volumes at the reservoir from the rainfall and discharge data that is being obtained from the network stations inside the basin (Sepúlveda et al., 1996).

The National Weather Service (NWS) establishes Flash Flood Guidance estimates in real time based on the Sacramento soil moisture accounting model. Flash Flood Guidance is performed by region or River Forecast Center, and Puerto Rico belongs to the Southeast River Forecast Center. The analysis allows for the development of the curves that relate threshold runoff to flash flooding of a given duration as a function of soil moisture deficit (Sweeney, 1992; Georgakakos, 2006a; Smith et al., 2004; Reed et al., 2004). Vieux and Vieux (2006) tested a physics-based distributed model in the Loíza basin of Puerto Rico. A long term and event-based simulation were conducted to calibrate the streamflow volume. The soil moisture values calculated in the long term model were fed back into the event-based simulation to enhance the calibration for several individual storm events. A sensitivity analysis to initial soil moisture showed some persistence in antecedent soil conditions, with about one year of warm up the model to obtain stable results.

To establish a flood alarm system in Puerto Rico, first it is imperative to know how the watershed behaves under different environmental conditions, parameter spatial variability, input aggregation and associated biases and how these differences are propagated to the solution. This knowledge enhances the forecast skills using distributed models such as Wechsler (2006); Vieux, et al. (2004), Viglione et al. (2010), Müller et al. (2005) and Bloschl, et al. (2008).

Hydrologic parameters play an important role in the hydrologic prediction where high slope exist, and where soil as well as land use characteristics change over short distances. Hydrologic models average the hydrologic parameters and topographic characteristics in lumped, semi-distributed and distributed models to simplify or reduce computational time. In addition, calibrations are usually limited to the watershed outlet, hence, not producing accurate flood prediction within the sub-watershed's internal outlets.

Loss of accuracy occurs in flood prediction with topographic and parameters aggregation, however, how much loss of accuracy can we expect? Limited number of studies have evaluated the effects of grid size on basin response and the prediction of discharge in tropical environments and complex topography (e.g., Bormann, 2006; Shrestha et al., 2002; Vieux, 1993; Wechsler, 2006; Western et al. 2004). Therefore, this research will investigate these aspects as they are related to model calibration and flood prediction.

The hydrologic model used in this research is *Vflo*<sup>TM</sup> (for convenience in this dissertation *Vflo*<sup>TM</sup> will be referred to as Vflo), a fully distributed hydrologic model

(Vieux and Vieux, 2002; and Vieux et al. 2003). Vflo uses the finite element numerical method to resolve overland and channel flow. The Green Ampt equation is used to represent rainfall infiltration through the soil (Rawls et al., 1983). The digital revolution in geospatial data has helped to promote the development of physically-based models capable of producing excellent results in flood prediction at internal basin points.

To understand the system predictability we will conduct various experiments within a small sub-watershed laboratory (test-bed) covering a 4 km x 4 km Geostationary Operational Environmental Satellite (GOES) pixel. This “real world” laboratory has a rain gauge network with a resolution well below that of the NWS radar products; a stage elevation station at the outlet; high topography resolution information (Digital Elevation Model raster map, DEM 10 x 10 m), remotely sensed data (e.g., LandSat Thematic M) and several field measurements to represent the channel geometry. The test-bed sub-watershed is located in Western Puerto Rico and belongs to the Rio Grande de Añasco watershed. To establish a flood alarm system in the region of the study area, it is necessary to know the performance and the prediction limits associated with the small sub-watersheds.

## 1.1 Justification

A study which considers different input (rainfall) resolutions, parameter aggregation effects and hydrologic model resolutions, at scales lower than the current radar products, has not been conducted in Puerto Rico or anywhere as of the writing of this thesis. With the new emergent radar technologies it is necessary to recommend to the hydrology community which grid size is necessary to capture the spatial variability of rainfall and hydrologic model that generate reliable flood prediction. The prediction limits related to this input grid size and, at the same time have a cell size that minimizes the computational time for real-time applications.

The grid size and the watershed response are interrelated. Therefore, it is imperative to know the combination of grid sizes needed to produce reliable results within the study area and to know the probabilistic distribution function (PDF) of flow peaks, time to peak and runoff volume associated with each resolution. The optimal grid size is defined as the largest grid size which will produce reliable results, beyond which flood prediction accuracy degrades.

The time required to run the model in real-time operation mode is critical. Therefore, the grid size should be courser to decrease the computational time, while maintaining sufficiently accurate results. An up-scaling evaluation of rainfall and hydrologic parameters consist in the creation of a high resolution hydrologic model, mentioned above, and then increasing the grid size to produce incrementally coarser resolution maps

of each parameter and input, resulting in different output responses. These hydrologic responses will be compared in terms of their probability distribution functions (PDFs) to observed values. A decision can be made in terms of which aggregation technique should be used to aggregate the data and which parameters will be used in the evaluation at small scales.

## **1.2 Research Questions and Objectives**

Real time hydrologic predictions require estimation of stream stage, peak flow, time to peak, and storm volume with high reliability. To obtain reliable estimates it is necessary to know and understand the predictability and prediction limitations of the system.

The general objective of this research was to evaluate the hydrologic predictability of flood predictions in complex terrain located at Mayagüez Bay drainage basins due to rainfall inputs and hydrologic model resolutions. To identified representative parameters at each scale that will enhance the flood prediction when the modeler uses different grid size resolution inputs within the distributed hydrologic models.

Three basic research questions (RQ) addressed in this research are summarized below and were based on a Workshop on Predictability and Limits to Prediction in Hydrologic Systems by the National Research Council (Entekahbi et al., 2002) and suggestions made by several investigators in the field (e.g., Vieux et al., 2004, 2005, 2006; Georgakakos, 2006a, 2006b).

**RQ1. How flow prediction is affected by the spatial variability of point rainfall at scales below that of the typical resolution of radar-based products?**

The error propagation due a rainfall spatial resolution in the distributed models has been a goal in the hydrologic community in recent years. Different studies that have been conducted have been done at scales courser or same than resolution of the radar rainfall products using distributed models (Gourley and Vieux, 2005 and 2006; Vieux and Farajalla, 1996 or Cole and Moore, 2009) or using lumped model (Bell and Moore, 2000).

The accuracy of current precipitation estimates over a basin must be known; and moreover, the accuracy of these estimates must be improved before the uncertainty in hydrologic forecasts can be quantified and ultimately reduced. As pointed out in Droegemeier and Smith (2000), hydrologic forecast uncertainty cannot be reasonably assessed until the uncertainty in the rainfall observations has been determined a priori. Entekahbi et al. (2002) identified the uncertainty in model inputs as one of the major limitations to improved hydrologic predictability.

One important contribution will be to find the current rainfall product uncertainty over small watersheds. Also, evaluate how uncertainties due to quantitative precipitation estimates at different resolutions (below 2 km) from point rainfall are propagated through the hydrologic solution. By this means we can determine which rainfall resolution is required to encompass the rainfall variability and produce the least uncertainty and highest accuracy for flood predictions at scales below radar products and small subwatersheds.

The Collaborative Adaptive Sensing of the Atmosphere (CASA) project has instrumented a 4 km by 4 km area with a network of 28 rain gauges, producing high spatial rainfall resolution with the objective to test and validate CASA radars. Inside the pixel a small sub-watershed was delineated and instrumented with a pressure transducer to measure stage at a determined cross section. The small area was named Test Bed Subwatershed (TBSW) and serves as a field laboratory to test how the uncertainty due to rainfall resolution input propagates through the distributed hydrological model to the streamflow prediction.

**RQ2. How does parameter and hydrological model resolution affect the model's predictive capabilities and the errors of the hydrologic system?**

To develop a real time hydrologic model, a coarse grid size resolution is desirable in order to minimize computational time. However, this choice could have an important impact on the hydrologic simulation, because the calibration is grid-cell size dependent. The effects observed in the grid size aggregation are flattening of the slope and shortening of the drainage length, changes in flow direction, channel and overland cells and smoothness of the soil parameters and roughness. Both effects can be compensated for or reduced depending on the topographic characteristics of the basin and the methods used to calculate them (Brasington and Richards, 1998; Quinn et al., 1991; Tarboton et al., 1991; Vieux, 1993).

Mountainous areas with large slopes are more sensitive to digital elevation model resolution. The resolution of the terrain model needed to capture the basin properties is

the same for slope as it is for other parameters such as hydraulic roughness derived from land use obtained from satellite remote sensing and soil properties. Understanding the influence of resolution and parameter aggregation on the hydrologic model would enhance the model prediction. This will be accomplished using the highest resolution data available and then producing coarser resolution maps of each parameter through up-scaling (various methods could be tested here), and evaluate how the coarser resolution degrades the solution obtained at the finest resolution. We suggest, as an hypothesis, that the finer hydrologic model resolution ensemble will have the best flow prediction behavior. However, this model is not operational for future flash flood forecasting. The goal is to find a practical grid size resolution for real time applications and address reliable results at small watersheds.

**RQ3. Would the assumptions developed for the small scale enhance the hydrologic predictability at larger scales?**

The hypothesis formulated is that if we can enhance the flood forecasting in small sub-watersheds we can enhance the flood forecasting at larger scales where all major mountainous basins are a composite of similar sub-watersheds that have similar slope conditions, land use coverage and soil properties. Lessons learned in this study about the small watershed's behavior could be applied to watersheds of major sizes where the cost of using high resolution data could result in better flood forecasting. However, if it is necessary to apply coarse resolution data to large scale, real time applications, the predictability limits could be known a priori. Recommendations related to which terrain

and rainfall grid sizes and parameter estimations to use in the distributed hydrologic model will be available, and will be tested in watersheds of major size. Only a few rain gauges and NEXRAD rainfall estimates are provided to major areas.

The specific objectives of this study, required for the achievement of the major research goal and the research questions are:

1. Configure a hydrologic distributed model for the Mayagüez Bay Drainage Basin (MBDB) and extract a small subwatershed (TBSW) having similar slope characteristics to the MBDB subwatersheds, for the purpose of performing detailed studies. (Chapter 5)
2. Analyze the MBDB hydrologic model sensitivity in the flow response due to propagation of parameter and rainfall perturbations using spider plots and relative sensitivity analyses. (Chapter 6)
3. Quantification of MBDB hydrologic model flow response due to two rainfall interpolation methods and radar sources. (Chapter 6)
4. Evaluate the rainfall detection accuracy of the current radar product (multisensor precipitation estimator, “MPE”) at scales below 2 km using a high density rainfall network. (Chapter 7)
5. Evaluate ensemble behavior for rainfall resolutions exposed to uncertainties in parameter quantifications and hydrologic model resolutions. (Chapter 8)
6. Evaluate ensemble behavior of hydrologic model resolutions due to propagation of parameter uncertainties and rainfall resolutions. (Chapter 8)

## CHAPTER 2

# 2 THEORETICAL BACKGROUND

### 2.1 Quantitative Precipitation Estimates

A major source of error in hydrologic models is the poor quantification of the areal distribution of rainfall, typically due to the low density of rain gauges. A rain gauge located at a single point may not represent an extensive area, with only one value. The spatial distribution of rainfall can have a major influence on the corresponding runoff hydrograph, errors may occur in the resulting hydrograph when the spatial pattern of the rainfall is not preserved. These errors will be magnified for intense, short duration and localized events especially in areas of high topographic variability subject to convective storms (Wilson and Brandes, 1979).

Rain gauges themselves may produce errors, a major source of error being from turbulence and increased winds around the gauge, affecting precipitation quantification in events where the wind is an important factor (e.g., hurricanes). Nevertheless, the rainfall measured in a gauge station is generally assumed to be the most reliable measurement of rainfall, but when measurements are extrapolated to the entire basin for hydrologic models, the rainfall has a great uncertainty and can affect the watershed response. Bevan and Hornberger (1982) have stated, "... an accurate portrayal of spatial variation in rainfall is a prerequisite for accurate simulation of streamflows".

Investigators have used mean areal precipitation as calculated by, for example Thiessen polygons, (Wilson and Brandes et al. 1979; Viessman and Lewis, 1996), and interpolation methods, such as Spline, Inverse Distance Weights, and Krigging and polynomial surface. But all of these methods are limited by the number of rain gauges.

Ball and Luk (1998) present the results of a study investigating the accuracy and reliability of hydroinformatic tools (e.g. GIS) for modeling the spatial and temporal distribution of rainfall over a catchment. It was found that using spline surfaces with a geographic information system produced robust and accurate estimates of rainfall and enable real-time estimation of spatially distributed patterns.

Currently, sophisticated methods attempt to fill gaps between rain gauges, by sensing the atmosphere with remote sensors like the space-borne Tropical Rainfall Measuring Mission (TRMM), the U.S. National Weather Service's (NWS) Next Generation Radar (NEXRAD), the National Oceanic and Atmospheric Administration's (NOAA) Hydro-Estimator (HE) algorithm (Scofield and Kuligowski, 2003), the satellite precipitation estimation /radar rainfall merging algorithm of the NOAA-CREST Group at City University of New York (Mahani and Khanbilvardi, 2009), and the MPE (Seo, 1998; Lawrence, et al., 2003; Kondragunta, et al., 2005). The HE utilizes data from the GOES geostationary satellite to estimate rainfall, and has, for example, an approximate pixel size of 4km x 4km.

These quantitative precipitation estimation (QPE) techniques are evaluated and adjusted or calibrated using existing rain gauges, however, these adjustments depend on

the rain gauge density and their spatial distribution (Harmsen et al., 2008). Studies that have compared radar and rain gauge–derived rainfall documented large discrepancies between them (e.g., Baeck et al., 1998; McGregor et al., 1995; Woodley et al., 1975).

In order to address the need to obtain more rainfall estimates for basin analysis, in 1997 The National Weather Service (NWS) put into operation the WSR-88D Next Generation Radar (NEXRAD) in the United States of America. NEXRAD radar enhances covertures with a 1 degree x 1 km base resolution. Since 1999, NEXRAD has been used by the NWS to estimate rainfall in Puerto Rico. The NEXRAD facility is located near the City of Cayey at 860 m above mean sea level and at approximately 120 km from Mayagüez. The radar measures reflectivity in decibel, or dBZ, and uses empirically derived Z-R relationships to transform reflectivity to rain rate. The Marshall and Palmer (1948) equation is the default Z/R relationship employed by the WSR-88D and is described by the empirical power law which can be expressed as:

$$Z = aR^b \quad (2-1)$$

where  $Z$  is the reflectivity in decibels (dBZ) and  $R$  is the rain rate in mm/hr; “ $a$ ” and “ $b$ ” are coefficients and their respective values depend on the type of precipitation.

The coefficients depend on location, season, rain type, drop size distribution, and are event dependent. Battan (1973) presents more than 50 Z/R relationships. At this time there exist at least five different relationships depending on climatological zones approved by the NWS. For example for a convective rainfall “ $a$ ” and “ $b$ ” values are 300

and 1.4, respectively. Similarly, for a tropical condition, values of 250 and 1.2, respectively, are used and for a warm stratiform rainfall values of 200 and 1.6 are used.

The default Z-R relationship used in Puerto Rico is the convective one and is not representative of tropical rain events due to the drop size distribution (smaller rain drops than convective with fewer and larger rain drops). It is necessary to define a maximum precipitation rate threshold for decibels above 51, because equation 2-1 with the tropical coefficients can produce nonsensical rain rates. High dBZ are due to possible hail formations or, very heavy precipitation or extreme winds, which also may be produced by thunder and lightning, and wet ground returns. The radar default setting is 4.09 in/hr and if rainfall rates are greater, a deep warm cloud layer exists. Therefore, warm rain processes govern, which is typical of tropical events (Maddox et al., 1978). Operationally the Z/R relationship should be changed to the tropical equation and the maximum precipitation rate threshold changed to 6.00 in/hr.

Vieux and Bedient (1998) found an improved Z-R relationship comparing slopes of the best fit regression lines of each Z-R relationship to daily rain gauge accumulation. With the current Z-R relationship used in Puerto Rico, NOAA has reported low estimates of accumulated rainfall by the radar as compared to gauge accumulations.

The MPE algorithm is a product of NEXRAD, and recently has been used to improve quantitative precipitation estimates (Kondragunta and Shrestha, 2006; Mahani and Khanbilvardi, 2009). MPE is based on the Digital Precipitation Array (DPA) product (hourly and 4km x 4km resolution) and performs a mean field bias correction over the

entire radar coverage area, based on (near) real-time hourly rain gauge data (Seo et al., 1999). The MPE is mapped onto a polar stereographic projection called the Hydrologic Rainfall Analysis Project (HRAP) grid. This data is often used in hydrologic modeling, availing the bias correction made by the MPE algorithm. Nevertheless, in long term hydrologic simulations and watersheds with small numbers of rain gauges, a bias verification would be evaluated, because the bias quantification has a high variability over the radar coverage area and time (Harmsen et al., 2008; Ramírez-Beltrán et al., 2008a and 2008b) affecting the hydrologic calibration and validation.

Gourley and Vieux (2005) developed a method for evaluating the accuracy of Quantitative Precipitation Estimates (QPE) for isolated events. A hydrologic approach to QPE evaluation may also become complicated because model parameters can be judiciously adjusted or calibrated to account for errors in model inputs. Systematic biases, which are originally present in the model inputs, can be mitigated or corrected in order to yield accurate streamflow forecasts.

Probabilistic calibration methods exist, such as the generalized likelihood uncertainty estimation (GLUE) used by Beven and Binley (1992), to compute the probability that a given parameter set adequately simulates the observed system behavior. Furthermore, it was suggested in Freer et al. (1996) that the GLUE technique should be expanded to include the uncertainties associated with different rainfall inputs. Extension of the GLUE provides a consistent methodology to independently evaluate the hydrologic response to each input.

Georgakakos (2006b) expressed the need of future research in the context of short term hydrologic forecasting with QPF driven distributed hydrologic models which include:

- Development of high resolution reliable QPF, especially in mountainous areas.
- Sensitivity analysis of distributed models with operational data to assess the relative importance of parameter uncertainty and QPF hydrologic models that include characterization of the errors in distributed QPFs.

## **2.2 Physically-based distributed hydrologic models**

Vieux and Moreda (2003) explain that the goal of distributed modeling of streamflow is to better represent the spatial-temporal characteristics of a watershed governing the transformation of rainfall into runoff that relies on conservation equations for the routing of runoff through a distributed representation of a watershed.

The term physics-based or physically-based distributed (PBD) models, includes such models as Vflo (Vieux and Vieux, 2002); r.water.fea (Vieux and Gauer, 1994; Vieux, 2001), CASC2D (Julien and Saghafian, 1991; Ogden and Julien, 1994; Julien, et al., 1995), Systeme Hydrologique European (SHE) (Abbott et al., 1986a,b) and the Distributed Hydrology Soil Vegetation Model (DHSVM) (Wigmosta, et al., 1994). PBD models are well suited to simulating specific events at locations where streamflow records may not exist.

Conceptual rainfall-runoff (CRR) models simulate runoff generation by a variety of conceptual parameters and route the runoff using unit hydrographs to an outlet. CRR models are inherently non-physics based and lump parameters at the basin or sub-basin level. CRR models include Precipitation-Runoff Modeling System (PRMS) by Leavesley et al. (1983), the Sacramento Soil Moisture Accounting Model (SAC-SMA) (Burnash, et al. 1973), and the HEC-HMS model (Hydrologic Engineering Center, 2006). CRR models differ from event-based models, simulating continuous cycles of rainfall and runoff. The CRR models breakdown the hydrologic cycle into a series of reservoirs that represent physical phenomena such as infiltration, runoff, etc. (Vieux and Moreda, 2003).

Physics-based models use conservation of mass, momentum, and energy equations to represent hydrologic processes, whereas conceptual models use empirical relationships together with buckets to represent component processes. Moore and Grayson, (1991) describe an array of physics-based models that capitalize on digital models of elevation, GIS and remotely sensed (GIS/RS) geospatial data. The term physics-based model means that conservation of mass in combination with momentum and/or energy is employed to compute hydrologic fluxes.

The model used in this research is a fully-distributed, physics-based hydrologic model named Vflo (Vieux, 2002 and 2004) that derives its parameters from soil properties, land use/cover, topography, and can obtain input from radar or multi-sensor precipitation estimates. Vflo incorporates routing of unsteady flow through channel and overland elements comprising a drainage network.

The following Vflo description and mathematical formulation was obtained (in some cases verbatim) from Vieux and Vieux (2002) and states that the model uses the kinematic wave analogy (KWA). The KWA has better applicability where the principal gradient is the land surface slope. Thus in almost all watersheds except for very flat areas, the KWA may be used. The simplified momentum equation and the continuity equation comprise the KWA. One-dimensional continuity for overland flow resulting from rainfall excess is expressed by:

$$\frac{\delta h}{\delta t} + \frac{\delta(uh)}{\delta x} = R - I \quad (2-2)$$

where  $R$  is rainfall rate;  $I$  is infiltration rate;  $h$  is flow depth;  $u$  is overland flow velocity;  $t$  is the time and  $x$  is the distance. In the KWA, the bed slope is equated with the friction gradient. In open channel hydraulics, this amounts to the uniform flow assumption. Using this fact together with an appropriate relation between velocity,  $u$  (m/s), and flow depth,  $h$  (m), such as the Manning equation, we obtain the velocity for very wide open channel and metric system:

$$u = \frac{S_o^{1/2}}{n} h^{2/3} \quad (2-3)$$

where  $S_o$  (m/m) is the bed slope or principal land surface slope, and  $n$  is the hydraulic roughness as expressed by the Manning's coefficient. Velocity and flow depth depend on the land surface slope and the friction induced by the hydraulic roughness. For

channelized flow, Eq. 2-2 is written with the cross-sectional area  $A$  instead of the flow depth  $h$ :

$$\frac{\delta A}{\delta t} + \frac{\delta Q}{\delta x} = q \quad (2-4)$$

where  $Q$  ( $\text{m}^3/\text{s}$ ) is the discharge or flow rate in the channel, and  $q$  is the rate of lateral inflow per unit length in the channel.

Combining equations 2-3 and 2-4 results in:

$$\frac{\delta h}{\delta t} + \frac{s^{1/2}}{\beta n} \frac{\delta h^{5/3}}{\delta x} = \gamma R - \alpha I \quad (2-5)$$

where the three scalars  $\alpha$ ,  $\gamma$  and  $\beta$  are the multipliers for the values contained in the spatially variable parameter maps according to the Ordered Physics-based Parameter Adjustment (OPPA) calibration method. Differential application of the roughness scalars ( $\beta n$ ) to channel and overland are used ( $\beta c$  for channel and  $\beta o$  for overland).

Overland flow is modeled with equations 2-2 and 2-3, and channels with equation 2-4 and appropriate form of the Manning uniform flow relation in Eq. 2-4 using the finite element method.

Digital maps of soils, land use, topography and rainfall rates are used to compute and route rainfall excess through a network formulation based on the Finite Element Method (FEM) computational scheme described by Vieux (1988) and Vieux et al. (1990). Special treatment is required to achieve a FEM solution to the KWA over a surface with spatially

varying roughness, slope, or other parameters. Vieux et al. (1990) presented such a solution using nodal values of parameters in a finite element solution. This method effectively treats changes in parameter values by interpolating nodal values across finite elements.

Vieux (2001) and Vieux and Gauer (1994) describe the development of a rainfall-runoff model based on a drainage network comprised of finite elements. The advantage of this approach is that the kinematic wave analogy can be applied to a spatially variable surface without numerical difficulty introduced by the shocks caused by non-continuous parameter variation that would otherwise propagate through the system. The finite element methodology results in execution times that are fast enough to allow real-time computation before the next radar update.

Accounting for unsteady flow in mild slopes, Vflo allows a looped rating curve for channel elements. Essentially, the acceleration (deceleration) induced by the rising (falling) limb of the hydrograph is accounted for through the Jones Formula (Henderson, 1966). In mild slope hydraulic conditions, looped rating curves may cause important effects when maximum flow rate is observed. Vflo incorporates both distributed runoff generation, and routing of unsteady flow through channel and overland elements (Vieux, and Vieux, 2002).

Vieux and Bedient (2004) used spatial resolution of radar rainfall as input to a distributed model which affected prediction error. Also, Vieux and Imgarten (2012) studied the scale-dependent propagation of hydrologic uncertainty using high-resolution

X-band radar rainfall estimates for watershed areas less than about 20 km<sup>2</sup>. Results of experiments using historical radar events, including the tropical storm Allison, indicate that accurate rainfall-runoff predictions in real time are possible and useful for site-specific forecast in Houston, TX. They found that the achievable model accuracy with radar bias correction was approximately a mean absolute percentage error of 11.8% in peak discharge, 11.1% in runoff depth and average difference in arrival times of 12 min at the Main Street gauge with a drainage area of 260 km<sup>2</sup>.

The complex interaction of input with drainage network presents challenges to the design of storm-water drainage infrastructure, the management of flooding, flood mitigation, and real-time forecasting of multi-scale urban drainage systems with multi-scale inputs (Vieux and Vieux, 2005).

## **2.3 Calibration Process**

### *2.3.1 Sensitivity Analysis*

The classification of the sensitivity analysis methods refers to the way that the parameters are treated. Local techniques concentrate on estimating the local impact of a parameter on the model output. This approach means that the analysis focuses on the impact of changes in a certain parameter value (mean, default or optimum value). Opposed to this, global techniques analyze the whole parameter space at once. Global sampling methods scan in a random or systematic way the entire range of possible

parameter values and possible parameter sets. The sampled parameter sets can give the user a good idea of the importance of each parameter. These in turn can be used to quantify the global parameter sensitivity or the uncertainty of parameters and outputs.

### *2.3.2 Calibration of distributed models*

Vieux and Moreda (2003) developed an OPPA procedure for a distributed model. The OPPA calibration process involves estimating the spatially distributed parameters from physical properties, assign channel hydraulic properties based on measured cross-sections, study the sensitivity of each parameter, and find the optimum parameter set that minimizes the respective objective function. Runoff depth should be adjusted first, followed by timing and peak flow and re-adjust hydraulic conductivity if necessary to account for changes in infiltration opportunity time. The Vflo model does not simulate base flow directly, only direct runoff. It can be taken in account by assigning a fixed value to channel cells for one simulated event. For long term analyses it is necessary to quantify the base flow using known methodologies (Gupta, 1989; Sepulveda, et al., 1996) and subtract it from the observed hydrograph to compare with direct runoff simulated by the Vflo model.

The agreement between the observed and simulated runoff depth, time to peak and peak flow may be expressed in terms of a bias or spread. The bias indicates systematic over or under prediction. The departure, whether expressed as an average difference,

percentage error, coefficient of determination, or as a root-mean-square error, serves as a measure of the prediction accuracy.

McMichael, et al., (2005) calibrated a distributed physically based hydrologic model (MIKE-SHE) in California and estimated uncertainty. They used the GLUE methodology for model calibration, testing and predictive uncertainty for estimating monthly streamflow. The catchment in Central California was 34 km<sup>2</sup> in area and the model grid size was fixed at 270 m x 270 m. A Monte Carlo simulation was used to randomly generate one thousand parameters sets for a 20 yr calibration period encompassing variable climatic and wildfire conditions. Many studies have demonstrated the difficulties that arise in identifying, calibrating and validating physically-based hydrologic models. Such difficulties stem from uncertainties in model structure, boundary conditions, and catchment parameterization, as well as errors in inputs and observed variables.

The GLUE methodology (Binley and Beven, 1991; Beven and Binley, 1992) explicitly recognizes the coexistence of alternative parameter set and models and it provides a suitable framework for model calibration and uncertainty estimation under non-uniqueness. The non-uniqueness recognizes the existence of several set of parameters and structures that would produce good agreement with the observed data, and satisfy the calibration. With the limited measurements available and the application of a distributed hydrological model it may not be possible to identify an optimal model. Implementing GLUE requires making Monte Carlo simulations using a large number of parameter sets, assessing the relative performance of each set by comparing model

estimates with observed data, and retaining only those parameter sets that provide behavioral (acceptable) predictions. The relative performance of each parameter set is evaluated on the basis of a likelihood measure calculated by comparing model predictions with observed data. A parameter set is classified as behavioral if the corresponding likelihood value is equal to or greater than a specified threshold value. Parameters sets that do not meet this criterion are rejected as non-behavioral.

The final step in the GLUE procedure is to establish predictive uncertainty bounds for comparison with observed values. First, the set of behavioral likelihood values is rescaled to archive a cumulative sum of unity by dividing each value by the sum of the likelihood values. Next, behavioral model predictions for each time step are ranked in ascending order and each prediction is assigned to a user-specified bin. The rescaled likelihood values associated with the ranked predictions in each bin are summed to calculate the height of the corresponding bar in the density plot. A cumulative density plot is constructed by graphing the cumulative sum of the likelihood values versus the ranked model predictions. Typically, the 5th and 95th percentiles calculated at each time step are used to calculate the predictive uncertainty bounds over the period of observations. The GLUE based prediction limits the capture of uncertainty in model output associated with uncertainty in model parameterization.

GLUE provides a useful modeling approach for advancing beyond globally optimized, unique, parameter sets. Working within a framework of Monte Carlo-generated

parameters sets allows modelers to explicitly recognize and quantify the effects of uncertainties on model prediction (McMichael et al., 2005).

Sahho et al., (2006) performed a calibration and validation of MIKE SHE in a flashy mountainous Hawaii stream. The model was calibrated with a single hydraulic conductivity value and produced consistent results with correlation coefficients greater than 0.7. In the sensitive analysis the Manning's roughness coefficient and the hydraulic conductivities (vertical and horizontal) of the saturated zone had the most pronounced effects in determining the shape of the flood's peaks.

Griensven, et al. (2006) made a global sensitivity analysis tool for the parameters of multi-variable catchment models. An analysis of Monte Carlo simulations was conducted with statistical methods such as Kolmogorov–Smirnov (K-S) test (Stephens, 1970) or with the computation of regression and correlation based sensitivity measures to define whether a parameter is sensitive (Spear and Hornberger, 1980). An advantage of the method is the logical combination of calibration, identifiable analysis, and sensitivity and uncertainty analysis within a single modeling framework (Van der Perk and Bierkens, 1997). The method can be applied to problems with absolutely no probabilistic content as well as to those with inherent probabilistic structure. It has been widely used in catchment modeling, for assessing parameter uncertainty and input uncertainty, e.g. for rainfall variability (Krajewski et al., 1991).

The Monte Carlo method provides approximate solutions to a variety of mathematical problems by performing statistical sampling experiments on a computer (Fishman, 1996).

This method performs sampling from a possible range of the input parameter values followed by model evaluations for the sampled values. An essential component of every Monte Carlo experiment is the generation of random samples. Techniques, such as the latin-hypercube methodology, are also available for minimizing the number of required runs to reproduce the selected probability distributions of the input datasets (Harmsen, 1991). These generating methods produce samples drawn from a specified distribution (typically a uniform distribution). The random numbers from this distribution are then used to transform model parameters according to some predetermined transformation equation.

## **2.4 Flood Prediction**

In an attempt to determine flood occurrence, Birikundavyi et al. (1997) used two approaches commonly used for the probabilistic analysis of extreme flood magnitudes that are based on the annual maximum series (AMS) and the partial duration series (PDS). In the AMS approach the highest flood peak in the year is used, while in the PDS approach all those events that exceed a specified value are used. In the study, the Poisson distribution and generalized Pareto distribution (GPD) were used to describe the occurrence of flood and the flood magnitudes. Two neighboring flood peaks were independent if (1) they are separated by at least seven days and (2) the flow between them drops below 50% of the smaller peak.

In the Brays Bayou watershed (334 km<sup>2</sup>) in southwest Houston Texas, Bedient et al. (2000) developed a flood warning system using radar-based rainfall (NEXRAD) and delivery systems on the internet. In 1950-1960 the Army Corps of Engineers constructed a concrete and rip-rap lined channel to contain a greater than 100-years storm event with bankfull capacity, currently the same channel only can contain the 10 year design level due to increased urbanization. In this system HEC-1 is used to predict the flow at different interest points with known rainfall distribution and the results are modeled in HEC-2 to determine the maximum height of water in the channel. These two models are often used together for flood prediction and are the basis for calculating the Flood Alert System nonograph used to translate rainfall rates into peak flow and levels. After, generating the system nonograph, calibration was conducted with hypothetical storms.

The HCOEM ALERT (Harris County Office of Emergency Management Automated Local Evaluation in Real-Time) exists within the Brays Bayou watershed with a high density of rainfall and flow gauges available real time via the internet (HCFCD, 1984 and Bedient et al., 2000 and 2004). Data received from these gauges can be used to predict possible flooding conditions and were used to calibrate the watershed HEC-1 model.

NEXRAD used with GIS can calculate the rainfall rates within the sub-watersheds and to estimate rainfall rates from approaching storms and visualize the development of the storm. These are powerful tools for storm prediction and flood alert. Bedient et al. (2000) reported an excellent accuracy using HEC-1 and NEXRAD in several storms. However the NEXRAD data is only used to track the storm.

Currently, the next generation flood alert system (FAS2) started its operation in 2004 with more than 30 storm events (Fang and Bedient, 2007). FAS2 utilizes available radar (NEXRAD) data coupled with real-time hydrologic modeling, and provides visual and quantitative identification of severe storms producing heavy rainfall, as well as a linkage between the rainfall and likelihood of flooding. The accuracy of the current FAS2 is adequate for regional events over a large basin (129 mi<sup>2</sup>), but is lacking for events where the regional/local scale interactions, local scale precipitation, infiltration losses, or local hydraulics are important.

In the CASA Annual Report; year 3, Volume II, (2006), three projects were cited that are in development which are employing state of the art techniques. In the S22 project uses rainfall data derived from radar images to run real-time, physically-based distributed models for flood prediction and generation of flooding maps. This project explores the drainage density in an urban area, because it has been demonstrated in FAS that a small urban watershed could not predict flow with sufficient accuracy with the current Vflo model, when the area was classified as overland flow.

Project S23 is concerned with testing different QPE resolutions derived from radar and the impact in flow at different basin scales with the same grid size resolution. Project S24 is developing a Vflo model that incorporates a secondary drainage system and evaluating the methodology in Harris Gully (FAS's urbanized watershed). A distributed pipe network linked to topography is a unique combination of new urban hydrologic

models. All these projects are guided to enhance the accuracy in flood prediction especially at small watershed scales.

Making predictions in real-time with a hydraulic model is difficult because of inaccuracies in model parameters, rainfall input inaccuracy, or unknown upstream flow rates. Real-time systems for mapping expected areas of inundation require input of flow rates from other sources to generate inundated areas using sophisticated 2-D hydrodynamic models. Even the inflow between river gauging stations requires some model estimation of watershed response in the intervening areas. Upstream gauging points and rainfall-runoff models are viable sources of real-time flow information. Both lumped and physics-based distributed rainfall-runoff models may be used for this purpose (Bedient, et al., 2004).

Georgakakos (2006a) studied the theoretical basis of developing operational flash flood guidance systems using analytical methods. The Sacramento soil moisture accounting model is used operationally in the United States to produce flash flood guidance estimates of a given duration from threshold runoff estimates. The study attempted to: (a) Shed light on the properties of this model's short term surface runoff predictions under substantial rainfall forcing. (b) Facilitate flash flood computations in real time.

Various characteristics of the flash flood guidance to threshold runoff relationship are discussed and considerations for real-time application are offered. Uncertainty analysis of the threshold runoff to flash flood guidance transformation is also performed.

Vieux et al. (2003) in collaboration with Taiwan government agencies and the United States Government began a program initiative for the research and development of a flood alert and water resources management system to unify monitoring and prediction of floods within a single system in Taiwan. Enhancing the accuracy and efficiency of information disseminated from the central government to the public, and to regional and local water management and emergency response agencies is the major goal of this project. A limited sensitivity analysis was conducted. Knowing which parameters cause the most response in stage or discharge, helps to identify where efforts should be expended to improve parameter specification.

Vieux et al. (2002) developed a proposal for Arizona to utilize a sophisticated hydrologic modeling approach coupled with QPe-SUMS. This model will help 1) manage reservoir operations, 2) minimize losses through spills, and 3) predict flood levels in selected basins. The authors emphasize the need to perform a flood hazard analysis a priori to the modeling.

The U.S. Army Corps of Engineers (USACE, 1996) define the “*maximum potential warning time*”, as the response time after initiation of the flood-producing rainfall and is related to the arrival time of the peak stage or discharge, and is the interval during which mitigating responses can reduce property damage, loss of life, or business interruption.

In this chapter, various studies related to flood prediction and uncertainty were reviewed. In the next chapter the study area in which this research was conducted is described.

## **CHAPTER 3**

### **3 STUDY AREA**

This investigation considered two study areas, the Mayagüez Bay Drainage Basin model (MBDB) and the Test Bed Sub Watershed (TBSW). A description of the two study areas is given below.

#### **3.1 Mayagüez Bay Drainage Basin Study Area**

##### *3.1.1 General description and stations in the area*

The study area is over the region of western Puerto Rico and has 819.1 km<sup>2</sup>. The area includes three principal courses: Río Grande de Añasco, Río Guanajibo and Río Yagüez. Numerous hydrologic and hydraulic studies by the US Geological Survey (USGS) and the University of Puerto Rico have been conducted in this area (Prieto, 2006; Villalta, 2004; Rojas, 2004; Sepulveda et al., 1996). The area encompasses the municipalities of Mayagüez, Añasco, Las Marías, San Sebastián, Lares, Maricao, Yauco, Adjuntas, Sabana Grande, Cabo Rojo, San Germán and Hormigueros. Of these municipalities, Mayagüez has the highest population (89,080 habitants), followed by Cabo Rojo (50,917 habitants). The lowest population density is for Maricao with 6,276 habitants, according to the U.S. Census Bureau, 2010. Changes in elevation vary from zero meters mean sea level in the

coastal areas to 960 m in the mountainous areas, producing abrupt slope changes in short distances (Figure 3-1).

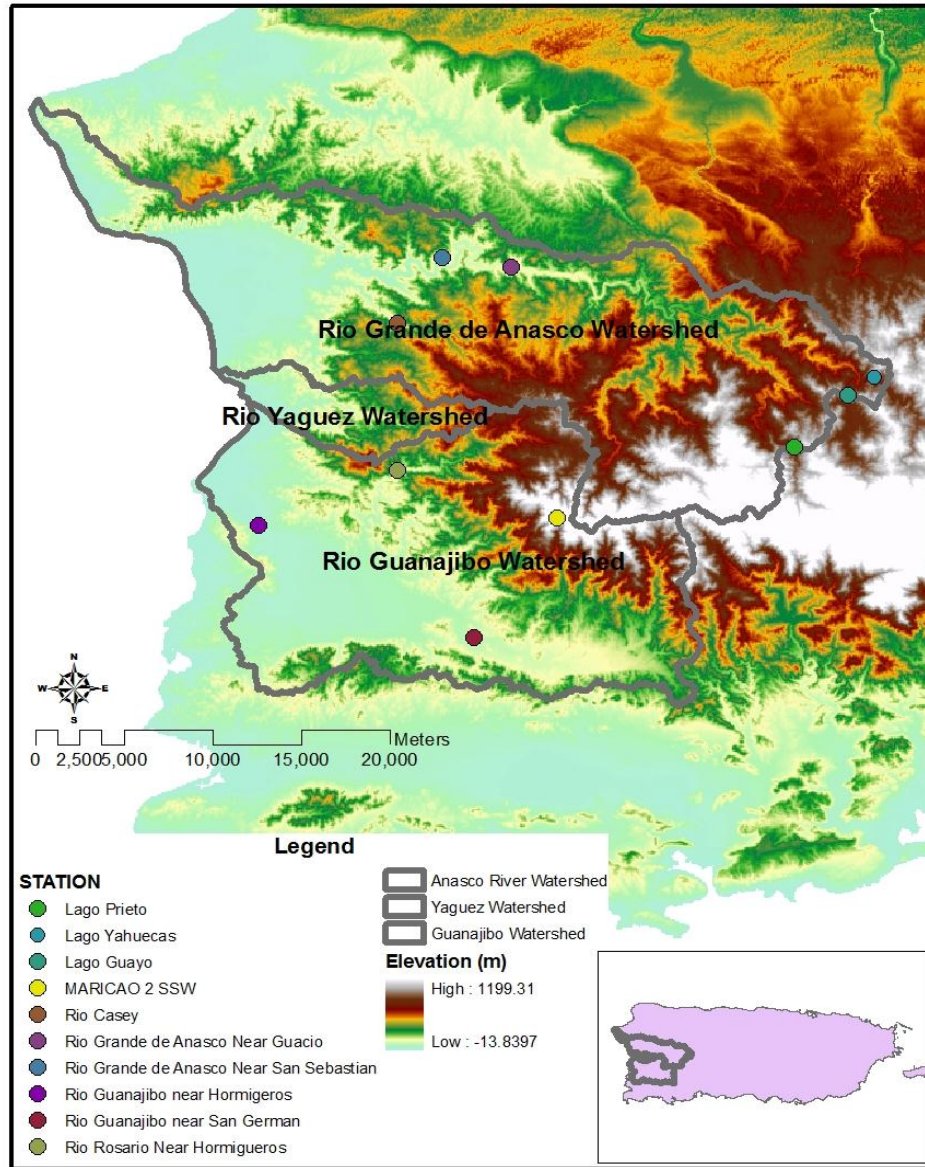


**Figure 3-1 Digital Elevation Model and Rio Guanajibo, Yaguez, and Grande de Añasco watersheds, rain gauges and flow gauging stations.**

The Río Grande de Añasco basin (Figure 3-1) has an area of 370.36 km<sup>2</sup>, including the reservoir lakes, tributary areas and river, which has a length of 64 km. Lakes Yahuecas, Prieto, Guayo and Toro were constructed by the Puerto Rico Water Resources Authority (PRWRA), presently the Puerto Rico Electric Power Authority, during the decade of the 50's. These were constructed to supply water to the Luchetti Lake for energy production and irrigation. According to Figueroa et al. (2006), the area above Lago Guayo, Lago Yahuecas, and Lago Prieto dams contributes flow to the Río Grande de Añasco only during high floods. For the purpose of the present study it was assumed that the contribution of water from the Lago Guayo, Lago Yahuecas, and Lago Prieto sub watersheds to the Añasco watershed downstream of the lakes is not significant for regional water budget estimation (Prieto, 2006). Therefore, those subwatersheds were not included as part of the Añasco watershed in this study. The total lake drainage area is about 116.55 km<sup>2</sup> and was used as a boundary condition in the model.

The coastal plain associated with Río Grande de Añasco basin is characterized by an alluvial fan having an area of 41.5 km<sup>2</sup> and 0.08% average slope. The alluvial fan has a length of 15.6 km reaching a width of 8.8 kilometers at the coast shore (Rojas, 2004).

According to FEMA (2009), the estimated 100 years return period flood flows was 5,130 m<sup>3</sup>/s (cms) and 3,797 cms for 50 years return period at the river's mouth and at USGS Gage No. 50144000 Rio Grande de Añasco near San Sebastian were reported to be 4,078 cms for 100 years and 3,278 cms for 50 years return period. The major flood measured in that station was for Hurricane Georges in September 22, 1998, reporting a

stage of 10.52 m (34.5 ft) and peak flow of 4,587 cms, followed by Hurricane Eloise in September 16, 1975 with a stage of 10.33 m (33.9 ft) and peak flow of 3,964 cms.

The station has different flood categories; the flood stage is 3.35 m (11 feet), a stage greater than 4.27 m (14 ft) is a moderate flood and stages greater than 5.59 m (19 ft) are categorized as major floods. The station shows that the river had been flooded in thirty one times from 1963 according to the records (NOAA, No date).

The Federal Emergency Management Agency (FEMA) performed a Flood Insurance Study (FIS) for the Commonwealth of Puerto Rico (FEMA, 2009) in which regulatory peak flow values for the study basins were established. The Río Grande de Añasco FIS presents the magnitude and frequency of floods in accordance with the application of the U.S. Geological Service (USGS) regression equations for estimating peak flow on stream in Puerto Rico (USGS, 1999). This report presented regression equations developed from gages sites having 10 to 43 years of records that can be used to estimate peak flows at ungaged sites or gaged sites with short periods of records. The equations utilized the mean annual rainfall (MAR), the contributing drainage area (CDA) and the depth to rock (DR), as variables that govern the peak streamflow. The MAR was obtained from the Puerto Rico 1971-2000 Mean Annual Precipitation map developed by NOAA (2006) , with the variations of rainfall across Puerto Rico calculated.

The Río Guanajibo basin (see Figure 3-1) has an area of 328.9 km<sup>2</sup> and 38 km river length. The topography of the area is diverse, including mountains, foothills, and valleys.

The predominant rocks in this area are serpentine and volcanic-related. The main tributaries are Rio Rosario, Rio Daguey, Rio Cain, Rio Cupeyes, Rio Cruces, Rio Loco, and Rio Viejo, and to the south exists relatively small tributaries. Major floods have been monitored in this basin since 1974, with the largest flood registered occurring in September 16, 1975 (Hurricane Eloise) with a reported peak flow of 3,625 cms and 8.7 m (28.54 ft) stage elevation at the USGS 50138000 Río Guanajibo near Hormigueros station. In this location FEMA calculated a flow of 5,343 cms and 5,745 cms at the river's mouth for the 100 year return period. The 50 years return period flows were 3,637 at USGS station (50138000) and 3,896 cms at mouth (FEMA, 2009).

The station has different flood categories; flood stage greater than 7.93 m (26 ft) is categorized as a major flood, 6.7 m (22 ft) is a moderate flood stage, 6.1 m (20ft) is the flood stage and at 4.88 m (16 ft) is the stage at which action is required. The area had been flooded twenty-four times from 1974 according to the records (NOAA, No date). The percent annual chance recurrence intervals were developed using rainfall-frequency relationships presented in Technical Paper 42 (U.S. Department of Commerce, 1961) and an unit hydrograph was carried out using the HEC-1 computer program (USACE, 1990).

The Rio Rosario is a tributary of the Rio Guanajibo and the subwatershed in this study is defined by the outlet point defined at the USGS 50136400 Rio Rosario near Hormigueros station.

The Río Yagüez basin (see Figure 3-1) has an area of 35.48 km<sup>2</sup>, a river length of 20 km with average slope from 0.004 % to 0.025 % for the channelized river section at city of Mayagüez. Río Yagüez originates in the western slopes of the Cordillera Central and flows westerly into the Mayagüez Bay. The drainage basin is narrow, having a length-width ratio of approximately 10 to 1. In 1968, a flood protection project for the City of Mayagüez was initiated and the lower reach of the river was channelized to protect the city from floods. The channel has a capacity of 326 cms, but the maximum capacity of the channel at the PR Highway 2 Bridge is approximately 425 cms. To determine the discharges for the different percent annual chance floods in the basin reported in the FIS (FEMA, 2009), a regional flood-frequency analysis (USGS, 1977) was used based on log-Pearson Type III analyses of individual station records and regionalization using multiple regression techniques. The 100, 50 and 10 year return period flows at the mouth were estimated to be 770 cms, 595 cms and 292 cms, respectively (FEMA, 2009).

Nine flow gauge stations operated by the United States Geological Survey (USGS), 3 NOAA rain gauge stations, 2 Soil Climate Analysis Network (SCAN) sites from the United States Department of Agriculture (USDA) Natural Resources Conservation Service (NRCS), and 4 owner stations published at the Wunderground web page (<http://www.wunderground.com/US/PR/>), 2009, exist within the study area (see Figure 3-1), . Currently there are only 4 flow gauge stations with precipitation data and 2 river stage measurements; see **Error! Reference source not found.** for the source and data type details.

**Table 3-1 Climatic and river flow stations located within the study area**

Source	ID Station	Station Name	Lat.	Long.	Elev. (m)	Data
NOAA		Maricao 2 SSW	18.15	-66.98	863.4	Meteorological
NOAA		Hacienda Constanza	18.11	-67.05	146.3	Rain
NOAA		Mayagüez Airport	18.25	-67.13	11.6	Meteorological
NOAA		Maricao Fish Hatchery	18.16	-66.98	457.3	Rain
NOAA		Mayagüez City	18.18	-67.13	22.6	Rain, Temp
USGS	50131990	Rio Guanajibo at Hwy 119 at San German	18.09	-67.03	45.0	Rain, Stage
USGS	50136400	Rio Rosario near Hormigueros	18.17	-67.07	50.0	Rain, Stage, Flow
USGS	50138000	Rio Guanajibo near Hormigueros	18.14	-67.15	2.2	Rain, Stage, Flow
USGS	50141500	Lago Guayo at Damsite near Castaner	18.21	-66.83	426.8	Rain, Stage
USGS	50142500	Lago Prieto near Adjuntas	18.19	-66.86	600.2	Rain, Stage
USGS	50146073	Lago Daguey above Añasco	18.301	-67.13	40.0	Rain, Stage
USGS	50141100	Lago Yahuecas near Adjuntas	18.22	-66.82	426.8	Rain, Stage
USGS	50143930	Rio Grande de Añasco at Bo. Guacio	18.28	-67.02	64.9	Rain, Stage
USGS	50144000	Rio Grande de Añasco Near San Sebastian	18.285	-67.05	31.6	Rain, Stage, Flow
USGS	50145395	Rio Casey above Hacienda Casei	18.25	-67.08	75.0	Rain, Stage, Flow
NRCS		Mayagüez TARS	18.217	67.13	13.7	Meteorological
NRCS		Maricao Forest	18.15	67	747.0	Meteorological
Wunder ground	MMGZP4		18.218	-67.16	0	Meteorological
Wunder ground	KPRMAYAG8	Miradero Mayagüez	18.23	-67.14	23.2	Meteorological
Wunder ground	KPRMAYAG7	Mayagüez	18.211	-67.14	0	Meteorological
Wunder ground	KPRMAYAG3		18.168	-67.15	48.8	Meteorological
Wunder ground	KPRSANGE3	Vivoni	18.083	-67.04	47	Meteorological

The climate in the area is tropical, with moderate temperatures year round, and the mean high annual temperatures are 26.4 C in the mountains (Maricao 2SSW station) and 31.4 C in Mayagüez City station (Table 3-2)

**Table 3-2 Temperature and Precipitation Normals for NOAA stations within the study area (NOAA, 2006).**

Station Name		Jan	Feb	Mar	Apr	May	Jun	Jul	Aug	Sep	Oct	Nov	Dec	Annual
Mayagüez City	High Temp (C)	30.1	30.2	30.7	31.0	31.7	32.6	32.6	32.7	32.5	32.2	31.4	30.3	31.4
	Low Temp (C)	17.9	17.7	18.1	19.2	20.3	20.9	21.1	21.0	21.2	21.1	20.2	19.1	19.8
	Rain (mm)	40.4	64.0	77.5	102.6	184.4	160.5	220.5	232.7	269.2	226.8	119.4	45.7	1744.0
	Days with Rain	6.7	6.7	8.3	10.9	14.2	13.6	15.6	17.2	17.1	16.1	11.8	7.9	146.1
Hacienda Constanza	Rain (mm)	48.5	67.1	80.3	120.7	200.2	195.6	247.1	253.7	279.4	242.6	138.4	34.0	1908.3
	Days with Rain	2.4	2.4	2.9	5.3	8.4	7.1	8.7	9.3	9.6	9.2	4.9	1.7	71.9
Maricao 2SSW	High Temp (C)	24.8	25.2	25.7	26.2	26.7	27.8	27.6	27.8	27.4	26.8	26.2	24.8	26.4
	Low Temp (C)	16.4	16.2	16.2	16.8	17.9	18.8	18.9	19.2	19.0	18.9	18.2	16.9	17.8
	Rain (mm)	76.5	95.3	134.1	172.5	239.5	159.5	216.4	287.0	348.0	378.5	236.0	86.6	2428.2
	Days with Rain	10.2	9.4	10.1	11.9	13.5	10.6	13.4	14.8	15.5	17.1	13.7	10.8	151
Mayagüez Airport	Rain (mm)	41.4	51.1	71.4	98.8	191.3	178.1	237.5	251.0	266.7	223.5	123.2	37.8	1771.4
	Days with Rain	6.9	6.4	8.4	11.5	16.6	15.5	17.4	19.3	18.7	18	12.2	8.4	159.3
Maricao Fish Hatchery	Rain (mm)	67.8	80.8	124.5	178.6	243.8	204.0	228.1	294.6	391.2	365.8	215.1	70.4	2463.8
	Days with Rain	5.5	5.3	6.9	10.2	11.3	8.5	11	13.3	15.4	15.7	10.5	7	120.6

Table 3-2 presents a summary of the mean monthly average air temperatures and rainfall for five locations within the study area. Puerto Rico has a bimodal rainfall

distribution in the wet season from April to November, with drier conditions in June and July (Capiel and Calvesbert, 1976); and a dry season from December to March.

The mean annual precipitation varies greatly across the study area due to the abrupt changes in elevation by the mountains causing wide variation in local wind speed and direction, which results in a sea breeze effect in the western area. Table 3-2 presents annual rainfall accumulations from 2463.8 mm for Maricao Fish and 1743.96 mm for Mayagüez City stations.

### 3.1.2 Soils Classification

A soil map describing the textural or soil class distribution is necessary to assign the values of the Green-Ampt infiltration parameters. The soil map was obtained from the Soil Survey Geographic (SSURGO) database for the Arecibo, Mayagüez, Lajas Valley and Ponce areas (USDA, 2006a; 2006b; 2006c; 2006d) provided by the NRCS. Figure 3-2 and Figure 3-3 depict the soil and textural classes occurring within the study area.

The soil textures present are clay with 558.68 km<sup>2</sup> area, loam with 176.84 km<sup>2</sup>, clay loam with 53.88 km<sup>2</sup>, sand with 14.28 km<sup>2</sup>, rock with 10.32 km<sup>2</sup> and gravel with 4.72 km<sup>2</sup>. The SSURGO data base provides additional information for each soil type, for example, bulk density, percent of sand and clay and soil depth.

The soils series with a major presence in the area are Consumo (184.4 km<sup>2</sup>), Humatas (132.9 km<sup>2</sup>) and Mucara (78.9 km<sup>2</sup>). The three soil types are classified clays for texture

class, but have different infiltration capacities. Therefore, they are classified in the Hydrologic Soil Group as B for Consumo, C for Humatas and D for Mucara.

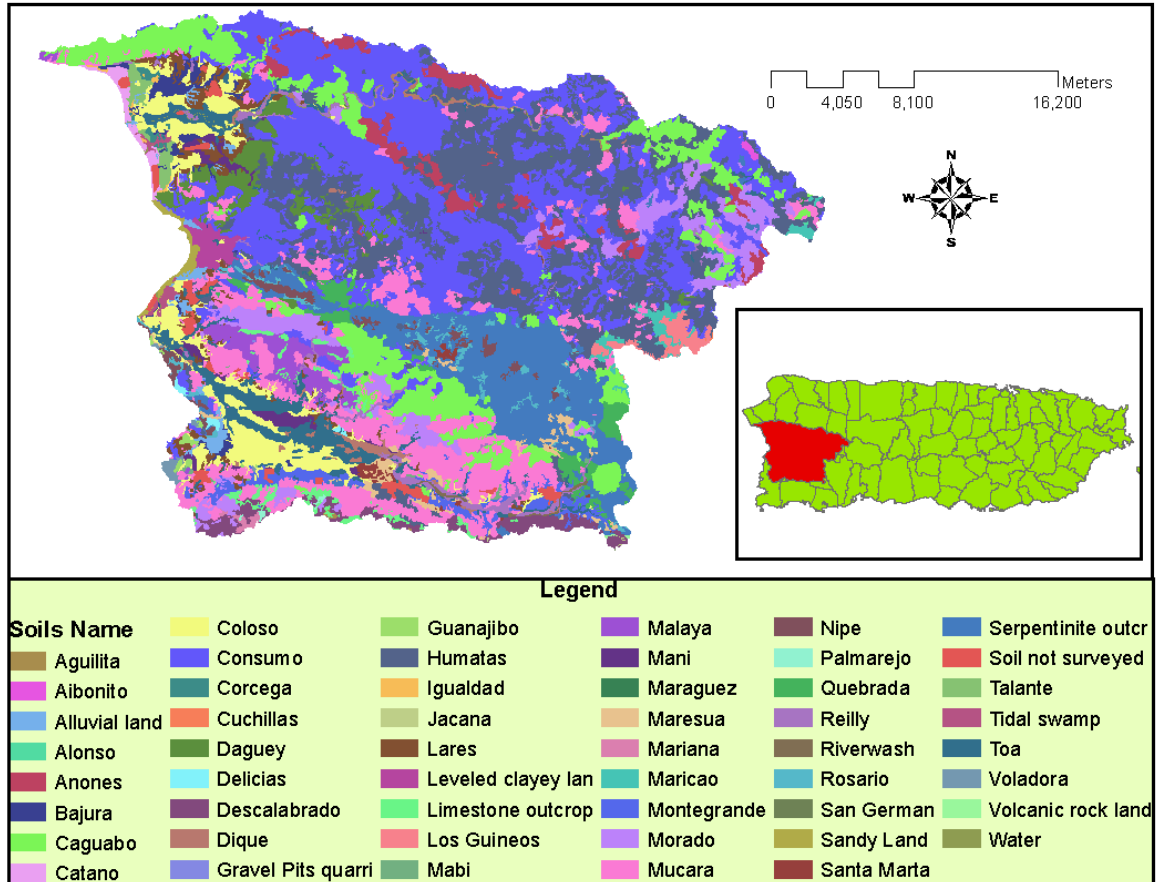


**Figure 3-2 Soil Map distribution for the study area. Source: SSURGO data base, (USDA, 2006a, b, c, d).**

### 3.1.3 Land Use Classification

To conceptualize the hydrologic model it is necessary to obtain land use or land cover classes to assign roughness values and crop coefficients according to the classes. A digital map of the forest type and land cover was developed for Puerto Rico using

LandSat enhanced Thematic images at 30 m resolution (Helmer et al., 2002), applying a supervised classification approach. In total, twenty-five classes were obtained from supervised classification (Figure 3-4). Prieto (2006) reclassified the detailed classification into six major categories, grouping similar categories such as different forest types, shrub land, wood land or shade coffee.

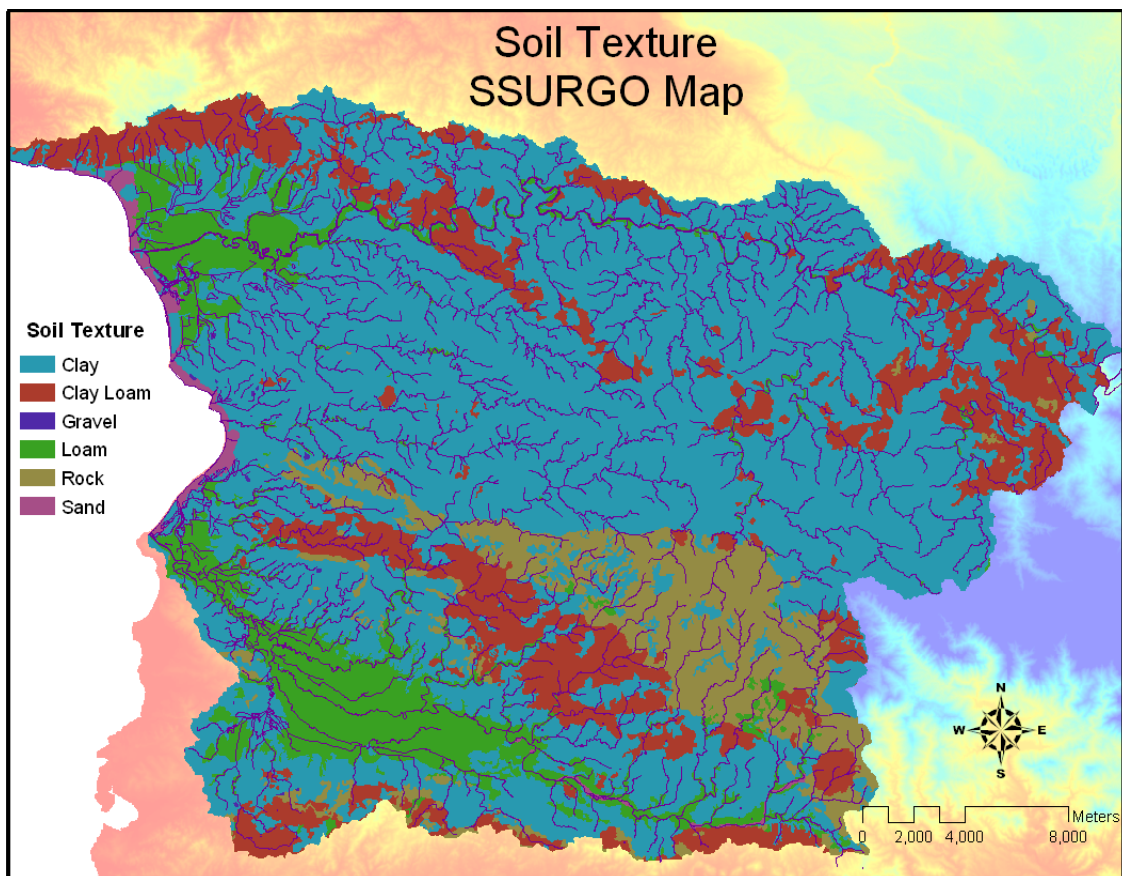


**Figure 3-3 Soil Texture for the study area, SSURGO map (USDA, 2006a, b, c, d)**

The final land use classification is shown in Figure 3-5 and exhibits the predominant land use classification of forest, shrub, wood land and shade coffee with an area of 529.16 km<sup>2</sup>, followed by pastures with an area of 172.84 km<sup>2</sup> and Urban and barren land with 60.02 km<sup>2</sup>. Preliminary, hydrologic model for the Mayagüez Bay basin area was configured using the Land use classification of Figure 3-5, provided by Prieto, 2006 and some analysis were developed using this data. In the upcoming sections will be indicated which land use classification was used, because new information was collected for land use.

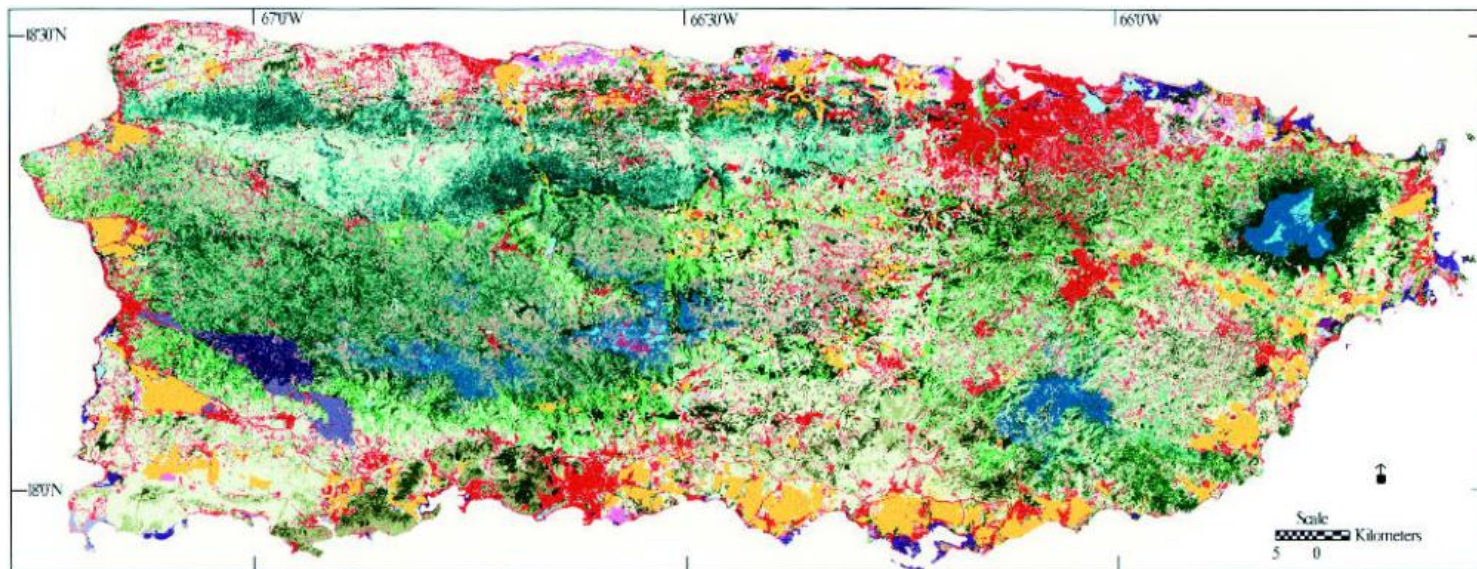
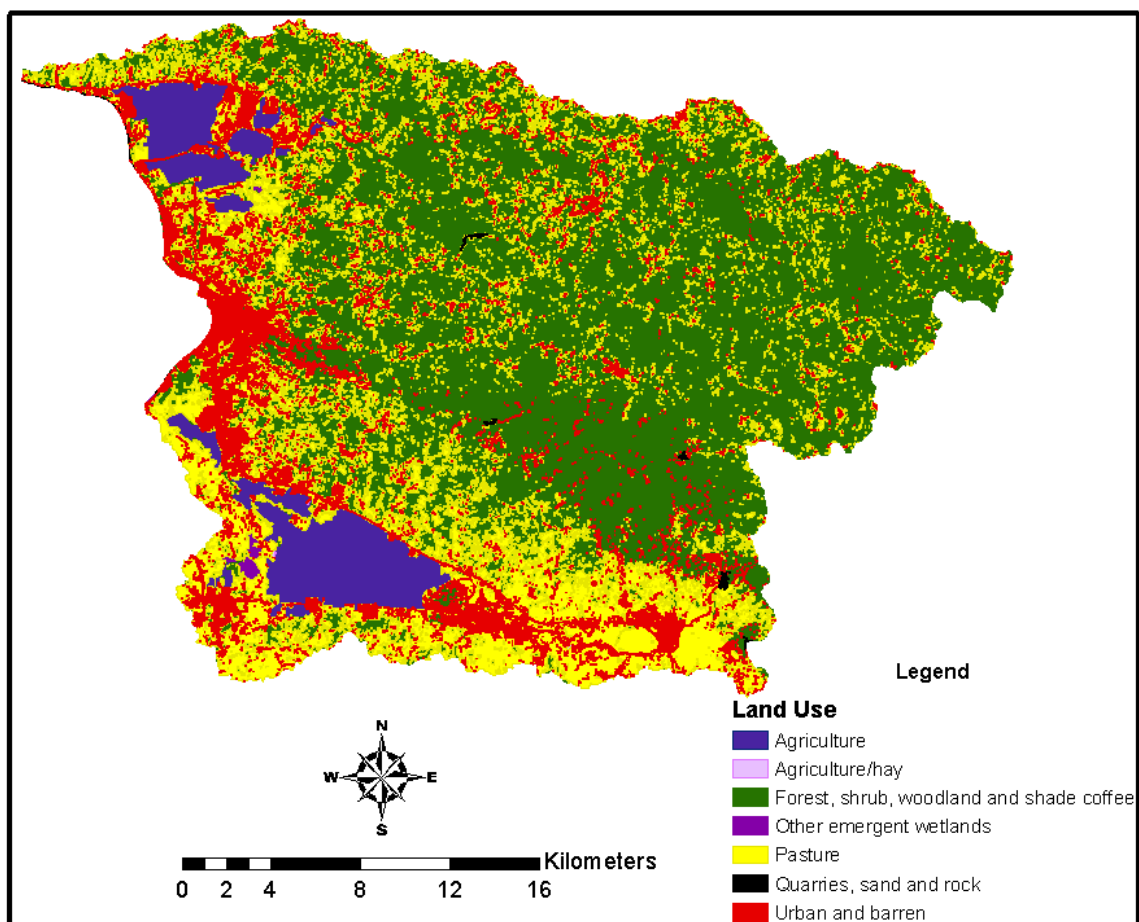


Figure 3-4 Map of Puerto Rico natural vegetation and land cover. Source: Helmer, E.H. et al., 2002



**Figure 3-5 Land Use Classification at 30 m resolution from LandSat ETM, 2000. Source: Prieto (2006) and Helmer et al. (2002)**

The second source of land use classification was provided by Puerto Rico Water Resources and Environmental Research Institute (PRWRERI, 2004), who developed the project titled *Land Use Classification of the Mayagüez Bay Watershed, (Río Grande de Añasco, Río Yagüez, and Río Guanajibo Watersheds)*, supported by the Puerto Rico Environmental Quality Board (Figure 3-6). The sensor used for this classification was LANDSAT 7 TM satellite image from 2004 with 30 m resolution for a general land use classification with field visits verification as needed. Thirty five classes were found in

this product where the most important area is cover by Forest low density (274.68 km<sup>2</sup>), fallow by Shrub and brush rangeland (253.05 km<sup>2</sup>), Forest high density (183.20 km<sup>2</sup>) and Urban or built-up land (103.71 km<sup>2</sup>).

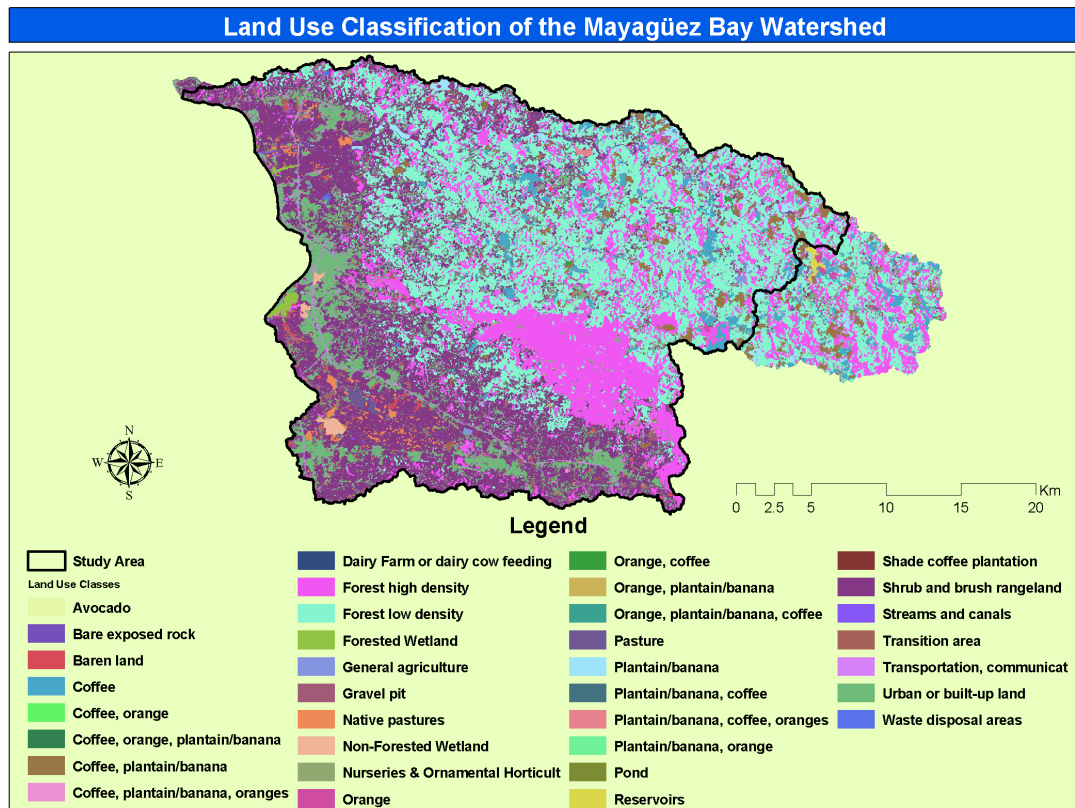


**Figure 3-6 Land Use classification of the Mayagüez Bay Watershed**  
*Source: PRWRERI, 2004.*

### 3.2 Test Bed Sub-Watershed

The “test-bed sub-watershed” (TBSW) study area is located within the Río Grande de Añasco Basin, more specifically in the Río Cañas sub-watershed (Figure 4-6). In this study, the TBSW, with an area of 3.55 km<sup>2</sup>, is characterized and used for analysis

purposes as a “field laboratory” to test the scale influence in the hydrologic prediction. The terrain elevation within the TBSW varies from 25.4 m (above mean sea level [amsl]) to 305.7 m amsl., (CRIM, 1998) (Figure 3-7). The area is characterized with large terrain elevation changes over small distances, with slopes varying from 0.265 % to 91.96% (39.03% average slope). Therefore, the study area is classified as a mountainous sub watershed which is very typical of the Puerto Rican upland sub watersheds. Prior to this investigation, no rain or flow gauges were present within the area. Figure 3-7 shows the TBSW location within the Mayagüez Bay model, the color contoured terrain map and the rain gauge network installed and used in the study area for this research, a detailed description is addressed in the next chapters.

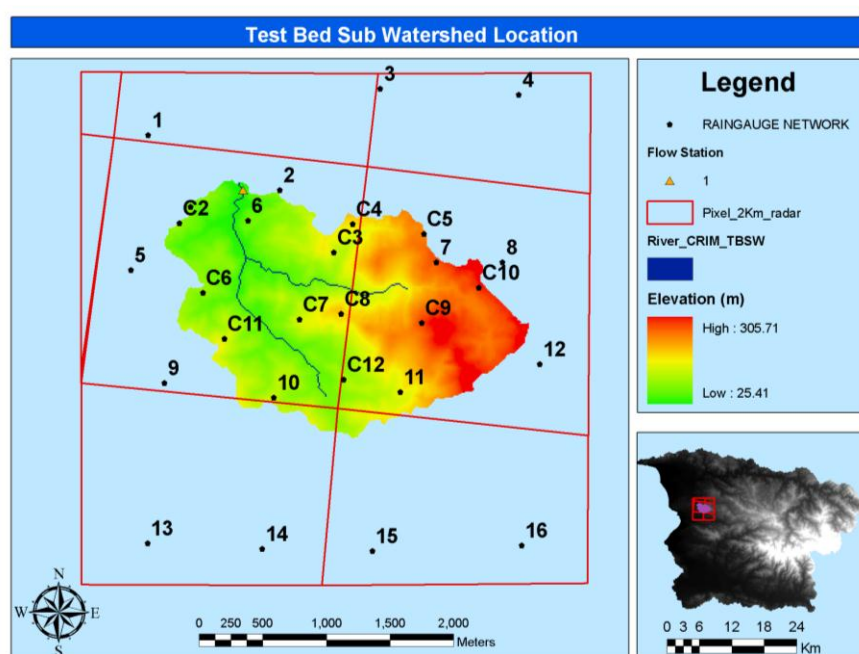


**Figure 3-7 TBSW location within the 4 km by 4 km NEXRAD pixel and rain gauge network.**

## CHAPTER 4

### 4 HYDROLOGIC MODEL CONFIGURATION AND SLOPE ANALYSIS

A detailed description of the components of a hydrologically distributed model is presented in Section 4.1. The configuration for the MBDB model was developed using available data for soils, land use, digital elevation models and field measurements. This model will be used for uncertainty analysis, rainfall tests and posterior flood alarm predictions (not addressed in this research). Therefore, the TBSW model set up was conducted by extracting data from the MBDB model. A slope analysis was developed according to an aggregation method to be used in the up-scaling experiment, without loss of slope information for mountainous subwatersheds. Additionally, an evaluation between different evapotranspiration methods was developed to quantify the uncertainty associated with this term.

The hydrologic model used in this study is Vflo (Vieux and Associates, Inc., 2004), which is capable of ingesting distributed radar rainfall data. Vflo is a finite element model and the equations are used to solve overland and channel flow. A detailed description of Vflo was presented in Chapter 2.

The configuration of the proposed physically-based distributed model used in this study was based on products described in Chapter 3 for the Mayagüez Bay Watershed and TBSW as well, such as soils, land use and digital elevation model maps. Generally, to create both high resolution models, it is necessary to derive the topographic characteristics from a digital elevation model with high resolution. For this purposes we used the digital elevation model quadrangles derived from the base map data of the “Center for Municipal Tax Revenues of Puerto Rico” by its acronym in Spanish (CRIM, 1998): xyz mass points, ridgelines, road cuts, and hydrographic features. The CRIM data were collected by AEROMETRIC, Inc. Ground control eastings, northings and elevations were surveyed by RLDA Surveying & Mapping of San Juan, Puerto Rico. The elevation maps were developed by phototriangulation with a root mean square error of ground-control residuals of 0.6 m for vertical control elevation coordinates and root mean square error of airborne-GPS exposure-station residuals of 0.184 m for vertical control elevation coordinates.

Most of the input data for the Vflo model was prepared using ArcGIS 9.3 and Arc Hydro Tools. The basin and river characteristics were extracted from the 7.5-Minutes Series topographic maps from USGS, 30 m x 30 m digital elevation model (DEM) quadrangles and from the digital elevation model at 10 m spatial resolution from CRIM.

The Green Ampt infiltration model is used by the distributed hydrological model to calculate the initial abstractions due to infiltration and runoff produced by rainfall. The parameters are derived from soil characteristics assigned to the SSURGO soil

classification maps, digitally available (Figure 3-3). Values of soil suction at wetting front ( $\psi$ ), saturated hydraulic conductivity ( $K_s$ ), effective porosity, soil depth and initial degree of soil saturation ( $\theta$ ) will be obtained from the literature (Vieux and Vieux, 2006; Sepúlveda, 1996), field measurements (USDA, 2006a; 2006b; 2006c; 2006d) and computations using the percent of sand and clay, soil bulk density and percent of organic matter in combination with the Soil Water Characteristics Hydraulic Properties Calculator (Saxton and Rawls, 2006).

Vflo also requires soil depth (cm), initial abstraction (cm) and percentage of impervious area. Required channel data include base flow, roughness (Manning's  $n$ ), channel and side slopes, and the infiltration parameters mentioned above. Overland flow properties include flow direction, overland slope and infiltration parameters.

#### **4.1 Flow direction and stream definition**

For MBDB, the model comprises the Rio Grande de Añasco, Rio Guanajibo and Rio Yaguez watersheds. Overland slope, flow direction, and stream locations were determined from the USGS 30 m x 30 m digital elevation model (DEM) quadrangles and resized to 200 m spatial resolution. During this step the streams were “burned” into the model grid using a multi-step process in ArcGIS, in which the flow direction is forced to follow the rivers. This step is necessary because the flow direction calculation tends not to be accurate in low slope areas (e.g., floodplains of the rivers). The final resized digital

elevation model has correct flow direction based on the hydrological maps of the topographic quadrangles.

The flow direction and subsequent products were calculated with Arc Hydro Tools and ArcGIS 9.3. A flow direction map is necessary to calculate the flow accumulation map and create the stream network map. The flow accumulation is an accounting of cells contributing flow to a selected observation point, increasing the contributory area for observation points located further downstream. A cell located at the watershed outlet has the total cell number that drain to this point. The stream definition required 90 cells of flow accumulation to begin a channel. The river grid generated was utilized to define the channel cells in Vflo (Figure 4-1).

The TBSW model was developed using the same procedure described above but using the 10 m DEM (CRIM, 1998). The flow direction and stream definition were used to define the overland and channel cells respectively; based on the sub watershed delineation and river definition shown in Figure 3-7.

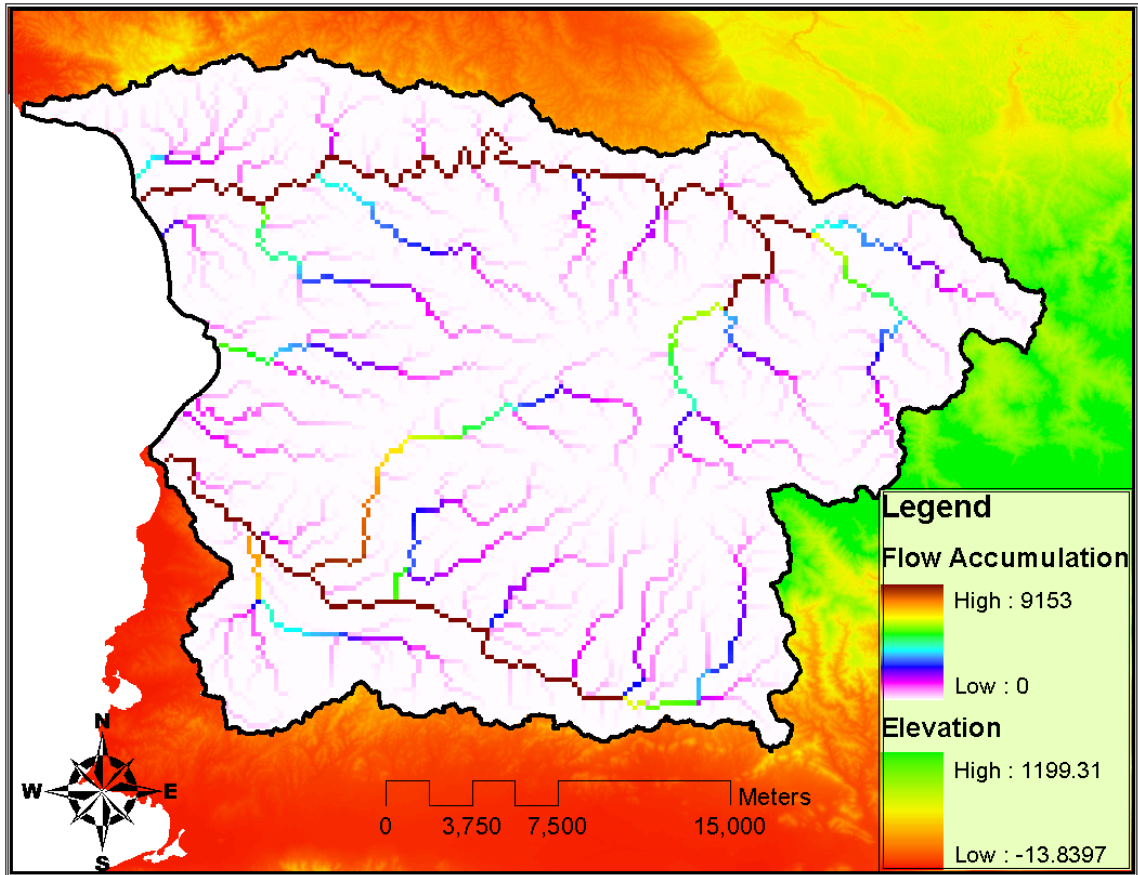


**Figure 4-1 Flow accumulation and stream definition for Rio Grande de Añasco, Rio Guanajibo and Yaguez basin model.**

## **4.2 Channel geometry**

Channel geometry in the hydrologic model is necessary for the channel cells or cross section cells in the model and includes the sides slopes, cross sectional data or base width for trapezoidal assumption and channel slope. The geometry would affect the flow response, increasing the stages for narrow rivers and decreasing stages for wide rivers, principally due to the storage. MBDB is not characterized by large width variations over short distances; typically widths are within the range of 3-5 m for upland rivers and

creeks and up to 32 m for low lands according to measurement samples in aerial photos taken December, 2006 (Google Earth) over the study area.

The channel side slopes were assumed to be 1:1 for the streams where no cross section information was available. The stream geometry was defined with data collected in 2002 by the PRWRERI (Villalta, 2004). At Río Grande de Añasco, 25 cross sections were measured along the river; 10 cross sections were surveyed in Río Guanajibo, located downstream of PR-114 and in Río Yagüez only four cross sections were measured upstream of the channelized section. To define the flood plain within the cross sections, an extending process was made using the digital terrain model (10 m resolution) and creating interpolation lines to extract the entire cross section and new cross sections. Additional cross sections were extracted from DEM (10 m resolution) to characterize the flood plain where no field cross sections were surveyed and a simple trapezoidal river section was used measuring the river width from 2006 aerial photos of Google Earth, 2006 and the side slope set to 1:1. Figure 4-2 shows the locations of cross sections extracted from the DEM for the Río Guanajibo and Río Grande de Añasco. The channel slope was determined using the stream definition raster layer (Figure 4-1) and the slope map calculated with the DEM at 10 m resolution for the stream reaches where no survey data was available.

The stream map generated with the DEM at 10 m resolution was utilized to define the channel cells in Vflo for the TBSW model; channel side slopes were assumed to be 1:1; and bed channel width was set to 5 m. In most of the river sections (measured from

Google Earth), the channel width is about 5 to 10m, supposing bed width is about 4 to 8 m. Streamflow and flow volume are not sensitive to bed width; however, the stream stage is sensitive to bed width according to some tests realized.

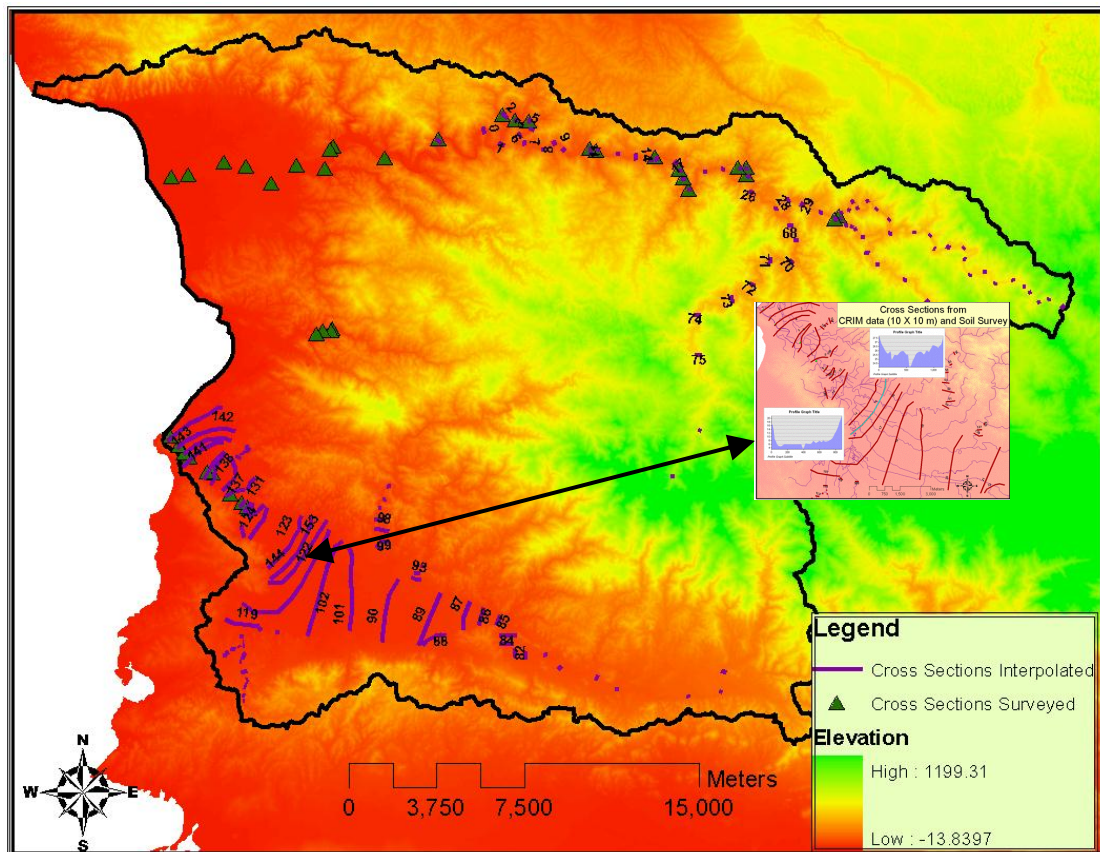


**Figure 4-2 Cross Sections Surveyed and interpolated for Mayagüez Bay Model**

### **4.3 Stage and Rating Curve for the TBSW creek**

A pressure transducer was installed at the TBSW outlet to collect flow stage measurements every 5 minutes from October 20, 2007 to May 2009. The instrument was located at 18.232667° latitude; -67.119533° longitude and elevation of 25 m amsl (see

Figure 4-4). Daily minimum barometric pressures were used to correct the factory calibrated stage measurements using the Miradero KPRMAYAG1 weather station (18.2° north latitude, 67.13° west longitude and elevation of 22.86 meter above mean sea level), available at [www.weatherunderground.com](http://www.weatherunderground.com). The average adjusted stage value was calculated in 0.847 m with 0.0225 m standard deviation. This value was using the minimum pressure measured at Miradero KPRMAYAG1.

Stream cross sections and bed slopes were measured in the field (Figure 4-3) and the rating curve was generated using HEC-RAS 4.0 hydraulic model (Hydrologic Engineering Center, 2006) with 3 cross sections and slopes observed. The downstream boundary condition was assigned as critical depth and flows were assigned with subcritical flow condition. The full bank stream rating curve was fitted to the following third order polynomial equation (Equation 4-1) with a regression coefficient of 1, where flow is in cubic meters per second and stage in meters. Equation 4-1 was used to convert stage elevations to flow discharge for the events.

$$\mathbf{Flow = -0.6331stage^3 + 5.33stage^2 + 0.003stage - 0.061} \quad \mathbf{(4-1)}$$

To setup the distributed model at TBSW, information was assigned to selected model cells corresponding to the principal stream channel. The bed channel slopes for the TBSW model were assigned by segments using the average longitudinal slope between cross sections digitized from the DEM (10 m) and corroborated with field measurements. Figure 4-4 shows pictures of the outlet section and the pressure transducer location. The

TBSW creek was divided in three creeks (Figure 4-5), the Lower Creek has a longitudinal average slope of 1.25%. The Upper Creek has 2.22% slope. Upper Creek2 shown in Figure 4-5 was divided into two segments, the upstream segment shows a slope of 11.27% and the downstream segment is 3.27%. Figure 4-5 shows the Vflo model with the channel and overland cells at 10 m resolution and the locations of the creeks named above.

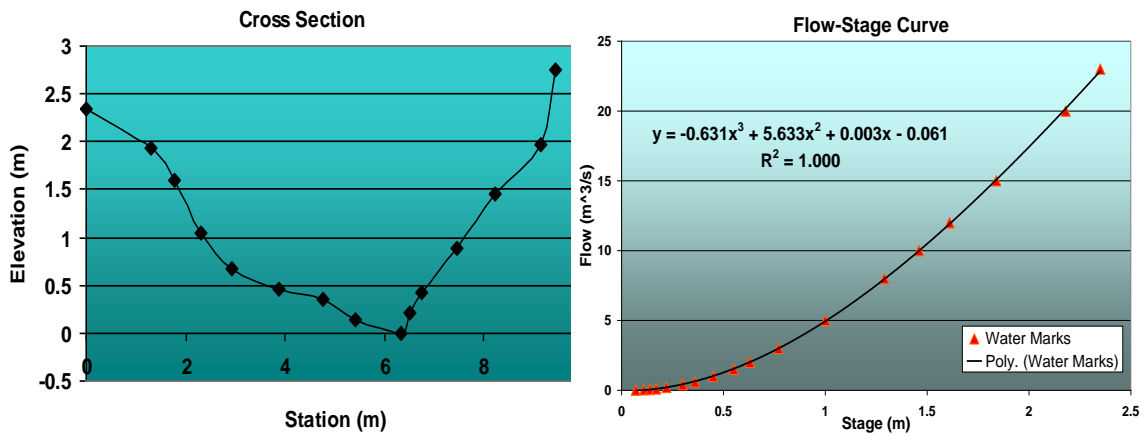


**Figure 4-3 Cross section measured at the instrumentation place and rating curve to full bank condition**



**Figure 4-4 Photos of principal channel bed at TBSW (right) and location of the pressure transducer (left)**

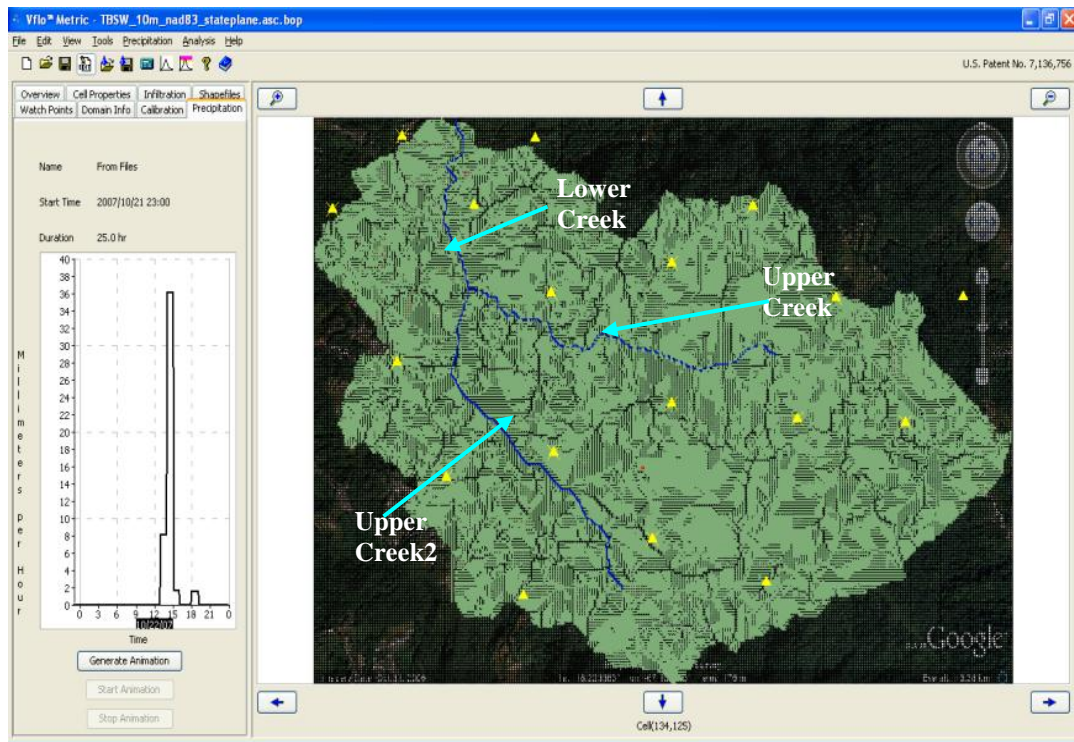


**Figure 4-5. TBSW hydrologic model configured in Vflo and identification of the river reaches**

## 4.4 Slope Analysis

Land surface slope is another important source of uncertainty in hydrologic modeling. High (low) slopes affect the time to peak producing early (retarded) peaks, less (more) infiltration, increasing (decreasing) discharge volume and increasing (decreasing) peaks. The average and standard deviation of the slope for Río Grande de Añasco basin were 34.6 % and 21.7% respectively; for Río Guanajibo basin 28.2% and 22.4 %, respectively; for Río Yagüez 29.8% and 18.0%, respectively; and for TBSW were 31.0% and 14.9%, respectively, calculated with the DEM at 10 m resolution. Figure 4-6 and Table 4-1 show

the subwatershed map and the average land surface slope values and standard deviation for each watershed and subwatersheds for MBDB area. In total, 24 subwatershed were identified for the most important tributary rivers and coastal areas, the majority of those exhibiting high slopes and similar conditions to the TBSW, indicating that the TBSW could be a representative sample of the MBDB, in terms of the slope parameter.

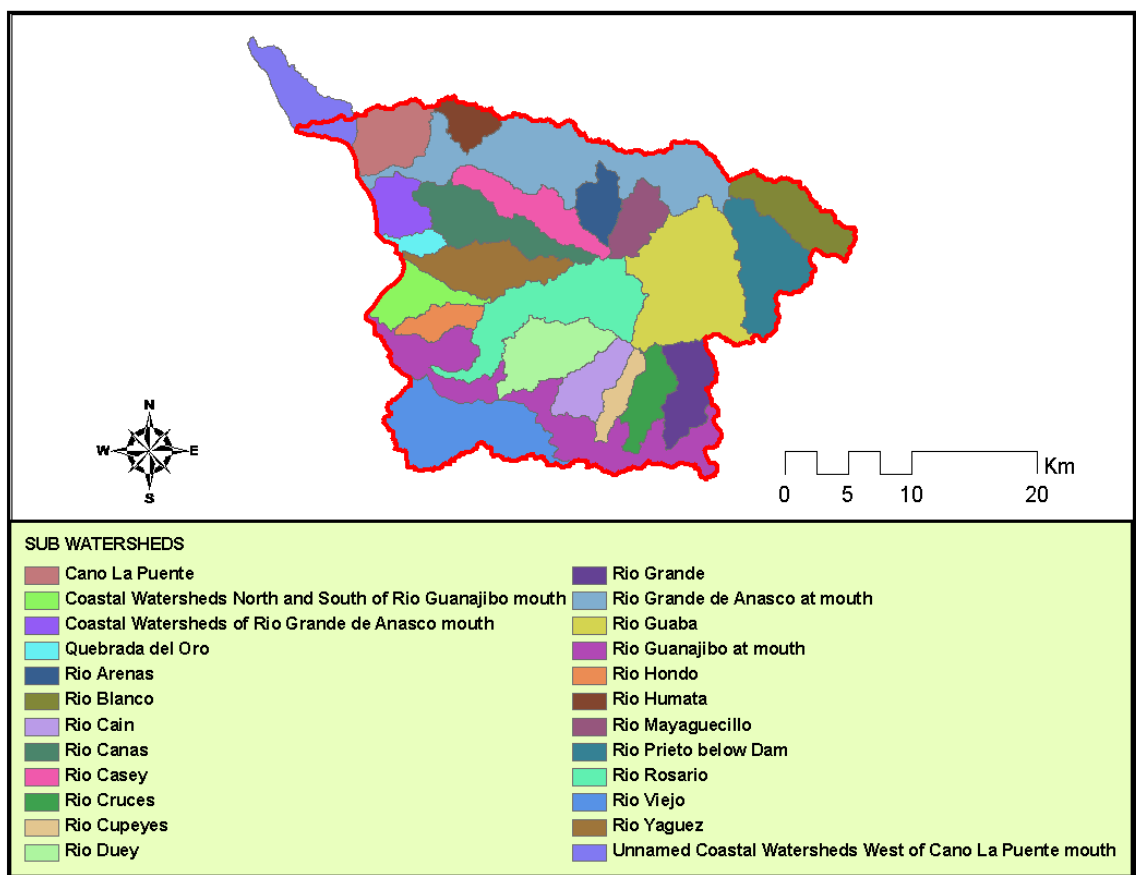


**Figure 4-6. Sub Watersheds map belonging to MBDB**

**Table 4-1. Mean land surface slope and standard deviation for the sub-watersheds.**

<b>Watershed Name</b>	<b>Sub Watershed Name</b>	<b>Area (km<sup>2</sup>)</b>	<b>Mean Slope (%)</b>	<b>Standard Deviation (%)</b>
<b>Río Grande de Añasco</b>	Unnamed Coastal Watersheds West of Cano La Puente mouth	28.78	28.70	21.70
	Río Humata	12.65	35.75	17.79
	Cano La Puente	28.37	20.11	25.65
	Río Grande de Añasco at mouth	101.91	32.30	20.85
	Río Arenas	15.41	28.72	14.57
	Río Casey	29.64	37.11	18.87
	Río Blanco	31.45	44.09	20.17
	Coastal Watersheds of Río Grande de Añasco mouth	18.13	7.39	10.69
	Río Mayaguecillo	18.11	37.81	17.75
	Río Cañas:	38.00	26.72	16.10
	<b>Test Bed Sub-Watershed</b>	<b>3.56</b>	<b>31.03</b>	<b>14.93</b>
	Río Guaba	83.20	46.06	19.38
	Río Prieto below Dam	43.31	41.51	18.43
	<b>Total area and average slope</b>	<b>448.95</b>	<b>34.60</b>	<b>21.67</b>
<b>Río Yagüez</b>	Quebrada del Oro	6.74	19.76	16.56
	Río Yagüez	35.24	31.67	17.69
	<b>Total area and average slope</b>	<b>41.98</b>	<b>29.76</b>	<b>18.05</b>
<b>Río Guanajibo</b>	Río Rosario	62.15	38.02	20.59
	Coastal Watersheds North and South of Río Guanajibo mouth	21.03	11.92	15.83
	Río Hondo	12.52	25.49	17.06
	Río Guanajibo at mouth	81.35	17.81	17.07
	Río Duey	35.70	37.25	19.06
	Río Cain	21.13	39.02	17.99
	Río Grande	25.41	47.21	23.64
	Río Cruces	19.55	38.39	22.83
	Río Cupeyes	11.03	39.55	19.14
	Río Viejo	60.65	15.71	18.37
	<b>Total area and average slope</b>	<b>350.52</b>	<b>28.17</b>	<b>22.38</b>

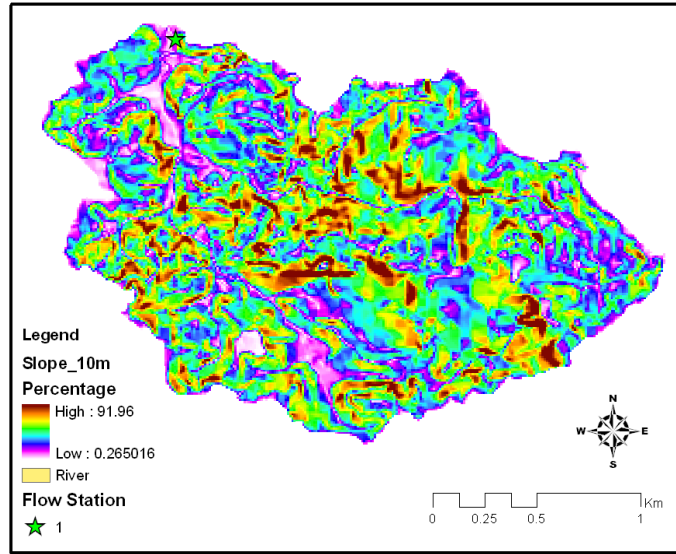
Maintaining the land surface slope values when resampling techniques are used would improve the flow prediction at larger terrain scales. A method to calculate slope at different grid size resolutions was investigated without decreasing of slope. Different methods can be applied to calculate the resampled slope while the up scaling is being done. The slope up-scaling was performed using 2 methods and 3 resample techniques for the TBSW model using ArcGIS 9.3. The TBSW presents an average slope of 31.03% with a standard deviation of 14.93 %.

Figure 4-7 presents the slope map for the TBSW and the base slopes for the resampling analysis derived from the DEM at 10 m resolution. The resample techniques used were Bilinear, Cubic and Nearest Neighbor Methods. The up-scaling methods used to achieve an adequate slope were:

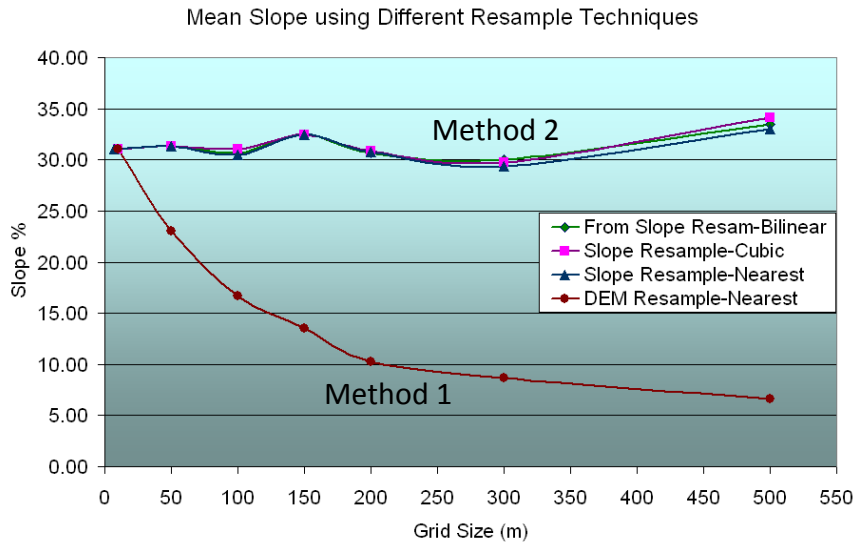
1. Use the DEM at 10 m and resample it to the desire resolution and then calculate the slope from the resample DEM.
2. Use the DEM at 10 m, calculate the slope at 10 m and resample the slope product to the desire resolution.

The worst method was found to be up-scaling the DEM to the required resolution and then calculating the mean land surface slope, (Method 1, brown line in Figure 4-8). The original slope was more or less preserved when the slope was calculated to 10 m resolution and the slope was up scaled to the required resolution. Negligible differences were found between the three techniques used, (Figure 4-8). From these findings the

method chosen to resample the digital elevation information was Method 2 described above using cubic interpolation.

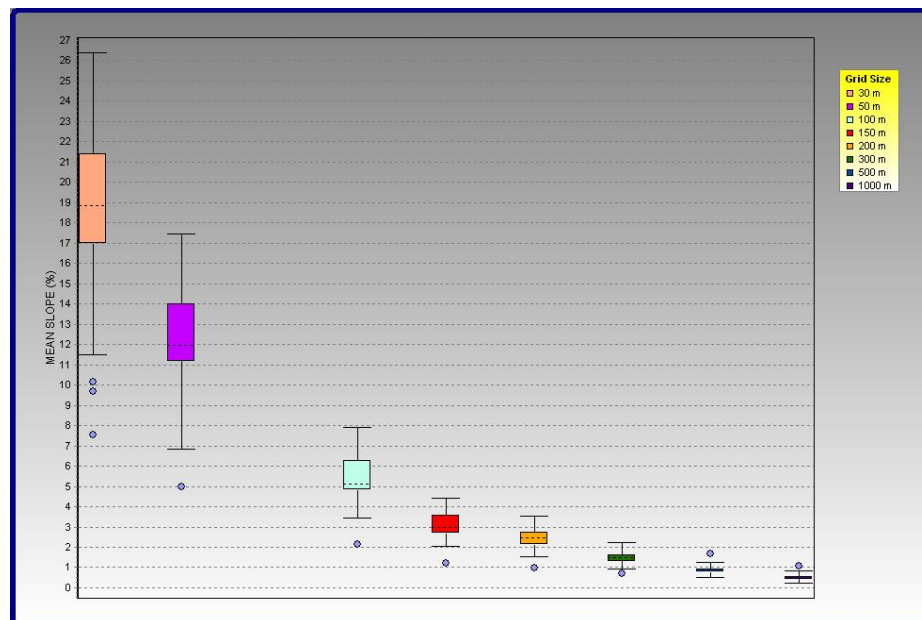


**Figure 4-7** Land Surface slope map for the TBSW, slope values are given in percent



**Figure 4-8** Slope calculated for TBSW using different resample techniques

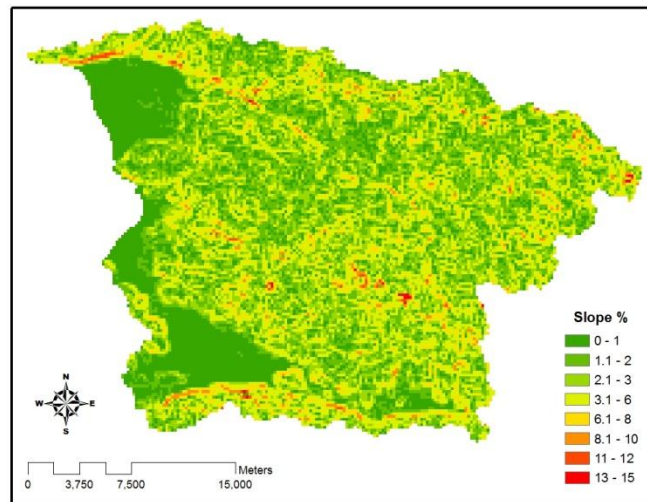
To verify the results and obtain a box plot of the change and degradation in slope using Method 1, a slope analysis was developed for the MBDB model, which included the sub-watersheds presented in Figure 4-6. The results show the same degradation of the mean slope (dashed lines Figure 4-9) using Method 1 and the nearest neighbor resampling technique for DEM resolutions of 30, 50, 100, 150, 200, 300, 500 and 1000 m.



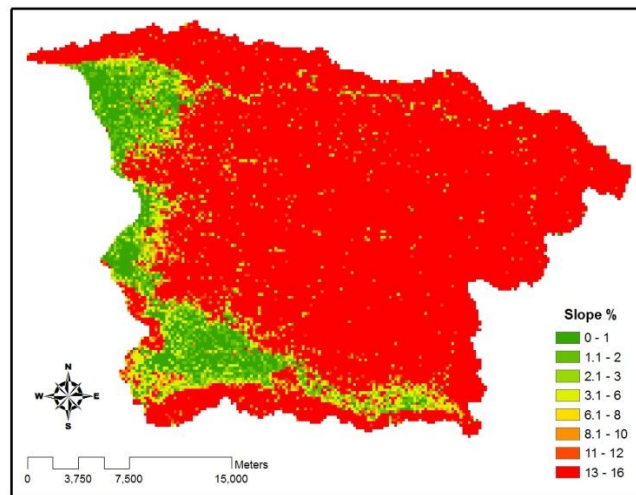
**Figure 4-9 Slope box plots (quartiles 25 and 75) for the MBDB study area calculated with Method 1 and nearest neighbor resample technique, mean slope (dashed lines), quartiles 5 and 95 (solid lines) and outliers (dots)**

Figure 4-9 presents slope degradation in terms of the interquartile 25-95 (solid boxes), interquartile 5-95 (solid lines) and outliers (dots). Figure 4-10 and Figure 4-11 present a spatial graphical representation of the slope degradation using the two methods described above. The same interval classes were chosen to represent the slope, Method 2 in Figure

4-11 presents much more area in red color than Method 1 in Figure 4-10, because it presents more areas without degradation and slope values greater than 16%. Therefore, Method 2 is the recommended for up-scaling both the slope of TBSW and Mayagüez Basin model.



**Figure 4-10 Visual comparison between resample methods at 200 m resolution for the MBDB model by Method 1**



**Figure 4-11 Visual comparison between resample methods at 200 m resolution for the MBDB model by Method 2**

## **4.5 Green Ampt infiltration parameters assignment**

The abstractions in the distributed hydrologic model are calculated with the Green Ampt infiltration model. The principal parameters are: saturated hydraulic conductivity; effective porosity, soil depth, and wetting front. Parameter values were assigned using the SSURGO maps and data base from the USDA (2006 a,b,c,d), which contains the soil classes for Puerto Rico. Initially, the soil map was classified into 6 basic textures (Figure 3-3) and the hydraulic conductivity, wetting front and effective porosity values were assigned from literature as shown in Table 4-2, (Vieux, 2004, Bear, 1972; Freeze and Cherry, 1979, McWhorter and Sunada, 1977). Using the Book Reference values of infiltration parameters from Table 4-2, average parameter values were calculated for the tributary area at the streamflow gauge stations, located in the watersheds.

At Río Grande de Añasco near San Sebastian for example, the average hydraulic conductivity is 0.05 cm/hr, the wetting front is 28.29 cm, the effective porosity is 0.364, and the soil depth assigned uniformly to the basin area was 20 cm. Average parameter values in several flow meter stations are found in Table 4-2. A preliminary study was developed with the infiltration values shown in Table 4-2 using the Vflo model and different events.

**Table 4-2 Summary of the infiltration values for the Green Ampt Model**

<b>Basin</b>	<b>Texture</b>	<b>Effective Porosity</b>	<b>Wetting Front (cm)</b>	<b>Hydraulic Conductivity (cm/h)</b>
Book Reference	Sand	0.42	4.95	11.78
	Loam	0.43	8.89	0.34
	Clay Loam	0.31	20.88	0.10
	Clay	0.39	31.63	0.03
	Gravel	0.24	1.5	2.27
	Rock	0.17	1	0.036
<b>Average Values over the Watersheds</b>				
Añasco near San Sebastian	--	0.364	28.29	0.05
Guanajibo near Hormigueros	--	0.33	22.5	0.1
Río Rosario	--	0.328	25.2	0.03
TBSW	--	0.382	31.21	0.03
Río Casey	--	0.376	30.41	0.03
<b>New Average Infiltration Values</b>				
Añasco near San Sebastian	--	0.412	28.61	0.75
Guanajibo near Hormigueros	--	0.363	22.85	6.35
Río Rosario	--			
TBSW	--	0.43	31.57	0.69
Río Casey	--	0.418	30.41	0.64

The volume calculated was over predicted in almost all cases; therefore an exhaustive analysis was conducted to enhance the infiltration parameter values since the literature shows low hydraulic conductivity values for the texture classes approach. In Puerto Rico, the soils present high organic matter content and some clays are well drained, and are considered as hydrologic group B, for example Alonso, Consumo, Delicias and Maricao soils (SSURGO, 2006a, b, c, d). New values for hydraulic conductivity, total porosity and

effective porosity were obtained using the percentage of sand, silt and clay and average bulk density from the SSURGO database and Rosetta Lite program (Schaap et al., 2001, Schaap, 2003) from HYDRUS-1D, (Simunek et al., 2005). Rosetta implements pedotransfer functions to predict van Genuchten (1980) water retention parameters and saturated hydraulic conductivity ( $K_s$ ) by using textural class, textural distribution, bulk density and one or two water retention points as input. Rosetta follows a hierarchical approach to estimate water retention and  $K_s$  values using limited or more extended sets of input data (Schaap et al., 1998, Schaap and Leij, 1998a). The calibration data for Rosetta has a set of 2134 samples for water retention and 1,306 samples for  $K_s$  (Schaap and Leij, 1998b) distributed in USA and some from Europe. The authors suggested that the usage of Rosetta for other climate zones, and hence other pedogenic processes, could lead to inaccurate predictions.

#### *4.5.1 Assumptions for unclassified soil classes*

Some soils did not have bulk density and percentage of sand, silt and clay. In these cases assumptions were made for alluvial land, leveled clayed classification, limestone, gravel, pits and quarries, serpentine rock, volcanic rock and limestone rock as described below.

##### **4.5.1.1 Alluvial land**

Alluvial land has a variable profile, is a fine-grained fertile soil deposited by water flowing over flood plains or in river beds. Clay or silt or gravel are carried by rushing streams and deposited where the stream slows down. The Soil Conservation Service

classified this soil in the hydrologic group D and reports that the alluvial land has 0-1 inches of ponding depth range, very long ponding duration and floods frequently during the year, (USDA, 2006 a, b, c, d). Therefore, it is assigned a classification of Clay with an effective porosity of 0.475, 31.63 cm suction head and 0.06 cm/hr saturated hydraulic conductivity.

#### 4.5.1.2 Leveled Clayed

Leveled Clayed presents a hydrologic group C. The hydraulic conductivity value assigned to this classification was the average value between clay texture and hydrologic group C and it was 1.225 cm/hr with a range between 0.801 and 2.789 cm/hr. The same procedure as was used for alluvial land was used for leveled clay where the effective porosity was assigned the average value of 0.427 and a value of 31.63 cm for suction head, as recommended for clay.

#### 4.5.1.3 Limestone

Limestone is a sedimentary rock composed largely of the mineral calcite (calcium carbonate:  $\text{CaCO}_3$ ). The hydraulic conductivity was 570 cm/hr, taken from Freeze and Cherry (1979), the range for this value varies from 0.11 to 1,142 cm/hr. The effective porosity is 0.14, (McWorter and Sunada, 1977). The wetting front suction head was set to 1 centimeter, the minimum for sand reported by Vieux (2003).

#### 4.5.1.4 Gravel, pits and quarries

Gavel, pits and quarries have a hydrologic group A, assigned in SSURGO database (USDA, 2006a, b, c, d) meaning that they possess very good infiltration. The values assumed for their classification was medium gravel with a moderate degree of sorting and without silt content. For this material, the saturated hydraulic conductivity was assigned a value of 297 cm/hr, (EPA, 1986) and an effective porosity of 0.24 (McWorter and Sunada, 1977). The wetting front suction head was the minimum for sand reported by Vieux (2003) of 1 cm.

#### 4.5.1.5 Serpentine rock

According to Freeze and Cherry (1979), the saturated hydraulic conductivity (Ks) for fractured metamorphic and igneous rocks is between 0.00114 and 11.4 cm/hr, the average is 5.71 cm/hr. The effective porosity assigned was obtained from McWorter and Sunada (1977) for metamorphic rock and is 0.26.

#### 4.5.1.6 Volcanic rock

Volcanic rocks are usually fine-grained or aphanitic to glassy in texture and are named according to both their chemical composition and texture. Basalt is a very common volcanic rock with low silica content. For Basalt rock we assumed a total 0.17 (reported range of 0.03 to 0.35), effective porosity 0.1, and saturated hydraulic conductivity 570 cm/hr for fractured basalt (10 to 10<sup>5</sup> m/yr).

The values assigned to “*Soil not Surveed*” classification were the average hydraulic conductivity for clay texture in the whole study area: 1cm/hr; and the effective porosity

and wetting front suction values correspond to clay as reported by Vieux (2003). For the TBSW model, all the parameters were assigned to a grid model resolution of 10 m from the MBDB model (Figure 3-3). Average infiltration parameters for the TBSW are tabulated in Table 4-3 with detailed soil names and parameter values used. Bouwer (1966) suggested multiplying the hydraulic conductivity by 0.5 for the saturated hydraulic conductivity in Green-Ampt model. Therefore the average saturated hydraulic conductivity for the TBSW is 0.69 cm/hr.

**Table 4-3. Soil classification (SSURGO), hydrologic group and infiltration parameters at TBSW**

Soil Name	Texture	Hydrologic Group	Area (%)	Wetting Front (cm)	K <sub>s</sub> (cm/hr)	Depth (cm)	Effective Porosity
Consumo	Clay	B	59.85	31.63	1.273	300	0.415
Dagiëy	Clay	C	15.11	31.63	1.266	300	0.451
Humatas	Clay	C	25.03	31.63	1.736	300	0.454
Serpentine	Rock Serpentine	D	0.01	3.00	5.7	300	0.26
Toa	Silty Clay Loam	B	0.01	27.30	0.294	300	0.377
<b>Average</b>				<b>31.62</b>	<b>1.38</b>		<b>0.43</b>

## 4.6 Soil Depth

The soil depth is a very important parameter to calculate the infiltration losses. The USDA (2006 a, b, c, d) reports the soil depth for each soil when some restrictive layer or lithic rocks exist at a shallow depth. In other cases a maximum soil depth is assigned a value of 152 cm (60 inches), corresponding to the depth surveyed. Lithic is a continuous hard rock and less permeable, in some cases it is encountered at as small a depth as 10 cm from the soil surface. For some soils a paralithic rock is present under the layered soil.

The paralithic rock is a broken rock in contact with fissures less than 10 cm apart, which allow roots to penetrate the underlying rock. Major hydraulic conductivity is allowed, and works like fractured rock. Soils that present this condition are allowed to increase the soil depth to 600 cm indicating no depth restriction, and other soils without any restrictive layer or lithic rock were set to 300 cm, almost double that of the survey. In this way the soil depth assigned to the soil map will be the maximum possible and reductions would be considered for calibration proposes. Values assigned for the TBSW area are shown in Table 4-3.

#### **4.7 Overland Roughness, Impervious and Crop Coefficient Assignment**

Overland roughness is an input parameter in hydrologic models; this parameter affects principally the peak flow in a hydrograph. Two sources were analyzed to determine the land use in the area. One source was obtained from Land Use/ Land Cover map for Puerto Rico (Figure 3-4, Helmer et al. (2002)), which was reclassified by Prieto, 2006 (Figure 3-5) into 6 Land Use classes, and appropriate Manning's and impervious values were assigned to each class at 30 m resolution (Table 4-4). A resize from 30 m to 200 m changed the area distribution of some land use would affect the flow response (e.g., flow volume). The land class most affected by resizing is the urban area showing a decrease in area of 1.33 km<sup>2</sup>, followed by an increase in Agriculture by a 0.99 km<sup>2</sup>, areas of special interest in terms of flooding, (Table 4-4).

**Table 4-4 Resized Grid Area for the land use map.**

<b>Re-class Name</b>	<b>Manning Roughness (n)</b>	<b>Impervious %</b>	<b>Area with 30 m (Km<sup>2</sup>)</b>	<b>Area with 200 m (Km<sup>2</sup>)</b>	<b>Δ Area (Km<sup>2</sup>)</b>
Agriculture	0.166	5	54.93	55.92	0.99
Agriculture /hay	0.190	4	0.13	0.12	-0.01
Forest, shrub, woodland and shade coffee	0.191	2	529.16	529.12	-0.04
Other emergent wetlands	0.050	1	1.26	1.24	-0.02
Pasture	0.225	5	172.84	173.2	0.36
Quarries, sand and rock	0.020	95	0.75	0.56	-0.19
Urban and barren	0.080	81	60.02	58.68	-1.33

The sum of the land use map areas between 30 m and 200 m are different due to pixel sizes; 200 m is rougher and covers more area, while the 30 m pixel can adjust much better to the basin form.

The second land use source was from remote sensing classification and field verification from PRWRERI (2004) shown in Figure 3-6, with thirty five classes. The land use classification was reclassified into 13 classes and is shown in Figure 4-12. The roughness values were specified for each class according to literature and expertise and shown in Table 4-4. A value of 0.118 is the average roughness value for the MBDB model and 0.12 for the TBSW.

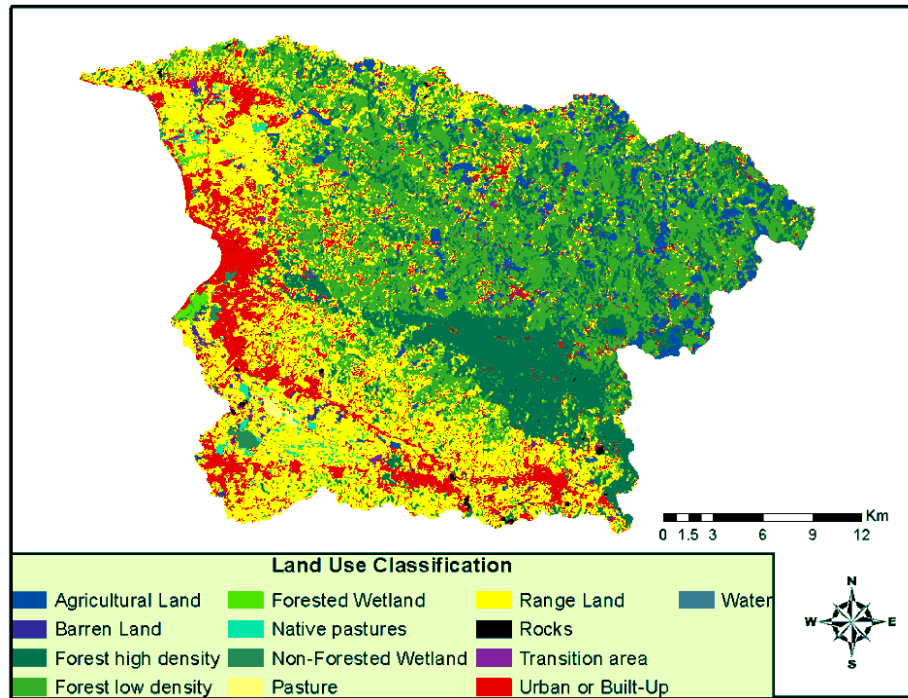


**Figure 4-12 Land Use general reclassification from Land Sat<sup>ET</sup>, 2004, PRWRERI (2004)**

Another parameter that is contingent upon the land use classification is the crop coefficient. Its coverage was determined using the land use classes derived in Figure 4-12 at 30 m resolution; values of  $K_c$  (mid-season crop stage) were assigned from Allen et al. (1998) and are shown in Table 4.5. Allen et al. (1998) did not present  $K_c$  values for forest land use. Therefore, an apples tree with active ground cover class value was assumed (for possible representation of forest), with a maximum of 1.2  $K_c$ . The TBSW exhibits a predominant forest land use (see Figure 4-13, 30 m resolution) of low density with 39.36 % of the area; brush rangeland with 38.17 % of the area and 14.51 % urban land use, respectively (Table 4-6). The Figure 4-14 shows some pictures taken for the forest representation and urban area.

**Table 4-5 Land Use Classification with the Manning Roughness values and crop coefficient ( $K_c$ ) for MBDB**

Classes	Re-classification	Manning Roughness ( $n$ )	$K_c$	Area (m <sup>2</sup> )
Coffee	Agricultural Land	0.080	1.100	15.76
Coffee, orange		0.080	1.000	0.01
Coffee, orange, plantain/banana		0.080	1.000	0.01
Coffee, plantain/banana		0.080	1.100	12.73
Coffee, plantain/banana, oranges		0.080	1.025	0.33
Dairy Farm or dairy cow feeding		0.050	0.400	0.03
General agriculture		0.080	1.000	1.17
Nurseries & Ornamental Horticulture		0.080	1.000	0.39
Orange		0.080	0.850	0.66
Orange, coffee		0.080	0.950	0.64
Orange, plantain/banana		0.080	0.900	0.29
Orange, plantain/banana, coffee		0.080	1.000	0.02
Plantain/banana		0.080	1.200	7.21
Plantain/banana, coffee		0.080	1.150	0.06
Plantain/banana, coffee, oranges		0.080	1.200	0.49
Plantain/banana, orange		0.080	1.025	0.11
Shade coffee plantation		0.080	1.100	0.06
<b>SUB-TOTAL</b>			<b>0.078</b>	<b>0.992</b>
Barren land	Barren Land	0.015	0.300	10.18
Forest high density	Forest high density	0.150	1.200	156.19
Forest low density	Forest low density	0.150	1.100	234.31
Forested Wetland	Forested Wetland	0.070	1.200	2.83
Native pastures	Native pastures	0.045	0.850	6.73
Non-Forested Wetland	Non-Forested Wetland	0.050	1.100	2.16
Pasture	Pasture	0.035	0.950	1.50
Shrub and brush rangeland	Range Land	0.130	1.000	248.92
Bare exposed rock	Rocks	0.015	0.100	0.04
Gravel pit		0.015	0.100	2.07
Transition area	Transition area	0.050	0.300	0.79
Transportation, communication	Urban or Built-Up	0.015	0.300	11.78
Urban or built-up land		0.015	0.300	97.40
Waste disposal areas		0.015	0.300	0.44
Pond	Water	0.030	1.050	0.24
Streams and canals		0.030	1.050	2.97
<b>TOTAL</b>		<b>0.188</b>	<b>0.966</b>	<b>818.53</b>

Source: PRWRERI,2004 for classes and Allen et al.(1998) for  $K_c$

**Table 4-6 Land use classification, Manning Roughness (n) values and  $K_c$  for Evapotranspiration quantification in the TBSW**

Land use Classification	Manning Roughness (n)	$K_c$	Area (km <sup>2</sup> )	Area Percent
Forest low density	0.1500	1.100	1.3994	39.36
Shrub and brush rangeland	0.1300	1.000	1.3570	38.17
Urban or built-up land	0.0150	0.300	0.5157	14.51
Forest high density	0.1500	1.200	0.2083	5.86
Baren land	0.0150	0.300	0.0378	1.06
Transition area	0.0500	0.300	0.0216	0.61
Transportation, communication	0.0150	0.300	0.0083	0.23
Streams and canals	0.0300	1.050	0.0045	0.13
Gravel pit	0.0150	0.100	0.0018	0.05
Native pastures	0.0450	0.850	0.0009	0.03

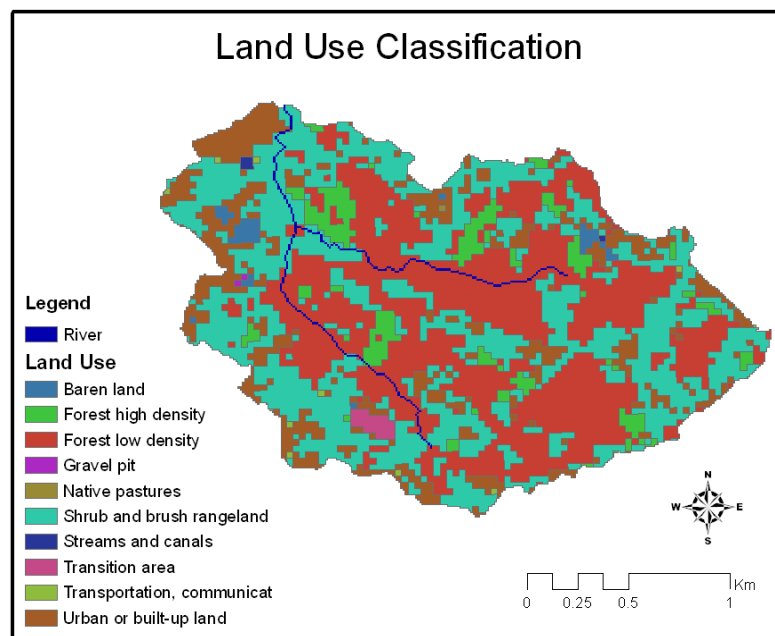


**Figure 4-13 Land use classification for the TBSW extracted from Figure 4-12**



**Figure 4-14 Photos describing the land use of the TBSW**

## **4.8 Evapotranspiration**

The hydrologic model requires potential or reference evapotranspiration as input to dry the soil in a long term simulation. This section identifies the uncertainties associated with the evapotranspiration quantification, because this parameter is time and scale dependent and is related to the meteorological stations located within the area of interest. Reference evapotranspiration can be calculated by the Penman-Monteith method (Allen et al., 1998, Equation 4-2) and the Hargreaves Samani method (Equation 4-3) using data from the NRCS Soil Climate Analysis Network (SCAN) weather stations located in western and southern Puerto Rico. Two stations are located within the MBDB and relatively close to the TBSW (i.e., the USDA Tropical Agricultural Research Station (TARS) at Mayagüez and Maricao Forest, PR). Penman Monteith and Hargreaves

Samani methods were compared at the stations mentioned with a daily time step from October, 2007 to October 2009. The FAO56 Penman Monteith evaporation equation is presented below (Allen et al., 1998):

$$ET_o = \frac{0.408 \cdot \Delta \cdot (R_n - G) + \gamma \cdot \left( \frac{900}{T + 273} \right) \cdot u_2 \cdot (e_s - e_a)}{\Delta + \gamma \cdot (1 + 0.34 \cdot u_2)} \quad (4-2)$$

where  $ET_o$  is reference evapotranspiration (mm/day),  $\Delta$  is slope of the vapor pressure curve (kPa/°C),  $R_n$  is net radiation (MJ/m<sup>2</sup>day),  $G$  is soil heat flux density (MJ/m<sup>2</sup>day),  $\gamma$  is psychrometric constant (kPa/°C),  $T$  is mean daily air temperature at 2 m height (°C),  $u_2$  is wind speed at 2 m height (m/s),  $e_s$  is the saturated vapor pressure and  $e_a$  is the actual vapor pressure (kPa). Equation 4-2 applies specifically to a hypothetical reference crop with an assumed crop height of 0.12 m, a fixed surface resistance of 70 sec/m and an albedo of 0.23.

The Hargreaves-Samani equation for reference or potential evapotranspiration is given below (Hargreaves and Samani, 1985):

$$PET = 0.0135 * R_s * (T_{ave} + 17.8) \quad 4-3$$

where  $R_s$  is solar radiation in units of mm/day and  $T_{ave}$  is average air temperature (°C).  $R_s$  is readily converted from units of MJ/m<sup>2</sup>day to equivalent depth of water in mm/day by dividing by the latent heat of vaporization (2.45 MJ/m<sup>2</sup>day).

The Pearson correlation coefficient ( $R^2$ ) between Equations 4-2 and 4-3 was 0.9375 and the bias was 0.956 for this period, indicating that the Hargreaves Samani constant (0.0135) presented in Equation 4-3 could be corrected by a factor of 0.956 for the current study area using a more simplistic formula than FAO-Penman-Monteith equation (Equation 4-2).

Goyal et al. (1988) developed monthly linear regression equations for air temperature (mean temperature ( $T_{ave}$ ), maximum temperature ( $T_{max}$ ) and minimum temperature ( $T_{min}$ ) for Puerto Rico, which depend on the surface elevation (m). PET can be calculated using these linear regressions (Goyal et al., 1988) and Hargreaves Samani equation extended (Equation 4-4) for places where no solar radiation data is measured.

$$PET = 0.0023 * R_a * (T_{ave} + 17.8)(T_{max} - T_{min})^{0.5} \quad 4-4$$

where PET is potential or reference evapotranspiration (mm/day) and  $R_a$  is the extraterrestrial radiation (mm/day).

Solar radiation is highly spatially variable in Puerto Rico (Harmsen et al., 2009 and 2010), therefore, the effectiveness of Equations 4-3 and 4-4 to estimate PET using the temperature versus elevation relationships developed by Goyal at short time scales (daily) was evaluated in the current study. Constants in Goyal's monthly linear regressions were interpolated to daily constants. All input parameters needed in the Hargreaves-Samani methods (Equations 4-3 and 4-4) are measured by the SCAN stations.

The elevation in the TARS is 13.72 amsl with an average temperature ( $T_{ave}$ ) of 23.9 C for the period of analysis (October, 2007 to October, 2009); and in Maricao Forest the elevation is 747 m with  $T_{ave}$  19.7 C. The results show that the Goyal regressions at a daily time step predict the  $T_{ave}$  with a coefficient of determination  $R^2$  of 0.46 for TARS and 0.62 for Maricao. However, if PET is calculated with the solar radiation measured at the stations along with the  $T_{ave}$  derived from the Goyal regressions, the improved  $R^2$  of 0.987 and 0.992 are obtained at TARS (Figure 4-15) and Maricao Forest (Figure 4-16), respectively. Values of  $R^2$  of 0.2145 for TARS and 0.0013 for Maricao were obtained using Goyal's elevation model and Equation 4-4. The  $R^2$  is increased to 0.2254 for the Maricao station if the PET is calculated using the  $T_{ave}$  from the Goyal equations and the solar radiation is assumed to be equal to the TARS solar radiation (Figure 4-15). These results show that solar radiation is a spatially sensitive parameter in the PET calculation and that solar radiation cannot be assumed equal at locations distant from each other. Remotely sensed satellite measurements are suggested for a better spatially distributed solar radiation dataset, such as the method used by Harmsen et al. (2009 and 2010). For a long term hydrologic model, simulations for the TBSW, we used the PET calculated using Equation 4-3 and assuming that the solar radiation is the same as TARS, due to its relatively close proximity to the TBSW, around 2.5 km, compared to 16.3 km between the TBSW and Maricao Forest stations. Although not used in this study, another option would have been to use the daily operational solar radiation data described by Harmsen et al. (2009) for Puerto Rico (<http://pragwater.com/solar-radiation-data-for-pr-dr-and-haiti/>).

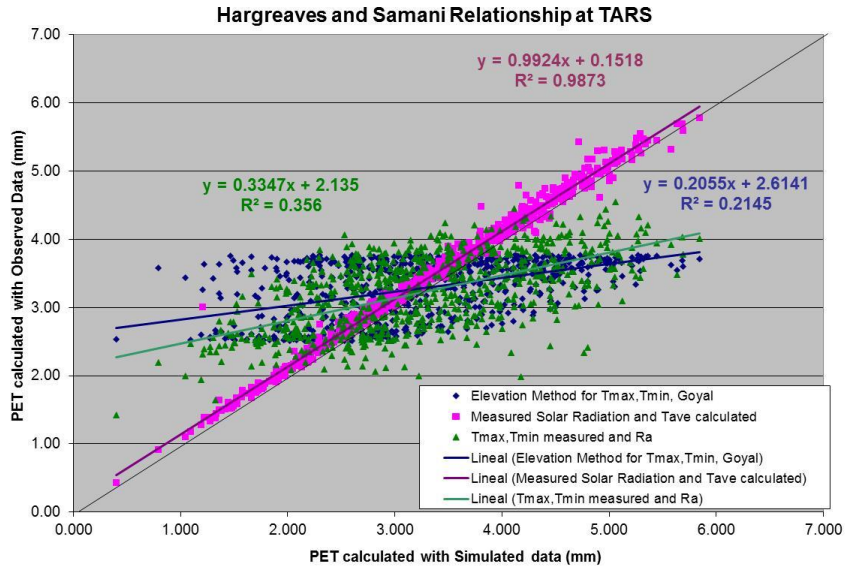


**Figure 4-15 Potential Evapotranspiration with Hargreaves-Samani relationship for observed  $T_{max}$ ,  $T_{min}$ ,  $T_{ave}$ , solar radiation, extraterrestrial radiation; and temperatures predicted by Goyal relationships at TARS station.**

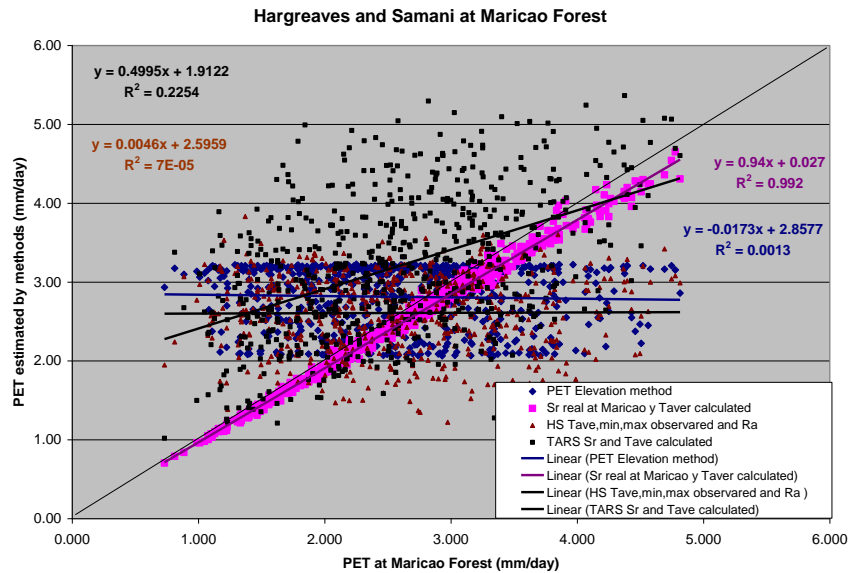


**Figure 4-16 Potential Evapotranspiration with Hargreaves-Samani relationship for observed  $T_{max}$ ,  $T_{min}$ ,  $T_{ave}$ , solar radiation, and extraterrestrial radiation; and temperatures predicted by Goyal relationships at Maricao Forest station.**

## CHAPTER 5

# 5 METHODOLOGY

This chapter presents the technical methodologies used in this research to address the research questions presented in Chapter 1. A determination of parameter sensitivity in the MBDB model is described in Section 5.1, where various parameters were first perturbed by multiplication factors to generate spider plots, and then the factors 0.5 and 1.5 (representing  $\pm 50\%$ ) were used to calculate the relative sensitivity ( $S_r$ ) for different variables and events. Using the TBSW model, in Section 5.2, some parameter aggregation techniques are evaluated for later use in the up-scaling experiment. Section 5.3 presents the evaluation of uncertainties in Quantitative Precipitation estimates from MPE by comparison with a high density rain gauge network. In Section 5.4 a methodology to evaluate uncertainty due to hydrologic model (grid spacing) and rainfall resolution were addressed.

To establish a flood alarm system in the MBDB, first, we need to know the likelihood and uncertainty associated with a prediction due to the inputs and parameters variations. Some initial sensitivity tests were developed in the Mayagüez Bay model to understand how some parameters and inputs affect the flow prediction. The major sources of uncertainties are associated with inputs such as rainfall estimation, terrain slope, parameter values and initial conditions; and all these sources of uncertainty are

resolution-dependent. How much rainfall variation is there at scales below the radar pixel size and how much does rainfall variation and DEM resolution affect predictability? These questions will be addressed in the TBSW analysis.

The TBSW is useful for research purposes and represents a “real world” laboratory to study the predictability limits due to aggregation of high resolution inputs in a hydrologic model. In the TBSW (Figure 3-7) a dense rain gauge network was installed as part of this investigation and a pressure transducer for water level measurements. Other high resolution data exists for the TBSW including topography (digital elevation model, CRIM, 1998); soils and land use maps, etc. These sets of information are ideal to define how much detail is necessary in the physical modeling process and the value of increasing the rainfall resolution, as well as the hydrologic model grid resolution within small watersheds. Carpenter (2004) mentioned that the uncertainty in the model output is inversely proportional to the watershed area. In other words, for a small hydrologic model, a large degree of uncertain exists at the subwatershed scale. Therefore, the magnitude and behavioral impact of the rainfall errors in the hydrologic forecasts help to define the precision and accuracy necessary in new rainfall algorithms and radar technologies. New radar technologies are being developed on the CASA project at UPRM and are available for western Puerto Rico, promising higher resolution than NEXRAD, and will be a critical component in the flood alarm system. Evaluating possible CASA radar resolution in this study with the rain gauges information, we will determine the predictability and quantify the uncertainty due to terrain and rainfall grid

size resolution at scales below the typical radar resolution (2 by 2 km cell size) in small subwatersheds.

After finding the predictability limits and assessing the predictability in the TBSW, we will formulate recommendations to initialize the larger model (MBDB) and enhance the flood prediction in mountainous basins. All statistical analyses in this research were performed using Minitab 16 (Minitab, Inc., 2010).

In the following sections, we will describe the methodology and activities required to achieve a successful investigation and to address the research questions presented before in Section 01.2. For convenience, a summary of the research questions are listed here:

1. How flood prediction is affected by the spatial variability of point rainfall at scales below that of the typical resolution of radar-based products?
2. How does the DEM and parameter aggregation affect the model's predictive capabilities and the errors of the hydrologic system?
3. Would the assumptions developed for the small scale enhance the hydrologic predictability at larger scales?

## **5.1 Additional Field Measurements**

A dense network of rain gauges (28 tipping bucket rain gauges with data loggers) were installed within a single GOES Satellite Hydro-Estimator (HE) pixel (4 km x 4 km) and 64% of the rain gauges are within TBSW with the objective to obtain high resolution

rainfall within the area. Complete records were collected since June, 2007 when the last 12 rain gauges were installed within the TBSW (Harmsen, et al., 2008) with a temporal resolution of 5 minutes. The Euclidian distance was calculated between rain gauges within the TBSW, exhibiting a maximum range distance of 563.2 m and the mean distance was 218 m with a standard deviation of 99.5 m. The calculated mean Euclidian distance within the Hydro-Estimator pixel was estimated to be 334 m with a standard deviation of 171 m, Figure 3-7 showed the location of the rain gauges network within the Hydro-Estimator pixel. Figure 5.1 shows the rain gauge network, the TBSW outline and the distance between rain gauges.

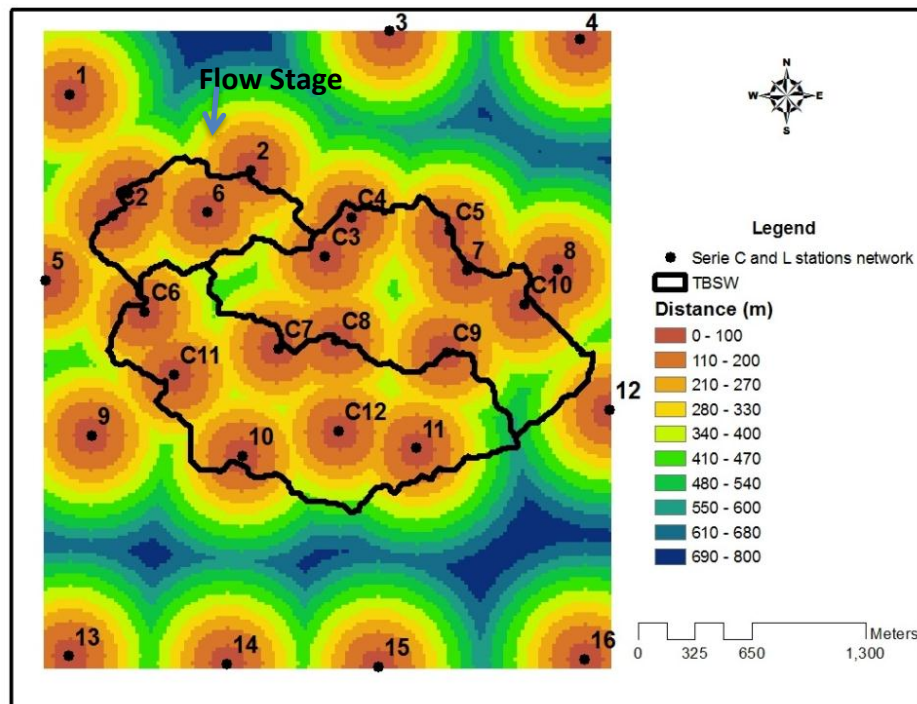


**Figure 5-1 Rain gauge distribution and location within the HE pixel; TBSW location and Euclidean Distance between the stations**

Additionally, a pressure transducer was installed at the TBSW outlet, which measured stage elevation data since October 2007 to May 2009 at 5 minutes temporal resolution.

## **5.2 Evaluation of Parameter Aggregation Techniques within the TBSW**

To develop the up-scaling experiment or set up any hydrologic model is necessary to evaluate which methodology will be addressed to create the hydrologic models at different resolutions. Several aggregation techniques are used in GIS to develop the parameters up-scaling. The aggregation consists of using data from the cells that will fall within the larger up-scaled cells and then applying to them mathematical operations to calculate a new aggregated cell value. All these aggregation techniques produce different results which can affect the hydrologic response. Also, the order in which the slope is generated can alter the results. Two different orders would be developed using different techniques and they are listed below:

1. Aggregate the terrain to a new resolution and calculate the slope for this resolution; or
2. Calculate the slope from high resolution terrain model and then aggregate it to a new resolution.

The aggregation techniques and the order to derive slope were tested in the TBSW using Arc GIS tools. The tested resolutions were 10, 50, 100, 175, 250, 500 m, which generated graphs of how the slope has been degraded. A decision was taken as to which

aggregation technique is best for the purposes of this research. Additionally the methodology was tested to see the degradation slope degree in the MBDB Model.

### **5.3 Determination of hydrologic model sensitivity due to parameters and rainfall perturbations for the MBDB Model**

To develop a distributed hydrologic model it is necessary to create an ensemble of different layers that represent the physical characteristics of the basin. Uncertainties associated with the model parameter values and their scales can be quantified by evaluating the hydrologic response given a range of parameter and rainfall perturbations.

The objective of this evaluation was to determine which parameters and rainfall are most sensitive in the mountainous areas, of the physical conditions present in Western Puerto Rico. Then these parameters were evaluated in the up scaling analysis presented in Section 5.5. For this purpose we used the MBDB model at 200 m by 200 m cell resolution with three outlet points, summarizing different watershed characteristics in terms of area, shape and slopes.

The sensitivity analysis considered parameter and input perturbations by changing the magnitude of the parameter value, but not its spatial distribution. The multiplicative factors used to perturb the model and input (rainfall) were 0.5, 1.0, 1.5 and 2.0. The parameters used in the analysis were: overland and channel Manning roughness coefficient, the overland and channel saturated hydraulic conductivity, soil depth, and

initial fraction of soil saturation. By demonstration in other studies, hydrologic models have been found to be sensitive to these parameters (Moreda and Vieux, 2003). In this study, for completeness, we additionally evaluated the model response to variations in land slope.

Three important events that produced flash flooding in Puerto Rico were evaluated. The most important event with a recurrence greater than 100 year return period for Río Grande de Añasco River was Hurricane Georges in September 21-23, 1998. FEMA, (2009) estimated 4,078 cms at Rio Grande de Añasco near San Sebastian for 100 yr return period and the measured event had a peak of 4,587 cms. Other important events analyzed were November 11-16, 2003; and the Tropical Storm Jeanne in September 14-17, 2004. Interpolations of the rainfall amounts each time step (15 minutes) using the USGS rainfall stations available for each event in the MBDB area were made to obtain a distributed rainfall over the basins. The interpolation method used was the Exponential Weighted method.

The parameter and rainfall perturbations were evaluated at three basin outlets, which are: USGS 50144000 Río Grande de Añasco near San Sebastian, USGS 50136400 Río Rosario near Hormigueros and USGS 50138000 Río Guanajibo near Hormigueros.

Spider plots were used to evaluate the model response to the entire range of the parameters and to determine if there is a portion of the parameter range that yields

unrealistic results. Spider plots for runoff depth and peak flow show the percent change in model output variable versus parameter value change (perturbation) by a given factor.

The Relative Sensitivity Coefficient ( $Sr$ ) is defined as the ratio of the difference in the model output to the value of the output when the input parameters are set to their base values, divided by the ratio of change in the input parameter to the initial value of the input parameter as shown in Eq. (4-1).

$$Sr = \frac{(O_{P+\Delta P} - O_{P-\Delta P})}{\frac{O}{P}} \quad (5-1)$$

where,  $O$  is model output with input parameters set at base values,  $P$  is the value of the input parameter,  $O_{P+\Delta P}$  and  $O_{P-\Delta P}$  are model outputs with the input parameter plus or minus a specified perturbation (in this case  $\pm 50\%$ ).

The behavior of the relative sensitivity coefficient was evaluated using two variables: discharge volume in millimeters and peak discharge in cubic meters per second.

## 5.4 Evaluation of current Quantitative Precipitation Estimates

The NEXRAD radar is located near the City of Cayey at 860 m mean sea level and approximately at 120-130 kilometers from Mayagüez city. It has been operational since 1999. Some errors exist associated with radar measurements due to factors such as distance from radar to the study area; the coverage gap between the terrain and radar

beam (at western flood plains with a radar beam of 0.5 degrees a coverage gap between 1.8 to 2 km was found); and Z-R relationship applied. Mountain blockage at lower beam angles (0.35 to 0.45 degrees) affects the reflectivity received from some locations within the Añasco and Mayagüez flood plains. Figure 5-2 shows the detail of mountain blockage at beam angle of 0.35 degrees; for 0.5 degrees and higher blockage does not occur.

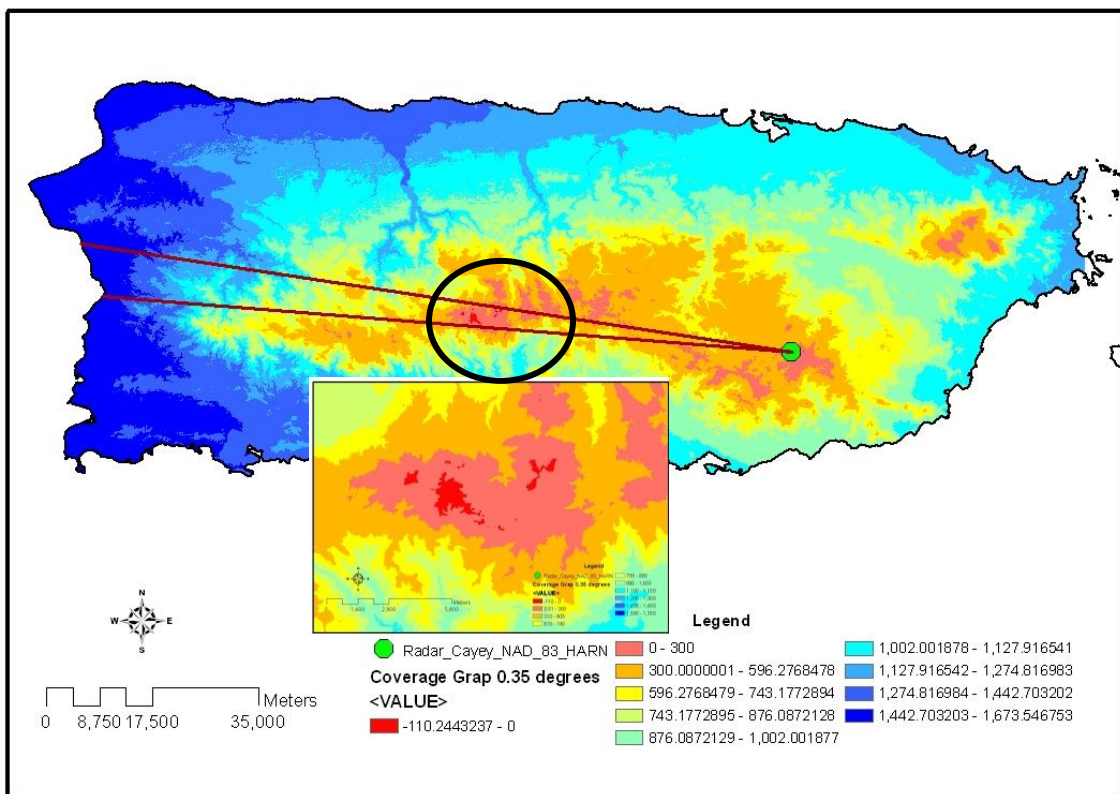


**Figure 5-2 Coverage gap between terrain elevation and radar beam of 0.35 degrees with the detail of blockage at mountainous area**

The NEXRAD radar resolution gives a spatial rainfall variability that fills the gaps between rain gauges enhancing the spatial rainfall quantification. However, it is necessary to remove some bias between radar and rain gauges due to radar errors and rain

rate quantification. Nevertheless, we don't know the rainfall variations at scales below the actual radar products (2 km x 2 km or 4 km x 4 km), because rain gauge networks do not exist at these scales within the island.

#### *5.4.1 Evaluating rainfall detection accuracy and long term Bias quantification*

Obtaining a long term bias quantification between the radar and rain gauge network is an essential part of the uncertainty quantification. It is possible to observe and quantify how much the bias changes in time and magnitude. An evaluation of the MPE rainfall product and bias performance at hourly and daily temporal scales is evaluated within the Hydro-Estimator pixel for the year 2007 using the rain gauge network located in western Puerto Rico near the University of Puerto Rico – Mayagüez Campus, where the TBSW is located (described Section 5.1). Some rain gauges were not operating during some periods owing to gauge damage or low logger batteries, these data were eliminated from the analysis. Five-minute rain gauge data was accumulated to 1-hour and 1-day intervals, with the intention of comparing data with the original MPE temporal resolution and daily accumulations.

MPE pixels are based on a HRAP (Hydrologic Rainfall Analysis Project) grid projection. Therefore, a geographic coordinate transformation from Stereographic North Pole to NAD 1983 State Plane Puerto Rico and Virgin Islands was performed for each hour using the ArcGIS project raster tool. The re-sampling technique algorithm used was the nearest neighbor assignment at 4 x 4 km resolution.

The N1P rainfall product is calculated from NEXRAD as a rainfall rate every 5 or 6 minutes when the radar detects rainfall, and a 10 minutes N1P product is archived when no rainfall is detected. The N1P NEXRAD product originally has a polar geographic coordinate system (GCS) and using the NOAA Weather and Climate Toolkit program (NOAA National Climatic Data Center available at <http://www.ncdc.noaa.gov>) it is possible to transform the coordinates to GCS\_WGS\_1984. Different formats are available to export the data. The GIS shapefiles maintain the original orientation; however, in a distributed hydrologic model it is necessary to use raster or ASCII files to represent the spatial rainfall variation in the model. Due to raster characteristics it is not possible to maintain the original orientation.

The study was made with the projected and raster pixels, with the aforementioned in mind, 4 MPE pixels were obtained around the HE pixel. Area weights were calculated for intersecting areas between the MPE pixels and the HE pixel which are 0.281, 0.344, 0.169 and 0.206, respectively. These area weights are used to calculate an average map precipitation for each time step. Weights for the N1P radar product were also estimated for 9 partial N1P pixels within the HE pixel.

Long term continuous validation between sensor rainfall estimates and rain gauge observations should be evaluated. The accuracy of rainfall estimates can be measured by decomposing the rainfall process into sequences of discrete and continuous random variables (Ramírez-Beltran et al., 2008a;b, Wilks, 1995).

The discrete variables were evaluated with contingency tables, where the rain gauges are the “ground truth” values and the MPE are the estimated values. In this way, the accuracy of the rainfall detection in terms of hit rate “H”, probability of detection “POD”, false-alarm rate “FAR” and discrete bias “DB” can be evaluated.

**Error! Reference source not found.** shows an example of a two-way contingency table. The variable “**a**” is the number of times that the rain gauge identifies a rainfall event and the estimator also correctly identifies a rainfall event at the same time and space. The variable “**d**” represents the number of times the rain gauge does not observe a rainfall event and the estimator correctly determines that there is no rainfall event. The variable “**b**” indicates the number of times the rain gauge does not observe a rainfall event but the estimator incorrectly indicates that there is a rainfall event. The variable “**c**” shows the number of times that the rain gauge detects a rainfall event but the estimator fails to detect the rainfall event (Ramírez-Beltran et al., 2008a).

**Table 5-1 Two-way contingency table**

		Observed Rainfall (Rain gauges)	
		Yes	No
Estimated MPE Rainfall	Yes	<b>a</b>	<b>b</b>
	No	<b>c</b>	<b>d</b>

Hit rate ( $H$ ) is the fraction of the estimating occasions when the categorical estimation correctly determines the occurrence of rainfall event or nonevent. Probability of detection ( $POD$ ) is the likelihood that the event would be estimated, given that it

occurred. The false-alarm rate (*FAR*) is the proportion of estimated rainfall events that fail to materialize. Bias is the ratio of the number of estimated rainfall events to the number of observed events (Wilks, 1995).

The typical scores that measure the accuracy of categorical estimation are:

$$H = \frac{a + d}{n_0}, \quad (5-2)$$

$$POD = \frac{a}{a + c} \quad (5-3)$$

$$FAR = \frac{b}{a + b} \quad (5-4)$$

$$DB = \frac{a + b}{a + c} \quad (5-5)$$

where  $n_0 = a + b + c + d$ . The mean field bias (*Bias*) is used to remove systematic error from radar estimates and used to correct the radar quantifications in the hydrologic simulation. The mean field bias is defined as the ratio of the “true” mean areal rain gauge rainfall to the corresponding radar rainfall accumulations (Casale and Margottini, 2004; Vieux, 2004). The average of the rain gauge network is evaluated each time step with an arithmetic mean, because the area weights change in time according to malfunctions errors in some gauges. The mean MPE rainfall at each time step is calculated using the area weights as stated above.

The indicators to evaluate the accuracy of MPE rainfall estimations over the HE pixel at different temporal scales are the Bias and root mean square error (*RMSE*).

$$Bias = \frac{\sum_{i=1}^{N_t} G_i}{\sum_{i=1}^{N_t} R_i} \quad (5-6)$$

$$RMSE = \left( \frac{1}{N_t} \sum_{i=1}^{N_t} (G_i - R_i)^2 \right)^{\frac{1}{2}} \quad (5-7)$$

where  $N_t$  is the number of hours,  $G_i$  is the areal mean rain gauge-based rain rate value at time “ $i$ ”, and  $R_i$  is the corresponding areal mean radar rain rate value.

For MPE Pixel 1, the associated rain gauges are: C01, C02, C03, C06, C07, C11, L01, L02, L05, L06 and L09, and for MPE Pixel 2 the associated rain gauges are: C04, C05, C08, C09, C10, C12, L03, L04, L07, L08, L10, L11. A mean field bias was calculated at 1 hour time resolution. Percentage of rainfall detection by rain gauges and MPE were calculated, and divided into three categories:

- 1) Rainfall not detected by MPE in percent, referred to as “No Radar Detection” or “c”.
- 2) Rainfall not detected by rain gauges in percent, referred as “No Rain gauge Detection” or “b”.
- 3) Rainfall detected by both sensors in percent, referred as “Coincident” or “a”.

The gauges L06 and L08 showed systematic errors in the records and, therefore, were ignored in the calculations. In addition to the statistics computed in the MPE Pixel 1 and

MPE Pixel 2, calculations were made using the 4 MPE pixels and the 26 rain gauges for hourly, daily and monthly data accumulations. The PDF was calculated to represent the probability distribution of the daily bias which represents the average total storm correction along one year.

#### *5.4.2 Evaluation of flow response to Rainfall interpolation Methods*

Different interpolation methods can be used to predict areal rainfall between rain gauges or areas where non-areal rainfall information exists. It's important to evaluate how different sources and interpolation methods affect the hydrologic response.

Two interpolation methods are analyzed and compared to produce aerial rainfall from existing rain gauges, which are exponential weighted (EW) and inverse distance weighted (IDW) methods. Additionally, NEXRAD rainfall product level 3 was compared with them. The events analyzed were the Tropical Storm Jean, passing over northern Puerto Rico on November 11-16, 2003.

The interpolations between USGS rain gauges were realized at 200 by 200 m cell resolution and 15 minutes temporal resolution for each event using the ArcGIS tools. The Hydrologic model (Vflo) with the prepared rainfall information and the MBDB model configuration described in Chapter 4 and aggregated to 200 by 200 m cell resolution was run with each rainfall product at the same resolution.

Analysis of bias quantification (Eq. 5-5) between rain gauges and radar were generated for each event and graphical comparisons between scenarios were generated.

## **5.5 Evaluation of predictability due to hydrologic model parameters and inputs resolutions at TBSW**

The previous sections describe which parameters, inputs and initial conditions, up-scaling and interpolation methods can be expected to affect runoff prediction and a hydrologic distributed model in mountainous tropical sub-watersheds. With the evolution of instruments to sense the atmosphere (CASA radars, NEXRAD, HE and others), as well as distributed hydrologic models that can predict runoff at even smaller scales, it is necessary to evaluate how the combined effect of model inputs and parameter uncertainties at different scales are spread through the hydrologic model and its impact on reliable operational flood prediction.

The hydrologic evaluation methodology must be objective and unbiased towards a given rainfall input or hydrologic model resolution. Global optimization methods in model calibration seek a unique parameter set that best simulate the observed behavior and if the rainfall resolution or rainfall source is changed, Gourley and Vieux (2005) indicate that the model needs to be recalibrated. They proposed a methodology to evaluate the accuracy of the inputs at the hydrologic scale using a hydrologic ensemble. Computing probabilities by examination of the allowable parameter space for each quantitative precipitation estimation algorithm, independently and thus remain unbiased towards a given rainfall source. Model parameter ensembles are created for each rainfall input, the spread and accuracy of the compilation of individual simulations are determined based on comparisons with observed streamflow.

An extension of this methodology will be addressed in this research to include the uncertainties associated with the parameter scale-dependence, in order to determine the accuracy of a given hydrologic model resolution. The combined effect of model parameters, rainfall and model resolution uncertainties are evaluated to produce the predictability limits, computing probabilities by examination of the allowable parameter space for each hydrologic scale and rainfall resolution in combination using ensemble predictions. The TBSW is the ideal scenario to evaluate the predictability limits where a network of rainfall sensors and a flow meter were installed in order to produce rainfall estimates at different scales and then compare the hydrologic prediction to observations for this research.

#### *5.5.1 Estimation of Uncertainty due to hydrologic model at TBSW*

Distributed hydrologic model configurations evaluated in this study are applied to represent the real world without any acknowledgment of how they affect the hydrologic prediction and how these uncertainties are propagated in the model at small upland watersheds. Previous evaluation in Section 5.3 at MBDA indicates input and parameters most sensitive in the model, which were used to be tested at the TBSW.

The DEM-derived parameters are well defined for each configuration and are scale-dependent, because they are mainly related to scale issues and aggregation techniques. This type of parameter include: flow accumulation; flow direction; slope; and stream definition indicating implicitly the stream density (as channel cells and overland cells).

The infiltration parameters depend on field measurements of soils and are treated as polygons representations on a map. The soil maps are available for Puerto Rico (USDA, 2006 a,b,c,d) and infiltration point measurements are attached to the polygons with the most probable realistic value to represent the area. The polygons are converted to gridded information and, therefore, become scale-depend. The same applies to the roughness map which is, related to the uncertainties associated with the remote sensing techniques, and a probable “realistic roughness value” is used to represent the land use. An up-scaling to the hydrologic model resolution will be addressed to evaluate the effect of parameter uncertainties due to scale.

The effect of slope degradation in the flow quantification was not evaluated. Instead, the aggregation methodology (determined in the Section **Error! Reference source not found.**) was used to preserve the average slope in the model and decrease the uncertainty and errors due to slope reduction.

The hydrologic evaluation of the resolution models was addressed using parameters ensembles at different resolutions. Every hydrologic parameter was calculated to 50 x 50 m, 100 x 100 m, 200 x 200 m and 400 x 400 m resolution from the high resolution hydrologic model at 10x 10 m. The hydrologic evaluation consists of making multiple runs using sets of parameters tested within their distribution`s physical bounds and the combinations of inputs for each hydrologic model. Some parameters, such as saturated hydraulic conductivity ( $K_s$ ), Manning roughness coefficient ( $n$ ) and initial degree of soil

saturation ( $\theta$ ) will be perturbed within their known space, while preserving the spatial variability at a determined scale.

The hydrologically distributed model (Vflo), controls this sampling space by multiplicative factors as illustrated by Moreda and Vieux(2003) in the OPPA method used to calibrate a distributed model. When no information is known *a priori* about the parameter distributions, an uniform distribution can and will be assumed. The scalar factors used to perturb the parameter maps (saturated hydraulic conductivity, Manning roughness coefficient) are determined by the following function and are different from the values used at Section 5.3, which permits computation of probabilities by examination of the allowable parameter space:

$$N_i = \frac{1}{8} (2 + 3i) \Big|_{i=0,2,3,4} \quad (5-8)$$

where  $N_i$  is the adjustment factor, (Moreda and Vieux, 2003).

The initial saturation parameter was tested with factor values of 0.25% (dry), 0.4, 0.6, 0.8 and 0.95% (almost fully saturated) covering a sample of the possible parameter space. Vieux and Vieux (2006) tested a long term distributed model at Loiza, Puerto Rico and found initial saturation factors around 0.75 in the uncalibrated model and 0.9 in the calibrated model. Additionally the initial soil saturation did not fall below 0.25 in the run time.

Each initial condition (rainfall event and one hydrologic setting resolution) and parameter perturbation was run in the hydrologic model (Vflo) producing a deterministic prediction called “ensemble member”, which are treated collectively and are samples of the PDF, representing the true initial state distribution. The three parameter perturbation in combination with one determined hydrologic and rainfall resolution event will produce a hydrologic ensemble. Each ensemble required 125 Vflo runs or ensemble members obtaining a simulation sample space for each hydrologic resolution model and rainfall are stored in a separate folder.

Results of each simulation are compared to the observed streamflow at the TBSW outlet. Three variables are important to evaluate in a flash flood forecasting, providing information of the flood magnitude (peak to flood), spread (volume normalized by the area) and lead time (time to peak) for the emergency management agencies. Box plots of each ensemble permit visualization of the spread of the solution due to parameters perturbations at each rainfall and model scale.

The estimation of uncertainty due to hydrologic model up-scaling was performed re-grouping the ensembles mentioned. The ensembles here are formed by the perturbations of the parameters and rainfall resolutions. Then, a hydrologic model resolution is evaluated according its size and is not dependent on rainfall resolution, because, it is tested with all rainfall resolutions. An important tool for the modeler is to understand the implications of using one specific hydrologic model resolution to estimate the flow discharge reliably.

Different objective functions exist, such as the least square error or maximum likelihood, to evaluate the variables in a verification step. The least square error is computed for each streamflow prediction giving a better understanding of the shape of the hydrograph.

The forecast or prediction verification method of an ensemble is the process of assessing the quality of the prediction with the corresponding observation. The quantitative statistics provide a simple way to evaluate the quality of an ensemble. To average the members of the ensemble to obtain a single prediction, provide a prediction that is more accurate than the single prediction initialized with the best estimate of the initial state of the hydrologic parameters. The mean ensemble is an overall indicator of the ensemble's behavior and is considered to be the best estimate (Stensrud et al. 2000)

The spread skill relationship for a collection of ensemble forecasts often is characterized by the correlation between the variance or the square of the standard deviation of the ensembles members around their ensemble mean. The accuracy is often characterized using the mean squared error.

The mean Time, Peak and Volume of each ensemble is computed and compared with observations. Additionally, the following statistics were used: *Bias*, Mean Absolute Error (*MAE*) and Root Mean Square Error (*RMSE*). Their definitions are formulated below:

$$\mathbf{Bias} = E[y_k] / O \quad \mathbf{5-9}$$

$$\mathbf{MAE} = \frac{1}{n} \sum_{k=1}^n |y_k - O| \quad \mathbf{5-10}$$

$$RMSE = \sqrt{\frac{1}{n} \sum_{k=1}^n (y_k - o)^2} \quad 5-11$$

where  $y$  represents the prediction from the  $k$ th simulation for Time, Peak and Volume, and  $O$  is the observation. The *Bias* measures the correspondence between the average forecast and the average observed value of the predictand. The *MAE* is the arithmetic average of the absolute values of the differences between the members of each pair. The *MAE* and *RMSE* values near to zero are desirable while *Bias* near to one are expected. Another diagnostic variable for representing runoff generation is the runoff coefficient defined as observed discharge volume divided by the basin-average rainfall event. These spread skill correlations have been found to be fairly modest, accounting for 25% or less of the accuracy variations (Atger, 1999; Gritmit and Mass, 2002; Hamill et al. 2004). Alternative approaches to the spread skill problem using probability distributions for forecast skill, conditional on ensemble spread were analyzed by Moore and Kleeman (1998). The conditional PDF are a statistical tool more robust than a simple ensemble mean to compare to an observation. PDF's were calculated for Time to Peak, Volume and Peak flow using the 625 ensemble members for the combination of hydrologic resolution model and rainfall event. The most widely used and important continuous probability distribution is the Gaussian or normal distribution described as:

$$p_x(x) = \frac{1}{\sqrt{2\pi\sigma^2}} e^{-\frac{1}{2}\left(\frac{x-\mu}{\sigma}\right)^2} \quad 5-12$$

where  $\mu$  and  $\sigma^2$  the mean and the variance of  $X$ , respectively. Thus, the normal distribution is a 2 parameter distribution which is bell-shaped, continuous, and symmetrical about the mean.

With the PDF, measures of the central tendency, prediction spread, limits and skill can be estimated. The central tendency is represented by the 50% simulation limit, or median, corresponding to 0.5 on the cumulative distribution function (CDF). The spread of the forecast represents the forecast uncertainty due to uncertain initial conditions, rainfall inputs, slopes and scale dependent parameters, etc; by determining the distance between the 5% and 95% confident limit simulation bounds.

The ensemble skill is assessed using the ranked probability score or RPS (Epstein, 1969; Murphy, 1971) which is capable of penalizing forecasts increasingly as more probability is assigned to event categories further removed from the actual outcome and the ensemble are encouraged to report their “true beliefs” (Wilks, 1995). Brier scores and reliability diagrams are used to evaluate each of the derived binary forecasting situations, but the RPS is an option for verification forecasts for multi category ordinal predictants.

The ranked probability score is the sum of squared differences between the components of the cumulative forecast and observation vectors as:

$$RPS = \sum_{m=1}^J (Y_m - O_m)^2 \quad 5-13$$

$$RPS = \sum_{m=1}^J [(\sum_{j=1}^m y_j) - (\sum_{j=1}^m o_j)]^2 \quad 5-14$$

where  $Y_m$  and  $O_m$  are the cumulative forecast and observation, respectively,  $y_j$  is the cumulative probability assigned to the category or vector component,  $o_j$  is the cumulative probability of the observation in the  $i$ th category or vector component and  $J$  is the number of categories and therefore also the number of probabilities included in each forecast. The sum of  $Y_m$  and  $O_m$  are always both equal to one by definition.

The PDFs statistics and RPS generated for each grid size will contain the predictability limits for small watersheds and will be useful information that can help the modeler to decide which grid size resolution is appropriate for larger watersheds where it is important to quantify flash flooding at upstream and ungauged sites.

The Figure 5-3 summarizes the evaluation of uncertainty propagation through flow prediction. The flow chart used a combination of hydrologic parameter perturbations within the physical bounds, rainfall input and model resolution or structure set up.

Knowing the uncertainty at the small scale and associated with the resolution selection, it will produce more realistic parameter estimations and flood quantification for the larger scale model. In other words, if the small scale, high resolution model, is characterized by a degree of uncertainty, then the goal of the modeler is to up-scale the resolutions, while maintaining a similar degree of uncertainty. In this way, the modeler hopes to maintain accuracy at the subwatershed scale.

### *5.5.2 Estimation of Uncertainty due to Rainfall up-scaling and temporal variations*

The same methodology described in the previous section (5.5.1) was used to calculate the uncertainty due to rainfall up-scaling and temporal variations. The amounts of rainfall measured by the rain gauge network within the TBSW are assumed to represent the “true” rainfall. The rain gauges are the most reliable method to sense precipitation and are widely used to correct other sensors methods (eg., radar, satellite and laser sensors) and remove sensor bias.

By interpolating to various resolutions, it is possible to measure the importance of spatial rainfall variation in hydrologic prediction while the average rainfall falling on the watershed is maintained, taking into account that the average distance between the rain gauges is approximately 218 m with a standard deviations of 100 m.

Precipitation total variations between rain gauges were calculated and presented for each event, demonstrating the high rainfall variability at small scales due to orographic effects in mountainous subwatersheds. The rainfall events were interpolated to the following resolutions: 100 m, 200 m, 400 m, 1000 m, and 2000 m to compare them in a probabilistic and deterministic sense. The interpolation method used was the inverse distance method. Each ensemble had 625 runs or ensemble members. These were the combination of parameter perturbations described in Section 5.5.1; (125 runs), model structures (5 different model resolutions) and one rainfall event (Figure 5-3). Observed and simulated values are compared by using objective functions. The compared variables

were time to peak, peak flows and volume. In addition, PDFs are computed using the Gaussian kernel density estimation technique and computation of non-parametric statistics provided information for the 0.05, 0.5 and 0.95 quartiles, given the central tendency and spread of the ensemble. The PDFs are treated as conditional probabilities and not as the true probability distribution. RPS's were calculated to compare the skill of each rainfall input. Rainfall events were tested through the year using different antecedent soil moisture conditions and temporal patterns. The dates tested were: October 22, 2007; May 2, 2008; June 5, 2008; August 28, 2008 and September 3, 2008. Performing the statistics previously described for each rainfall configuration ensemble, it was possible to evaluate the reliability of one rainfall resolution and compare them event by event and assess if there exists variations between events.

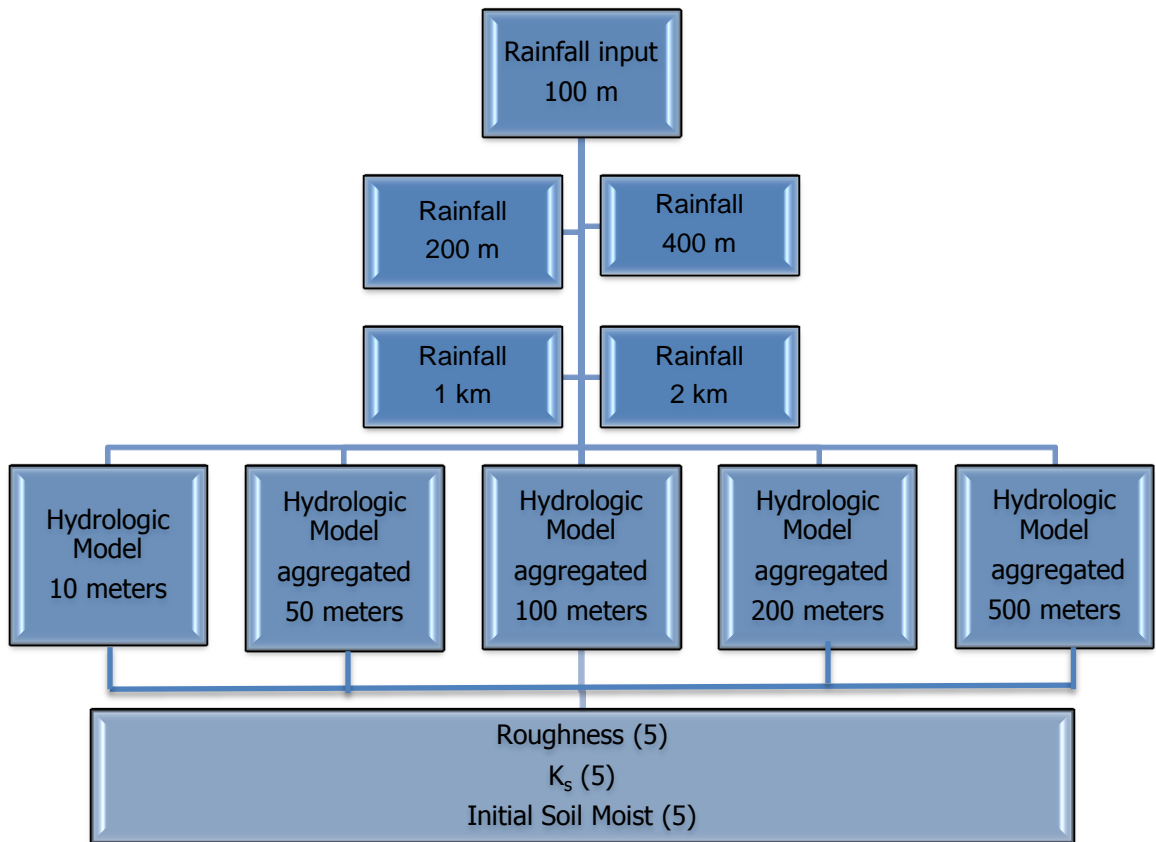


**Figure 5-3 Flow chart of the ensemble for predictability limits**

## CHAPTER 6

### 6 SENSITIVITY ANALYSIS RESULTS

Chapter 6 includes results for the sensitivity analysis performed in the MBDB (Section 6.1) for different hydrologic parameters and rainfall input. Spider plots for percentage changes in peak flow and runoff depth versus scalar factors (0.5, 1, 2.5 and 2)

were plotted. Additionally, relative sensitivity coefficient analysis was addressed for  $\pm$  50 % of parameter and input change (or 0.5 and 1.5 multiplicative factors). The most sensitivity parameters found were used in the up-scaling experiment to be perturbed in the TBSW. Section 6.2 describes the methods to fill the gaps between rain gauges and radar data in the MBDB.

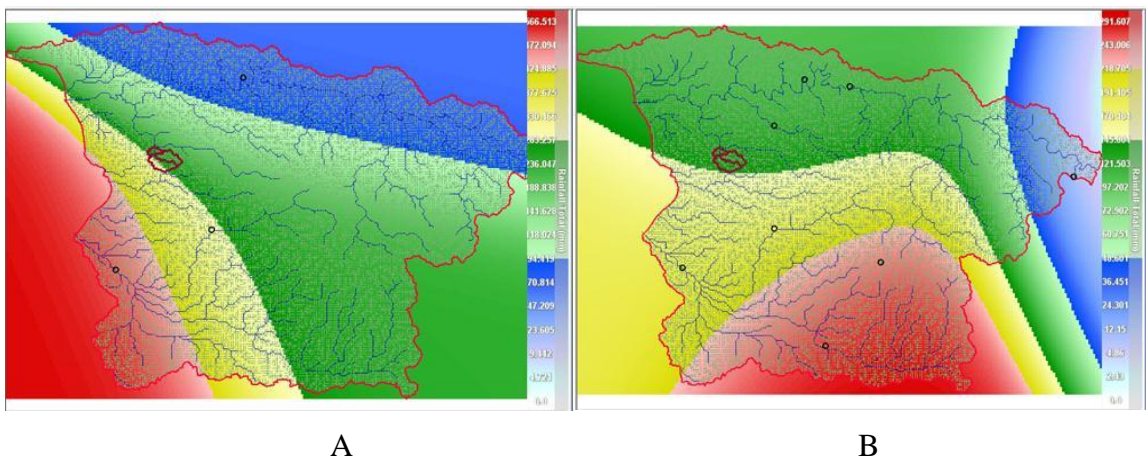
## **6.1 Parameters and Input Sensitivity Results**

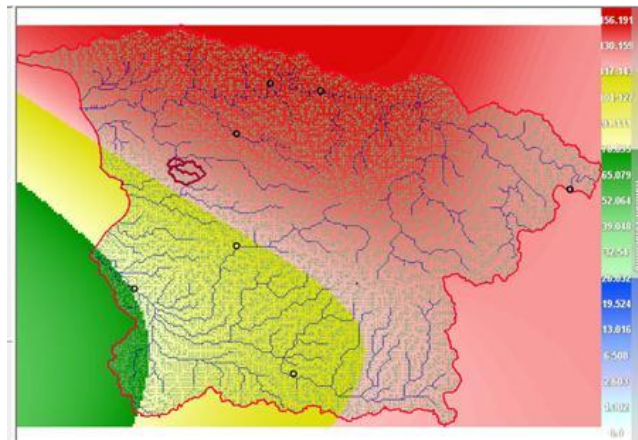
To identify the parameters for which the MBDB model is most sensitive for the mountainous condition considered, a sensitivity analysis was conducted. Uncertainties associated with the model parameters and inputs can be quantified by evaluating the hydrologic response given a range of parameter and input perturbations at 0.5, 1, 1.5 and 2 multiplicative factors or scalars. Within the study area, 3 USGS flow stations were identified, Rio Grande de Añasco near San Sebastian, Rio Guanajibo near Hormigueros and Rio Rosario near Hormigueros. The parameters within the drainage area upstream of the USGS flow stations were perturbed by the multiplicative factors conserving the spatial distribution. Sets of parameter used in the hydrologic model were shown in Table 4-2 and Table 4-4 as well as very shallow soil depth (20 cm) and initial saturation fraction of 0.5 was selected as a preliminary hydrologic model configuration at 200 m resolution.

The rainfall was created using additional USGS stations upon availability for each event. The point rainfall estimates at 15 minutes were interpolated at 200 m resolution

using the exponential weighted interpolation. For hurricane Georges (September 21 to 23, 1998) only three USGS stations mentioned above were working. For November 11 to 16, 2003 event, eight USGS station were interpolated and for September 14 to 17, 2004 seven stations. Figure 6-1 shows the storm total maps for the interpolations performed for each rainfall event at 200 m resolution using the stations available; the dots within each figure are the station locations with data each 15 minutes. The maximum rainfall accumulation during each event was 566.5 mm for September 1998 (red color in Figure 6-1 A), 291.6 mm for November, 2003 (Figure 6-1 B) and 156.2 mm for September, 2004 (Figure 6-1 C).

Spider plots were drawn for the parameters and rainfall perturbed additionally, relative sensitivity coefficients ( $S_r$ ) (Equation 4.1) were calculated with changes of  $\pm 50\%$  using the hydrologic distributed model for 3 events mentioned and 3 outlet points; considering the behavior of 2 output variables (runoff depth and peak discharge).





C

**Figure 6-1 Total storm maps, (A) September, 1998; (B) November 2003; (C) September 2004.**

Spider plots are used to evaluate the model response to the entire range of the parameter and determine if there is a portion of the parameter range that yields unrealistic results. Figure 6-1, **Error! Reference source not found.** presents the spider plots for peak flow as percent change in the model output variable versus change in rainfall value by a multiplicative given factor. Variations in the hydrologic response are linear; doubling the rainfall input increase the peak flow from 131.7% to 203.2% for Rio Guanajibo near Hormigueros depending on the rainfall event. In the case of Rio Grande de Añasco near San Sebastian the range is between 135.3 % and 168.5% and for Rio Rosario near Hormigueros is between 127.7% and 145.3%.

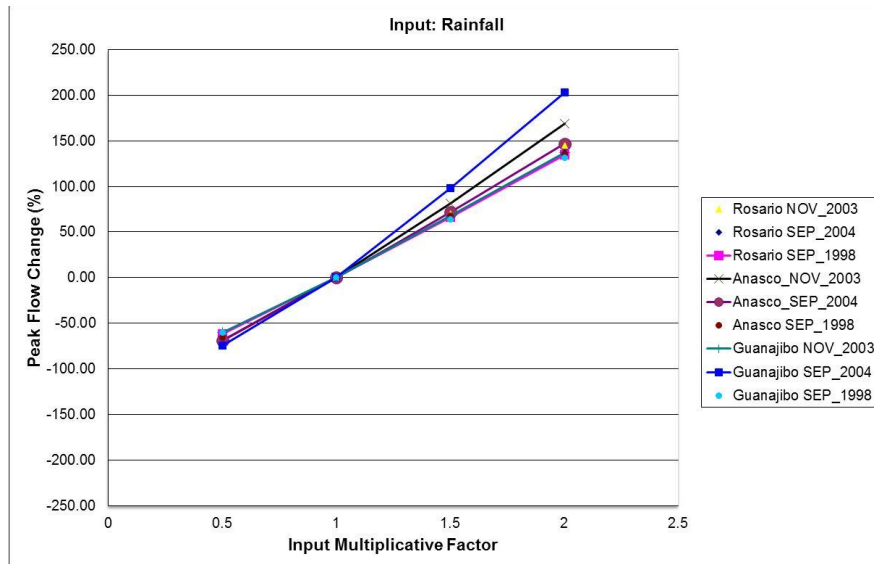


**Figure 6-2 Spider plot for percentage change in peak flow due to rainfall multiplicative factors at 3 USGS station outputs**

**Error! Reference source not found.** present the spider plot for runoff depth where the linearity between rainfall perturbations and hydrologic response was not conserved. For example doubling rainfall generates a runoff depth change between 111.5% and 145% for Guanajibo and for Añasco 131.4 % and 135.0 %; and for Rosario between 112.4 % and 120.6%. These results indicate that the infiltration is decreased with increasing the rainfall intensity providing the volume to the runoff that could not be infiltrated. Decreasing the rainfall intensity by 0.5 multiplicative factor, favors infiltration and decreases the runoff depth with percent changes between 25.5% and 64.8%. Lower percentages are presented for September 2004 (25.5% - 31.8%), which has a rainfall pattern different from the others (Figure 6-1 C). This event is characterized by high

rainfall intensity (red color) in the upland and lower in the flood plains. Minor percent variations occur with the peak flow for Añasco and Rosario discharge points (61.9% to 69.1%) compared with Guanajibo (50 % to 74%).

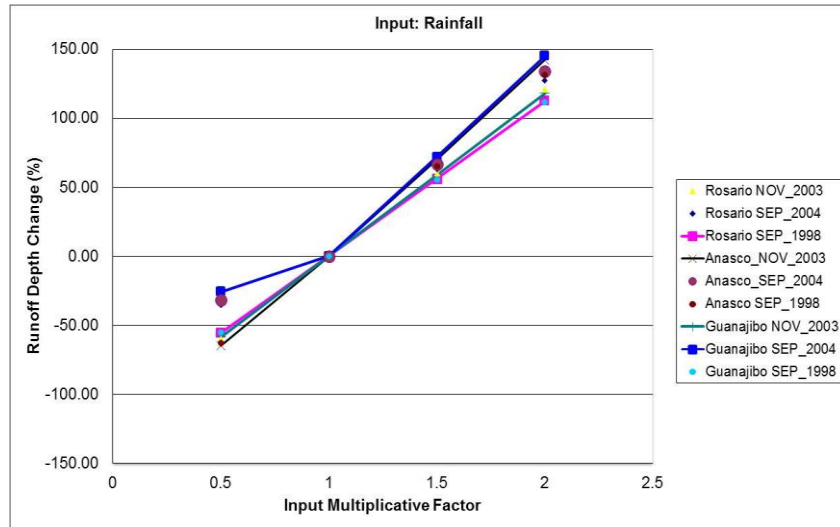
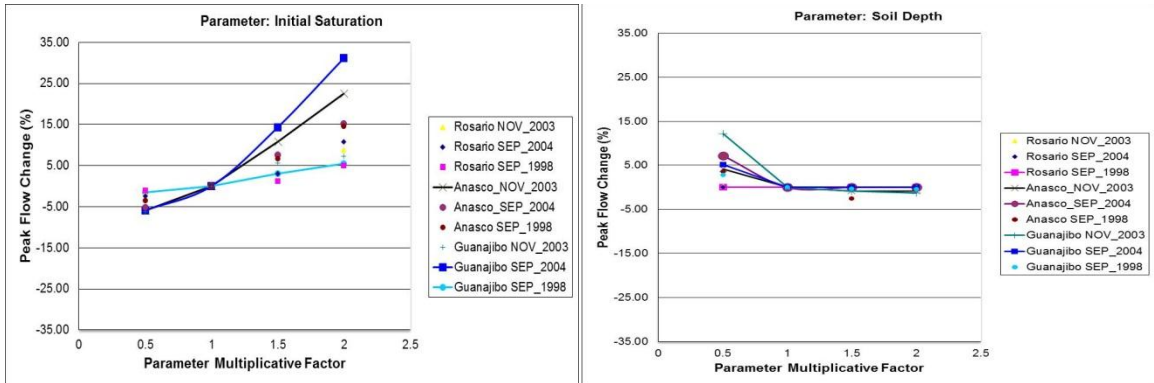


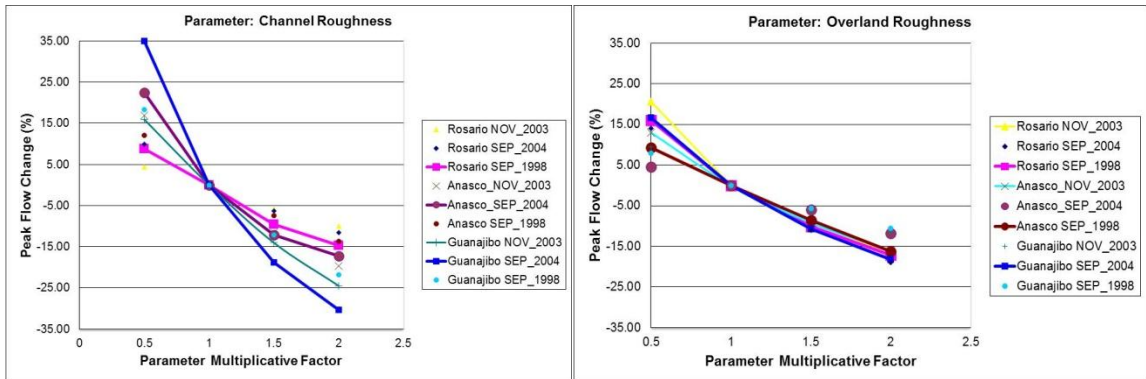
**Figure 6-3 Spider plots for percentage change in runoff depth due to rainfall multiplicative factors at 3 USGS station outputs**

Increasing channel roughness decreased the peak flow (Figure 6-4C), while increasing initial soil saturation increased the peak flow (Figure 6-4A), especially in Rio Guanajibo near Hormigueros outlet point, for September, 2004. Low variations were founded in peak flow with variations of soil depth and hydraulic conductivity for all events (Figure 6-4B, E, F).



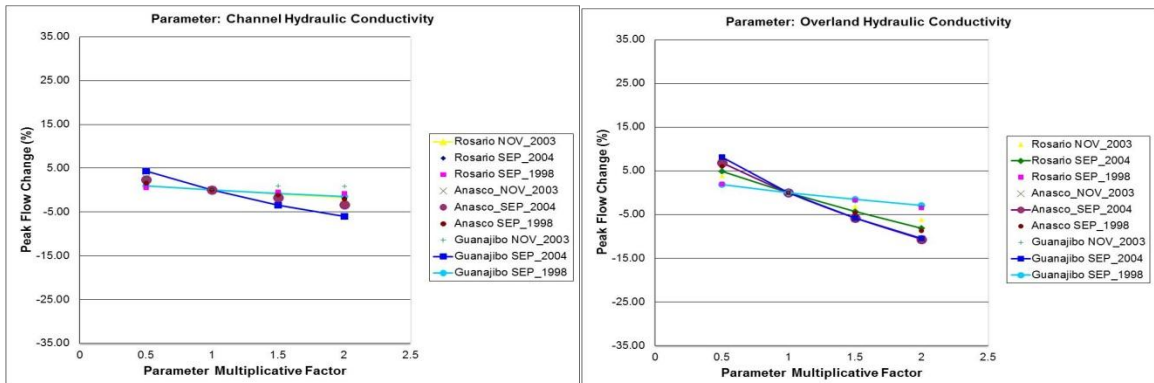
A

B



C

D

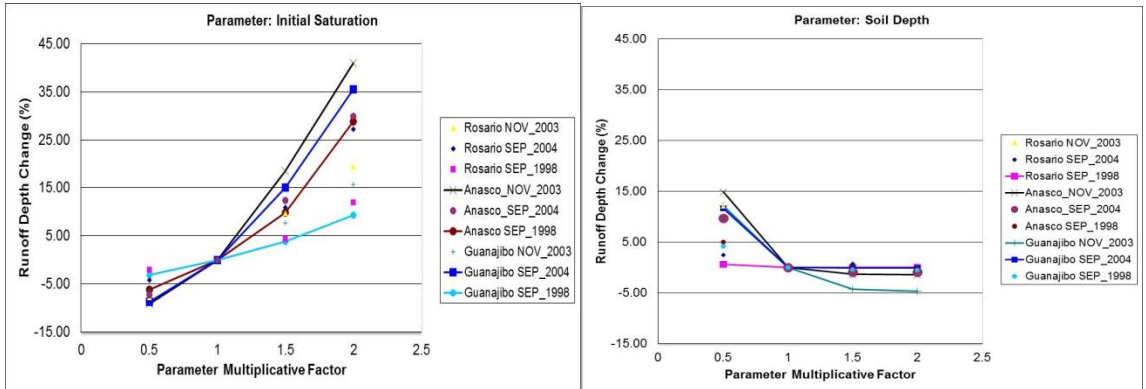


E

F

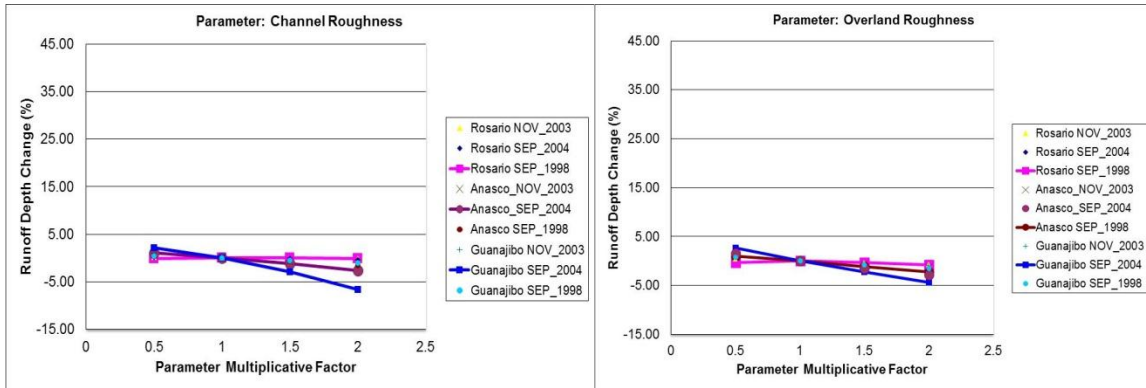
**Figure 6-4 Spider plots for changes in peak flow due to parameters multiplicative factors evaluated at USGS stations and 3 events. Parameters: A) Initial Saturation, B) Soil Depth, C) Channel Roughness, D) Overland Roughness, E) Channel hydraulic conductivity, F) Overland hydraulic conductivity.**

Additionally, spider plots graphs for runoff depth changes were calculated and presented in Figure 6-5 for each parameter evaluated. As for peak flow, the spider plot percent changes were graphed for different events and outlet points. The parameter that produced the greatest percentage change in runoff depth was the initial soil saturation (Figure 6-5A), for Añasco near San Sebastian outlet point for November 2003 and September 1998 and Guanajibo near Hormigueros for September, 2004. Generating a change between 30% and 40% in runoff depth due to doubling in the initial soil saturation, where the baseline was 0.5 and doubling produced a value of 1 (i.e., saturated conditions). Low variations were found with changes of the other parameters (Figure 6-5, B, C, D, E, F). The magnitude of change varied with the event indicating that the rainfall spatial distribution and intensity are important aspects for quantification of initial parameters.



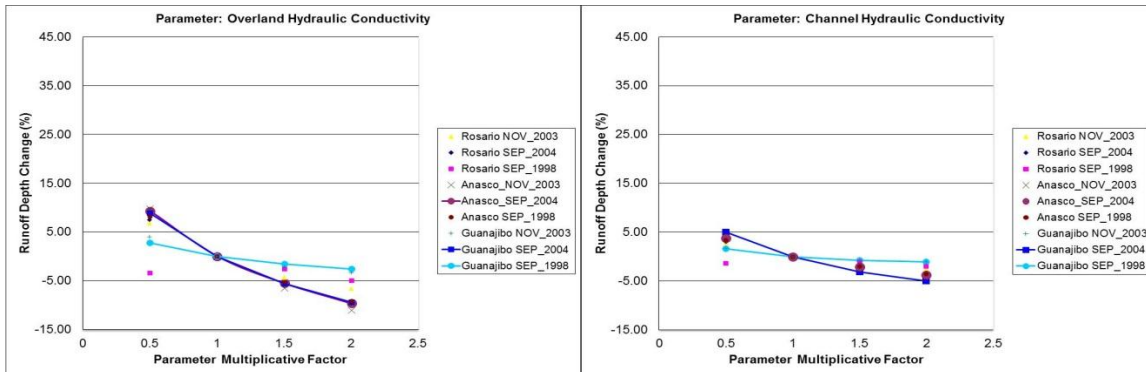
A

B



C

D



E

F

**Figure 6-5 Spider plots for changes in runoff depth due to parameter multiplicative factors evaluated at USGS stations and 3 events. Parameters: A) Initial Saturation, B) Soil Depth, C) Channel Roughness, D) Overland Roughness, E) Channel hydraulic conductivity, F) Overland hydraulic conductivity.**

Relative sensitivity coefficients were calculated for parameters and rainfall input using each event and outlet point. Results are presented in Table 6-1 for the peak flows and Table 6-2 for runoff depth as well as averages and standard deviations.

Results given below indicate that variations for both output variables (peak flow and runoff depth) are most sensitive to the rainfall input with a Sr of 69.1 and 56.5, respectively. Runoff depth was affected by initial saturation, increases in this parameter increased the runoff and a Sr value of 8.2 was obtained. Followed by overland hydraulic conductivity with a Sr of -5.5, increase in this parameter decreased the runoff depth; and increasing soil depth produced a decrease in peak flows (Sr of -4.4). Low variations were observed when soil depth was doubled, indicating that soil depths greater than 40 cm will produce little runoff depth changes (Figure 6-4 B).

The peak discharge was affected by roughness with a Sr of -13.4 for channel cells and Sr of -10.6 for overland cells; increases in roughness parameter decreased the peak flows and retarded the time to peak. The slope-distributed map produced a Sr of 12.6, increasing this parameter increased peak flow. The initial soil saturation parameter produced a Sr of 5.2 and is placed in the fifth place. Average relative sensitivities coefficients were plotted in Figure 6-6 and Figure 6-7 with observed variations in terms of basin outlet points or events.

**Table 6-1 Relative sensitivity analysis for peak flow evaluating 3 events and 3 USGS station outlet points for peak flow**

	<i>Rosario</i>				<i>Añasco</i>				<i>Guanajibo</i>				<i>Average Sr</i>	<i>STD</i>
	<i>Nov-03</i>	<i>Sep 04</i>	<i>Sep 98</i>	<i>Mean</i>	<i>Nov 03</i>	<i>Sep 04</i>	<i>Sep 98</i>	<i>Mean</i>	<i>Nov 03</i>	<i>Sep 04</i>	<i>Sep 98</i>	<i>Mean</i>		
<b><i>Rainfall</i></b>	66.85	66.86	63.87	65.9	75.3	70.4	66.7	70.8	63.8	86.1	62.1	70.7	69.1	7.5
<b><i>Rough Ch</i></b>	-5.07	-8.13	-9.14	-7.4	-14.3	-17.3	-9.8	-13.8	-15.0	-26.9	-15.2	-19.0	-13.4	6.4
<b><i>Slope</i></b>	10.76	10.20	11.85	10.9	13.1	11.9	10.5	11.8	12.7	20.6	11.9	15.1	12.6	3.1
<b><i>Rough over</i></b>	-15.47	-12.55	-13.07	-13.7	-11.1	-5.3	-9.0	-8.5	-8.1	-13.7	-6.8	-9.5	-10.6	3.4
<b><i>IS</i></b>	4.42	2.75	1.18	2.8	8.3	6.4	5.1	6.6	5.9	10.1	2.3	6.1	5.2	2.9
<b><i>K<sub>S</sub> Over</i></b>	-3.52	-4.55	-1.89	-3.3	-6.8	-6.3	-5.3	-6.1	-3.4	-7.0	-1.7	-4.0	-4.5	1.9
<b><i>Soil Depth</i></b>	-0.10	0.00	-0.03	0.0	-2.5	-3.6	-3.1	-3.0	-6.5	-2.6	-1.5	-3.6	-2.2	2.1
<b><i>K<sub>S</sub> Chan</i></b>	-0.97	-1.07	-0.44	-0.8	-2.5	-2.1	-1.4	-2.0	-0.9	-3.9	-0.8	-1.9	-1.5	1.1

**Table 6-2 Relative sensitivity analysis for 3 events and 3 USGS station outlet points for runoff depth**

	<i>Rosario</i>				<i>Añasco</i>				<i>Guanajibo</i>				<i>Average</i>	<i>STD</i>
	<i>Nov-03</i>	<i>Sep-04</i>	<i>Sep-98</i>	<i>Mean</i>	<i>Nov-03</i>	<i>Sep-04</i>	<i>Sep-98</i>	<i>Mean</i>	<i>Nov-03</i>	<i>Sep-04</i>	<i>Sep-98</i>	<i>Mean</i>		
<b><i>Rainfall</i></b>	60.00	49.22	55.82	55.0	67.5	49.2	64.1	60.3	58.6	48.7	55.5	54.3	56.5	6.74
<b><i>IS</i></b>	8.75	7.55	3.18	6.5	13.8	9.9	8.0	10.6	7.0	11.9	3.5	7.5	8.2	3.50
<b><i>K<sub>S</sub> Over</i></b>	-5.57	-6.42	-3.04	-3.9	-8.1	-7.4	-6.7	-7.4	-3.1	-7.2	-2.2	-4.2	-5.5	2.20
<b><i>S Depth</i></b>	-6.04	-0.86	-0.28	-2.4	-8.1	-5.3	-2.6	-5.3	-8.2	-5.8	-2.3	-5.4	-4.4	2.98
<b><i>K<sub>S</sub> Chan</i></b>	-2.28	-2.57	1.24	-1.6	-3.4	-3.0	-2.7	-3.0	-1.2	-4.1	-1.2	-2.2	-2.4	1.30
<b><i>Slope</i></b>	0.39	0.88	0.28	0.5	1.4	2.2	1.0	1.5	0.9	3.9	0.9	1.9	1.3	1.12
<b><i>Rough over</i></b>	-0.37	-1.06	-0.35	-0.5	-0.7	-1.5	-1.1	-1.1	-0.5	-2.5	-0.8	-1.3	-1.0	0.67
<b><i>Rough Ch</i></b>	-0.09	-0.15	-0.05	-0.1	-0.6	-1.2	-0.6	-0.8	-0.6	-2.5	-0.4	-1.2	-0.7	0.77

Legend: IS= initial saturation, K<sub>S</sub> Over = overland hydraulic conductivity; K<sub>S</sub> Chan = channel hydraulic conductivity; Rough Ch = channel roughness; Rough over = overland roughness; S Depth = soil depth.

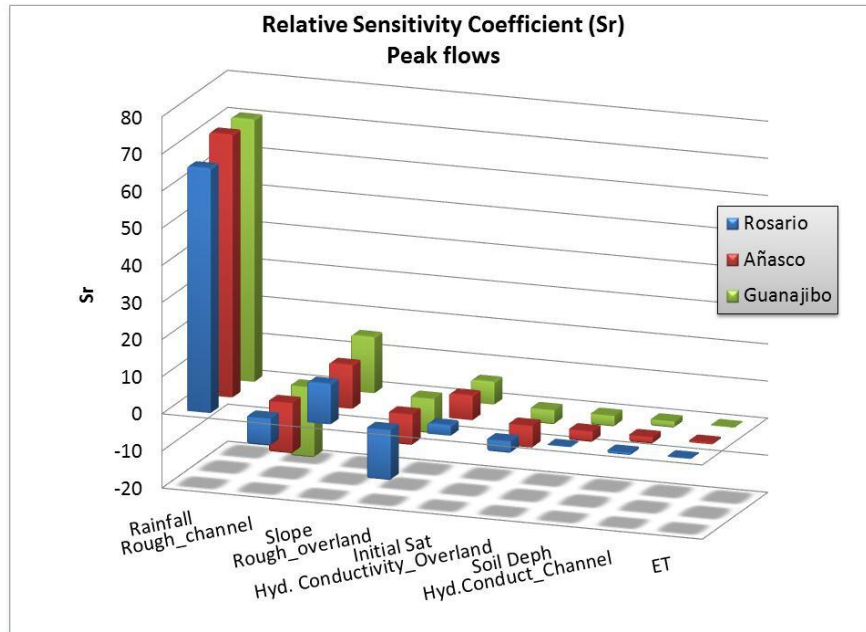


**Figure 6-6 Mean relative sensitivity coefficients for peak flows at three USGS outlet points**

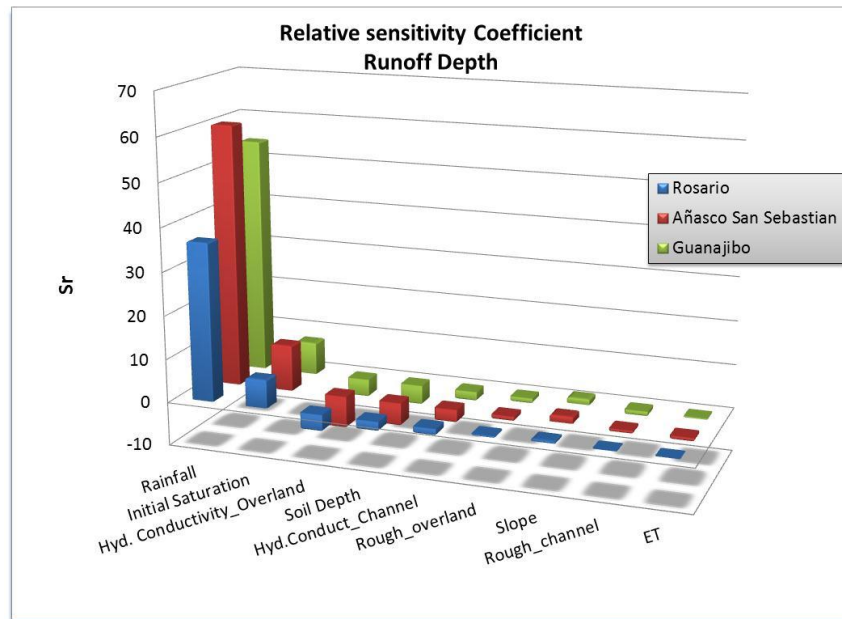
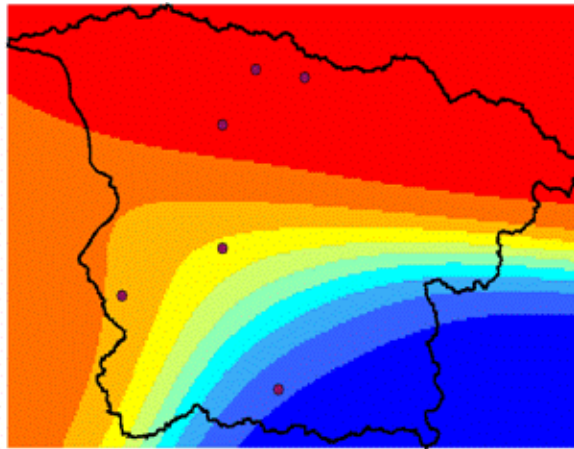


**Figure 6-7 Mean relative sensitivity coefficient for runoff depth at three USGS outlet points**

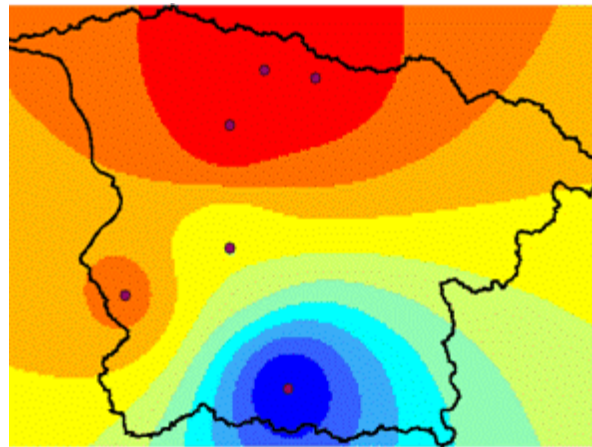
## 6.2 Sensitivity due to quantitative precipitation estimation within gap areas

The Vflo model has the capability to support distributed rainfall and rain gauge data in real time, ideal for a flood alarm system. However, rainfall itself is the principal source of uncertainty in the model as observed in the previous section. The number of rain gauges in a basin are frequently sparse and therefore do not capture the spatial variability.

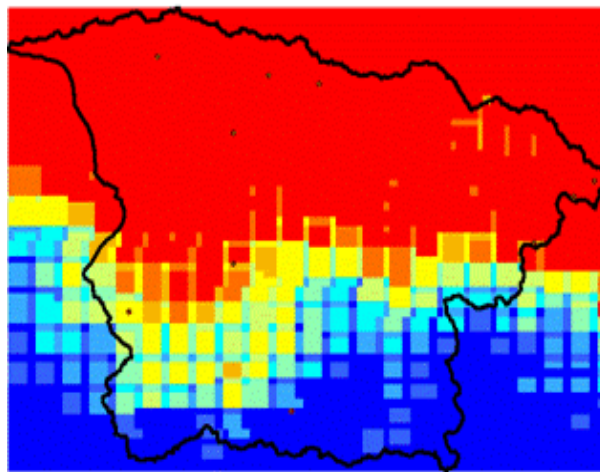
Two interpolation methods, exponential weighted (EW, Figure 6-8**Error! Reference source not found.**A), and inverse distance weighted (IDW, Figure 6-8**Error! Reference source not found.**B), were compared with radar rainfall from NEXRAD level 3 as seen in Figure 6-8**Error! Reference source not found.**C, for the November 11-16, 2003 period. The average total storm rainfall calculated at an outlet point is different between interpolation methods and radar source. For example for the USGS station Rio Grande de Añasco near San Sebastian the precipitation average depth is 122.8 mm for IDW, 114.8 mm and for EW and 77.8 mm for radar. In the USGS station at Rio Guanajibo near Hormigueros, the total storm was 230.6 mm with IDW, 237.1 mm and for EW and 199.8 mm for radar. It should be noted that the radar is partially dependent on the rain gauge data and number of stations. Furthermore, when we use radar, it is necessary to remove systematic error by applying a calculated correction factor or bias (Vieux, 2004) for the event, which is the relationship between rain gauges and the radar data. For November, 2003 event, the bias calculated for the whole area was 1.3 (Equation 5-6). Figure 6-9**Error! Reference source not found.** displays the scatter plot of radar and rain gauges and the adjusted line.



A



B



C

**Figure 6-8 Total Storm Rainfall Maps at Mayagüez Bay Drainage Basin for November 11-16, 2003 using Interpolation Methods: (A) Exponential Weighted; (B) Inverse Distance Weighted; and Radar data (C)**

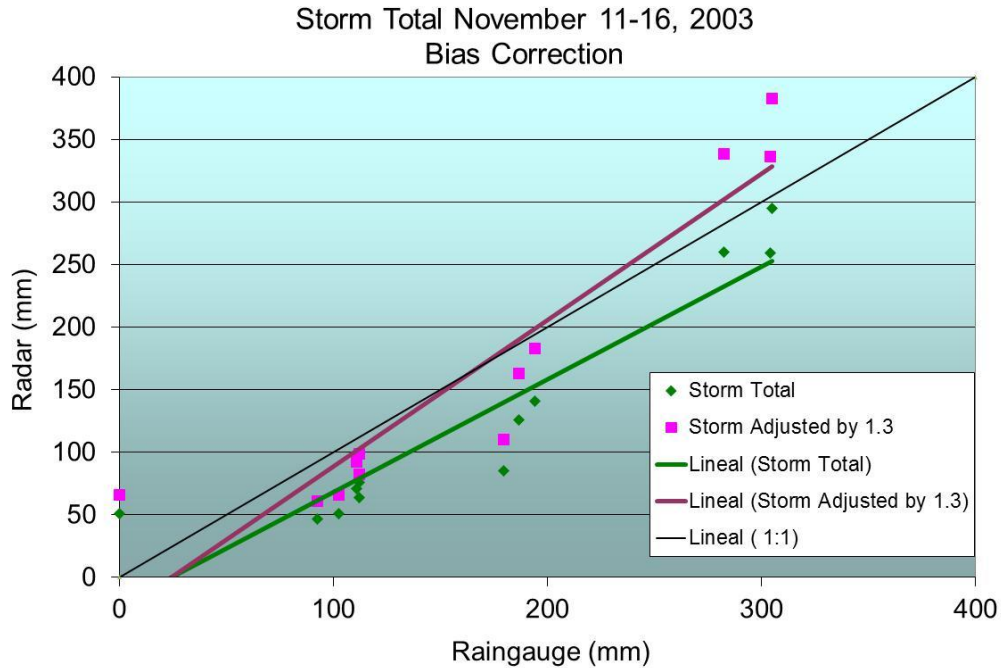


**Figure 6-9 Radar Bias correction for storm total, November 11-16, 2003**

Variations between methods to fill the gaps between rain gauges produce different responses in flow prediction. For example for the MBDB model we performed hydrologic simulations using the EW and IDW interpolation methods at 200 m resolution and NEXRAD radar level 3 at 2 km spatial resolution with a nominal resolution of 500 m. The results were compared at Rio Grande de Añasco near San Sebastian and Guanajibo near Hormigueros stations generating differences in peak flow runoff depth and average total rainfall (Table 6-3). The EW method produced greater peaks (2.4%) and runoff depth (2.5%) at Guanajibo outlet point, with a decrease in rainfall total storm (2.9 %) than IDW. The reverse effect was observed at Rio Grande de Añasco where decreasing

the rainfall total rainfall (-6.5%) generated proportional decrease in peak flow (-7.1%) and runoff depth (-6.8%). The radar rainfall quantification is -12.9 % and -36.7 % lower than IDW for Guanajibo and Añasco respectively, however the reduction in peak flow was not in the same proportion indicating that the rainfall intensity was maintained.

**Table 6-3 Comparison of hydrologic results and rainfall interpolation methods and radar**

	<b>Rio Guanajibo near Hormigueros</b>					
	<b>Peak Flow</b>		<b>Runoff depth</b>		<b>Rainfall</b>	
	<b>(cms)</b>	<b>Percent change</b>	<b>(mm)</b>	<b>Percent change</b>	<b>(mm)</b>	<b>Percent change</b>
<i>IDW</i>	394.1	reference	145.9	reference	230.6	reference
<i>EW</i>	403.4	2.4	149.6	2.5	237.1	2.9
<i>Radar</i>	376.6	-4.4	128.5	-11.9	200.9	-12.9
	<b>Rio Grande de Añasco near San Sebastian</b>					
<i>IDW</i>	668.4	reference	117.6	reference	122.8	reference
<i>EW</i>	620.9	-7.1	109.6	-6.8	114.8	-6.5
<i>Radar</i>	642.8	-3.8	72.4	-38.5	77.8	-36.7

## CHAPTER 7

### 7 BIAS ESTIMATION IN RADAR PRECIPITATION PRODUCT

In this chapter, an analysis of the rainfall spatial variability in a small area with a high density rain gauge network is described. Radar rainfall estimations were compared and evaluated with the rain gauge data. Statistical measurements of discrete and continuous validation scores were calculated for the radar estimates at hourly and daily time step. PDFs were calculated for the Bias with the purpose of knowing the rainfall uncertainty over a small area.

To compare the Multisensor Precipitation Estimates (MPE) with the rain gauge network rainfall accumulation time series, it is necessary to convert the MPE HRAP grid projection to a State Plane raster product, which will be used in the hydrological model. Due to changes in coordinates and raster conversions, the original pixels (HRAP projection) oriented with a certain angle, were reoriented horizontally (raster). Figure 7-1 displays the change in the orientation, including the MPE pixels (left) and Hourly Rainfall Product (N1P) from NEXRAD level 3 (right). The left image shows four square black boxes corresponding to the MPE raster-projected pixels, the colored pixels are the original raster with HRAP coordinates at 4 km x 4 km spatial resolution, and the red box corresponds to the Hydro-Estimator pixel at the same resolution as the MPE product.

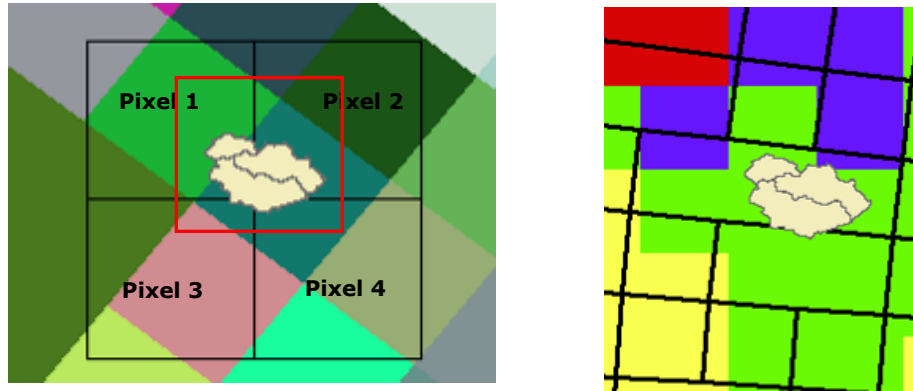


**Figure 7-1 HE pixel (red box) and MPE pixels (black and colored boxes) (left) and Hourly Rainfall Product (N1P) from NEXRAD level 3 (right) orientated in shapefile and raster formats.**

The annual 2007 rainfall accumulations for the 4 MPE pixels were 1546.2, 2212.1, 1949.8 and 2088.6 mm, with an annual standard deviation of 289.3 mm between them. Figure 7-2 shows the temporal variations in the cumulative rainfall during the year for each MPE Pixel. Large differences are found between Pixel 1 and Pixel 2.

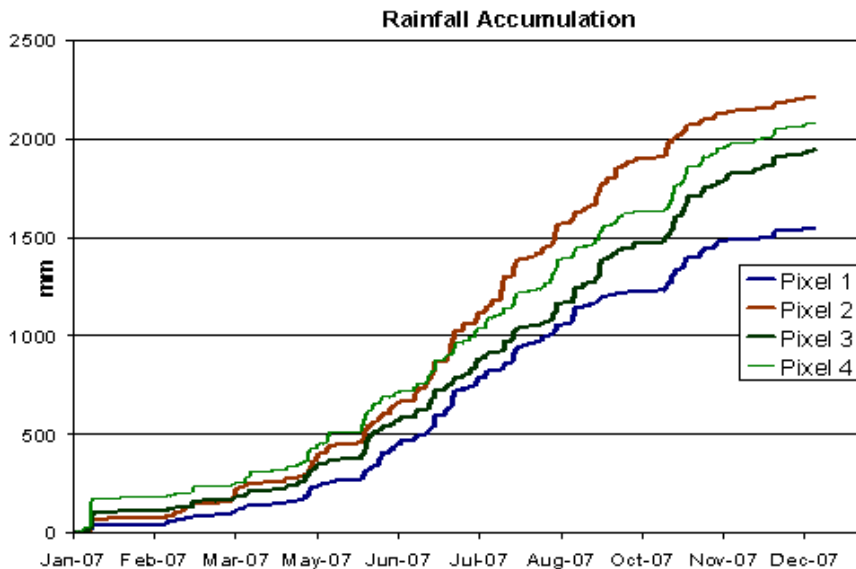


**Figure 7-2 Rainfall accumulation over the time for the MPE pixels.**

To show how variable the rainfall distribution within a specific pixel can be, we took the MPE Pixel numbers 1 and 2 and determined the rain gauges associated with each pixel. A plot of the monthly cumulative rainfall for MPE Pixel 1 and rain gauges are displayed in Figure 7-3.

The cumulative rainfall for the months of April and May are not representative of those months because we had missing rain gauge data for 11 days for April and 9 days for May, therefore, the computations were made with only the available data for these months. For the case of July, Figure 7-3 shows that only the C06 station reported an amount of rainfall (206.9 mm) that was similar to the MPE Pixel 1 rainfall (259.15 mm), and for almost all months, note that the MPE Pixel 1 underestimated the rainfall value with respect to rain gauges, except for the months of January, June and July.

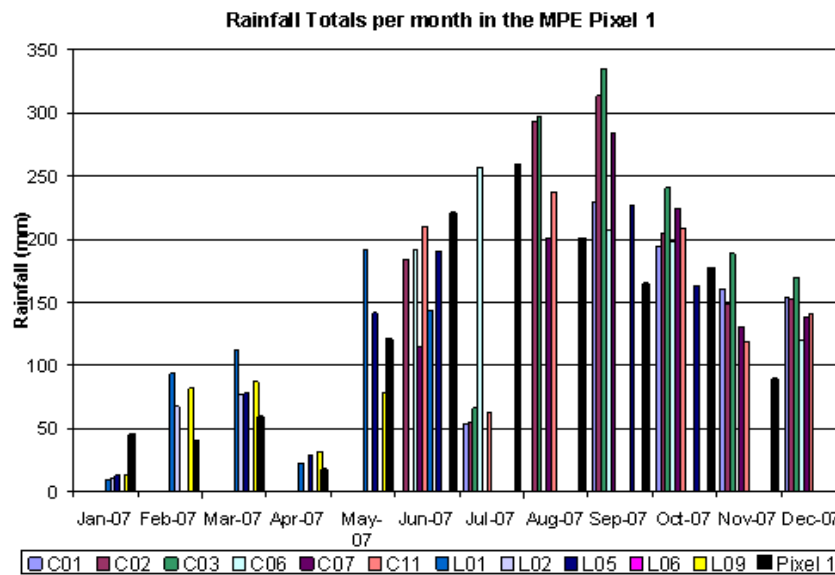


**Figure 7-3 Monthly Total Rainfall calculation for the rain gauge stations belonging to MPE Pixel 1, for 2007.**

Figure 7-4 displays the average rain gauge network rainfall in MPE Pixel 1 versus the standard deviation for 1-hour time step for 2007. The slope between standard deviation and mean rainfall is equivalent to the coefficient of variation (CV), and is a measure of the dispersion of the probability distribution. From the regression analysis, a  $R^2$  of 0.6627 and a CV of 0.3766 were obtained, indicating high rainfall variability in the MPE pixel 1, which cover an area of 4.5 km<sup>2</sup>.

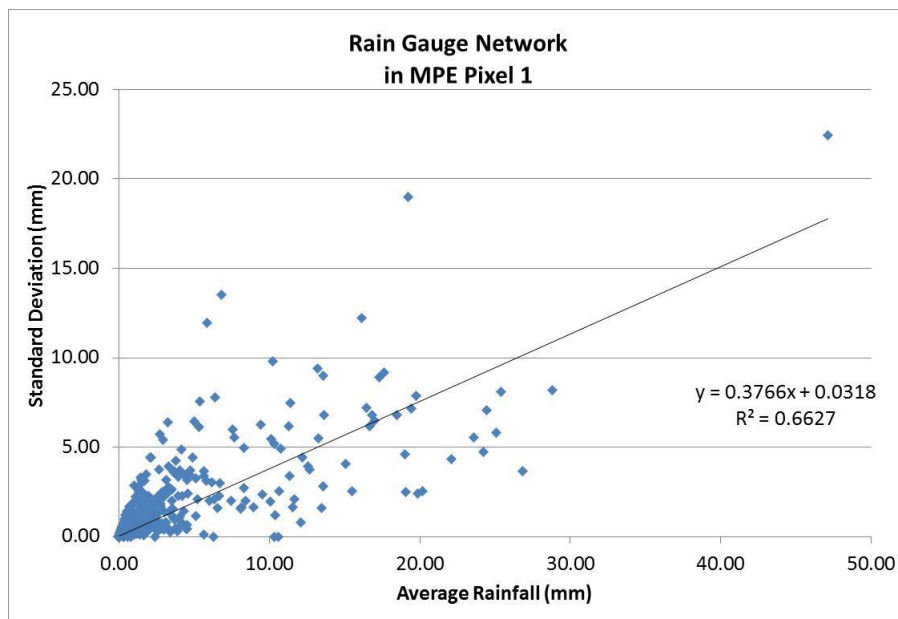


**Figure 7-4 Hourly average and standard deviation rainfall for the rain gauge network corresponding to MPE pixel 1 for 2007**

The rain gauge network covering an area of 16 km<sup>2</sup> shows that the relationship between mean rainfall and standard deviation has the trend of an increase in rainfall depth will produce an increase in standard deviation. The linear regression indicates a  $R^2$  of 0.78 and a slope of 0.45 (Figure 7-5). An increase in CV exists between Figure 7-5 and Figure 7-6, related to an expansion of the rain gauge area from 4.5 km<sup>2</sup> to 16 km<sup>2</sup>

indicating an increase in dispersion of the data. Therefore, the coefficient of determination increases, indicating that the standard deviation of a sample of mean rainfall can be obtained with more accuracy than in small areas.

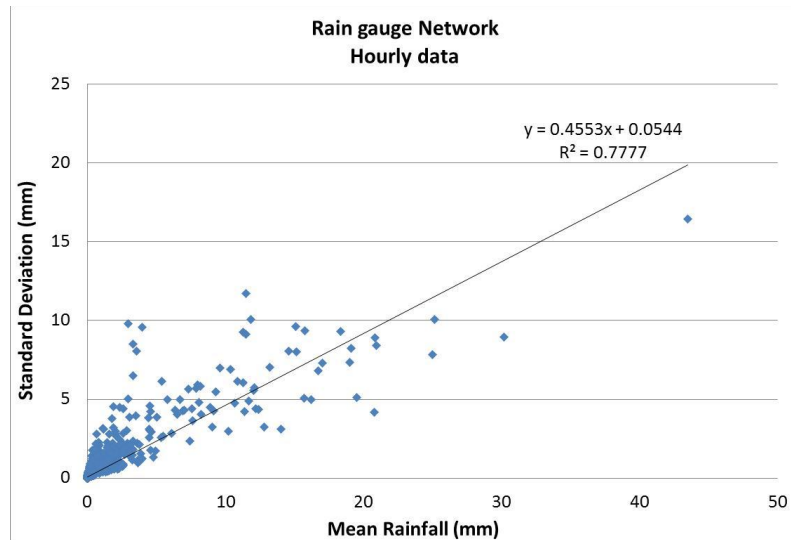


**Figure 7-5 Hourly average and standard deviation rainfall for rain gauge network for 2007**

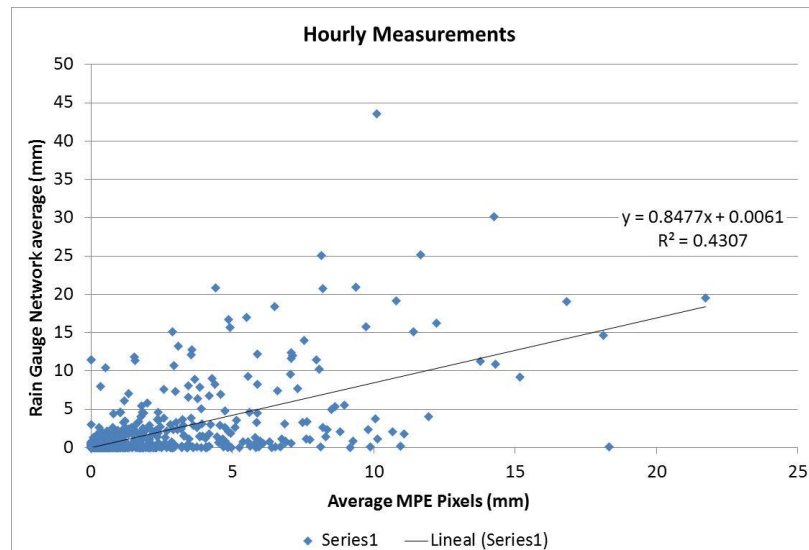


**Figure 7-6 Average rain gauge rainfall vs. MPE radar rainfall within HE pixel at hourly time step.**

Mean rain gauge network data and mean weighted MPE rainfall were graphed at the hourly time step and a linear regression equation was calculated (Figure 7-6) obtaining a slope line of 0.848 and a  $R^2$  of 0.43. The slope represents the Bias between the rainfall from the gauge network and the MPE radar product, and this value can be applied to the hourly MPE measurements as a correction. The MPE in general is overestimating precipitation with a coefficient of determination of 0.4307. The MPE exhibits problems of detection at low rainfall measurements principally (Figure 7-6).

The contingency tables and scores (**Error! Reference source not found.** and **Error! Reference source not found.**, respectively) were calculated to evaluate the Pixel 1, Pixel 2 and total 4 MPE pixels for hourly time step and daily rainfall accumulations for the four MPE pixels within the HE pixel. The number of estimated rainfall events were overestimated according to the discrete bias (DB) in the MPE pixel 1 (1.24) comparing with the Pixel 2 and the 4 MPE pixels, which have a values close to 1. For daily data the DB is underestimated by a factor of 0.956.

The hit rate (H) indicates the occasions when the categorical estimation correctly determined the occurrence of rainfall event or nonevent and was around 0.82 and 0.89; non-significant differences were found between hourly and daily accumulations at the 4 pixels.

Moreover, the probability of detection (POD) is the likelihood that the event would be estimated by the radar, increasing with the time step, with 0.833 for the daily data. Daily estimates eliminate the influence of light rainfalls that the radar cannot detect. For the

hourly time step, the Pixel 1 POD was higher than the POD for Pixel 2 and the average of 4 MPE pixels.

**Table 7-1 Contingency tables for the MPE pixels.**

Hourly Data MPE Pixel 1		Observed Rainfall (Rain gauges)	
		Yes	No
<b>Estimated MPE Rainfall</b>	Yes	638	653
	No	400	6581
Hourly Data MPE Pixel 2		Observed Rainfall (Rain gauges)	
		Yes	No
<b>Estimated MPE Rainfall</b>	Yes	630	464
	No	449	6729
Hourly Data 4 MPE Pixels		Observed Rainfall (Rain gauges)	
		Yes	No
<b>Estimated MPE Rainfall</b>	Yes	915	756
	No	693	5910
Daily Data 4 MPE Pixel		Observed Rainfall (Rain gauges)	
		Yes	No
<b>Estimated MPE Rainfall</b>	Yes	225	33
	No	45	341

**Table 7-2 Discrete validation scores for the MPE pixels and time scales.**

	Hourly Data			Daily Data
	MPE Pixel 1	MPE Pixel 2	4 MPE pixels	4 MPE pixels
<b>POD</b>	0.62	0.58	0.57	0.833
<b>FAR</b>	0.51	0.42	0.45	0.128
<b>DB</b>	1.24	1.01	1.04	0.956
<b>H</b>	0.87	0.89	0.82	0.879

False alarm rates or portion of estimated rainfall events that fail to materialize are similar in Pixels 1, 2 (0.50 and 0.42, respectively) and the four pixels average (0.45). For the daily time step there was a considerable reduction in the FAR (0.128). Figure 7-7 and Figure 7-8 show the distribution of false alarms and the probability of no detection by the radar during 2007. Events in which the radar did not detect rainfall and the rain gauges did measure rainfall (c) were assigned a value of 1 in the graph. Events in which the radar did detected rainfall and the gauges did not measure rainfall (b) were assigned a value of 2. Differences in time when false alarms and probability of no detection quantities occurred can be observed in the graphs, and detailed statistics are presented in **Error! Reference source not found.** and **Error! Reference source not found.**

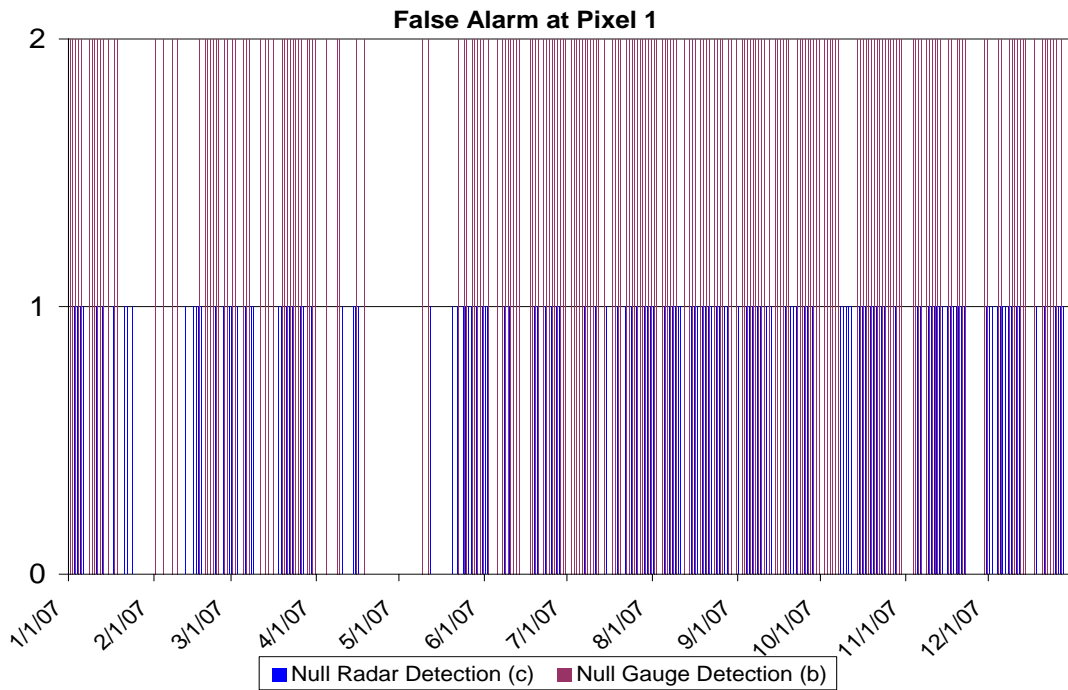


**Figure 7-7 Hourly False Alarm Time Series for the MPE Pixel 1 for 2007.**

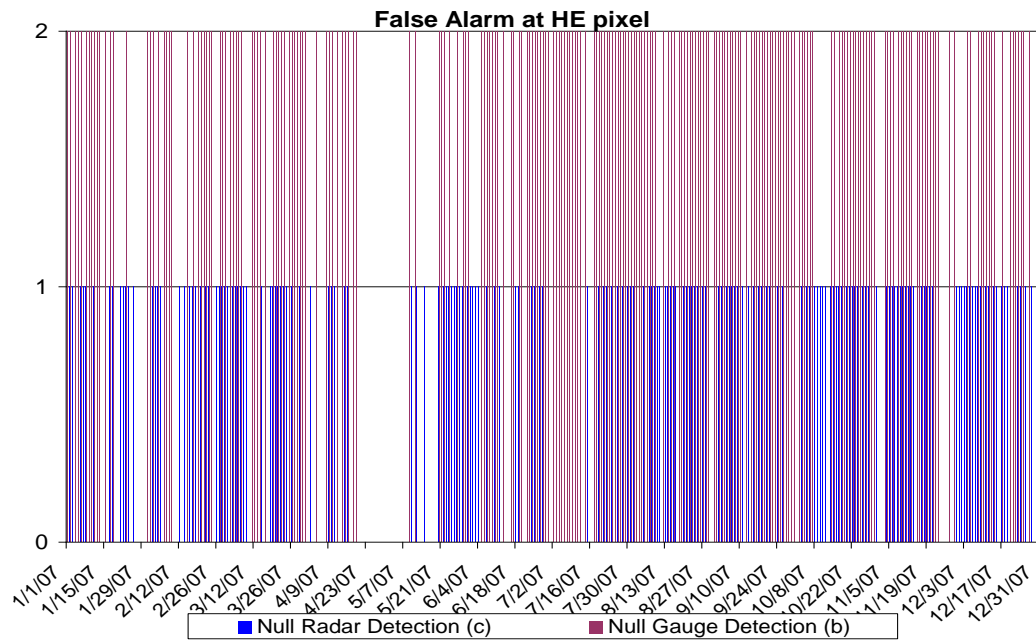


**Figure 7-8 Hourly False Alarm Time Series for the MPE Pixels within a HE Pixel for June to December 2007.**

**Table 7-3 Continuous validation scores for the MPE pixels and time scales.**

	Mean Hourly				Daily Data
	MPE Pixel 1	MPE Pixel 2	4 MPE pixels	4 MPE pixels Rain $\geq$ 0.3mm	4 MPE pixels
<i>RMSE</i>	-	-	0.012	-	0.368
<i>Bias</i>	3.85	1.58	2.77	1.55	1.23
<i>STD Bias</i>	4.21	2.73	8.18	2.14	1.65

A mean field bias (Bias) was calculated for the MPE Pixel 1, 2 and overall 4 pixels, as the ratio of the average of the rain gauge rainfall and the mean rainfall sensed for the MPE pixels using the area weights for each time step (hourly, daily, monthly and annually accumulations). Hourly mean field bias time series during the 2007 are

displayed in the Figure 7-9 for the MPE Pixel 1 only and Figure 7-10 for the mean four MPE pixels within the HE pixel.

Large biases were found at the hourly time step and are associated with small radar rainfall and rain gauge detections (Figure 7-9). The possible effect is that the radar minimum precipitation depth capable of being detected is 0.01 inches or 0.254 mm; while our rain gauge network has a rainfall depth resolution of 0.1 mm. In addition, the NEXRAD in Puerto Rico is located about 100 km from the study area in Cayey at a site elevation of 850 meters msl. Due to the earth curvature, the beam has an elevation of 600 m above the study site at Mayagüez, affecting the cloud's measurement in the lower troposphere.

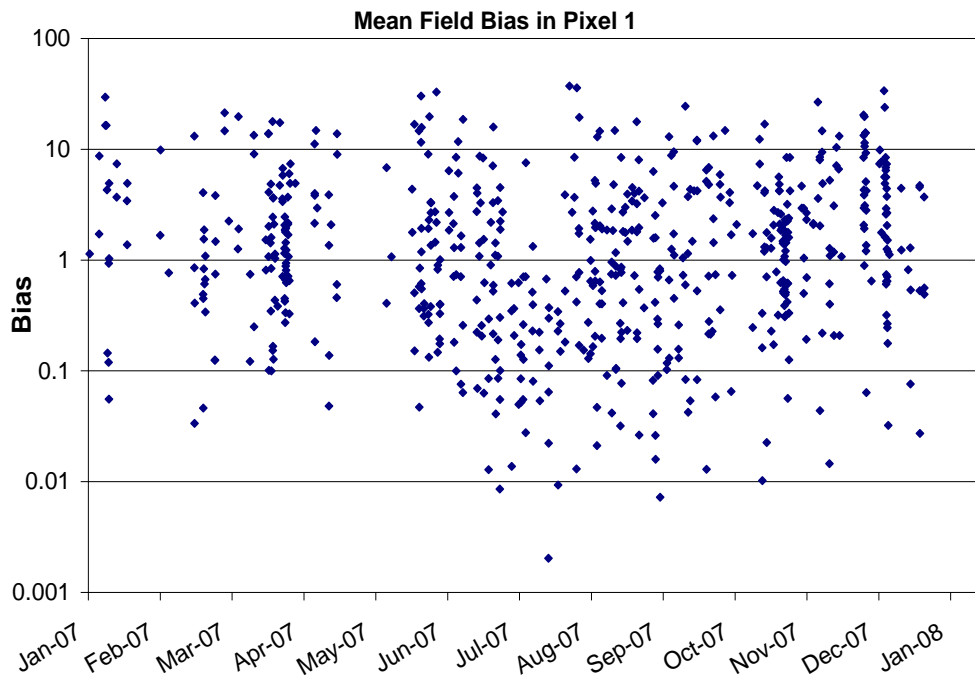


**Figure 7-9 Hourly Mean Field Bias for the MPE Pixel 1 during 2007**

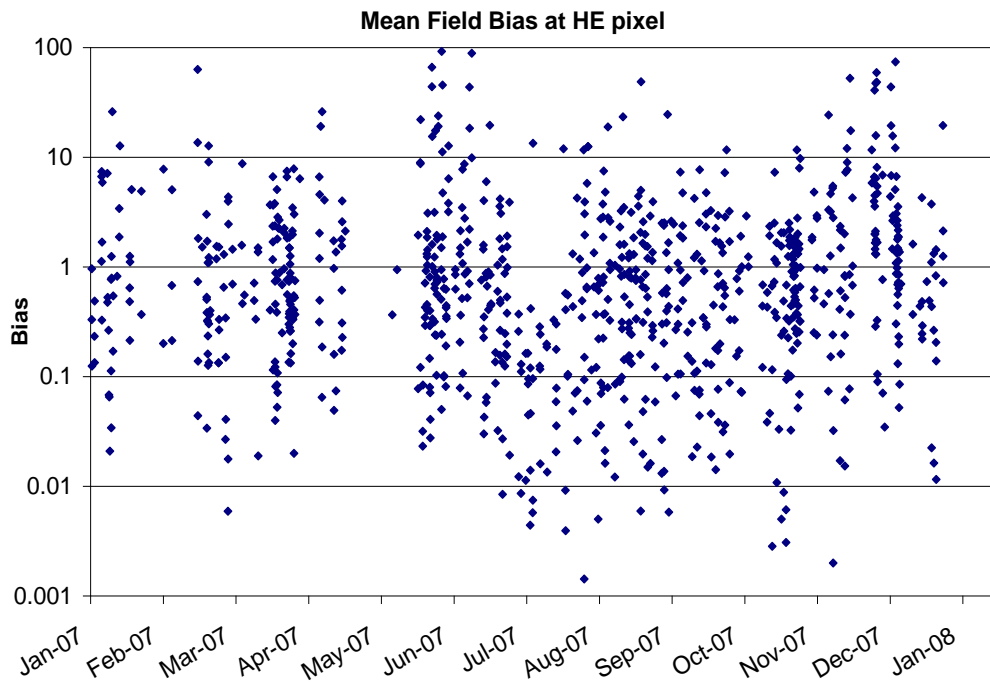


**Figure 7-10 Hourly Mean Field Bias for the four MPE Pixels during 2007 within a HE Pixel.**

To neutralize the noise effect of small rainfall quantifications in the hourly bias computation, rainfall depths less than 0.3 mm were eliminated. A considerable hourly bias reduction was observed in time (Figure 7-11) and in the average and standard deviation computation across the year as well as monthly (**Error! Reference source not found.** and **Error! Reference source not found.**).

The continuous validation scores for MPE rainfall validation (**Error! Reference source not found.**) show a root mean square error is greater (0.368 mm) in daily accumulations than in hourly (0.012 mm). The mean field bias average for 2007 in Pixel 1 is 3.85 with a standard deviation average of 4.21. The four MPE pixels present a lower

Bias (2.77) but a large standard deviation (8.18). The annual average Bias is improved after eliminating rainfall depths less than 0.3 mm, diminishing to 1.55 and a standard deviation of 2.14 for the four MPE pixels with rainfall greater than 0.3 mm.

In the months of April and May some data in the rain gauge network were missing, and as a consequence, the mean field bias was calculated only for the existing data. In addition, the MPE Pixels present the complete accumulations for these months while the rain gauge column showed only the existing data. The MPE total accumulations are 120.9 and 187 mm for April and May (Table 7-4), but the MPE accumulations only for the time window that correspond to the rain gauge data are 22.41 mm and 143.61 mm for April and May, respectively and these data were not considered in the computations of Bias.

The mean field bias tended to decrease when the calculation was performed for the whole HE pixel area (16 km<sup>2</sup>). Therefore, when the MPE is accumulated (e.g., over several hours or days) the bias is reduced and the standard deviation as well. Table 7-4 provides detailed bias computations for year 2007 results.

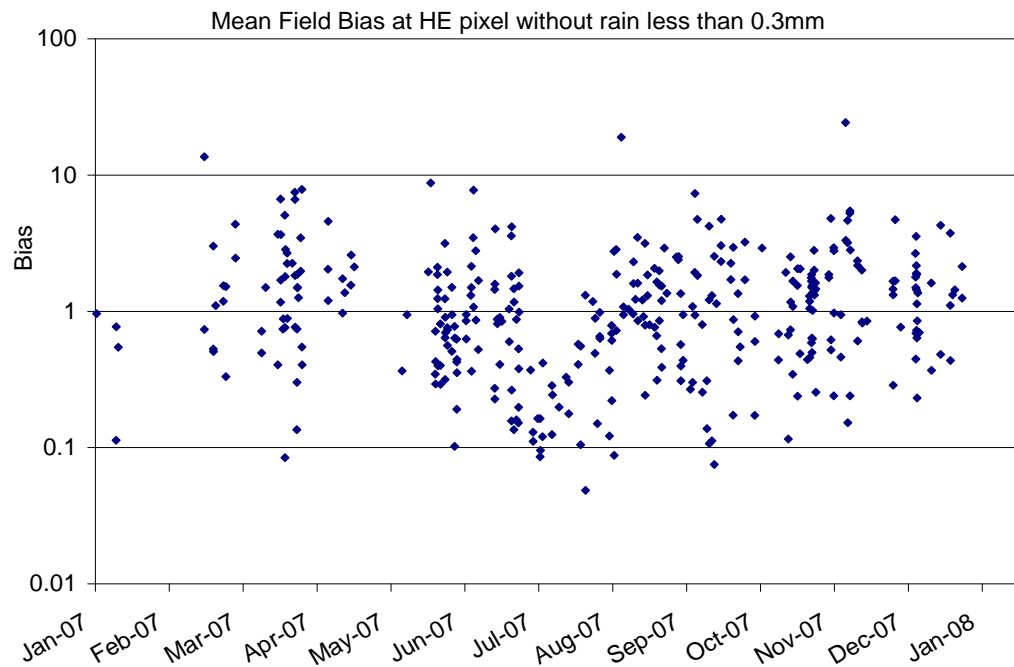


**Figure 7-11. Hourly Mean Field Bias for the overall MPE Pixels within a HE Pixel for January to December, 2007.**

The results indicate that the month with largest hourly bias was December (5.68), which also had the highest variability (STD =12.92). These results are decreased to 1.53 and 2.52 respectively, when the average rainfall less than 0.3 mm in radar and rain gauges were eliminated (Table 7.4). The greatest daily Bias occurred in November with 2.24 and a standard deviation (STD) of 2.6. The months with Bias close to 1 are June, July, August and September but only August and September maintain the value close to one in monthly accumulations.

**Table 7-4 Total rainfall in the MPE pixels and mean field daily bias calculation for year 2007.**

	MPE Pixel Rainfall				MPE Statistics		Rain Gauge	Month	Daily Bias		Hourly Bias		Hourly Bias Rain>0.3mm	
	1	2	3	4	Mean	STD	Total	Bias	Mean	STD	Mean	STD	Mean	STD
	(mm)	(mm)	(mm)	(mm)	(mm)	(mm)	(mm)							
<b>Jan</b>	45.3	77.3	110.4	179.2	94.9	57.3	15.51	0.16	1.43	1.81	2.47	4.77	0.60	2.02
<b>Feb</b>	39.9	72.6	53.0	54.9	56.5	13.4	71.50	1.27	1.20	1.91	2.89	9.11	2.57	2.80
<b>Mar</b>	59.5	106.7	56.6	74.8	78.4	23.0	94.62	1.21	1.36	1.38	1.48	1.89	2.18	1.98
<b>Apr</b>	91.6	129.5	128.4	140.7	120.9	21.3	-	-	-	-	-	-	-	-
<b>May</b>	142.8	203.2	182.7	223.7	187.0	34.5	-	-	-	-	-	-	-	-
<b>Jun</b>	220.5	283.3	196.0	206.0	235.0	39.2	192.01	0.82	1.02	0.85	3.25	10.59	1.26	1.44
<b>Jul</b>	259.2	430.3	245.7	263.5	316.6	87.4	82.22	0.26	0.97	1.51	1.04	2.68	0.39	0.88
<b>Aug</b>	200.4	268.2	195.9	252.6	233.7	36.5	223.69	0.96	0.93	1.60	1.98	5.45	1.66	2.44
<b>Sept</b>	164.4	312.4	277.9	227.1	247.4	64.4	241.45	0.98	1.08	1.50	1.49	3.01	1.61	1.58
<b>Oct</b>	177.2	187.9	261.9	239.2	208.0	40.6	204.23	0.98	0.72	0.50	1.14	1.74	1.19	0.99
<b>Nov</b>	89.2	72.2	124.4	117.4	95.1	24.4	162.49	1.71	2.24	2.60	3.92	8.16	2.92	4.55
<b>Dec</b>	55.7	68.0	111.7	104.0	79.4	27.2	109.86	1.38	1.72	2.38	5.68	12.92	1.53	2.52
<b>Year Total</b>	<b>1545.7</b>	<b>2211.4</b>	<b>1944.4</b>	<b>2083.2</b>	<b>1952.7</b>	<b>249.8</b>	<b>1542.3</b>							
<b>Aver</b>								<b>0.85</b>	<b>1.24</b>	<b>1.65</b>	<b>2.77</b>	<b>8.14</b>	<b>1.55</b>	<b>2.14</b>

Note: (-) No data values, Rain gauge total = rain gauge average for the months including the available network.

Different probability distributions were tested with a 95% of confidence to determine which particular distribution fits to the daily rainfall bias. The null hypothesis is that the data follow the distribution selected if P-value is greater than 0.05. The normal distribution with Box-crox transformation ( $\lambda = 0.15$ ) was the probability distribution that obtain a better fit to the data. Goodness of fit was evaluated using the Anderson Darling (AD) test (0.677) (Anderson and Darling, 1954) and P-value equal to 0.677. Additionally the exponential, lognormal and Weibull distributions were tested (Figure 7-12), but obtained P-values less than 0.05 and the hypothesis was rejected, although Anderson Darling values were small.

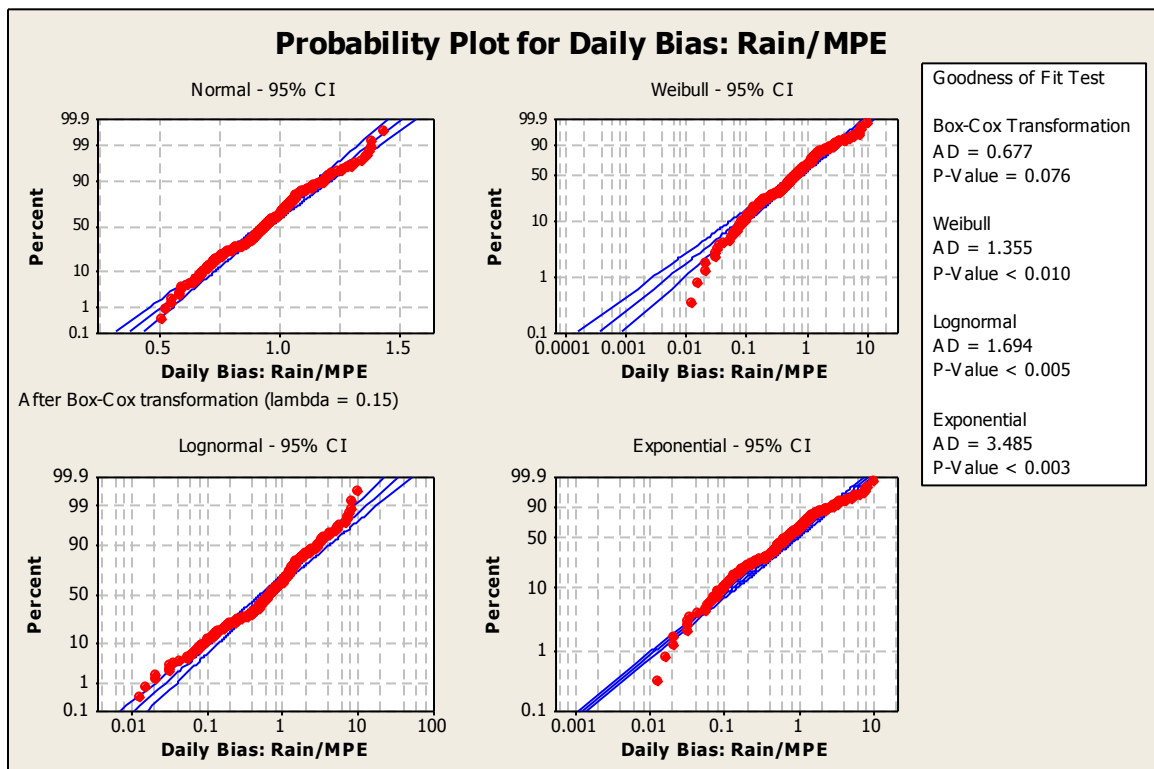


**Figure 7-122 Probability plots for daily rainfall bias between rain gauges and MPE product**

## CHAPTER 8

# 8 PREDICTABILITY LIMITS DUE TO UP-SCALING

Chapter 8, analyzes the uncertainty propagation through the model. Comparisons between rainfall resolutions and hydrologic model resolutions serve as a guide for modelers and radar developers to know how much detail is necessary to archive a reliable solution in small watersheds in terms of flow prediction using ensembles.

### 8.1 Parameter uncertainty propagation due to rainfall spatial variability and hydrologic model configurations

Hydrologic evaluation was performed at the TBSW to evaluate the uncertainty due to spatial rainfall variations. A most comprehensive methodology was used than in Section **Error! Reference source not found.**, where different interpolation methods represent rainfall coverage over MBDB model.

The ensemble forecast procedure in principle draws a finite sample from the probability distribution describing the uncertainty of the initial state of the atmosphere (rainfall) or hydrologic model. Each input, parameter or model configuration combination is called the ensembles of initial condition, and each one represents a possible initial state consistent with the uncertainties in observation and analysis. Using a deterministic model,

it is possible to evaluate the propagation of the entire initial state probability distribution by the governing physical laws. The evaluation would bring information reliable to a determined initial state and would be a decision support to evaluate procedures that would be applied to obtain goodness of fit models at different resolutions or selecting a rainfall cell size when rainfall information is available at scales below NEXRAD resolutions. Here, the word “probability” is treated as conditional, because parameters were perturbed in their physical bounds, using scalar factors, selection of possible hydrologic configuration and input resolution without giving any spatial weight.

Monte-Carlo method approximation is based on a large number of possible initial hydrologic states drawn up randomly from the PDF of initial-condition uncertainty in the phase space. The stochastic dynamic simulation is constructed by a substantial amount of hydrologic simulations, repeatedly running the model is where the knowledge of the real PDF's are required. It is important that the initial ensemble member be chosen well, their selection is further complicated by the fact that initial condition PDF in space required for a distributed model is unknown and it changes from day to day, so that the ideal of simple random samples from this distribution cannot be achieved in practice. As a practical manner, computing time is a limiting factor at operational flood forecast centers. The modeler must make a subjective judgment balancing the number of ensemble members to include in relation to the spatial resolution of the hydrologic model used taking into consideration their physical bounds.

Using methods to resample parameters was possible to reduce the uncertainty due to slope degradation that result in lowest peaks and volumes retarding the runoff and

smoothing the hydrograph. Five hydrologic model configurations at different scales were tested with a distributed model, computation of the parameter statistics are showed in Table 8-1.

**Table 8-1 Descriptive variables and statistical quantification for hydrologic model resolution TBSW configuration**

<i>Variable</i>		<i>RESOLUTION MODEL (m)</i>				
		<b>10</b>	<b>50</b>	<b>100</b>	<b>200</b>	<b>400</b>
<i>Area (km<sup>2</sup>)</i>		3.56	3.64	3.72	3.76	3.84
<i>Cells Number</i>		35235	1393	342	82	18
<i>Channel Cells Number</i>		318	61	30	12	6
<i>Channel Cells Ratio (%)</i>		0.90	4.38	8.77	14.63	33.33
<i>Roughness</i>	<i>Minimum</i>	0.02	0.02	0.02	0.02	0.02
	<i>Average</i>	0.12	0.11	0.11	0.10	0.10
	<i>Maximum</i>	0.15	0.15	0.15	0.15	0.15
<i>Slope (%)</i>	<i>Minimum</i>	27.00	10.00	10.00	0.10	1.25
	<i>Average</i>	30.98	29.83	27.69	26.21	24.63
	<i>Maximum</i>	97.00	87.54	86.10	70.84	60.28
<i>Hyd. Conductivity (cm/h)</i>	<i>Minimum</i>	0.15	0.64	0.64	0.64	0.64
	<i>Average</i>	0.69	0.69	0.69	0.69	0.70
	<i>Maximum</i>	2.84	0.86	0.86	0.86	0.86
<i>Wetting Front (cm)</i>	<i>Average</i>	31.62	31.62	31.62	31.62	31.62
<i>Effective Porosity</i>	<i>Minimum</i>	0.26	0.42	0.42	0.42	0.42
	<i>Average</i>	0.43	0.43	0.43	0.43	0.43
	<i>Maximum</i>	0.45	0.45	0.45	0.45	0.45
<i>Impervious</i>	<i>Minimum</i>	0	0	0	0	0
	<i>Average</i>	0.02	0.02	0.03	0.03	0.02
	<i>Maximum</i>	0.63	0.63	0.58	0.46	0.30
<i>Abstraction (cm)</i>	<i>Minimum</i>	0.08	0.00	0.15	0.15	0.15
	<i>Average</i>	0.80	0.80	0.78	0.80	0.84
	<i>Maximum</i>	1.25	1.25	1.25	1.25	1.25
<i>Channel Width (m)</i>	<i>Average</i>	5.00	5.00	5.00	5.00	5.00

Grid scales are from 10 m to 400 m, with changes in total area through 3.56 km<sup>2</sup> for a high resolution model (10 m) to 3.84 km<sup>2</sup> for coarser resolution (400 m). Average

parameter values were maintained through the up-scaling at the TBSW. Terrain slope is reduced from 30.98 percent to 24.63 percent for average values and from 97% to 60.28 % for maximum slopes. The most important change was due to channels cells ratio, because to increase the grid size the number of cells that represent overland and river cells are reduced. In the high resolution model the total cells were 35,235 in which 318 cells were attributed to channel representation with a ratio of 0.9%. For coarser model resolutions up to 400 m, 18 cells were dedicated to overland process, and 6 cells for channel processes.

Additionally, rainfall and stage information are necessary to feed and validate the model. Five important events were selected from the monitoring time period (October 2007 to May 2009) for stage and rainfall. Section 4.2 describes the methodology used to transform the pressure measurements of transducer installed at the outlet of the TBSW to stage measurements and posterior flow-stage curve generation. **Error! Not a valid bookmark self-reference.** shows important information for the selected events, as time to peak; peak flow and average runoff depth over the TBSW. These variables compared to observed data give more descriptive information of the hydrograph shape than statistics based on error variances. The observed hydrograph for each event are displayed in Figure 8-1. The base flow was removed as a constant value from the observations because this creek has a very short concentration time due its size and high slopes.

Events over the year represent different initial states of the parameters and atmospheric characteristics. Antecedent soil moisture represented by initial saturation in the model is a spatially distributed parameter and it is time dependent, affecting

principally the runoff depth. Low initial saturation values increase the infiltration capacity due to soil moisture and reduce the runoff depth. Rainfall information was collected from the rain gauge network described in Section **Error! Reference source not found.** and Section 7 for the events selected. Some rain gauges produced erroneous results or malfunctioned and were eliminated from the analysis. The minimum number of rain gauges used to produce a time step rainfall map were: 15 for May 2, 2008 and a maximum number of 18 rain gauges for October 22, 2007.

**Table 8-2 Inventory of observed events**

<i>Events</i>	<i>Observed Peak flow (m<sup>3</sup>/s)</i>	<i>Observed runoff depth (mm)</i>	<i>Observed Time to peak (hr)</i>
<b>22-Oct-07</b>	10.13	16.6	15:15
<b>2-May-08</b>	9.38	34.6	15:30
<b>5-Jun-08</b>	5.2	6.51	18:15
<b>28-Aug-08</b>	6.69	10.34	16:00
<b>3-Sep-08</b>	21.2	54.6	3:45

Table 8-3 presents storm totals for each rain gage, average storm total for all gauges and standard deviations. May 2 and September 3, 2008 events present the highest rainfall variability with a standard deviation of 24.3 mm and 20.8 mm between rain gauges; and totals rainfall of 80.4 mm and 95.7 mm respectively. Additionally, standard deviation at each rain gauge through the events were calculated at 10 minutes time step; presenting a maximum value of 3.29 mm, 4.29 mm, 3.23 mm, 2.88 mm and 2.59 mm for October 22, 2007; June 5, September 3, May 2, and August 28, 2008 respectively. The standard deviation calculated for both: partial and total storms reflect the spatial variability with a 4 by 4 km pixel (Table 8-3).

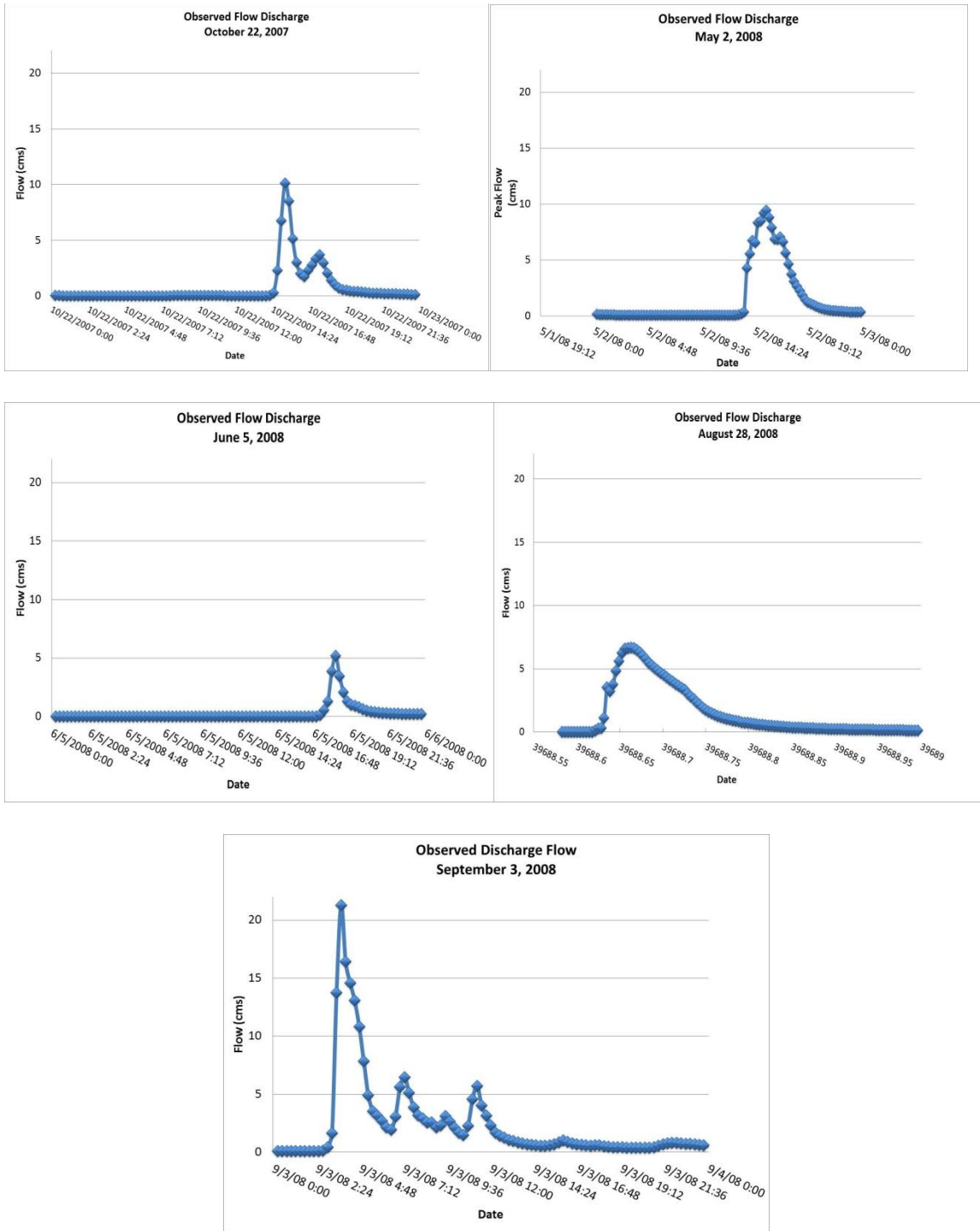


**Figure 8-1 Observed flows for the events studied.**

**Table 8-3 Total rainfall event measured in rain gauges network over 4 km x 4 km area**

Gauge Station	<i>Total Rainfall (mm)</i>				
	<b>22-Oct-07</b>	<b>2-May-08</b>	<b>5-Jun-08</b>	<b>28-Aug-08</b>	<b>3-Sep-08</b>
<b>C01</b>	32.4	57.5	51.7	35.7	105.3
<b>C02</b>	38.1	-	46.7	32.6	105.4
<b>C03</b>	47.8	83.8	52.2	34.5	117.5
<b>C04</b>	40.4	86.7	51	-	-
<b>C05</b>	42.4	101.1	49.5	44	112.2
<b>C06</b>	42.7	55.7	40	31.5	-
<b>C07</b>	49.5	70.3	-	23.6	107.6
<b>C08</b>	48.6	83.3	48.8	29.9	90.2
<b>C09</b>	51.7	96.3	43.5	30.5	97.3
<b>C10</b>	43.0	94.3	-	-	-
<b>C11</b>	48.6	-	-	28.1	108.9
<b>C12</b>	45.4	82.6	34.1	14.2	97
<b>L02</b>	-	-	-	33.2	94.3
<b>L03</b>	-	40.6	-	49.9	60.3
<b>L04</b>	-	-	52.3	-	-
<b>L05</b>	32.7	-	-	11.6	38.1
<b>L06</b>	-	-	18.5	-	-
<b>L07</b>	40.1	86.8	47	37.6	82.8
<b>L08</b>	-	-	-	-	-
<b>L09</b>	-	-	44.1	49.2	116.5
<b>L11</b>	-	-	40.2	-	-
<b>L13</b>	48.5	85.3	49.5	-	100.2
<b>L14</b>	28.1	-	-	-	-
<b>L15</b>	22.5	44.9	18.6	-	-
<b>L16</b>	64.0	136.7	39.8	45.3	97.9
<b>Average (mm)</b>	42.58	80.39	42.79	33.21	95.72
<b>STD (mm)</b>	9.63	24.28	10.49	10.93	20.79
<b>Antecedent rainfall, Average total rainfall previous 5 days (mm)</b>	51.61	64.27	2.66	24.06	4.41

Antecedent rainfall defines how much runoff will be produced and is an indicator of the antecedent soil moisture condition 5 days before the event occurred. The May 2 antecedent rainfall was 64.27 mm, while September 3 antecedent rainfall was only 4.41 mm. Therefore, initial soil moisture will be different for both events. Combinations of important smaller rainfall events with low and high antecedent rainfall accumulation were analyzed in this work.

Precipitation was interpolated using ArcGIS 9.3 software with the inverse distance weighted method at 10 minutes time steps. The method is a commonly used technique for generating weighted averaged surfaces of scatter points, and which places more weight (influence) by nearby points and less by distant points. The average storm for each event is shown in Table 8-3.

Convective and orographic rainfalls are the most common in western Puerto Rico and can occur daily during the wet season. In orographic events along the western coast of Puerto Rico, masses of wet air are transported by a sea breeze mechanism towards the east where it converges with the easterly trade wind over the mountains of western Puerto Rico. This, combined with the heating of the land causes the wet air to move vertically upward forming convective cloud, within which the air is cooled and moisture is condensed causing precipitation. Convective precipitation falls over a certain area for a relative short time with a limited horizontal extent and variable intensity, forming rainfall cells over limited areas. Figure 8-2 shows the temporal variation between two selected cells after interpolation was made at 10 minutes time scale. Table 8-4 indicates the total

storm rainfall averaged over the TBSW area, where the storm total is slightly different for each interpolation resolution.

**Table 8-4 Storm Total produced for different resolutions**

		<i>Total Rain (mm)</i>						
<i>Model Resolution (m)</i>	<i>Rainfall Event</i>	<i>Rain Grid Size (meter)</i>					<i>Average (mm)</i>	<i>Standard Deviation (mm)</i>
		<i>100</i>	<i>200</i>	<i>400</i>	<i>1000</i>	<i>2000</i>		
<b>Grid 10</b>	<b>2-May-08</b>	80.1	80.1	80.0	81.2	77.4	<b>79.8</b>	<b>1.4</b>
	<b>3-Sep-08</b>	100.5	100.6	100.4	97.5	101.3	<b>100.1</b>	<b>1.5</b>
	<b>22-Oct-07</b>	44.9	44.9	44.8	44.1	44.4	<b>44.6</b>	<b>0.3</b>
	<b>28-Aug-08</b>	30.2	30.3	30.3	30.2	34.6	<b>31.1</b>	<b>2.0</b>
	<b>5-Jun-08</b>	42.3	42.3	42.5	42.2	44.6	<b>42.8</b>	<b>1.0</b>
<b>Grid 50</b>	<b>2-May-08</b>	79.9	79.9	79.8	81.1	77.6	<b>79.7</b>	<b>1.3</b>
	<b>3-Sep-08</b>	100.5	100.5	100.4	97.2	101.2	<b>100.0</b>	<b>1.6</b>
	<b>22-Oct-07</b>	45.0	45.0	44.9	44.2	40.5	<b>43.9</b>	<b>1.9</b>
	<b>28-Aug-08</b>	30.0	30.0	30.0	29.8	34.4	<b>30.9</b>	<b>2.0</b>
	<b>5-Jun-08</b>	42.2	42.2	42.4	42.1	44.4	<b>42.7</b>	<b>1.0</b>
<b>Grid 100</b>	<b>2-May-08</b>	80.6	80.6	80.5	81.5	77.7	<b>80.2</b>	<b>1.5</b>
	<b>3-Sep-08</b>	100.7	100.7	100.6	98.1	101.5	<b>100.3</b>	<b>1.3</b>
	<b>22-Oct-07</b>	44.8	44.8	44.8	44.1	40.4	<b>43.8</b>	<b>1.9</b>
	<b>28-Aug-08</b>	30.8	30.8	30.8	30.8	34.9	<b>31.6</b>	<b>1.8</b>
	<b>5-Jun-08</b>	42.5	42.5	42.6	43.3	44.8	<b>43.1</b>	<b>1.0</b>
<b>Grid 200</b>	<b>2-May-08</b>	80.2	79.6	79.5	80.8	76.9	<b>79.4</b>	<b>1.5</b>
	<b>3-Sep-08</b>	100.5	100.3	100.1	96.6	101.4	<b>99.8</b>	<b>1.9</b>
	<b>22-Oct-07</b>	45.0	44.7	44.6	43.9	40.2	<b>43.7</b>	<b>2.0</b>
	<b>28-Aug-08</b>	30.3	30.4	31.7	30.0	34.7	<b>31.4</b>	<b>1.9</b>
	<b>5-Jun-08</b>	42.2	42.4	42.5	42.3	44.8	<b>42.8</b>	<b>1.1</b>
<b>Grid 400</b>	<b>2-May-08</b>	78.7	79.1	80.4	80.5	77.0	<b>79.1</b>	<b>1.4</b>
	<b>3-Sep-08</b>	100.3	100.4	100.7	94.0	101.5	<b>99.4</b>	<b>3.0</b>
	<b>22-Oct-07</b>	44.7	44.9	44.7	43.5	40.3	<b>43.6</b>	<b>1.9</b>
	<b>28-Aug-08</b>	29.9	29.7	30.9	29.2	34.8	<b>30.9</b>	<b>2.3</b>
	<b>5-Jun-08</b>	44.0	42.3	42.4	42.3	44.6	<b>43.3</b>	<b>1.2</b>

Additionally small differences across model resolutions are due to changes in area, where the grid is intended to represent the shape of the basin.

Ogden and Julien (1994) discussed the appropriateness of the correlation length as indicator of spatial structure and obtained an inter-gage distance of 2.5 km. Distances greater than this value will not capture the true rainfall spatial variability. With the existing average distance between the TBSW rain gauges network of 200 m, this work ensures to capture the real spatial variability for each time step through the event.

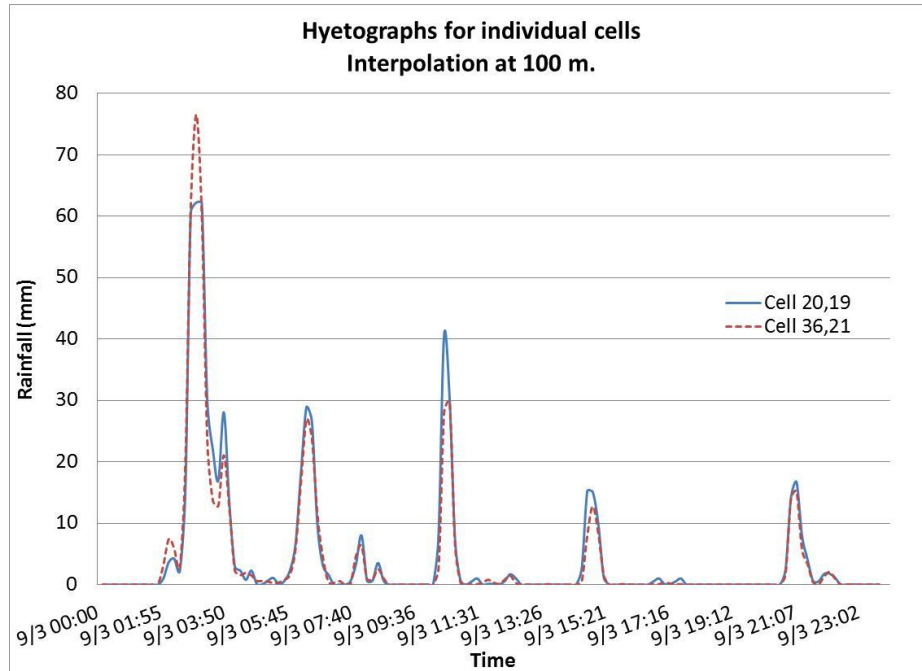


**Figure 8-2 Hyetographs extracted from two cell (100 m resolution) for September 3, 2008**

### 8.1.1 Evaluating predictability limits

The predictability analysis due to rainfall inputs and hydrologic models resolution was performed using a total of 15,625 runs with combinations of five parameter

perturbations to roughness, hydraulic conductivity and initial saturation; five hydrologic model configuration resolutions (10 m, 50 m, 100 m, 200 m, and 400 m); five rainfall resolutions (100 m, 200 m, 400 m, 1000 m and 2000 m) and five events presented in Table 8-3. The events were tested to evaluate temporal or season dependence and cover different mechanisms of rainfall generation as convective or orographic movements.

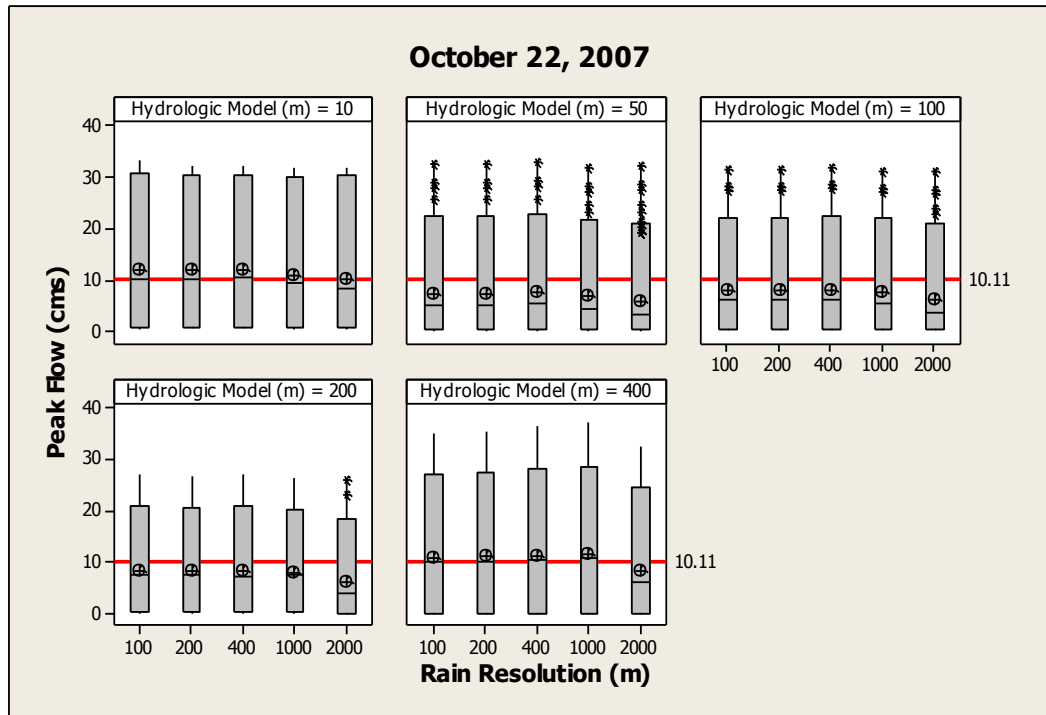
The total number of runs was reclassified in different ways depending on the type of analysis. Box plots summarize information about the shape, dispersion (confident levels of the ensemble at 5 and 95 quartiles), center of the data and outliers ; also are presented as exploratory measures A total of 125 runs that describes the dispersion of hydrologic predictions due to parameter perturbation were grouped, for each combination of model and rainfall resolution, where peak flows, runoff depth and times to peak were compared with observed data. In box plot graphs, the horizontal line represent the median of the data, the vertical lines extending from the box are called whiskers. The whiskers extend outward to indicate the lowest and highest values in the data, excluding outliers. Extreme values or outliers are represented by asterisks (\*).

The event of October 22, 2007 was one of the largest flows measured at the flow gauge during the testing period, with a discharge runoff depth of 16.6 mm and peak flow of 10.11 cms, and a runoff-rainfall ratio of 0.37 (Table 8-2). October 22, 2007 ensembles show a tendency almost constant between rain resolutions, with a slight decrease of mean peak flows with increase of the rainfall resolution. Additionally, hydrologic model results are shown in the different panels for 10 m, 50 m, 100 m, 200 m and 400 m resolution (Figure 8-3-A). The averages are around the observed peak flow (red line), and

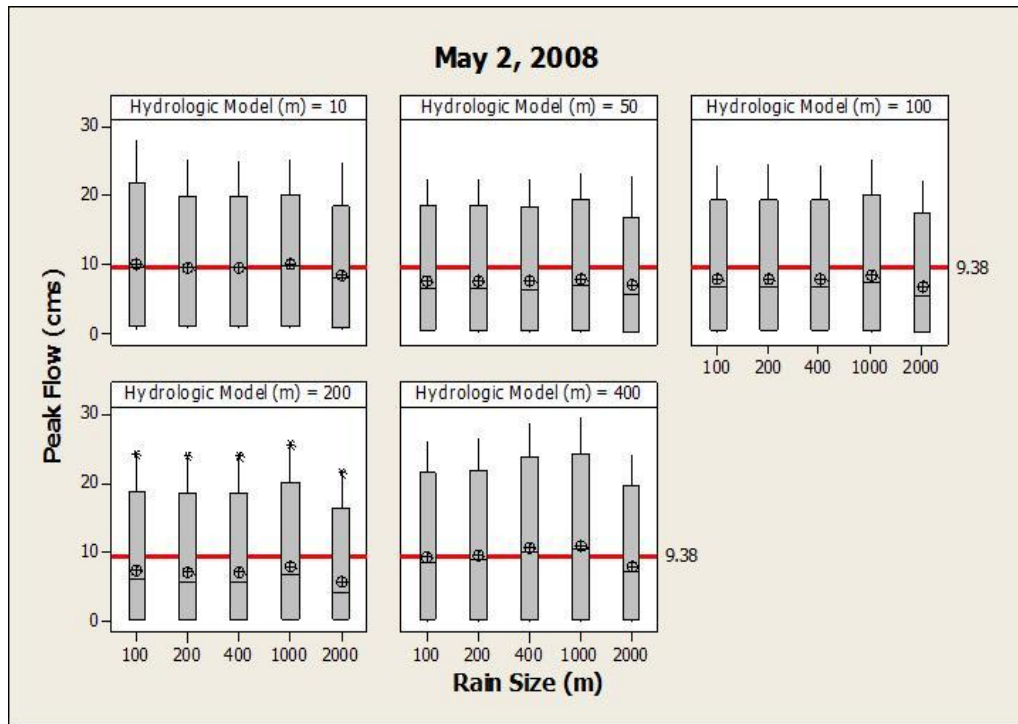
hydrologic model 50 m and 100 m present outliers for high peaks in all rain gauge resolutions. In the case of runoff depth Figure 8-6-A, the average ensembles are around the observed volume (red line) with a tendency to overestimate at 10 m hydrologic model and underestimate the observed volume for the others hydrologic model resolutions in all rainfall maps. No outliers were present in runoff depth box plots. The time to peak graphs (Figure 8-9-A) indicate low dispersions in modeled values for the 10, 100 and 200 m hydrologic models.

The event of May 2, 2008 with a discharge depth volume of 34.6 mm, and peak flow of 9.38 cms, and a runoff-rainfall ratio of 0.43 shows a tendency almost constant for the peaks through rain sizes and hydrologic models, with a slight decrease of mean peak flows with increase in the rainfall resolution, (Figure 8-3-,B). The average ensembles are around the observed peak flow, and hydrologic model 200 m presents some outliers for high peaks in all rain gauges sizes. In the case of runoff depth Figure 8-6-B, the average ensembles underestimate the runoff depth except for the 10 m hydrologic model with 100 m rainfall size. The average ensemble for runoff depth decreases with increasing of rainfall resolution and hydrologic model resolution. No outliers were present in runoff depth box plots. Figure 8-9-B shows the time to peak modeled where the average ensemble values are around the observed and low dispersions were found.

Box plots for June 5, 2008 are shown in Figure 8-4-A for peak flow and Figure 8-7-A for runoff depth. The event had a discharge volume of 6.51 mm and 5.2 cms flow, and a runoff-rainfall ratio of 0.154.



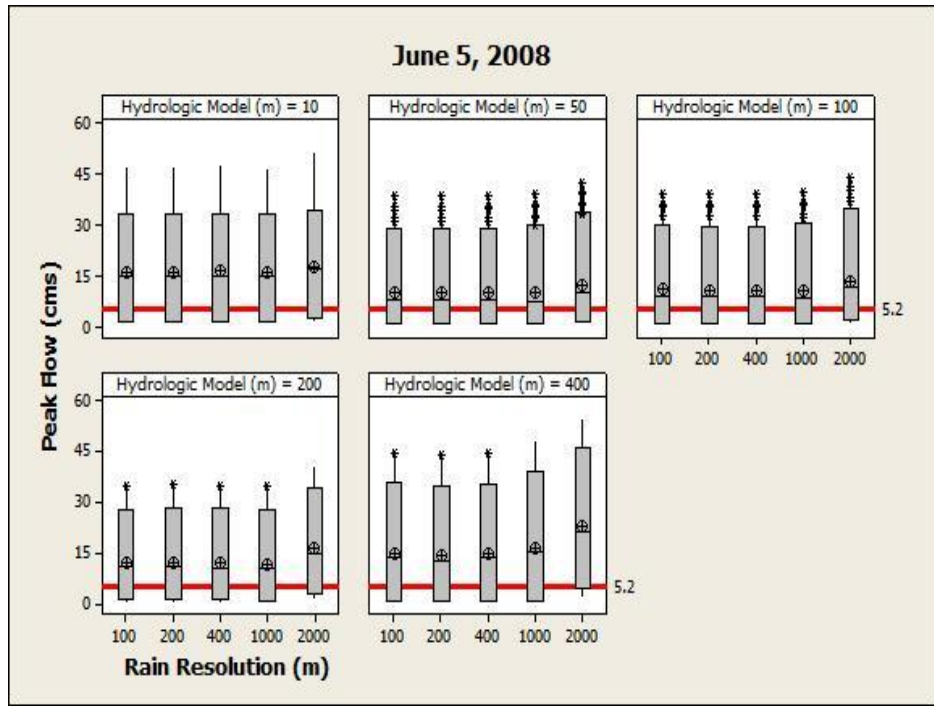
A



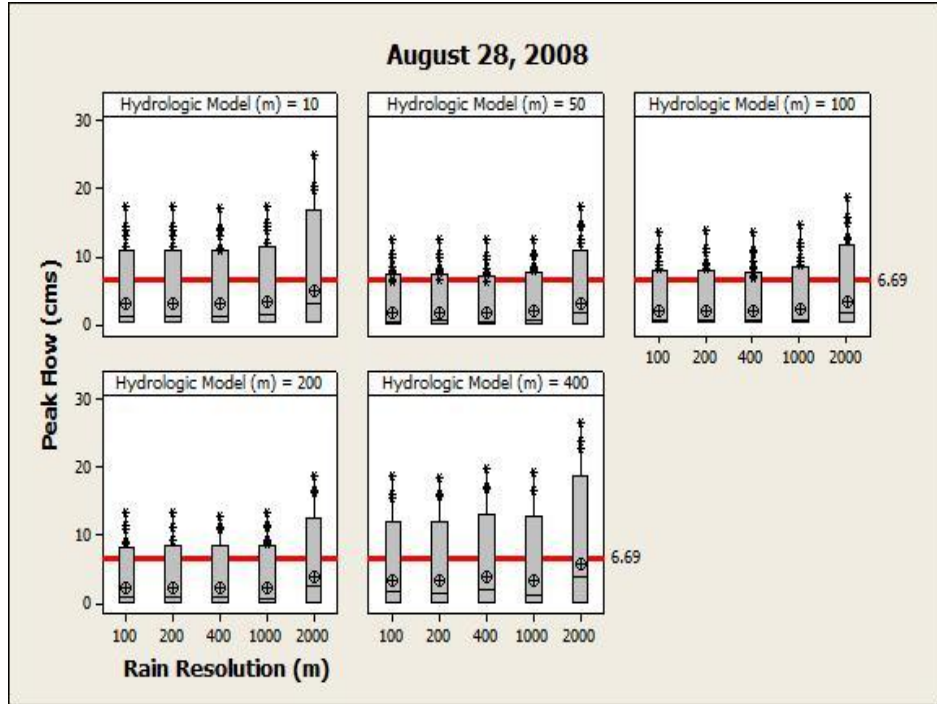
B

**Figure 8-3** Box plots of Peak flows for events on: (A) October 22, 2007; (B) May 2, 2008

The average ensembles tended to overestimate peaks and volumes as well, therefore, showing a tendency almost constant for the peak average through rain sizes and hydrologic models, with an increase of mean peak flows with increase rainfall resolution, (Figure 8-4-A) for the 400 m hydrologic model. Hydrologic models presented some outliers for high peaks in all rain gauges sizes, except for the 10 m hydrologic model. In the case of runoff depth, Figure 8-7-A, the simulations for 10 m resolution model were out of the observed volume and the others ones ensembles slightly covering the observed volume. The average resemble of runoff depth decrease to increase the rainfall resolutions and hydrologic model resolution. No outliers are presented in runoff depth box plots. Time to peak ensemble means presented in Figure 8-10-A are within the observed value of 18:15 min for June 5, 2008 with underestimation in hydrologic models greater than 50 m. For hydrologic models 200 and 400 m the quartile 95 are below the observed value.



A



B

**Figure 8-4** Box plots of Peak flows for events on: (A) June 5, 2008; (B) August 28, 2008

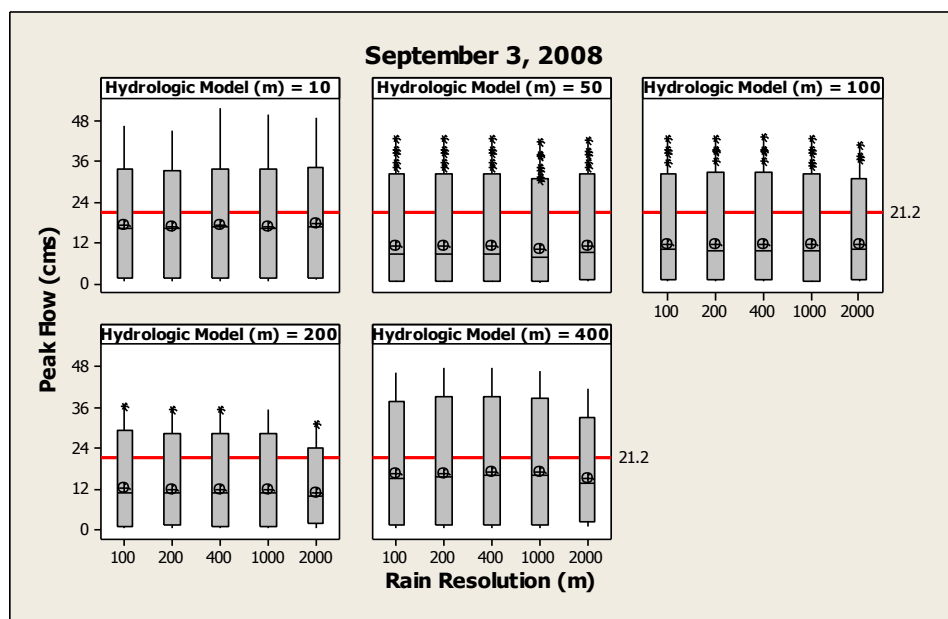


**Figure 8-5 Box plots of Peak flows for September 3, 2008 event**

The event of August 28, 2008 has a discharge depth volume of 10.34 mm, 6.69 cms peak flow, and a runoff-rainfall ratio of 0.34. It shows a tendency almost constant between rain sizes, with a slighter increase of mean peak flows with increase of the rainfall resolution, additionally the range between quartiles 5 and 95 is increased as well, Figure 8-4B. The average ensembles are below the observed peak flows, and all hydrologic models present outliers for high peaks in all rain gauges resolutions. In the case of runoff depth, Figure 8-7-B, the average ensembles are below the observed volume with a tendency to underestimate, except for 10 m hydrologic model and rainfall resolution of 2000 m. Therefore, for some ensembles the quartiles 95 are very close to the observed volume. No outliers were present in runoff depth box plots.

The reason is that computations with very low initial saturation (0.25) did not represent the antecedent soil moisture and high hydraulic conductivities. Figure 8-10-B

shows the time to peak box plots showing values around the observed (August 28 16:00) with low dispersion for the hydrologic model of 100 m resolution. The hydrologic models with more dispersion are 50 and 400 m resolution.

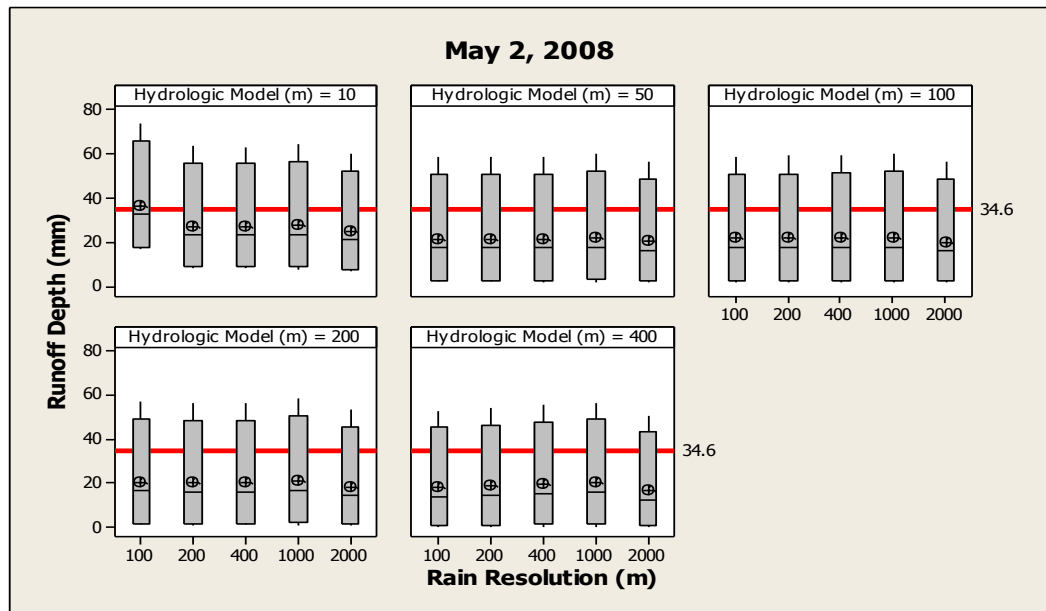
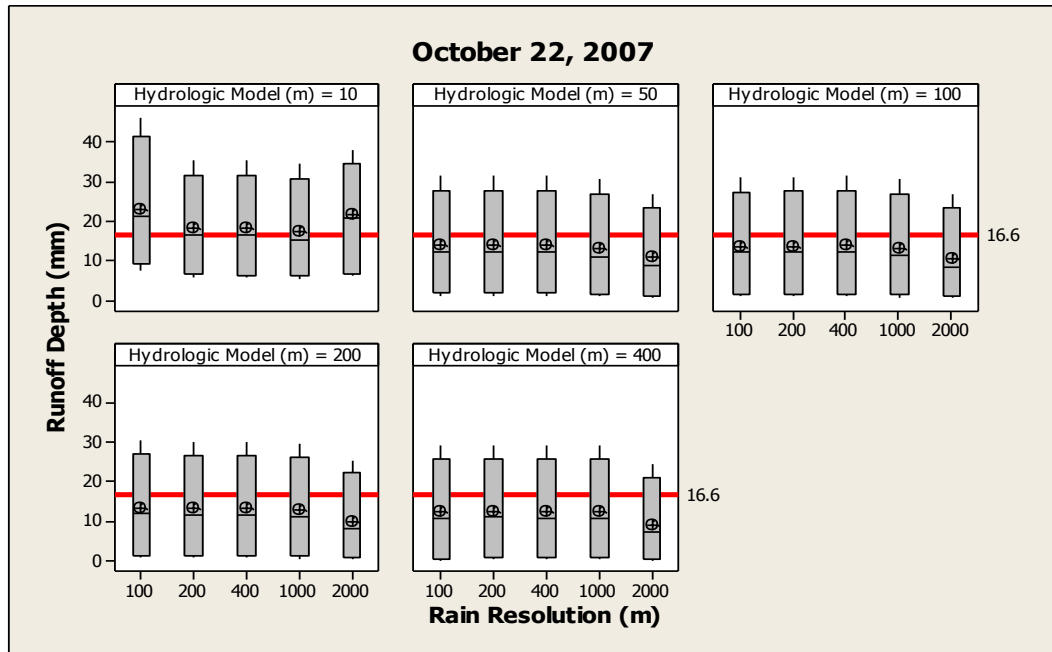
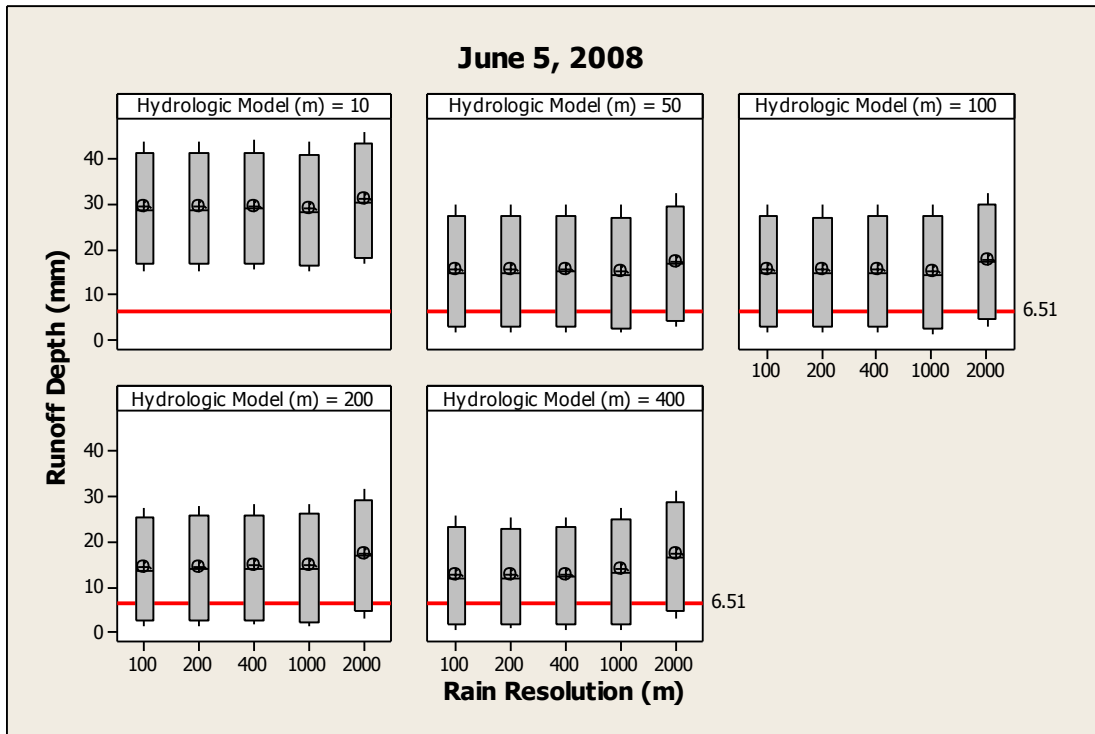
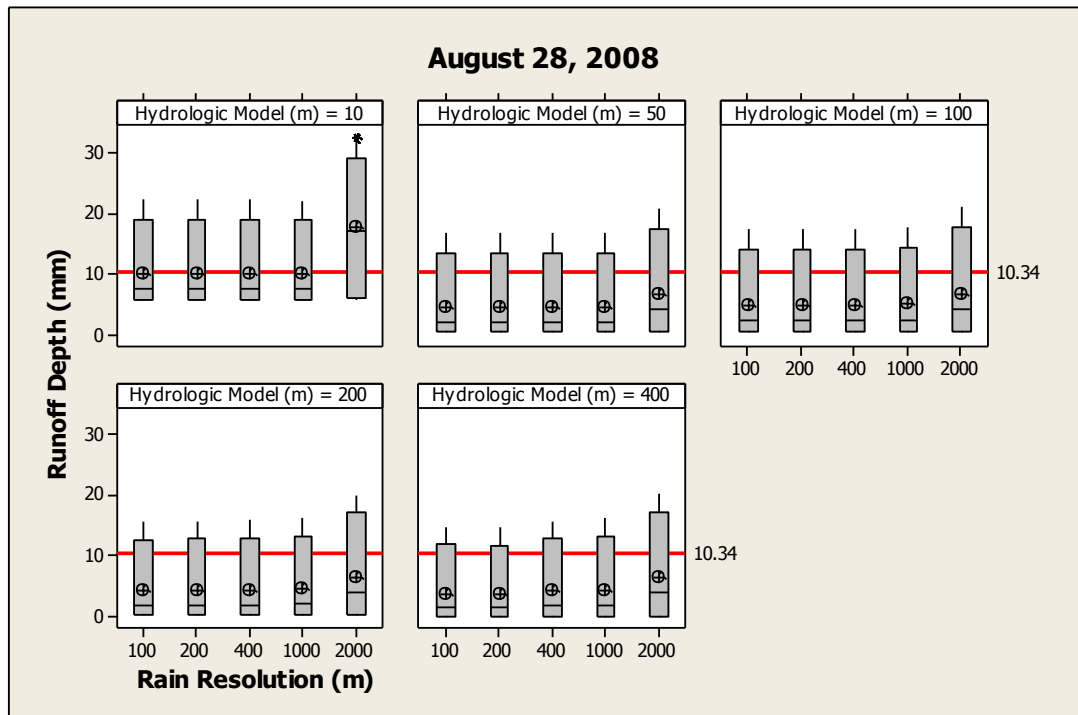


**Figure 8-6** Box plots for runoff depth: (A) October 22, 2007; (B) May 2, 2008



A



B

**Figure 8-7 Box plots for runoff depth: (A) August 28, 2008; (B) September 3, 2008**

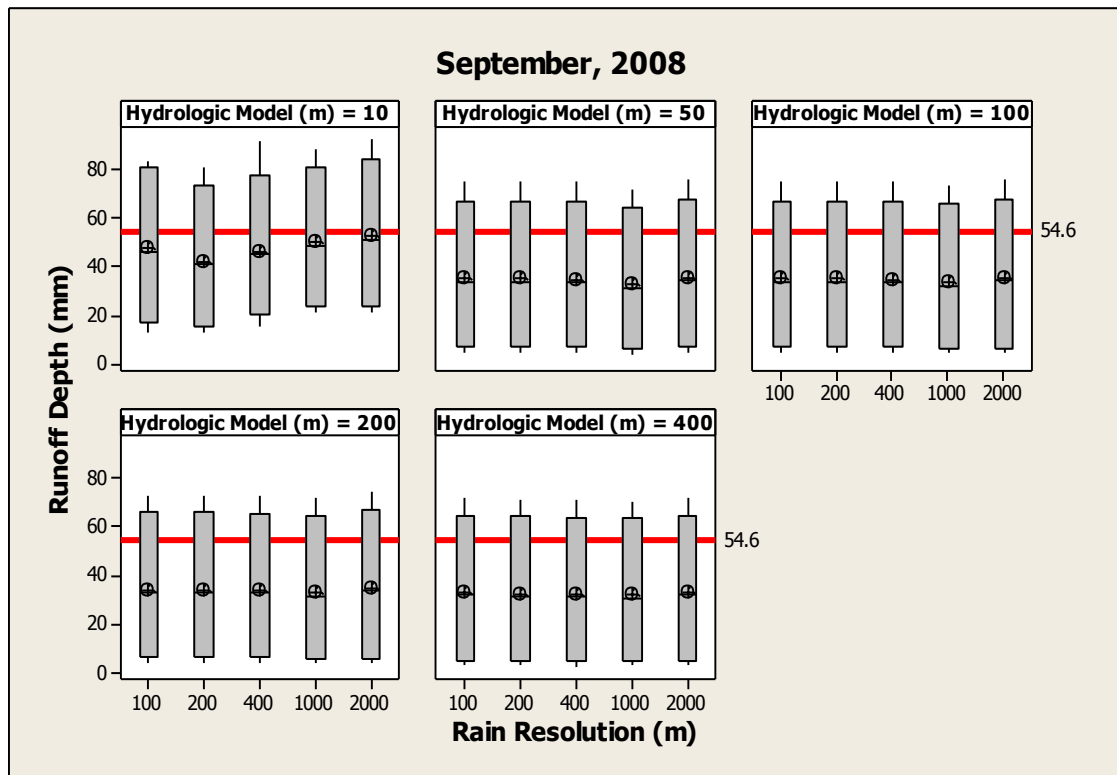
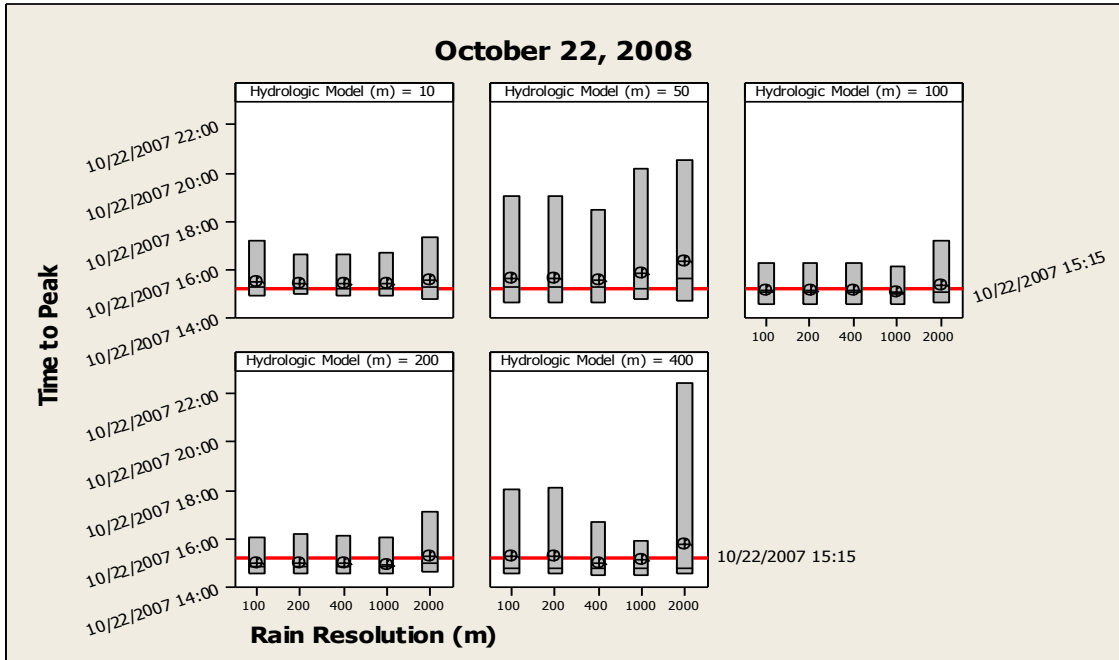


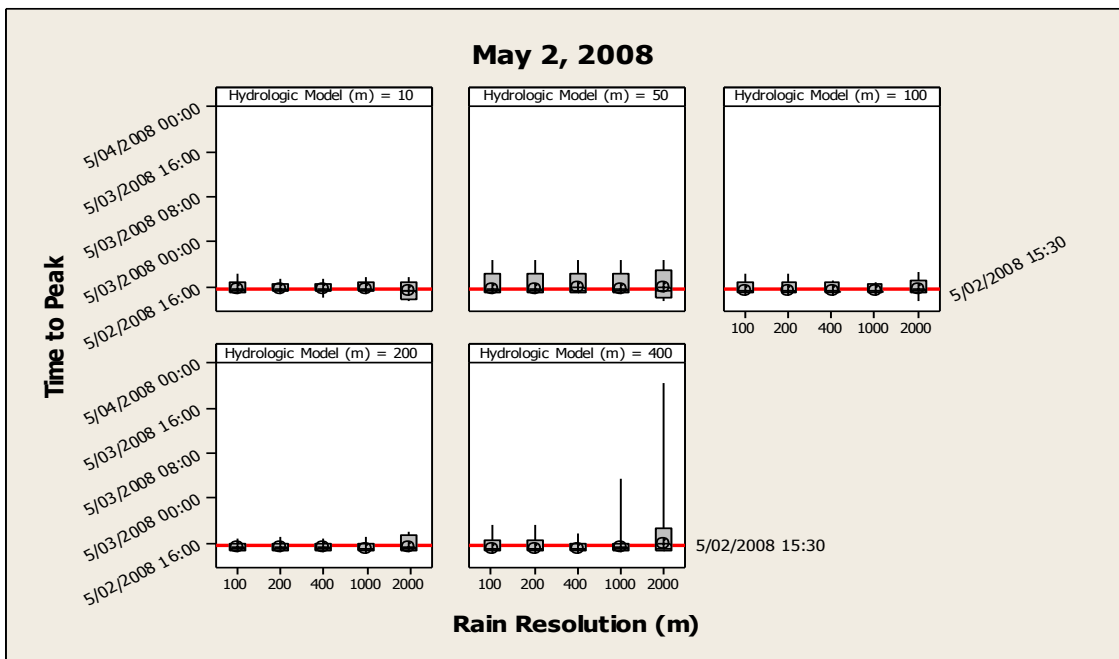
**Figure 8-8 Box plots for runoff depth for September 3, 2008**

The event of September 3, 2008 was the largest peak flow measured at the flow gauge in the studied period, with a discharge depth volume of 54.6 mm, 21.2 cms peak flow, and a runoff-rainfall ratio of 0.5. September 3, 2008 shows a tendency almost constant between rain sizes, with slight changes of mean ensemble peak flows (Figure 8-5). The ensemble averages are underestimating the observed peak flow, the 10 m hydrologic model results are closer to the observed values as is the 400 m resolution hydrologic model as well. Hydrologic model 50 m 100 m and 200 m present outliers for high peaks in all rain gauge resolutions. In the case of runoff depth Figure 8-8, the average ensembles at 10 m hydrologic model are around the observed depth volume with a tendency to underestimate the observed depth volume. The observed runoff depth volume

is near to the quartile 95 for 50, 100, 200 and 400 m hydrologic model resolutions. No outliers were present in volume depth runoff box plots.

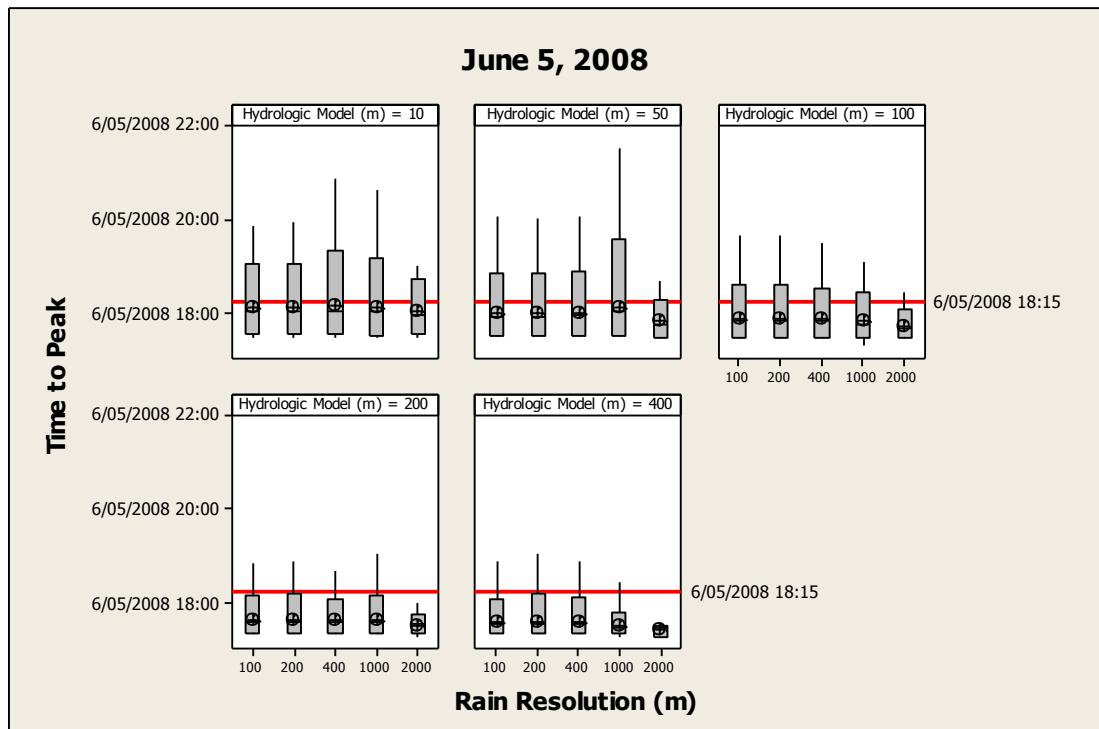


A

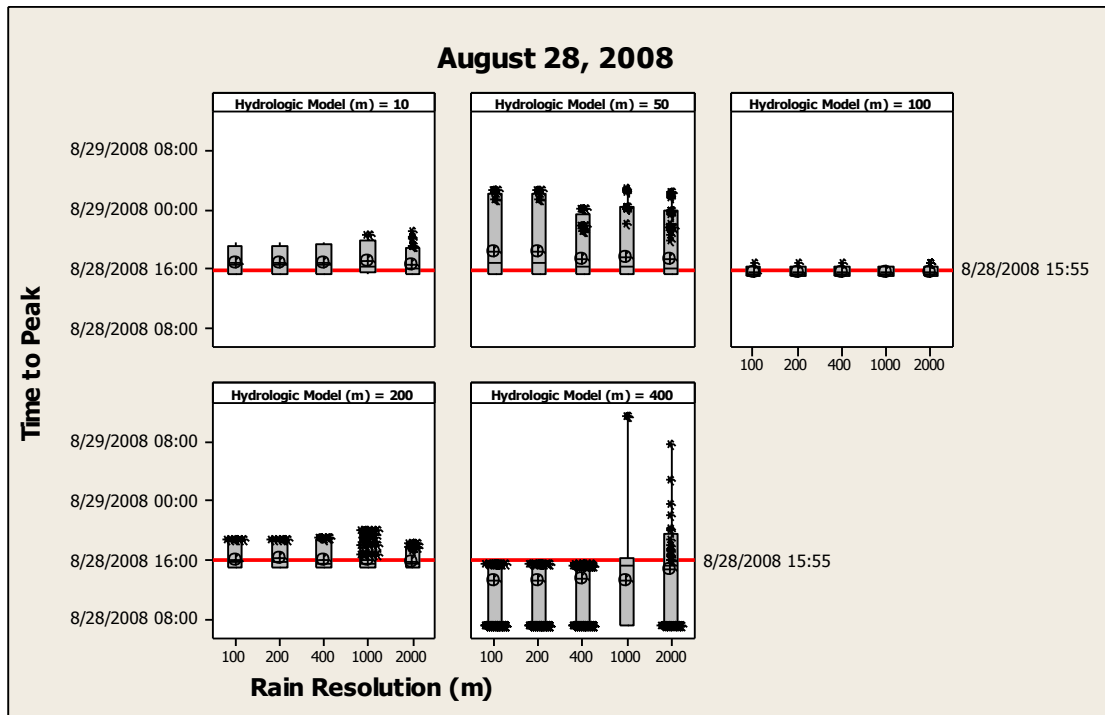


B

**Figure 8-9** Box Plot of time to peak for (A) October 22, 2007; (B) May 2, 2008



A



B

**Figure 8-10** Box Plot of time to peak for (A) June 5, 2008; (B) August 28, 2008

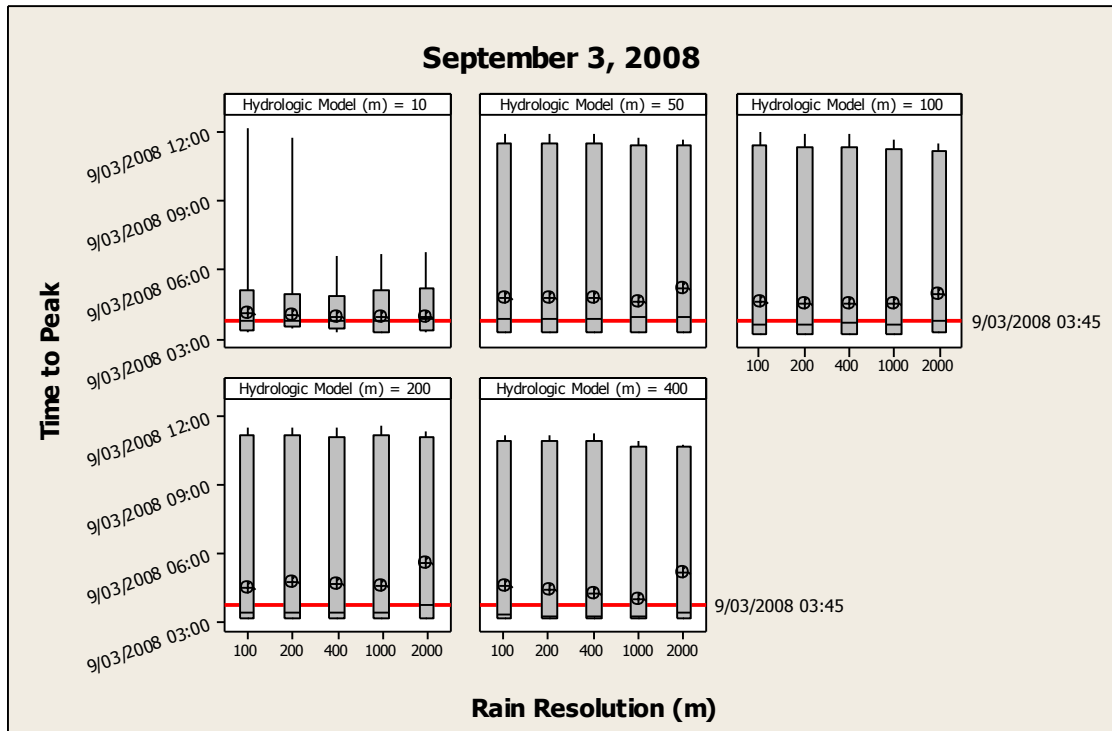


**Figure 8-11 Box Plot of time to peak for September 3, 2008**

Figure 8-11 indicated high dispersions for the 50, 100, 200 and 400 m hydrologic models resolutions and a tendency to overestimate the observed time to peak (September 3, was 3:35). The significant dispersions are due to the form of the observed hydrograph that consist in three limbs. With low initial saturations and high hydraulic conductivities the first jump is absorbed and peaks are greater in the second or third limb.

In general the average ensembles were underestimating the peak flow and runoff depth for the analyzed events, except for June 5, 2008 where the contrary situation was obtained. This event is characterized by an antecedent dry period and medium rainfall in a short time, revealing an anomaly for dry periods and lighter rainfall events.

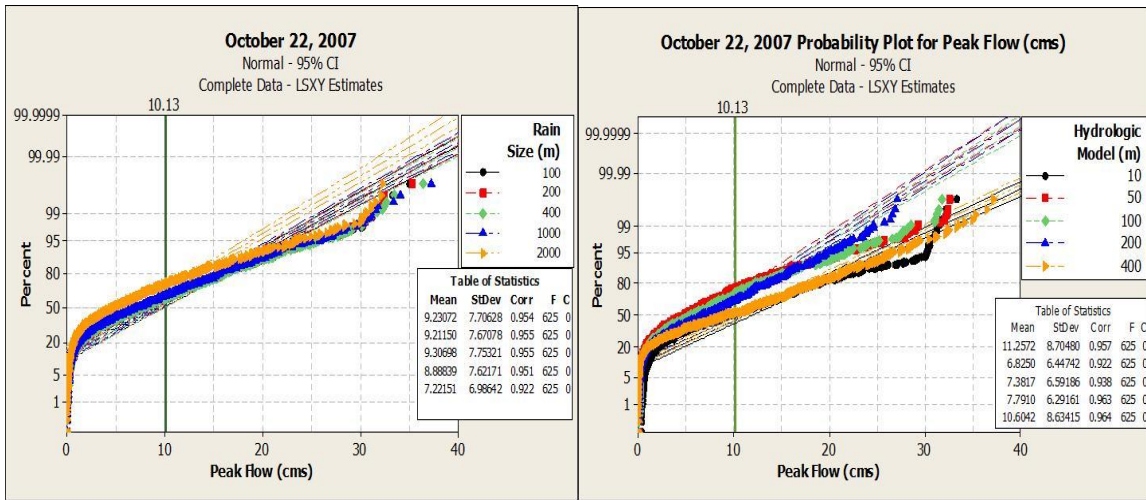
### 8.1.2 Evaluating hydrologic models resolutions and rainfall resolutions

The 15,625 runs were grouped in a different way that helps to explain differences between rainfall resolutions and hydrologic model resolutions as well. Probability with normal distribution and confident levels (5-95) were calculated and plotted for ensemble with observed values in Figure 8-12, Figure 8-13, Figure 8-14,

Figure 8-15 and Figure 8-16. The ensembles for example consist of 625 runs for each hydrologic model including the perturbation parameters and variations in rainfall sizes. Goodness of fit statistics were calculated to compare the data to probability distribution.

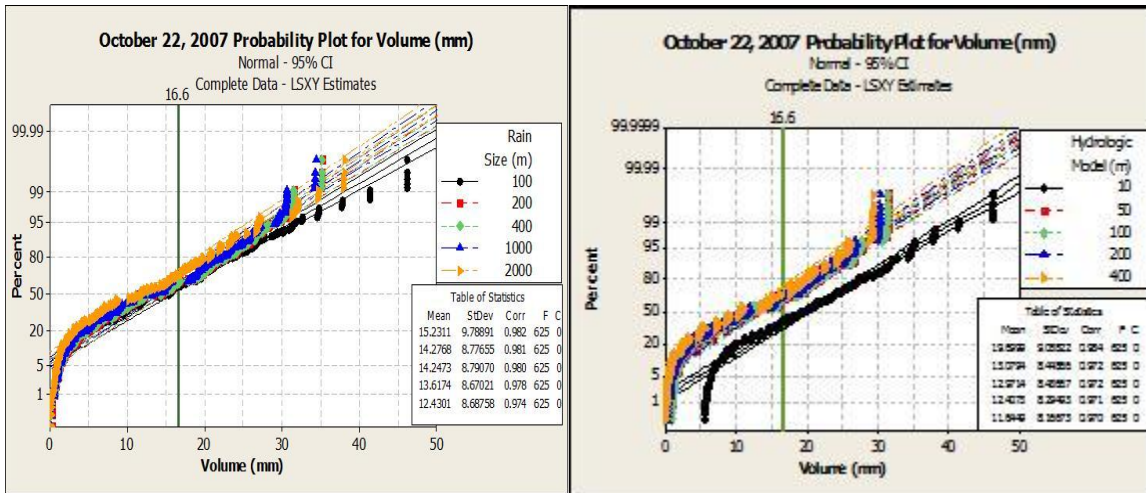
The Pearson correlation coefficient measures the strength of the linear relationship between the X and Y variables on a probability plot (a value close to 1 indicates that the relationship is highly linear). Almost all graphs present Pearson correlation coefficient values above 0.93. The event that presents the lowest was August 28, 2008 (Figure 8-15A) for peak flows with 0.875 coefficient of determination. Additional information such as mean and standard deviation of the ensemble are shown in Figure 8-12, Figure 8-13, Figure 8-14,

Figure 8-15 and Figure 8-16. The lowest extreme values in peak and runoff depth did not have good agreement with the PDF, and was produced by low initial soil saturation values (0.25) in combination with high hydraulic conductivities. In general, the ensemble means and standard deviation decreased with increasing rain resolution input or increase of model resolution.



A

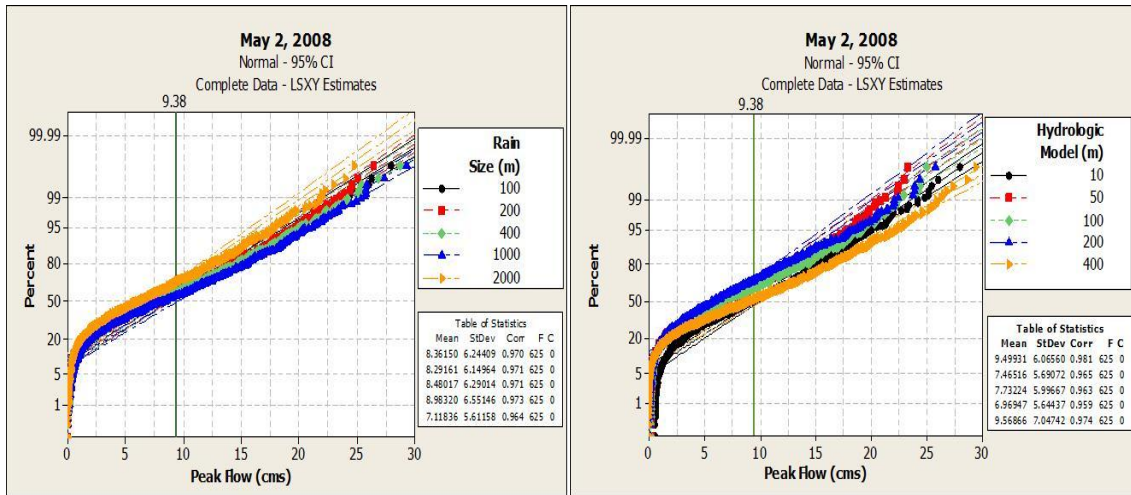
B



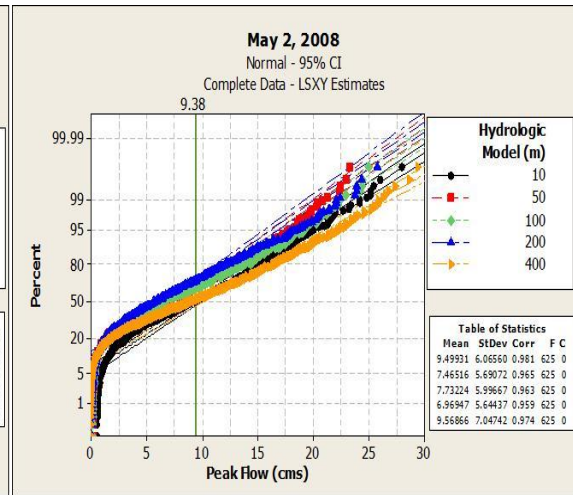
C

D

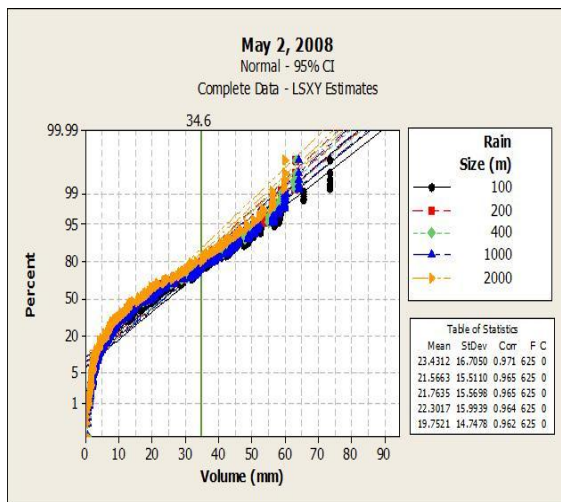
**Figure 8-12 Probability plots for (A) Rain ensembles for peak flow, (B) Hydrologic model ensembles for peak flow, (C) Rain Ensembles for discharge depth volume, (D) Hydrologic Model ensembles for discharge depth volume. October 22, 2007**



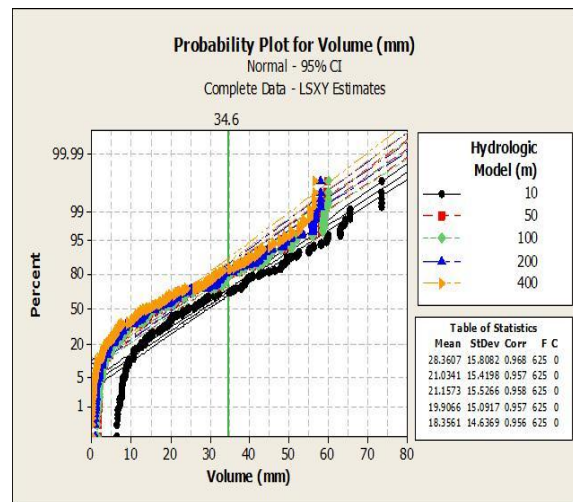
A



B

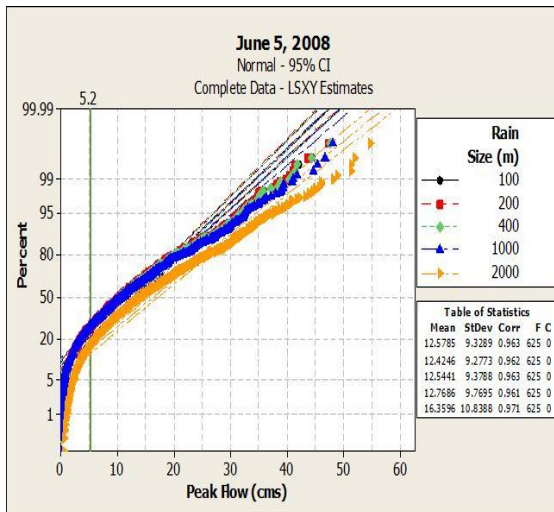


C

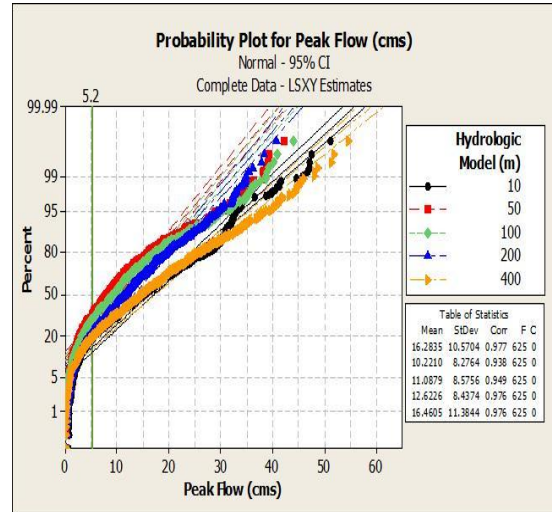


D

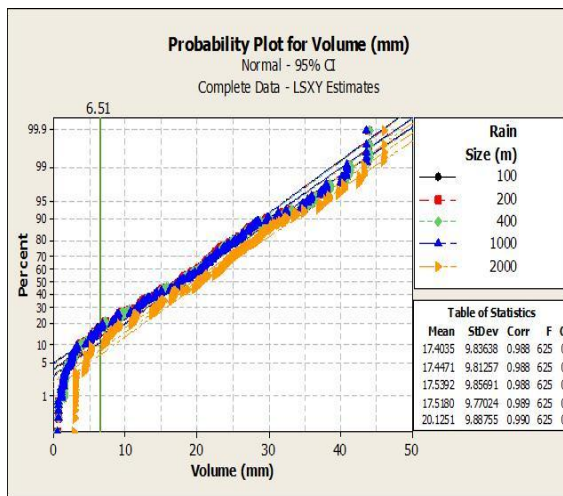
**Figure 8-13 Probability plots for (A) Rain ensembles for peak flow, (B) Hydrologic model ensembles for peak flow, (C) Rain Ensembles for discharge depth volume, (D) Hydrologic Model ensembles for discharge depth volume. May 2, 2008**



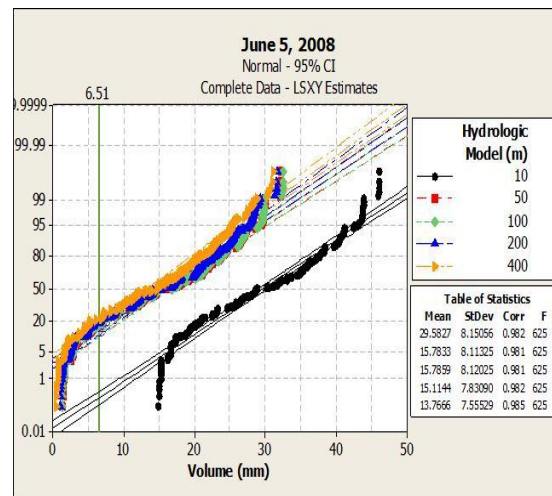
A



B



C



D

**Figure 8-14** Box and probability plots for (A) Rain ensembles for peak flow, (B) Hydrologic model ensembles for peak flow, (C) Rain Ensembles for discharge depth volume, (D) Hydrologic Model ensembles for discharge depth volume. June 5, 2008

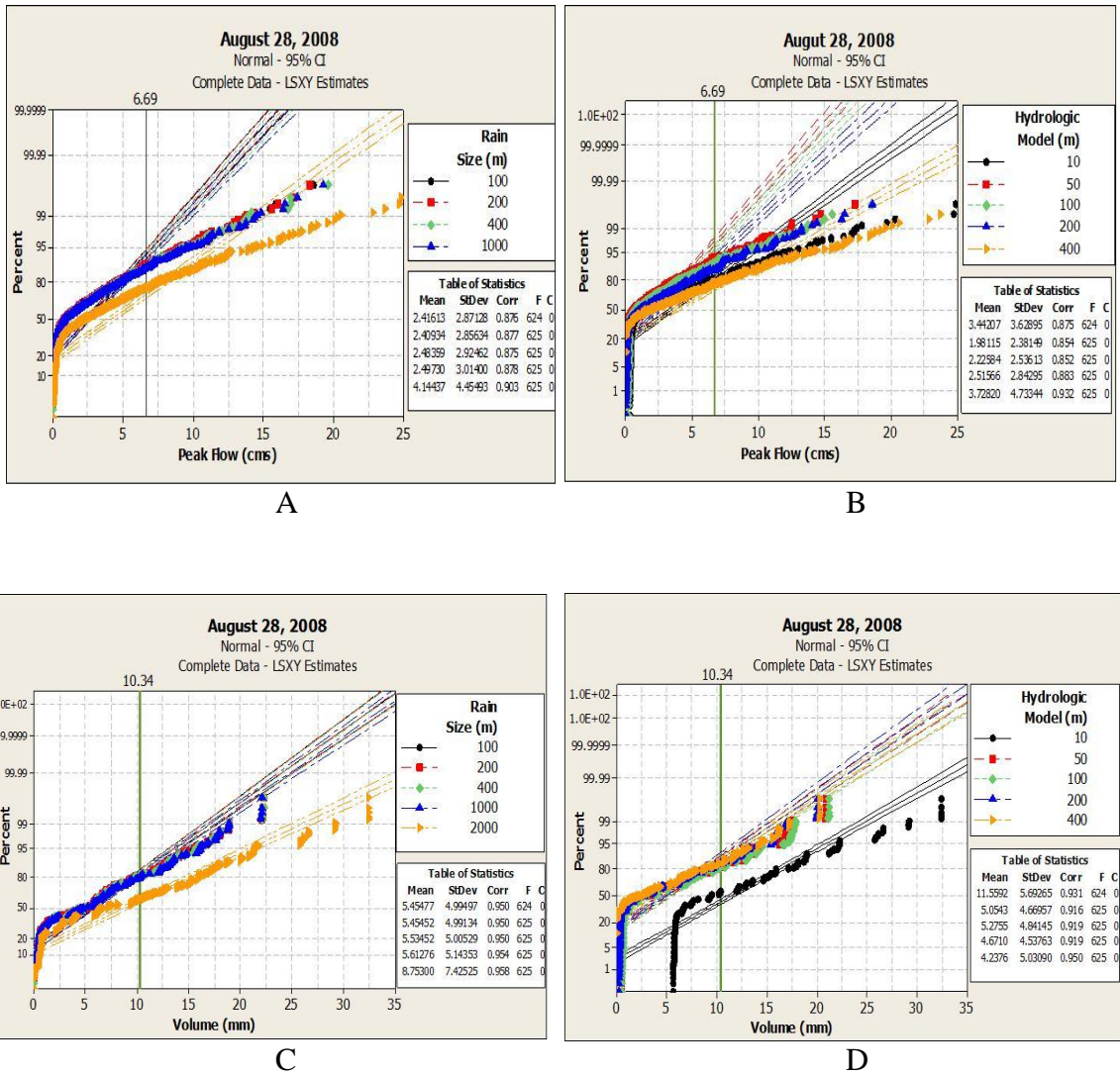


**Figure 8-15** Box and probability plots: (A) Rain ensembles for peak flow, (B) Hydrologic model ensembles for peak flow, (C) Rain Ensembles for discharge depth volume, (D) Hydrologic Model ensembles for discharge depth volume. August 28, 2008

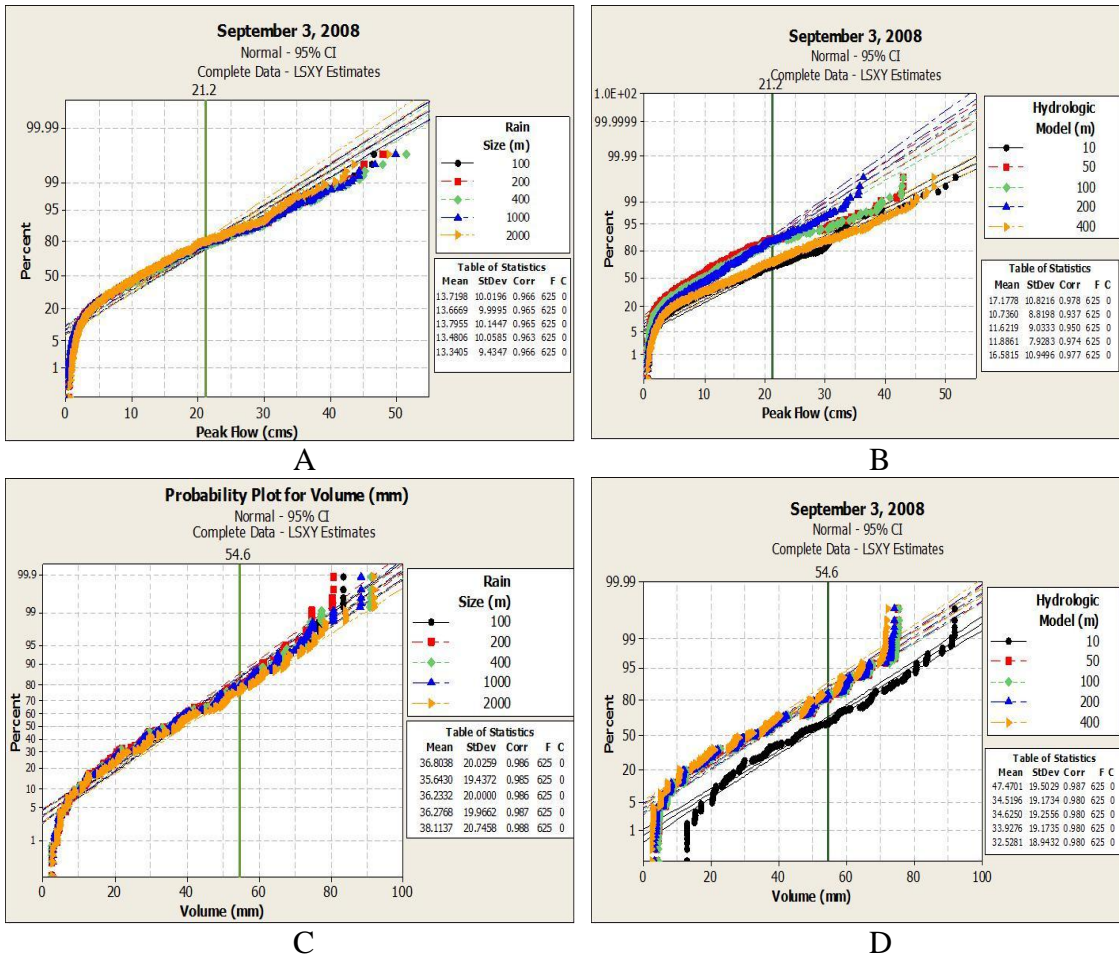


**Figure 8-16 Box and probability plots: (A) Rain ensembles for peak flow, (B) Hydrologic model ensembles for peak flow, (C) Rain Ensembles for discharge depth volume, (D) Hydrologic Model ensembles for discharge depth volume. September 3, 2008**

The statistical measures Bias, MSE, RMSE and the RPS were calculated for the 625 members for each ensemble explained above. The RPS compares each category with observed values; 12 categories were selected for the RPS computation. Table 8-5 the statistics calculated for October 22, 2007 where the lowest RPS for peak flow variable and different rainfall resolutions are for rainfalls of 100 m (0.79) and 400 m (0.79) with

similar RMSE (8.09 mm and 8.05 mm respectively); and 100 m (RPS: 0.7) follow by 200 m (RPS: 0.77) and 400 m (RPS: 0.77) for runoff depth. Therefore, the lowest RMSE (9.23 mm) is for 400 m rainfall resolution. The time to peak presents the best RPS (0.43) for 400 m rainfall with the lowest RMSE (49 minutes) and the Bias is close to one. When the ensembles grouped by hydrologic model were analyzed, the best RPS for peak flow are 0.78 and 0.79 for the 400 m and 200 m hydrologic models respectively. The best lowest RMSE, 6.91 cms is for 400 m and 7.52 cms for 200 m. Analyzing the runoff depth volume variable, the 10 m hydrologic model obtained a good RPS (0.75) as did the 50 m (RPS: 0.83) and 100 m (RPS: 0.83) m hydrologic model.

**Table 8-5 Ensemble statistics and skill of prediction according to rainfall resolution and hydrologic model resolution for October 22, 2007**

	Peak									
	Rainfall					Hydrologic Model				
	100	200	400	1000	2000	10	50	100	200	400
<i>Bias</i>	0.91	0.91	0.91	0.92	0.88	0.71	1.21	0.67	0.73	0.77
<i>MAE</i>	6.74	6.74	6.73	6.78	6.79	6.99	8.36	6.64	6.40	5.93
<i>RMSE</i>	8.09	8.09	8.05	8.13	8.08	8.09	10.16	7.71	7.52	6.91
<i>RPS</i>	<b>0.79</b>	0.80	<b>0.79</b>	0.83	1.08	0.86	1.10	0.95	0.79	<b>0.78</b>
	Volume									
	Rainfall					Hydrologic Model				
	100	200	400	1000	2000	10	50	100	200	400
<i>Bias</i>	1.50	1.41	1.41	1.34	1.23	2.05	1.29	1.28	1.22	1.15
<i>MAE</i>	8.32	7.92	7.94	8.05	8.24	8.99	8.05	8.07	8.12	8.32
<i>RMSE</i>	10.02	9.21	9.23	9.32	9.81	11.24	9.35	9.38	9.48	9.74
<i>RPS</i>	<b>0.70</b>	<b>0.77</b>	<b>0.77</b>	0.85	0.88	<b>0.75</b>	0.83	0.83	0.94	1.03
	Time									
	Rainfall					Hydrologic Model				
	100	200	400	1000	2000	10	50	100	200	400
<i>Bias</i>	1.002	1.002	0.998	1.002	1.026	1.014	1.036	0.993	0.986	1.001
<i>MAE</i>	0:34	0:34	0:29	0:35	0:50	0:24	0:51	0:25	0:29	0:54
<i>RMSE</i>	1:09	1:12	0:49	1:17	1:45	0:40	1:40	0:34	0:35	2:04
<i>RPS</i>	0.47	0.45	<b>0.43</b>	0.47	0.72	<b>0.38</b>	0.69	0.41	0.66	0.94

The hydrologic model that produced the best time to peak according to the RPS is 10 and 100 m resolution models with 0.38 and 0.41 RPS's, additionally, these resolutions present lower RMSE's of 40 and 34 minutes. Table 8-5 presents the ensemble statistics and skill of the prediction according to rainfall resolution and hydrologic model resolution for the event occurring on May 2, 2008. Evaluating peak flow and time to peak due to rainfall variations the RPS's do not clearly favor any resolutions. Therefore 100 m, 200 m and 400 m resolution obtain similar value of RPS. In the case of runoff depth volume, the RPS favors rainfall resolutions of 100 m and 1000 m with RPS values of 1.28 and 1.36, respectively.

Ensembles grouped by hydrologic resolution provide RPS values that favor the 10 and 100 m resolution for peak flow, volume and time to peak.

Table 8-7 shows the statistics and skills of the prediction for June 5, 2008 where the rainfall resolutions favor the 100 m, 200 m and 400 m hydrologic model for peak flow, depth volume and time to peak with the lowest RPS values around 0.6, 1.7 and 0.77 respectively. Therefore, the RMSE are very similar between the resolutions. There was no clarity in terms of the best hydrologic model resolution, because the peak flow favored the 50 and 100 m resolution; runoff depth volume favored the 200 and 400 m and time to peak favored the 10 and 50 m resolution model, respectively.

**Table 8-6 Ensemble statistics and skill of the prediction according to rainfall resolution and hydrologic model for May 2, 2008**

	<b>Peak</b>									
	<b>Rainfall</b>					<b>Hydrologic Model</b>				
	<b>100</b>	<b>200</b>	<b>400</b>	<b>1000</b>	<b>2000</b>	<b>10</b>	<b>50</b>	<b>100</b>	<b>200</b>	<b>400</b>
<i>Bias</i>	0.89	0.88	0.90	<b>0.96</b>	0.76	1.01	0.80	0.82	0.74	1.02
<i>MAE</i>	5.57	5.51	5.58	5.75	5.38	5.20	5.38	5.58	5.48	6.15
<i>RMSE</i>	6.49	6.40	6.51	6.72	6.22	6.16	6.18	6.41	6.34	7.21
<i>RPS</i>	<b>0.73</b>	<b>0.73</b>	<b>0.73</b>	0.76	0.75	<b>0.71</b>	<b>0.75</b>	0.78	0.79	0.80
	<b>Volume</b>									
	<b>Rainfall</b>					<b>Hydrologic Model</b>				
	<b>100</b>	<b>200</b>	<b>400</b>	<b>1000</b>	<b>2000</b>	<b>10</b>	<b>50</b>	<b>100</b>	<b>200</b>	<b>400</b>
<i>Bias</i>	2.50	2.30	2.32	2.38	2.11	3.02	2.24	2.26	2.12	1.96
<i>MAE</i>	17.63	18.01	17.94	17.95	18.67	15.23	18.31	18.31	18.79	19.55
<i>RMSE</i>	20.45	20.63	20.56	20.59	21.30	17.42	21.01	21.01	21.50	22.27
<i>RPS</i>	<b>1.28</b>	1.45	1.46	<b>1.36</b>	1.69	<b>0.95</b>	<b>1.49</b>	<b>1.47</b>	1.64	1.84
	<b>Time</b>									
<i>Time</i>	<b>Rainfall</b>					<b>Hydrologic Model</b>				
	<b>100</b>	<b>200</b>	<b>400</b>	<b>1000</b>	<b>2000</b>	<b>10</b>	<b>50</b>	<b>100</b>	<b>200</b>	<b>400</b>
<i>Bias</i>	0.992	0.992	0.990	0.991	1.003	1.001	1.014	0.991	0.981	0.985
<i>MAE</i>	0:30	0:29	0:29	0:32	0:46	0:22	0:41	0:27	0:29	0:46
<i>RMSE</i>	0:44	0:42	0:41	0:57	1:55	0:33	1:09	0:36	0:34	1:56
<i>RPS</i>	<b>0.20</b>	<b>0.18</b>	<b>0.18</b>	0.21	0.27	<b>0.14</b>	0.30	<b>0.15</b>	0.22	0.55

The August 28, 2008 event presented in

Table 8-8 indicates the statistics and skills of the ensembles where the RPS favored the rainfall resolution of 2000 m with 0.76 for peak flow and 1.11 for depth volume. Time to peak did not present differences between 100 m, 200 m and 400 m rainfall resolution. The skill ensemble by hydrologic models gave the lowest RPS for 50 m resolution for peak flow and the second lowest value for time to peak.

**Table 8-7 Ensemble statistics and skill of the prediction according to rainfall resolution and hydrologic model for June 5, 2008**

	<b>Peak</b>									
	<b>Rainfall</b>					<b>Hydrologic Model</b>				
	<b>100</b>	<b>200</b>	<b>400</b>	<b>1000</b>	<b>2000</b>	<b>10</b>	<b>50</b>	<b>100</b>	<b>200</b>	<b>400</b>
<i>Bias</i>	2.42	2.39	2.41	2.45	3.14	3.13	1.96	2.13	2.42	3.16
<i>MAE</i>	8.86	8.75	8.87	9.19	11.87	12.02	6.95	7.58	8.61	12.38
<i>RMSE</i>	12.14	12.01	12.16	12.63	15.74	15.45	10.11	10.75	11.36	16.17
<i>RPS</i>	<b>0.61</b>	<b>0.60</b>	<b>0.61</b>	0.63	0.99	1.06	<b>0.49</b>	<b>0.58</b>	0.62	1.19
	<b>Volume</b>									
	<b>Rainfall</b>					<b>Hydrologic Model</b>				
	<b>100</b>	<b>200</b>	<b>400</b>	<b>1000</b>	<b>2000</b>	<b>10</b>	<b>50</b>	<b>100</b>	<b>200</b>	<b>400</b>
<i>Bias</i>	3.34	3.35	3.37	3.36	3.86	5.68	3.03	3.03	2.90	2.64
<i>MAE</i>	11.90	11.92	12.01	12.01	14.06	23.07	10.22	10.23	9.69	8.69
<i>RMSE</i>	14.73	14.74	14.84	14.76	16.86	24.51	12.40	12.41	11.71	10.53
<i>RPS</i>	<b>1.70</b>	<b>1.71</b>	<b>1.72</b>	1.78	2.26	4.86	1.50	1.49	<b>1.43</b>	<b>1.15</b>
	<b>Time</b>									
	<b>Rainfall</b>					<b>Hydrologic Model</b>				
	<b>100</b>	<b>200</b>	<b>400</b>	<b>1000</b>	<b>2000</b>	<b>10</b>	<b>50</b>	<b>100</b>	<b>200</b>	<b>400</b>
<i>Bias</i>	0.978	0.978	0.978	0.978	0.971	0.991	0.984	0.976	0.966	0.963
<i>MAE</i>	0:30	0:29	0:30	0:32	0:33	0:23	0:25	0:28	0:37	0:41
<i>RMSE</i>	0:33	0:33	0:34	0:37	0:36	0:29	0:32	0:31	0:39	0:42
<i>RPS</i>	<b>0.78</b>	<b>0.77</b>	<b>0.77</b>	0.82	1.09	<b>0.36</b>	<b>0.53</b>	0.82	1.30	1.62

The mean ensemble for peak and volume are underestimated for the event occurring on September 3, 2008, where the RPS are similar between rainfall resolutions for peak flow and the 10 m and 400 m hydrologic model are favored. The depth volume variable and the time to peak favored the rainfall resolution of 2000 m and a hydrologic model of 10 m followed by 50 m.

**Table 8-8 Ensemble statistics and skill of the prediction according to rainfall resolution and hydrologic model for August 28, 2008**

	Peak									
	Rainfall					Hydrologic Model				
	100	200	400	1000	2000	10	50	100	200	400
<i>Bias</i>	0.36	0.36	0.37	0.38	0.62	0.51	0.30	0.33	0.38	0.58
<i>MAE</i>	4.94	4.93	4.92	4.94	4.79	4.74	5.12	4.99	4.82	4.87
<i>RMSE</i>	5.34	5.34	5.33	5.36	5.50	5.25	5.47	5.36	5.26	5.54
<i>RPS</i>	1.07	1.07	1.06	1.05	<b>0.76</b>	<b>0.87</b>	1.20	1.13	1.02	<b>0.78</b>
	Volume									
	Rainfall					Hydrologic Model				
	100	200	400	1000	2000	10	50	100	200	400
<i>Bias</i>	0.82	0.82	0.83	0.84	1.31	1.73	0.76	0.79	0.70	0.65
<i>MAE</i>	8.43	8.42	8.37	8.30	7.72	5.46	8.77	8.65	9.04	9.32
<i>RMSE</i>	9.41	9.41	9.36	9.34	8.93	6.35	9.72	9.62	9.97	10.25
<i>RPS</i>	1.73	1.73	1.68	1.67	<b>1.11</b>	<b>0.66</b>	1.95	1.91	1.96	2.07
	Time									
	Rainfall					Hydrologic Model				
	100	200	400	1000	2000	10	50	100	200	400
<i>Bias</i>	1.007	1.007	0.997	0.998	1.005	1.058	1.114	0.973	1.012	0.858
<i>MAE</i>	1:31	1:30	1:16	1:33	1:08	1:03	2:03	0:31	0:46	2:34
<i>RMSE</i>	2:47	2:46	2:19	3:01	2:18	1:30	3:27	0:36	1:07	4:24
<i>RPS</i>	<b>0.36</b>	<b>0.36</b>	<b>0.38</b>	<b>0.37</b>	0.40	<b>0.21</b>	0.49	0.57	<b>0.42</b>	0.92

**Table 8-9 Ensemble statistics and skill of the prediction according to rainfall resolution and hydrologic model for September 3, 2008**

	Rainfall					Hydrologic Model				
	100	200	400	1000	2000	10	50	100	200	400
<i>Average</i>	13.72	13.67	13.80	13.48	13.34	17.18	10.74	11.62	11.89	16.58
<i>Bias</i>	0.65	0.64	0.65	0.64	0.63	0.81	0.51	0.55	0.56	0.78
<i>MAE</i>	11.13	11.15	11.18	11.36	10.95	10.03	12.75	12.01	10.82	10.17
<i>RMSE</i>	12.75	12.77	12.82	12.95	12.50	11.72	14.04	13.46	12.34	12.07
<i>RPS</i>	<b>1.06</b>	<b>1.07</b>	<b>1.07</b>	1.11	<b>1.08</b>	<b>0.78</b>	1.54	1.35	1.24	<b>0.77</b>
	<b>Volume</b>									
	Rainfall					Hydrologic Model				
	100	200	400	1000	2000	10	50	100	200	400
<i>Average</i>	36.80	35.64	36.23	36.28	38.11	47.47	34.52	34.62	33.93	32.53
<i>Bias</i>	1.74	1.68	1.71	1.71	1.80	2.24	1.63	1.63	1.60	1.53
<i>MAE</i>	22.40	22.85	22.90	22.80	22.14	17.75	23.47	23.45	23.80	24.62
<i>RMSE</i>	26.94	27.31	27.30	27.23	26.63	20.93	27.97	27.96	28.40	29.29
<i>RPS</i>	1.20	1.28	1.26	1.25	<b>1.13</b>	<b>0.79</b>	1.35	1.33	1.37	1.54
	<b>Time</b>									
	Rainfall					Hydrologic Model				
	100	200	400	1000	2000	10	50	100	200	400
<i>Average</i>	4:30	4:29	4:25	4:20	4:58	3:58	4:47	4:37	4:49	4:30
<i>Bias</i>	1.20	1.20	1.18	1.16	1.32	1.06	1.28	1.23	1.28	1.20
<i>MAE</i>	0:30	0:29	0:29	0:32	0:46	0:22	0:41	0:27	0:29	0:46
<i>RMSE</i>	0:44	0:42	0:41	0:57	1:55	0:33	1:09	0:36	0:34	1:56
<i>RPS</i>	0.54	0.52	0.51	<b>0.48</b>	0.50	<b>0.22</b>	<b>0.32</b>	0.45	0.88	0.92

Beven (1991) has recognized that the non-uniqueness of a model, especially in distributed models similar to the one used in this research, can produce results close to the observed peak flow, runoff depth and time to peak, using different combination of parameters and inputs. Our work also reveals the coexistence of alternative parameter sets that provide a suitable framework for model calibration and uncertainty estimation. The configuration ensemble that was out of the range around the peak flow, 5 and 95

quartiles and minimum peak flow estimation, was the model at 10 m resolution with all rainfall resolutions. This ensemble overestimates simulated flows and cannot reproduce flows for June 5, 2008. For the time to peak the ensembles for hydrologic model 100 m and 2000 m rainfall; 200 m hydrologic model and rains: 400m, 1000m and 2000 m; 400 m hydrologic with rains: 100 m, 200 m, 1000 m 2000 m are out of 95% confident level. June 5, 2008 is characterized by dry conditions and low peak flow and volume.

The ensembles that can reproduce well the time to peak when the hydrographs present 2 limbs (October 22, 2007); or 3 bumps (September 3, 2008) are the 10 m hydrologic model for all rainfall resolution for September and the 10 m, 100 m and 200 m hydrologic models for all rainfall resolutions. For events with only one limb like August 28 and May 2, 2008 the best models with low dispersions around the observed time to peak were 10 m, 100 m and 200 m hydrologic models.

Based on the RPS calculated for the rainfall resolution ensembles in combination with all models resolution (625 members for each event) and parameter perturbations the best rainfalls simulations were observed at the 100 m for peak flow followed by 200 m and 400 m with RPS values very similar. For runoff depth the rainfall at 100 m gives the better RPS for 3 events and the exceptions favor 2000 m for August 28 and September 3, 2008. The RPS for time to peak favored 200 m followed by 400 m rainfall resolution. These findings reveal that the hypothesis that the 100 m rainfall resolution will produce the best ensemble behavior for any event is rejected. The rainfall quantification due to rainfall interpolation will produce similar hydrologic ensembles behavior. In the case of the hydrologic model resolution, the hypothesis formulated was that the hydrologic

model with high resolution (10 m) will generate the best ensemble behavior for the events analyzed. This statement is true only for 2 events evaluating the peak flow variable. For runoff depth, the 10 m hydrologic model did not produce the best RPS for dry conditions and light rainfall event (June 5, 2008) with a storm total rainfall of 42.79 mm. the high resolution model obtained the better behavior for time to peak. This resolution model is not operationally practical for larger basins, and therefore an alternative has to be selected. The RPS analysis favored the 200 m model resolution for time to peak (5 events), runoff depth (4 events) and peak flow (3 events) followed by 400 m model resolution principally for peak flow.

## **8.2 Selection of the Optimal Rainfall and Grid Resolution for the MBDB Model**

The goal of this project is to develop recommendations for rain and grid resolutions that will provide equal accuracy with a 100 m and 10 m rainfall and grid resolution model, respectively (i.e., the smallest resolutions evaluated). To achieve this objective, the RPS values summarized in Table 8-10 were evaluated in a Two-Way ANOVA test. The RPS data were determined to be normally distributed and have equal variances, which is a requirement for the Two-Way ANOVA test.

The goal of the evaluation is to determine significant differences between the mean of the RPS for the highest resolution (100 m rainfall resolution and 10 m grid resolution) and the means for the other resolutions. If there is no significant difference between the mean of the RSP for the finer resolution and a coarser resolution, then the model can be

upscaled to the coarser resolution without loss of accuracy relative to the finer resolution. A grey highlighted cell in Table 8-10 indicates that a significant difference exists between that resolution and the highest resolution. For rainfall resolution, there is a significant difference between the 100 m resolution and the 2000 m resolution. For the grid resolution, there is a significant difference between the 10 m resolution and the 200 and 400 m resolutions. Therefore, based on the Two-Way ANOVA analysis of the RPS, the recommended upscaled rainfall resolution, which will provide equivalent accuracy with the 100 m rainfall resolution, is 1000 m, and the recommended upscaled grid resolution, which will provide equivalent accuracy with the 10 m resolution, is 100 m.

**Table 8-10 Mean RPS values for Peak Flow, Volume and Time to Peak for 5 Storms, 5 Rainfall Resolutions and 5 Grid Resolutions**

	RAINFALL RESOLUTION					GRID RESOLUTION				
	100 m	200 m	400 m	1000 m	2000 m	10 m	50 m	100 m	200 m	400 m
<b>STORM</b>	<b>PEAK FLOW RPS</b>					<b>PEAK FLOW RPS</b>				
<b>3-Sep-2008</b>	1.06	1.07	1.07	1.11	1.08	0.78	1.54	1.35	1.24	0.77
<b>5-Jun-2008</b>	0.61	0.60	0.61	0.63	0.99	1.06	0.49	0.58	0.62	1.19
<b>28-Aug-2008</b>	1.07	1.07	1.06	1.05	0.76	0.87	1.20	1.13	1.02	0.78
<b>22-Oct-2008</b>	0.79	0.80	0.79	0.83	1.08	0.86	1.10	0.95	0.79	0.78
<b>2-May-2008</b>	0.73	0.73	0.73	0.76	0.75	0.71	0.75	0.78	0.79	0.80
<b>MEAN</b>	0.85	0.85	0.85	0.88	0.93	0.86	1.02	0.96	0.89	0.86
	<b>RUNOFF DEPTH RPS</b>					<b>RUNOFF DEPTH RPS</b>				
<b>3-Sep-2008</b>	1.20	1.28	1.26	1.25	1.13	-	1.35	1.33	1.37	1.54
<b>5-Jun-2008</b>	1.70	1.71	1.72	1.78	2.26	-	1.50	1.49	1.43	1.15
<b>28-Aug-2008</b>	1.73	1.73	1.68	1.67	1.11	-	1.95	1.91	1.96	2.07
<b>22-Oct-2008</b>	0.70	0.77	0.77	0.85	0.88	-	0.83	0.83	0.94	1.03
<b>2-May-2008</b>	1.28	1.45	1.46	1.36	1.69	-	1.49	1.47	1.64	1.84
<b>MEAN</b>	1.32	1.39	1.38	1.38	1.41	-	1.42	1.41	1.47	1.52
	<b>TIME TO PEAK RPS</b>					<b>TIME TO PEAK RPS</b>				
<b>3-Sep-2008</b>	0.54	0.52	0.51	0.48	0.50	0.22	0.32	0.45	0.88	0.92
<b>5-Jun-2008</b>	0.78	0.77	0.77	0.82	1.09	0.36	0.53	0.82	1.30	1.62
<b>28-Aug-2008</b>	0.36	0.36	0.38	0.37	0.40	0.21	0.49	0.57	0.42	0.92
<b>22-Oct-2008</b>	0.47	0.45	0.43	0.47	0.72	0.38	0.69	0.41	0.66	0.94
<b>2-May-2008</b>	0.20	0.18	0.18	0.21	0.27	0.14	0.30	0.15	0.22	0.55
<b>MEAN</b>	0.47	0.46	0.45	0.47	0.59	0.26	0.46	0.48	0.70	0.99

## CHAPTER 9

# 9 CALIBRATION/VALIDATION OF A DISTRIBUTED HYDROLOGIC MODEL AT MBDB

This section reveals findings in the previous sections applied to the MBDB using a distributed model with a resolution of 200 m and radar information for 2003. Predictability limits (maximum and minimum peak flows and runoff depths) were calculated for the calibration developed at the basins. The hydrologic model of 100 m was recommended in the previous section however the 200 m hydrologic model was tested because not significance differences were found for peak flow and runoff depth, variables analyzed here.

The rainfall source used to run one year simulation (2003) was the NWS MPE radar-rainfall products. This source has a mean systematic error (Bias) correction for Puerto Rico and in some places cannot remove the local bias, correctly, principally for small areas. In Chapter 7 an evaluation of the efficiency in removing the local Bias from MPE was conducted at the TBSW and additionally bias corrections need to be developed for small subwatersheds.

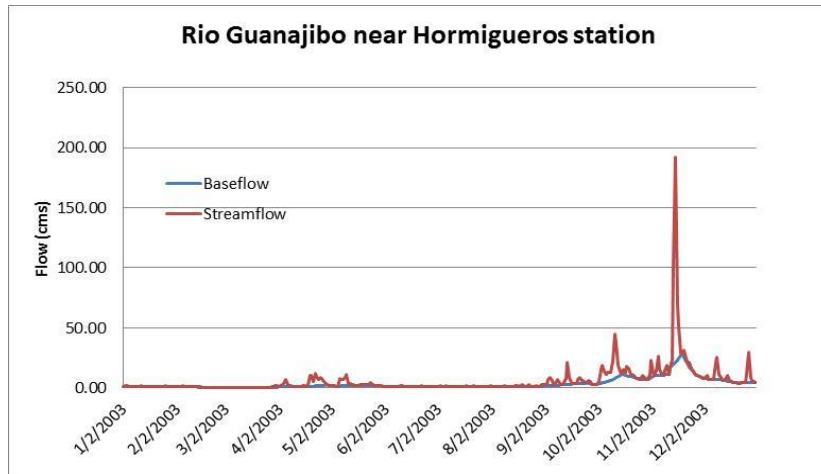
At observed flow locations, the base flow must be removed to obtain runoff observations. The PART computer program analyzes daily streamflow records and

estimates a daily ground water discharge. The method designates groundwater discharge to be equal to streamflow on days that fit a requirement of antecedent recession, linearly interpolates groundwater discharge for other days, and is applied to a long period of record to obtain an estimate of the mean rate of groundwater discharge and remove base flow at daily a time step (Rutledge, 1998).

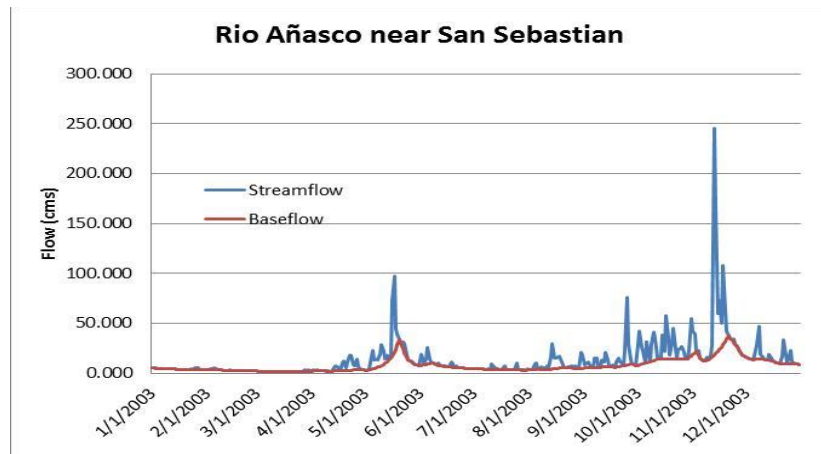
Table 9-1 shows the results for monthly base flow separation for 2003 at three USGS stream flow stations obtained from the PART computer model (Figure 9-1-A-B-C for Rio Guanajibo near Hormigueros, Rio Grande de Añasco near San Sebastian and Rio Rosario near Hormigueros, respectively). Additionally daily computations were obtained to add them to the Vflo runoff results for comparison with the observed stream flow.

**Table 9-1 Base flow separation at 3 USGS streamflow stations for 2003**

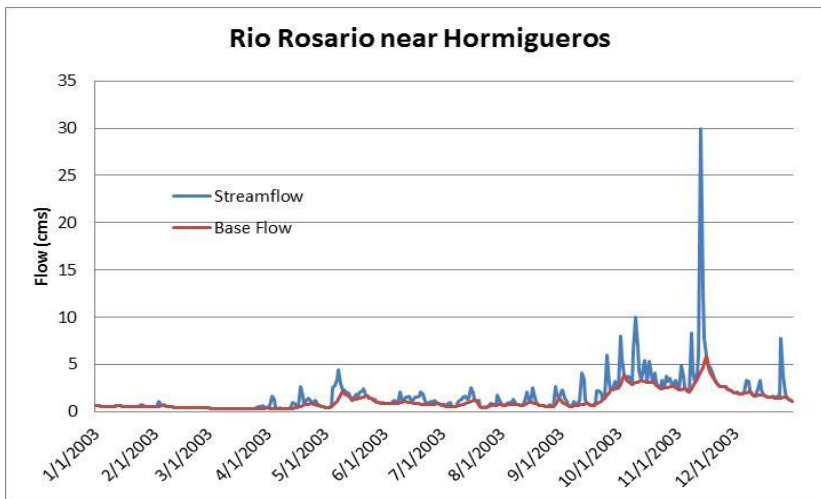
	Guanajibo near Hormigueros			Añasco near San Sebastian			Rosario near Hormigueros		
	Stream flow (mm)	Base flow (mm)	Runoff (mm)	Stream flow (mm)	Base flow (mm)	Runoff (mm)	Stream flow (mm)	Base flow (mm)	Runoff (mm)
<i>Jan</i>	10.2	9.4	0.8	44.2	41.9	2.3	32.0	30.7	1.3
<i>Feb</i>	4.8	4.1	0.8	28.2	25.7	2.5	25.1	23.6	1.5
<i>March</i>	4.1	2.8	1.3	20.6	18.5	2.0	19.3	17.3	2.0
<i>Ap</i>	33.3	14.7	18.5	59.9	30.0	30.0	45.0	26.7	18.3
<i>May</i>	28.2	18.5	9.7	231.6	139.4	92.2	97.3	70.4	26.9
<i>Jun</i>	8.9	7.6	1.3	90.4	70.6	19.8	66.5	48.5	18.0
<i>Jul</i>	9.7	6.9	2.8	46.5	37.8	8.6	57.7	41.4	16.3
<i>Aug</i>	12.2	8.4	3.8	97.3	53.3	43.9	59.9	42.7	17.3
<i>Sep</i>	45.7	25.4	20.3	136.7	68.6	68.1	99.1	61.5	37.6
<i>Oct</i>	123.4	76.7	46.7	280.7	142.7	137.9	234.4	167.4	67.1
<i>Nov</i>	235.0	122.9	112.0	454.2	255.5	198.6	265.4	170.4	95.0
<i>Dic</i>	72.6	48.5	24.1	170.2	125.5	44.7	122.4	94.5	27.9
<b>Total</b>	<b>588.0</b>	<b>345.9</b>	<b>242.1</b>	<b>1660.4</b>	<b>1009.7</b>	<b>650.7</b>	<b>1124.2</b>	<b>795.0</b>	<b>329.2</b>



A



B



C

**Figure 9-1 Daily stream flow and baseflow computation for 3 USGS stations, 2003.**

Figure 9-2 shows the simulated and observed accumulated runoff depth for the three USGS stations for 2003. The percent of errors for runoff depth around these values were 1.81 %, 1.07% and 4.47% for Guanajibo, Añasco and Rosario USGS outlet points. Nash–Sutcliffe model efficiency coefficients calculated for these outlet points were 0.46, 0.10 and 0.02, respectively.

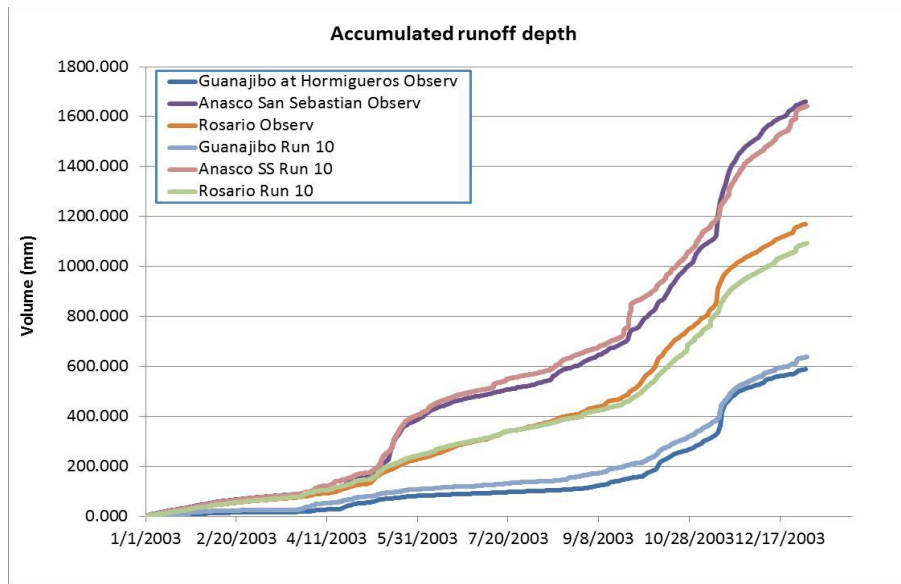
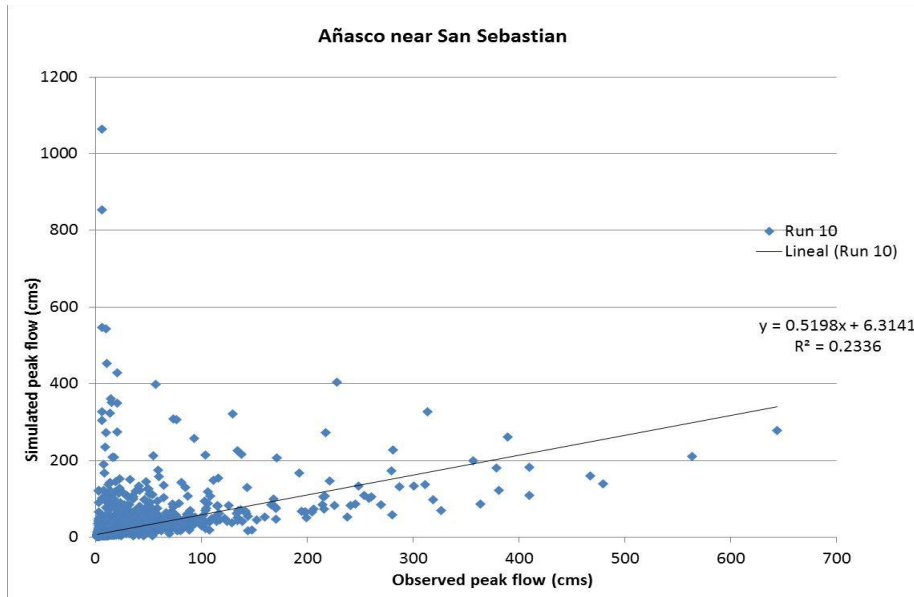


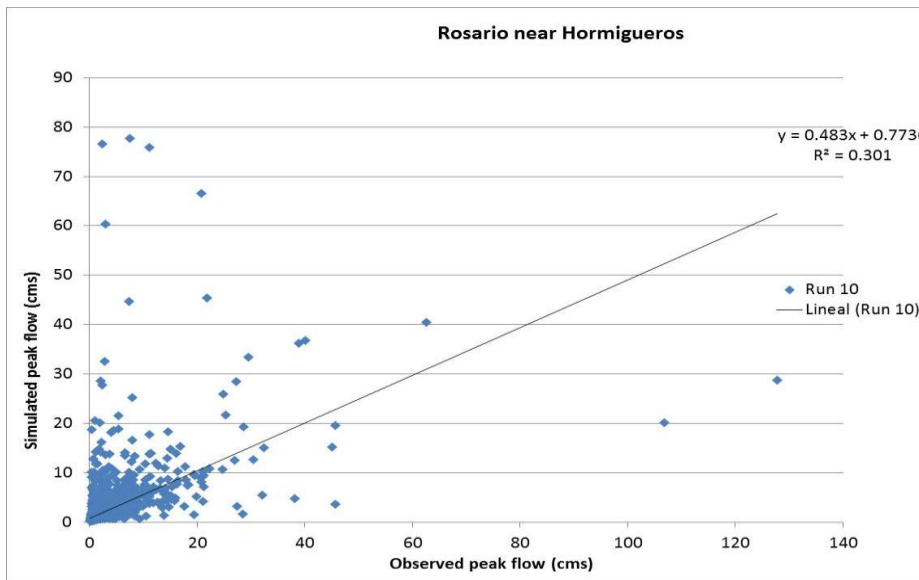
**Figure 9-2 Runoff depth accumulated for the USGS stations for 2003 year**

Some systematic errors in the MPE rainfall product were revealed in the simulation period, where the MPE sensed larger amounts of rainfall than actually occurred within the study MBDB area. In this cases the observed discharges were lower than the simulated (Figure 9-3-A-B) for Añasco and Rosario rivers. Additionally, maximum and minimum discharges were calculated perturbing the roughness and hydraulic conductivity within their limits evaluated in previous sections (0.25 and 1.75, respectively), while setting the initial saturation to 0.25 and 0.95, respectively. It is clear

that, for certain rainfall events, large differences between the modeled and observed data exist (Figure 9-4-A-B), indicating systematic errors due to MPE rainfall quantification, and limiting flood predictability in western Puerto Rico using the MPE radar product.

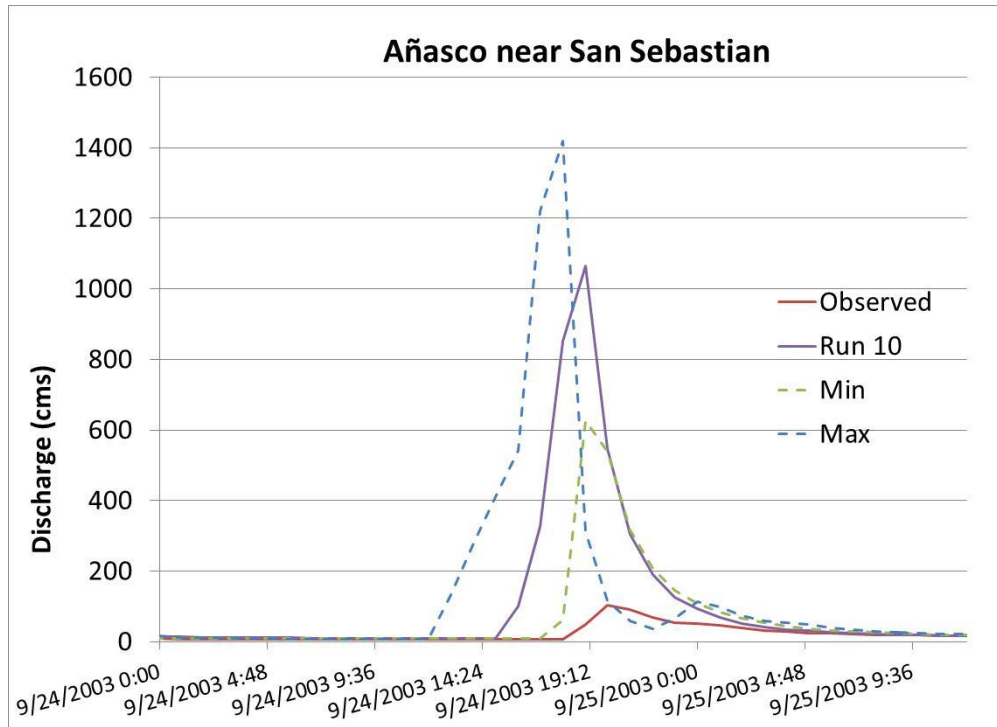


A

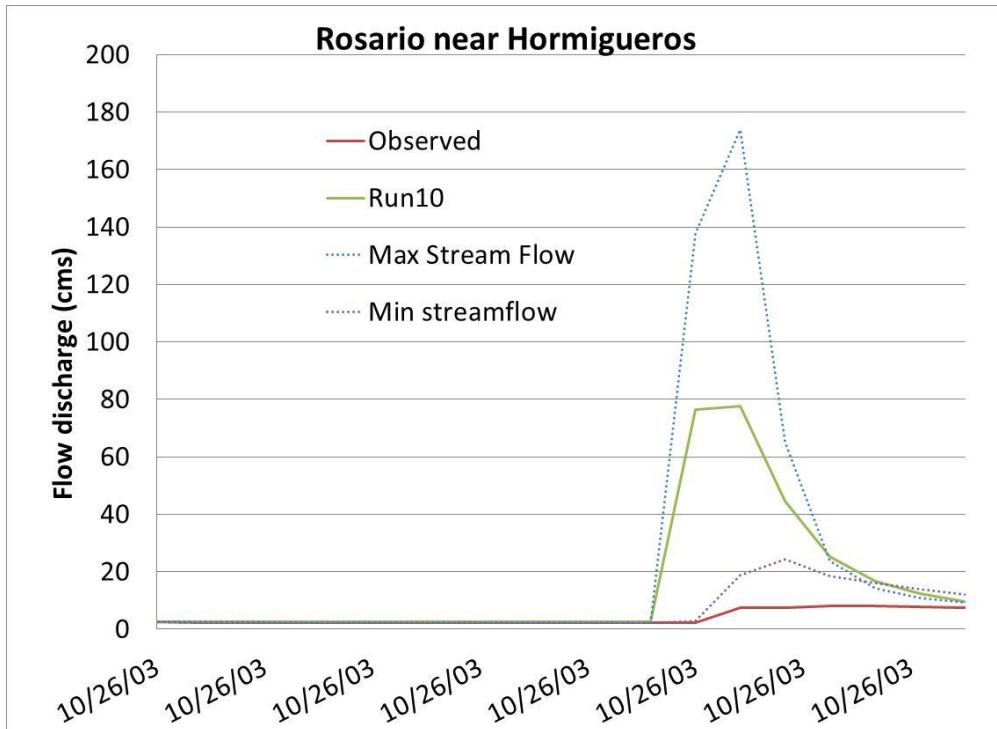


B

**Figure 9-3 Comparison between observed and simulated discharge for 2003 at hourly time step for: (A) Rio Grande de Añasco near San Sebastian and (B) Rio Rosario near Hormigueros stations.**



A



B

**Figure 9-4 Maximum, minimum and observed runoff for Añasco river (A) and Rosario river (B) outlet points for selected events**

The stream flow examples shown in Figure 9-4 A and B, illustrate cases in which the upscaled model could not reproduce the observed flow because the rainfall could not be quantified accurately using the MPE product. Forcing the model to produce maximum and minimum peak flows by judiciously parameterizing the model showed that the predictability limits of the model were well above the magnitude of the observed flow.

The implications of this result are that a better rainfall product is needed within the study area before accurate flood forecasts can be expected. It is hoped that the high resolution CASA radar product, currently under development, may fulfill this important need.

## CHAPTER 10

### 10 CONCLUSIONS AND FUTURE WORK

A hydrologic model was evaluated for its potential to perform real-time flood forecasting within the Mayagüez Bay drainage basin (819.1 km<sup>2</sup>), located in western Puerto Rico. Minimal run times, enhanced prediction skill, parameterization of variables and the understanding the dynamics of the system are issues that need to be faced to enhance flood prediction. In distributed models, the parameter values are physically based and the watershed is represented by grids, which approximates the parameter distribution and the initial conditions of the system. The modeler assigns the grid size resolution to the model, rainfall input scales and parameter values in a subjective way; subjective because the modeler has to select among various methods available for assigning grid point values (e.g., slope), and each method can influence the hydrologic result of the model. Each parameter and input are spatially and temporally scale-dependent, probability distributions are not known a priori, and the implications, in terms of uncertainty propagation through the system, are well understood.

This research provides a guide for the modeler to develop a hydrologic model knowing the implications of scale and parameter uncertainties on the flow response in small watershed where the uncertainties affect more the prediction and answers several important research questions. An objective of this research was to address the three

research questions given in Chapter 1. For convenience, the three research questions are restated below.

RQ1. How flood prediction is affected by the spatial variability of point rainfall at scales below that of the typical resolution of radar-based products?

RQ2. How does parameter resolution affect the model's predictive capabilities and the errors of the hydrologic system?

RQ3. Would the assumptions developed for the small scale enhance the hydrologic predictability at larger scales?

The main conclusions that can be drawn from this research are presented below:

- Rainfall variability was measured in a mountainous area of 4 km by 4 km (16 km<sup>2</sup>) using a high density rain gauge network. High spatial variability over short distances was measured. The standard deviation increased with increasing rainfall depth and the trend slope line (coefficient of variation) between average rainfall and standard deviation increased with increasing area of coverage (from 4.5 km<sup>2</sup> to 16 km<sup>2</sup>), [RQ1].
- NOAA's MPE (Multisensor Precipitation Estimation) product was evaluated in an area of 16 km<sup>2</sup> using the rain gauge network at hourly and daily time steps. MPE overestimated rainfall at the hourly time step and underestimated at the daily time step. Non significances were found in the hit rate between time steps. The probability of detection (POD) by the radar increased with the time step from 0.57

(hourly) to 0.833 (daily). False alarm rates were reduced with the larger time step, [RQ1].

- Large biases were found in the hourly time step and are associated with small rainfall detections and the resolution of both instruments. The bias between radar and the rain gauge network was event and time dependent. It is a random variable and follows a normal with box-crook distribution, [RQ1].
- Hydrologic predictability was studied as influenced by rainfall resolution inputs and hydrologic model resolutions, indicating their respective effects on flow response. The May 2 and September 8, 2008 events produced the greatest total average rainfalls and standard deviations, with high and low values of 5 days antecedent rainfall, respectively. No significant changes in total storm rainfall were observed with the interpolations at different scales, but produced important differences in rainfall intensity changes cell to cell through time, [RQ1].
- The slope map is an important input to the model. Decreases in the average slope will delay the time to peak and reduce peak flows. Up-scaling methods were tested to conserve the average slope and Method 2 was recommended to upscale a slope map in mountainous basins with high elevation variability over short distances, [RQ2].
- Rio Rosario watershed was most sensitive to overland roughness with a Sr average of -13.7 followed by channel roughness with -7.4, overland hydraulic conductivity with -3.3 and initial soil moisture with 2.8 for peak flow. Sr for Rio

Grande de Añasco and Rio Guanajibo watersheds indicate that the most sensitive parameters were channel roughness with -13.8 and -19.0, respectively, followed by overland roughness with -8.5 and -10.6 and initial soil moisture with 6.6 and 6.1 respectively, [RQ2]

- Rio Rosario, Grande de Añasco and Guanajibo watersheds were most sensitive to initial soil moisture followed by overland hydraulic conductivity and soil depth for runoff depth, [RQ2].
- Variations between events can change the ranking of the input parameters studied. This was observed in the case of both variables (peak flow and runoff depth) indicating time or event dependence in Sr computations related to antecedent soil moisture, [RQ2]
- Rainfall ensembles for different resolutions were evaluated and a guide was presented in which the modeler can decide or to know the uncertainties associated with each resolution. In general, the rainfall ensemble at 100 m, followed by 400 m and 200 m can represent very well the peak flow, volume and time to peak, three variables that indicate a good agreement between the observed hydrograph and the prediction, [RQ1, RQ2, RQ3].
- Hydrographs that present various bumps during the event can be represented very well with the hydrologic model at 10 m grid size spacing, locating the time to peak with the corresponding peak flow. However, this grid size has problems with volume computations for dry conditions. Another hydrologic model that can

capture the bumps is the 100 m grid size spacing and can produce the results for runoff depth very well, [RQ2, RQ3].

- Based on the analyses presented in this research, the recommended upscaled rainfall resolution, which will provide equivalent accuracy with the 100 m rainfall resolution, is 1000 m, and the recommended upscaled grid resolution, which will provide equivalent accuracy with the 10 m resolution, is 100 m, [RQ1, RQ2].
- Another useful result, but not specifically related to any of the research questions, pertains to the estimation of potential evapotranspiration (PET). The temperature/elevation linear regression equations of Goyal et al. (1988) were evaluated to calculate the PET at a daily time step using the Hargreaves-Samani equation and the results showed similar regression coefficients between observed and calculated  $T_{max}$ ,  $T_{min}$  and  $T_{ave}$  values with the temperature/elevation lineal regression equations by Goyal. The most sensitive parameter is the solar radiation, because the temperature model (Goyal et al., 1988) cannot represent the spatial variability of this parameter using the daily interpolation for extraterrestrial radiation and the  $T_{max}$  and  $T_{min}$  calculated with the elevation model. Therefore, the use of equation 5-3 is recommended with measured values of solar radiation and temperature values either measured or estimated using the Goyal et al. (1988) method.

For future works is recommended to include more events in the analysis for the TBSW, covering different event types, magnitudes and antecedent soil moisture condition as was covered in this research, from dry to wet conditions. Including more events would validate the findings in this research.

Include Bias as an additional perturbation parameter, using a normal with Box-cro transformation ( $\lambda = 0.15$ ) probability distribution function, to evaluate the uncertainty propagation through the hydrologic model.

The methodology used in this research to evaluate the rainfall resolution impact on hydrologic response using the bias corrected MPE product, could be reevaluated using the CASA radar data (when available) with high resolution grid size to decide which resolution is desirable from a hydrologic point of view.

Currently, a high density rain gauge network, extending over the MBDB area, which could be used to validate the NEXRAD rainfall estimates, does not exist. In the near future, it is hoped that this rainfall resolution gap will be filled by the CASA radars and that the hydrologic model formulated can be tested.

## 11 REFERENCES

- Abbott, M.B., J.C. Bathurst, J.A. Cunge, P.E. O'Connell, and J. Rasmussen, (1986a). "An introduction to European Hydrological System—Systeme Hydrologique Europeen, 'SHE'. 1. History and philosophy of a physically-based distributed modeling system." *J. Hydrol.* 87, 45–59.
- Abbott, M.B., J.C. Bathurst, J.A. Cunge, P.E. O'Connell, and J. Rasmussen, (1986b). "An introduction to the European Hydrological System—Systeme Hydrologique Europeen, 'SHE'. 2. Structure of a physically-based distributed modeling system." *J. Hydrol.* 87, 61–77.
- Anderson, T.W and D.A. Darling, (1954). "A Test of Goodness-of-Fit." *Journal of the American Statistical Association* 49: 765–769.
- Allen, R. G., L. S. Pereira, Dirk Raes and M. Smith, (1998). *Crop Evapotranspiration Guidelines for Computing Crop Water Requirements*. FAO Irrigation and Drainage Paper 56, Food and Agriculture Organization of the United Nations, Rome.
- Atger, F., (1999). "The skill of ensemble predictions systems." *Monthly Weather Review*, 127, 1941-1953.
- Baeck, M. L., and J. A. Smith, (1998). "Estimation of heavy rainfall by the WSR-88D." *Weather Forecasting*, 13, 416–436.
- Ball, J.E., and K.C. Luk, (1998). "Modeling the spatial variability of rainfall over a catchment." ASCE, *Journal of Hydrologic Engineering*, 3(2):122-130. DOI 10.1061/(ASCE)1084-0699(1998)3:2(122)
- Battan, L.J., (1973). *Radar observation of the atmosphere*. University of Chicago Press, 323 pp.
- Bear, J., (1972). *Dynamics of Fluids in Porous Materials*. American Elsevier, 784 pp.
- Bedient, P.B., B.C. Hoblit, D.C. Gladwell, and B.E. Vieux, (2000). "NEXRAD Radar for Flood Prediction in Houston." *Journal of Hydrologic Engineering*, 5(3): 269-277. ASCE, ISSN 1084-0699/00/0003-0269–0277

- Bedient, P.B., A. Holder, J.A. Benavides, and B.E. Vieux, (2004). "Radar-Based Flood Warning System Applied to Tropical Storm Allison." *Journal of Hydrologic Engineering*, 8(6): 308-318. ASCE, ISSN 1084-0699/2003/6-308-318
- Bell, V.A. and R.J. Moore, (2000). "The sensitivity of catchment runoff models to rainfall data at different spatial scales." *Hydrology and Earth System sciences*, 4(4):653-667.
- Bevan, K. J., and G.M. Hornberger, (1982). "Assessing the effect of spatial pattern of precipitation in modeling streamflow hydrographs." *Water Resources Bulletin*, 18(5):823-829.
- Beven, K., and A. Binley, (1992). "The future of distributed models: Model calibration and uncertainty prediction." *Hydrological Process.*, 6, 279-298.
- Binley, A.M., and K.J. Beven, (1991). "Physically-based modelling of catchment hydrology: a likelihood approach to reducing predictive uncertainty." In: Farmer, D.G., Rycroft, M.J. (Eds.). *Computer Modelling in the Environmental Sciences*. Clarendon Press, Oxford, pp. 75-88.
- Birikundavyi, S., and J. Rouselle, (1997). "Use of partial duration series for single-station and regional analysis of floods." *Journal of Hydrologic Engineering*, 2, 68-75
- Bloschl, G., C. Reszler, and J. Komma, (2008), "A spatially distributed flash flood forecasting model." *Environmental Modelling & Software*, 23(4):464-478. doi:10.1016/j.envsoft.2007.06.010.
- Bormann, H., (2006). "Impact of spatial data resolution on simulated catchment water balances and model performance of the multi-scale TOPLATS model." *Hydrology and Earth System Sciences*, 10(2):165-179. doi:10.5194/hess-10-165.
- Bouwer, H., (1966). "Rapid field measurement of air entry value and hydraulic conductivity of soil as significant parameters in flow system analysis." *Water Resources Research* 2(4):729-738.
- Brasington, K., and K. Richards, (1998). "Interactions between model predictions, parameters and DTM scales for TOPMODEL." *Comput. Geosci.*, 24(4):299-314.
- Burnash, R. J. C., R. L. Ferral, and R. A. McGuire, (1973). "A generalized streamflow simulation system—Conceptual modeling for digital computers." Tech. Rep. to the Joint Federal and State River Forecast Center, U.S. National Weather Service and California Department of Water Resources, Sacramento, 204 pp.

- CASA (2006). *CASA Annual Report Year 3, Volume II*. Engineering Research Center for Collaborative Adaptive Sensing of the Atmosphere. Cooperative Agreement No. EEC-0313747, National Science Foundation. March 20.
- Carpenter, T.M., and K.P. Georgakakos, (2004). “Continuous streamflow simulation with the HRCDHM distributed hydrologic model.” *Journal of Hydrology*, 298, 61-79.
- Casale, R. and C. Margottini, (2004). *Natural Disasters and Sustainable Development*. Springer, 398 pp.
- CRIM, (1998). Center for Municipal Tax Revenues of Puerto Rico. Digital Elevation Model.
- Cole, S. J., and R. J. Moore, (2009). “Distributed hydrological modelling using weather radar in gauged and ungauged basins.” *Advances in Water Resources*, 32(7):1107-1120. Elsevier Ltd. doi:10.1016/j.advwatres.2009.01.006
- Droegemeier, K. K. and J.D. Smith, (2000). “Hydrological aspects of weather prediction and flood warning: Report of the Ninth Prospectus Development Team of the U.S. Weather Research Program.” *Bull. Amer. Meteor. Soc.*, 81, 2665–2680.
- Entekahbi, D., M.P. Anderson, R. Avissar, R. Bales, G.M. Hornberger, W.K. Nuttle, M.B. Parlange, C. Peters-Lidard, K.W. Potter, J.O. Roads, J.L. Wilson, and E.F. Wood, (2002). *Report of a Workshop on Predictability and Limits to prediction in Hydrologic Systems*. Committee on Hydrologic Science, National Research Council, National Academy Press, ISBN 0-309-08347-8. pp. 118.
- Epstein, E.S., (1969). “A scoring system for probability forecast of ranked categories.” *Journal of Applied Meteorology*, 8, 985-987.
- Fang, Z. and P.B. Bedient, (2007). “NEXRAD Flood Warning System and Floodplain Library for Houston, TX.” ASCE Conf. Proc.: *World Environmental and Water Resources Congress: Restoring our Natural Habitat*. doi:http://dx.doi.org/10.1061/40927(243)302
- Fishman, G.S., (1996). *Monte Carlo: Concepts, Algorithms and Applications*. Springer, New York, USA. 723 pp.
- FEMA, (2009). *Flood Insurance Study*. Commonwealth of Puerto Rico, Volume 1 of 5, Revised: Nov. 18, 2009. Federal Emergency Management Agency

- Freer, J., K. Beven and B. Ambrose, (1996). "Bayesian estimation of uncertainty in runoff prediction and the value of data: An application of the GLUE approach." *Water Resour. Res.*, 32, 2161–2173.
- Freeze R. A. and J.A. Cherry, (1979). *Groundwater*. Prentice Hall Publishers, 604 pp.
- Figueroa-Alamo, C., Z. Aquino, S. Guzmán-Ríos, and A.V. Sánchez, (2006). *Water resources data Puerto Rico and the U.S. Virgin Islands*. Water Year 2004: U.S. Geological Survey Water-Data Report PR-04-1, 597 p.
- Georgakakos, K.P. (2006a). "Analytical results for operational flash flood guidance." *Journal of Hydrology*, 317, 81–103.
- Georgakakos, K.P., (2006b). "Hydrologic Short Term Forecasting with QPF Input." *White Paper in Proceedings of USWRP Warm Season Precipitation Workshop*, 5-7 March 2002, National Center for Atmospheric Research, Boulder, Colorado, 5 pp.
- Gourley, J. J. and B.E. Vieux, (2005). "A method for evaluating the accuracy of quantitative precipitation estimates from a hydrologic modeling perspective." *American Meteorological Society*. April, 115-133.
- Gourley, J. J. and B.E. Vieux, (2006). "A method for identifying sources of model uncertainty in rainfall-runoff simulations." *Journal of Hydrology*, 327, 68-80.
- Goyal, M. R., E.A. González and C. Chao de Báez, (1988). "Temperature versus elevation relationships for Puerto Rico." *J. Agric. UPR* 72(3):449-67.
- Griensven, A. van, T. Meixner, S. Grunwald, T. Bishop, M. Diluzio, and R. Srinivasan, (2006). "A global sensitivity analysis tool for the parameters of multi-variable catchment models." *Journal of Hydrology* 324, 10-23.
- Gritmit, E.P. and C.F. Mass, (2002). "Initial results of a mesoscale short-range ensemble forecasting system over the Pacific Northwest." *Weather and Forecasting*, 17, 192-205.
- Gupta, R.S., (1989). *Hydrology and Hydraulic Systems*. Waveland Press, Inc., Illinois. 302-307 pp. ISBN 0-88133-865-6.
- Hamill, T.M., J.S. Whitaker, and X. Wei, (2004). "Ensemble re-forecasting: improving medium-range forecast skill using a retrospective forecast." *Monthly Weather Review*, 132, 1434-1447.

- Hargreaves, G. H. and Z. A. Samani, (1985). "Reference crop evapotranspiration from temperature." *Appl. Eng. Agric.*, ASAE. 1(2):96-9.
- Harmsen E. W., J. C. Converse, and M. P. Anderson, (1991), "Application of the Monte-Carlo Simulation Procedure to Estimate Water-Supply Well/Septic Tank-Drainfield Separation Distances in the Central Wisconsin Sand Plain," *Journal of Contaminant Hydrology*, 8(1); 91-109.
- Harmsen, E. W., S.E. Gomez Mesa, E. Cabassa, N.D. Ramirez Beltran, S. Cruz-Pol, R.J. Kuligowski, and R. Vasquez, (2008). "Satellite sub-pixel rainfall variability." *WSEAS Transactions on Signal Processing*, 8(7):504-513.
- Harmsen, E. W. J. Mecikalski, M.J. Cardona-Soto, A. Rojas González and R. Vásquez, (2009). "Estimating daily evapotranspiration in Puerto Rico using satellite remote sensing." *WSEAS Transactions on Environment and Development*, 6(5):456-465.
- Harmsen, E. W., J. Mecikalski, A. Mercado, and P. Tosado Cruz, (2010). "Estimating evapotranspiration in the Caribbean Region using satellite remote sensing." *Proceedings of the AWRA Summer Specialty Conference, Tropical Hydrology and Sustainable Water Resources in a Changing Climate*. San Juan, Puerto Rico. August 30-September 1.
- HCFCDD, (1984). *Criteria Manual for the Design of Flood Control and Drainage Facilities*. Houston, Texas, Harris County Flood Control District.
- Helmer, E.H., O. Ramos, T.M. López, M. Quiñónez and W. Díaz, (2002). "Mapping the forest type and land cover of Puerto Rico, a component of the Caribbean biodiversity hotspot." *Caribbean Journal of Science* 38(3/4):165-183.
- Henderson, F. M., (1966). *Open channel flow*. Macmillan, New York. 544 pp.
- Hydrologic Engineering Center, (2006). *HEC-HMS, Hydrologic Modeling System*. U.S. Army Corps of Eng, Davis, CA.
- Hydrologic Engineering Center, (2008). *HEC-RAS River Analysis System*. Version 4.0 U.S. Army Corps of Eng, Davis, CA.
- Julien, P.Y. and Saghafian, B., (1991). *CASC2D user manual—a two dimensional watershed rainfall–runoff model*. Civil Engineering Report CER90-91PYJ-BS-12, Colorado State University, Fort Collins, p. 66.

- Julien, P.Y., Saghafian, B. and Ogden, F.L., (1995). "Raster-based hydrological modeling of spatially-varied surface runoff." *Water resources bulletin*. AWRA 31(3):523–536.
- Kondragunta, C.R., D. Kitzmiller, D.J. Seo, and K. Shrestha, (2005). "Objective integration of satellite, rain gauge, and radar precipitation estimates in the Multisensor Precipitation Estimator algorithm." *19th Conference on Hydrology, Amer. Meteor Soc.*, Seattle.
- Kondragunta, C.R. and K. Shrestha, (2006). "Automated real-time operational rain gauge quality control tools in NWS hydrologic operations." *20th Conference on Hydrology, 86<sup>th</sup> Amer. Meteor Soc. Annual Meeting*, Atlanta, GA.
- Koutsoyiannis, D. and N. Mamassis, (1993). "Univariate TO multivariate stochastic modelling of rainfall." Presented at *Fourth AFORISM Meeting*, Cork, Ireland. Published by Dept of Water Resources, Hydraul. & Maritime Engng.
- Leavesley, G. H., R. W. Lichty, B.M. Troutman. and L.G. Saindon, (1983). "Precipitation-runoff modeling system user manual." USGS Water Resources Investigations Rep. No. 83-4238, Denver.
- Lawrence, B. A., M.I. Shebsovich, M.J. Glaudemans, and P.S. Tilles, (2003). "Enhancing precipitation estimation capabilities at National Weather Service field offices using multi-sensor precipitation data mosaics." *83rd AMS Annual Meeting, 19th International Conference on Interactive Information Processing Systems for Meteorology, Oceanography, and Hydrology*, Long Beach, California, February 9-13.
- Maddox, R. A., L.R. Hoxit, C.H. Chappell, and F. Caracena, (1978), "Comparison of the meteorological aspects of the Big Thompson and Rapid City flash floods." *Mon. Wea. Rev.*, 106, 375-389.
- Mahani, S. E. and R. Khanbilvardi, (2009). "Generating Multi-Sensor Precipitation Estimates over radar gap areas." *WSEAS Transactions on Systems*, 8, 96-106.
- Marshall, J.S. and W. Palmer, (1948). "The distribution of raindrops with size." *J. Meteor.*, 5, 165-166
- McGregor, K. C., R.L. Bingner, A.J. Bowie, and G.R. Foster, (1995). "Erosivity index values for northern Mississippi." *Trans. ASCE*, 38, 1039–1047.
- McWhorter, D. B. and D.K. Sunada, (1977). *Ground-Water Hydrology and Hydraulics*. Water Resources Publications. 304 pp.

- McMichael, C. E., A.S. Hope and H.A. Loaiciga, (2005). "Distributed hydrological modeling in California semi-arid shrublands: MIKESHE model calibration and uncertainty estimation." *Journal of Hydrology*. 317, 307-324.
- Minitab Inc, (2010). "Meet MINITAB 16 for Windows®." English Version.  
[www.minitab.com](http://www.minitab.com)
- Moore, I. D., R. B. Grayson and A. R. Ladson, (1991). "Digital terrain modelling: a review of hydrological, geomorphological and biological applications." *Int. J. of Hydrological Process*, 5(1):3-30.
- Moore, A.M. and R. Kleeman, (1998). "Skill assessment for ENSO using ensemble prediction." *Quarterly Journal of the Royal Meteorological Society*, 124, 557-584.
- Müller, W. A., C. Appenzeller, F. J. Doblas-Reyes, M. A. Liniger, (2005). "A debiased ranked probability skill score to evaluate probabilistic ensemble forecasts with small ensemble sizes." *Journal of Climate* 18:10, 1513-1523
- Murphy, A.H., (1971). "A note on the ranked probabilistic predictions and probability score in the cost-loss ratio situation." *Journal of Applied Meteorology*, 5, 534-537.
- NOAA, (2006). *Puerto Rico Mean Annual Precipitation 1971-2000*. Hydrology and River Information. National Oceanic and Atmospheric Administration, National Weather Service Forecast Office, San Juan, Puerto Rico,  
URL:[http://www.srh.noaa.gov/sju/?n=mean\\_annual\\_precipitation](http://www.srh.noaa.gov/sju/?n=mean_annual_precipitation)
- NOAA, (No date). Advanced Hydrologic Prediction Service (Online). Available:  
<http://water.weather.gov/ahps2/hydrograph.php?wfo=sju&gage=horp4>
- Ogden, F.L. and P.Y. Julien, (1994). "Runoff model sensitivity to radar rainfall resolution." *J. Hydrol.* 158, 1–18.
- Prieto, M.G., (2006). "Development of a Regional Integrated Hydrologic Model for a Tropical Watershed." Master of Science Thesis, University of Puerto Rico at Mayagüez, PR.
- PRWRERI, (2004). Land Use Classification of the Mayagüez Bay Watershed (Río Grande de Añasco, Río Yagüez, and Río Guanajibo Watersheds. Puerto Rico Water Resources and Environmental Research Institute. Developed for the Puerto Rico Environmental Quality Board.

- Quinn, P., K. Beven, P. Chevallier and O. Planchon, (1991). "The prediction of hillslope flow paths for distributed hydrological modeling using digital terrain models." *Hydrol. Processes*, 5, 59–79.
- Ramírez-Beltran, N. R.J. Kuligowski, E.W. Harmsen, J. M. Castro, S. Cruz-Pol and M. Cardona-Soto, (2008a). "Rainfall estimation from convective storms using the Hydro-Estimator and NEXRAD." *WSEAS Transaction on Systems*. 10(7):1016-1027.
- Ramirez-Beltrán, N.D., R.J. Kuligowski, E.W. Harmsen, J. M. Castro, S. Cruz-Pol and M.J. Cardona-Soto, (2008b). "Validation and strategies to improve the Hydro-Estimator and NEXRAD over Puerto Rico." *12th WSEAS International Conference on SYSTEMS*, Heraklion, Greece, July 22-24.
- Rawls, W.J., Brakensiek, D.L., Miller, N., (1983). "Green-Ampt Infiltration Parameters from Soils Data." *Journal of Hydraulic Engineering* 109(1), 62 – 70.
- Reed, S., V. Koren, M. Smith, Z. Zhang, F. Moreda, D.J. Seo and DMIP Participants, (2004). "Overall distributed model intercomparison project results." *Journal of Hydrology*, 298, 27-60.
- Rojas-González, A.M., (2004). "Estudio Comparativo sobre hidráulica de ríos en valles aluviales", Master of Science Thesis, University of Puerto Rico at Mayagüez, PR., 140 pp.
- Rutledge, A.T., (1998). Computer programs for describing the recession of ground-water discharge and for estimating mean ground-water recharge and discharge from streamflow records-update. U.S. Geological Survey Water Resources Investigations Report 98-4148.
- Sahho, G.B, C. Ray and E. H. De Carlo, (2006). "Calibration and validation of a physically distributed model, MIKE SHE, to predict streamflow at high frequency in a flashy mountainous Hawaii stream." *Journal of Hydrology*, 327, 94-109.
- Saxton, K.E. and W. Rawls, (2006). *Soil Water Characteristics, Hydraulic Properties Calculator*. Hydrology and Remote Sensing Laboratory, USDA-ARS, Maryland, USA.
- Schaap, M.G., (2003). *Rosetta Lite Version 1.1*. George E. Brown Jr. Salinity Laboratory and UC Riverside, Department of Environmental Sciences, June.
- Schaap, M.G. and F.J. Leij, (1998a). "Database related accuracy and uncertainty of pedotransfer functions." *Soil Science* 163:765-779.

- Schaap, M.G. and F.J. Leij, (1998b). "Using neural networks to predict soil water retention and soil hydraulic conductivity." *Soil & Tillage Research*, 47:37-42.
- Schaap, M.G., F.J. Leij, and M. Th. van Genuchten, (1998). "Neural network analysis for hierarchical prediction of soil water retention and saturated hydraulic conductivity." *Soil Sci. Soc. Am. J.* 62,847-855.
- Schaap, M.G., F.J. Leij and M. Th. van Genuchten, (2001). "Rosetta: a computer program for estimating soil hydraulic parameters with hierarchical pedotransfer functions." *Journal of Hydrology*, 251,163-176.
- Scofield, R.A. and R.J. Kuligowski, (2003). "Status and outlook of operational satellite precipitation algorithms for extreme-precipitation events." *Weather Forecasting*, 18, 1037-1051.
- Seo, D.J., (1998). "Real-time estimation of rainfall fields using rain gauge data under fractional coverage conditions." *Journal of Hydrology*, 208, 25-36.
- Seo, D.J., J.P. Briedenbach and E.R. Johnson, (1999). "Real-time estimation of mean field bias in radar rainfall data." *Journal of Hydrology*, 223, 131-147.
- Sepúlveda, N., F. Pérez-Blair, L.L. DeLong and D. López-Trujillo, (1996). *Real-Time Rainfall-Runoff Model of the Carráizo-Reservoir Basin in Puerto Rico*, Water-Resources Investigations Report 95-4235, U.S. Geological Survey. San Juan, Puerto Rico.
- Shrestha, R. K., T. Yasuto, and T. Kaoru, (2002). "IC ratio concept in distributed hydrological modeling for optimal performance." *International Conference on Urban Hydrology for the 21st Century*, 14-16 October, Kuala Lumpur, 790-800.
- Simunek, J., M.Th. van Genuchten and M. Sejna, (2005). *Code for Simulating the one-dimensional movement of water, heat, and multiple solutes in variably saturated porous media*, Department of Environmental Sciences, University of California Riverside and US Salinity Laboratory, USDA, ARS, Riverside, CA, USA.
- Smith, M.B., D.J. Seo, V.I. Koren, S. Reed, Z. Zhang, Q.Y. Duan, F. Moreda and S. Cong, (2004). "The distributed model intercomparison project (DMIP): motivation and experiment design." *J. Hydrol. DMIP Special Issue*.
- Spear, R.C. and G. M. Hornberger, (1980). "Eutrophication in Peel Inlet II. Identification of critical uncertainties via generalized sensitivity analysis." *Cybernetics*, 14, 43-49.

- Stensrud, D.J., J.W. Bao, and T.T. Warner, (2000). "Using ensembles for short range forecasting." *Monthly Weather Review*, 127, 433-446.
- Stephens, M.A., (1970). "Use of the Kolmogorov-Smirnov, Cramer-Von Mises and related statistics without extensive tables." *Journal of the Royal Statistical Society. Series B (Methodological)*, 32(1):115-122.
- Sweeney, T.L., (1992). *Modernized Areal Flash Flood Guidance*. NOAA Technical Report NWS HYDRO 44. Hydrologic Research Laboratory, National Weather Service, NOAA, Silver Spring, MD, October, 21 pp. and an appendix.
- Tarboton, D.G., R.L. Bras, and I. Rodriguez-Iturbe, (1991). "On extraction of channel networks from digital elevation data." *Hydrolog. Process.*, 5, 81-100.
- U.S. Census Bureau, (2010). Census 2010 Data for Puerto Rico. U.S. Census Bureau.
- U.S. Army Corps of Engineers, (1990). *HEC-1 Flood Hydrograph Package*. Hydrologic Engineering Center, Davis, California, September.
- USACE, (1996). *Hydrologic Aspects of Flood Warning Preparedness Programs*. Department of the Army, U.S. Army Corps of Engineers, Engineering Technical Letter, ETL 1110-2-540.
- U.S. Department of Agriculture, Natural Resources Conservation Service, (2006a). *Soil Survey Geographic (SSURGO) database for Mayagüez area*. Puerto Rico Western Part, pr684, Fort Worth, Texas, Publication date: Dec. 26.  
URL:<http://SoilDataMart.nrcs.usda.gov/>
- U.S. Department of Agriculture, Natural Resources Conservation Service, (2006b). *Soil Survey Geographic (SSURGO) database for Lajas Valley Area*. Puerto Rico, pr687 Fort Worth, Texas, Publication date: Dec. 26.  
URL:<http://SoilDataMart.nrcs.usda.gov/>
- U.S. Department of Agriculture, Natural Resources Conservation Service, (2006c). *Soil Survey Geographic (SSURGO) database for Arecibo area*. Puerto Rico Western Part, pr682, Fort Worth, Texas, Publication date: Dec. 26.  
URL:<http://SoilDataMart.nrcs.usda.gov/>
- U.S. Department of Agriculture, Natural Resources Conservation Service, (2006d). *Soil Survey Geographic (SSURGO) database for Ponce area*. Puerto Rico Western Part, pr688, Fort Worth, Texas, Publication date: Dec. 26.  
URL:<http://SoilDataMart.nrcs.usda.gov/>

- U.S. Department of Commerce, (1961). *Technical Paper 42, Generalized Estimates of Probable Maximum Precipitation and Rainfall-Frequency Data for Puerto Rico and Virgin Islands*. National Oceanic and Atmospheric Administration, Weather Bureau.
- USGS, (1999). *Estimation of Magnitude and Frequency of Floods for Streams in Puerto Rico: New Empirical Models*. Water Resources Investigation Report 99-4142, U.S. Department of the Interior, Geological Survey, San Juan, Puerto Rico.
- U.S. Department of the Interior, Geological Survey, (1977). *Regional Flood Frequency for Puerto Rico*. Open-File Report, M. A. Lopez (author).
- Van der Perk, M. and M.F.P. Bierkens, (1997). "The identifiability of parameters in a water quality model of the Biebzra river, Poland." *Journal of Hydrology* 200, 307-322.
- van Genuchten, M.Th., (1980). "A closed-form equation for predicting the hydraulic conductivity of unsaturated soils." *Soil Sci. Am. J.* 44:892-898.
- Viessman, W. and G.L. Lewis, (1996). *Introduction to Hydrology*. 4th Edition, Harper-Collins, 760 pp.
- Vieux, B.E., (1988). "Finite Element Analysis of Hydrologic Response Areas Using Geographic Information Systems", Ph.D. Thesis , Department of Agricultural Engineering, Michigan State University, July, 199 pp.
- Vieux, B.E., V.F. Bralts, Segerlind and R.B. Wallace, (1990). "Finite element watershed modeling: one-dimensional elements." *J. Water Resour. Plan. Mgmt* 116(6):803–819.
- Vieux, B. E., (1993). "Surface runoff modeling." *Computing*, 7(3), 310-338.
- Vieux, B.E. and N. Gauer, (1994). "Finite element modeling of storm water runoff using GRASS GIS." *Microcomput. Civil Eng.* 9(4):263–270.
- Vieux, B.E. and N.S. Farajalla, (1996). "Temporal and Spatial Aggregation of NEXRAD Rainfall Estimates on Distributed Hydrologic Modelling." *Third Int. Conf. on GIS and Environmental Modeling*, Santa Fe, NM, Nat. Center Geog. Info. Annual, 199– 204.
- Vieux, B. E. and P.B. Bedient, (1998). "Estimation of rainfall for flood prediction from WSR-88D reflectivity: A case study, 17-18 October 1994." *American Meteorological Society*. June, 407- 415.

- Vieux, B.E., (2001). *Distributed Hydrologic Modeling Using GIS*. Water Science Technology Series, Kluwer Academic Publishers, Norwell, Massachusetts, 311 pp. ISBN 0-7923-7002-3.
- Vieux, B.E., C. Ester, C. Dempsey, and J.E. Vieux, (2002). "Prospects for a real-time flood warning system in Arizona." *Proceedings of the 26th Annual Conference, Breaking the Cycle of Repetitive Flood Loss, Association of State Floodplain Managers*, June 23-28, 2002, Phoenix, AZ.
- Vieux, B.E. and J.E. Vieux, (2002). "Vflo™: A real-time distributed hydrologic model." *Proceedings of the Second Federal Interagency Hydrologic Modeling Conference*, July 28-August 1, Las Vegas, NV 2002. Abstract and paper in CD-ROM.
- Vieux, B.E., C. Chen, J.E. Vieux and K.W. Howard, (2003). "Operational Deployment of a Physics-based Distributed Rainfall-runoff Model for Flood Forecasting in Taiwan." *IAHS General Assembly at Sapporo, Japan*, July 3-11, 2003.
- Vieux, B.E. and F.G. Moreda, (2003). "Ordered physics-based parameter adjustment of a distributed model" In: Duan, Q., Sorooshian, S., Gupta, H.V., Rousseau, A.N., Turcotte, R. (Eds.), *Water Science and Application Series*, vol. 6. American Geophysical Union, pp. 267-281, ISBN 0-87590-355-X (Chapter 20).
- Vieux, B.E. and Associates, Inc., (2004). *Vflo™ 3.0, Desktop User Manual*. [URL: www.vieuxinc.com](http://www.vieuxinc.com).
- Vieux, B. E., Cui, Z. and A. Gaur, (2004). "Evaluation of a physics-based distributed hydrologic model for flood forecasting." *Journal of Hydrology*, 298, 155-177. doi:10.1016/j.jhydrol.2004.03.035
- Vieux, B.E. and P.B. Bedient, (2004). "Assessing urban hydrologic prediction accuracy through event reconstruction." *Journal of Hydrology*, 299, 217-236. doi:10.1016/j.jhydrol.2004.08.005
- Vieux, B.E., P.B. Bedient and E. Mazroi, (2005). "Real-time urban runoff simulation using radar rainfall and physics-based distributed modeling for site-specific forecasts." *10th International Conference on Urban Drainage*, Copenhagen, Denmark, 21-26 August.
- Vieux, B.E. and J.E. Vieux, (2005). "Statistical evaluation of a radar rainfall system for sewer system management",

- Vieux, B.E. and J.M. Imgarten, (2006). “On the scale-dependent propagation of hydrologic uncertainty using high-resolution X-band radar rainfall estimates”, *Atmospheric Research*, 103, 96-105. doi: 10.1016/j.atmosres.2011.06.009.
- Vieux, B.E. and J.E. Vieux, (2006). “Evaluation of a physics-based distributed hydrologic model for coastal, island, and inland hydrologic modeling”, In *Coastal Hydrology and Processes*. Water Resources Publications, LLC, Highlands Ranch, CO, USA., Pp 453-464.
- Viglione, A., G.B. Chirico, J. Komma, R. Woods, M. Borga, and G. Blöschl, (2010). “Quantifying space-time dynamics of flood event types.” *Journal of Hydrology*, 394(1-2):213-229. Elsevier B.V. doi:10.1016/j.jhydrol.2010.05.041
- Villalta-Calderón, C.A., (2004). “Selección de Funciones de Transporte de Sedimentos para los Ríos de la Bahía de Mayagüez usando SAM”, Master of Science Thesis, University of Puerto Rico at Mayagüez, PR., 441 pp.
- Warner, T.T., E.A. Brandes, J. Sun, D.N. Yates and C.K. Mueller, (2000). “Prediction of a flash flood in complex terrain. Part I: A comparison of rainfall estimates from radar, and very short range rainfall simulations from a dynamic model and an automated algorithmic system.” *J. Appl. Meteor.*, 39, 797-814.
- Wechsler, S. (2006). “Uncertainties associated with digital elevation models for hydrologic applications : a review.” *Hydrol. Earth Syst. Discuss.*, 3, 2343-2384.
- Wunderground web page, (No Date). WenderMap. Available: <http://www.wunderground.com/US/PR/> [2010, June 5]
- Western, A., S. Zhou, R. Grayson, T. McMahon, G. Blöschl and D. Wilson, (2004). “Spatial correlation of soil moisture in small catchments and its relationship to dominant spatial hydrological processes.” *Journal of Hydrology*, 286(1-4):113-134. doi:10.1016/j.jhydrol.2003.09.014
- Whiteaker, T., O. Robayo, D. Maidment and D. Obenour, (2006). “From a NexRAD rainfall map to a flood inundation map.” *Journal of Hydrologic Engineering*, 11(1):37-45.
- Wigmosta, M.S., L.W. Vail and D.P. Lettenmaier, (1994). “A distributed hydrology-vegetation model for complex terrain.” *Water Resour. Res.* 30(6):1665–1679.
- Wilks, D.S., (1995). *Statistical Methods in the Atmospheric Sciences: An Introduction*. Academic Press, San Diego, 467 pp.

Wilson, J. W. and E. A. Brandes, (1979). "Radar measurement of rainfall A summary." *Bulletin of the AMS*, 60(9):1048-1058.

Woodley, W. L., A.R. Olsen, A. Herndon and V. Wiggert, (1975). "Comparison of gauge and radar methods of convective rain measurement." *Journal of Applied Meteorology*, 14, 909–928.